Cranfield University

Nicolas MAILH

Experimental investigation of Lift and Drag on the NACA 4412 near the water surface

School of Water, Energy and Environment

MSc by Research
Academic year : 2016-2017

Supervisor : Dr Florent Trarieux
June 2017

Cranfield University

School of Water, Energy and Environment

MSc by Research

Academic year : 2016-2017

Nicolas MAILH

Experimental investigation of Lift and Drag on the NACA 4412 near the water surface

Supervisor : Dr Florent Trarieux

June 2017

Abstract

This thesis deals with hydrofoils, appendages which are a growing trend in yacht design and aimed at alleviating boats (this reduces the wetted area and therefore the drag). This thesis acknowledges the research previously done relating to hydrofoils and the testing of hydrofoils from the 1900's until now, from a military and sailing point of view. It goes through the methodology used to extract lift and drag data from tank testing in Cranfield University. It goes through the approach to design a test process to extract consistent results from different foils in later stages. The works also details the manufacturing of the rig to test a hydrofoil in near surface conditions: the profile studied is the NACA 4412, the submergence ranges from 2.5 chords to 0.1 chords, the angle of attack ranges from 10 to -1 degrees and Reynolds Number ranging from 1500000 to 910000 (0.5 to 3.0 m/s). The resulting data showed that lift decreased as the foil got closer to the free surface. With significant effects being seen from a submergence of 1 chord. This project also points outs the limitations of tank testing and the effects of side struts holding the hydrofoil.

Acknowledgements

I'm very lucky to have had great support around me during my MSc by research in the Ocean Systems Test laboratory. The work presented here could never have been done without this support and I would therefore like to acknowledge the contributions of the people responsible. First and foremost, Dr Florent Trarieux, has taught me a lot about doing research and has always kept me on my toes. I would also like to thank Dr Maurizio Collu and Dr Joao Teixeira who have always been patient with me and have always found time to help me.
My friends and family are also to thank for their support during this long journey. Thank you to Coline Cuau for being there and supporting me, Léo Mougel because you always need a good friend to help you put things in perspective. My father for the sound advice he has given me during this period of my life. My mother for always making sure I was never lacking anything.
Without them, none of this would have been possible.

Table of Contents

List of Figures

List of Tables

List of Equations

Nomenclature

$F_y struts$	Drag force generated by the struts
$F_y total$	Total drag force generated by the hydrofoil
$-P_{min}$	Pressure coefficient at the point of minimum pressure
α	Angle of attack
α_W	Change in α due to wave effect
β_B	$\frac{1-\beta}{2\pi B}$
δ	Interference coefficient
Γ	circulation
Γ_∞	infinite fluid circulation
ρ	Density of the fluid
AR	Aspect ratio
B	2D Biplane correction factor
C_D	The Drag coefficient
C_L	The Lift coefficient
C_{DW}	Wave induced drag coefficient
D	Drag in Newtons
D_i	Induced Drag
e	span efficiency value
F_c	Froude number on chord
L	Lift in Newtons
P_a	Atmospheric pressure
P_v	Water vapour pressure

P_w	Hydrostatic head
S	Surface in m^2
s	semi-span
V	Velocity in m/s
W_{HV}	vertical velocity induced by horseshoe vortex
W_{IHV}	vertical velocity induced by the image horseshoe vortex

1 Introduction

1.1 Benefits of hydrofoils

The basic principle of the hydrofoil is to lift a vessel partially or completely out of the water to reduce drag. In sailing and shipping the main force that has to be overcome to achieve movement (momentum) is the drag of the hull. Hydrofoils are a good way to reduce displacement and therefore drag, which in turn lowers the energy used to move the vessel.

1.2 Historical development

The concept of the hydrofoil began in the 1860's with a boat from English engineer Thomas Moy [26]. In 1861, Moy towed a boat with wings underneath in the Surrey canal. Next, progress came in 1897 from the American William E. Meacham in Chicago [27]. In 1905, professor Enrico Forliani [28] experimented with the first known Ladder type hydrofoil on Lake Maggiore [1] to reach a speed of 39 knots, as shown in Figure 1. The next big leap came from Alexander G. Bell's HD-4 circa 1919 [29]. From then on, the Hydrofoil took two distinctive routes: The Military applications and the sailing applications. These two paths will be discussed in chronological order starting with the military branch.

One of the first occurrence of the hydrofoil was in the early 1900's. As shown on Figure (1) below.

Figure 1: Forlanini hydrofoil on lake Maggiore, 1911 [1]

1.2.1 Military applications

The Military were the first to have a practical use for the hydrofoil. In 1940-1941, the German navy built VS-6 hydrofoil as seen on Figure 2 [30]. However the boat never saw any major action.

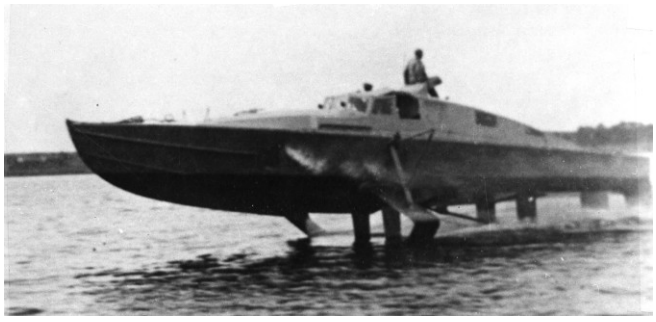

Figure 2: VS-6 hydrofoil warship [2]

A second surge came during the Cold war when Americans, Russians and Italians started building hydrofoil boats. In the mid-50s William P. Carl designed the XCH4 for the US Navy. Between 1977 and 1993 the Navy used the Pegasus class see Figure 3.

Figure 3: Us Navy's Pegasus Class [3]

On the other side of the iron curtain, the use of hydrofoils started in the 1970s with the Sarancha class missile boat, Figures 4 and 5, followed by the Turya class torpedo boat in 1972 seen on Figure 6 (still in service today). In the 80s came the Matka, Figure 7, class missile boat and the Muravey class patrol boat - also still in service.

Figure 4: USSR's Sarancha Class under way [4]

Figure 5: USSR's Sarancha docked with the hydrofoils lifted up [4]

Figure 6: USSR's Turya Class under way [5]

Figure 7: USSR's Matka docked with the hydrofoils lifted up [6]

Meanwhile, the Italians were building the Sparviero Class (also know as the P420 class) in the late 1970s this can be seen in Figure 8.

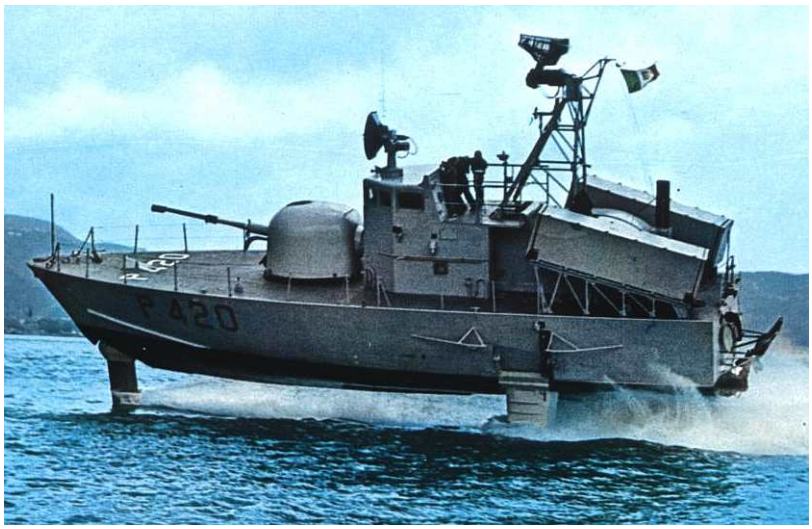

Figure 8: Italian P420 Class under way [4]

As seen above, most of these boats stopped being built after the late 70's. From that point on, navies moved on from this fade and started shifting their focus from speed to stealth.

1.2.2 Recreational applications

In addition to being used by navies around the world, hydrofoils have also become one of the most interesting and spectacular parts of the sport of sailing nowadays.

There are two distinct types of sailing rafts in this category: the smaller dinghy type, and the larger and often ocean-going vessel. The development of foils was seriously kicked off in the mid 2000's by the Hydroptere project in the later category (see Figure 9), which set the world 500 meters' record in 2009 with a speed of 51.36 knots (95.12kph) [7]. The next major push came with the change of the America's cup rules to allow multihulls (in 1988 [31] and then 2010 [32]). In 2013, hydrofoils arrived [16].

Figure 9: Hydroptere sailing under foil [7]

Being one of the most watched sailing event in the world, the America's Cup is also an event to which sailing firms and syndicates dedicate very large resources. As high profile boats started displaying hydrofoils, the public started paying attention to this new feature. This launched a small revolution which then reached every aspect of the sailing industry, from the small international Moth Class to the Gunboat. To this day, most of the foiling is still done on inshore multihulls like the Class A, Figure 10, Class C, Figure 11, Nacra 17, Nacra 20, Figure 12, Flying phamtom, Figure 13 and the SL33, Figure 15 just to name a few.

Figure 10: Foiling Class A catamaran [8].

Figure 11: Foiling Class C catamaran [9].

Figure 12: Foiling Nacra 20 catamaran [10].

Figure 13: Foiling Flying Phamtom catamaran [11].

Figure 14: Foiling International Moth dinghy [12].

Figure 15: Foiling SL33 catamaran [13].

Figure 16: Foiling GC32 [14]

Figure 17: Kite board fitted with Hydrofoils Foiling [15]

In recent years, offshore teams have started researching and using hydrofoils. The aim here is not to lift the entire hull out of the water for long periods of time but to alleviate forces on the hull, mostly to reduce drag. This can be seen on the new Imoca class boats such as Hugo Boss and No way back from VPLP architects, Banque Populaire VIII and Saint Michel Virbac [33]. This phenomenon is also due in a change of class rules: for many boats, class rules have evolved to allow hydrofoils, thus taking the sport a step further and adding extra interest to the races. The most recent development is with the new Figaro design [34].

The facilities in the Ocean Test Systems Laboratory can help provide a better understanding of the multiple uses of foils. As foils begin to be more in use within the boating community, better data and a better understanding of the phenomenon is needed. The foils on most boats in the future will not make the boat fly per say, but will alleviate part of the down force so that there is less displacement and thus less drag. Since most of the energy needed to move a ship is relative to drag and displacement, this gain is crucial and could have an impact on every aspect of the maritime world from the racing sphere to the shipping industry.

The range of foiling boats is wide: on one end are the International Moth, Figure 14 and the AC 45, Figure 18 which are completely airborne with only a few appendages in the water (mainly the foil/dagger and the rudder); on the other end are the ocean going 60 footer Imoca.

1.3 Foil development for high speed sailing applications

A hydrofoil is a lifting surface, or foil, that operates in water. They are similar in appearance and purpose to aerofoils used by aeroplanes. Boats that use hydrofoil technology are also generally called hydrofoils. As a hydrofoil craft gains speed, the hydrofoils lift the boat's hull out of the water, decreasing drag and allowing greater speeds for the same amount of energy.

There are two main types of hydrofoils: surface piercing ones and fully submerged ones.
On a sailing hydrofoil, rudder foils are fully submerged, whereas dagger-boards are now mostly surface piercing.
Historically, the first hydrofoils were either T or L shaped. As hydrofoiling developed, the foil evolved to more complex shapes such as the S, G or C variant.
Each shape has its advantages and drawbacks. For the T and L shapes, the main advantage is the consistency of the lift and drag developed. however it lacks refinement.
The other shapes have the opposite problem: they are more suited to specific ranges and therefore offer a more narrow range of possibilities. Most of the time, the more complex shapes are used as dagger-boards on each side of the vessel. They can be slid at different heights, and the upwind dagger-board is raised and doesn't come into contact with the water. If this wasn't the case, the drag would be greater than the lift generated.

Figure 18: Oracle's AC45 on hydrofoils during the America's cup [16]

1.3.1 Types of foil and Nomenclature

1.3.1.1 NACA

Before studying the interactions between the hydrofoil and the free surface, it is important to understand the behaviour of a foil or wing section in a flow. Fortunately, the behaviour of foils in simple conditions has been extensively researched over the last century, mostly for the aviation industry. Multiple profiles have been studied, and in this thesis we will be focusing on a NACA profile.
The NACA airfoils are a profile of foils that have been designed and developed by the American National Advisory Committee for Aeronautics since the beginning of the 1920's. The profiles are described by a set of numbers following the Word NACA (for example NACA 0012 or NACA 4414). The numbers are meant to give a precise definition of the airfoils and are to be inserted into equations to accurately generate the cross-section of the foil and calculate its properties.

In this thesis, the 4-digit series of hydrofoils will be used. The series can be further separated into two distinct categories: the symmetrical and cambered 4-digit NACA hydrofoil.
-The first number represents the maximum camber as a percentage of the cord.
-The second number represents where that camber is situated from the leading edge in 10% increments.
-The last two numbers indicate the maximum thickness of the foil as a percentage of the chord.
This means a symmetrical foil will always start with 00.

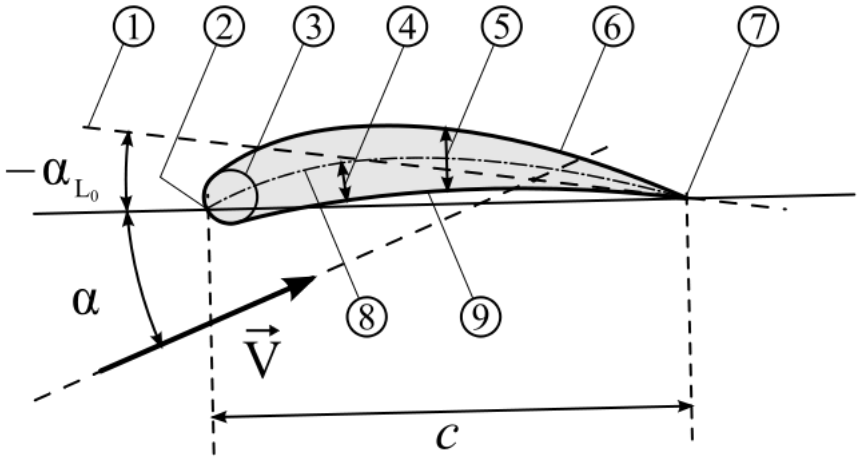

Figure 19: Profile Geometry [17]

In figure 19 : 1: Zero lift line; 2: Leading edge; 3: Nose circle; 4: Camber; 5: Max. thickness; 6: Upper surface; 7: Trailing edge; 8: Camber mean-line; 9: Lower surface

The advantage of the NACA Profiles is that they have been studied in great detail since their invention.

1.3.1.2 Lift and Drag generation

A hydrofoil works like a wing: because of the difference in length between the upper surface and the lower surface, it creates a difference in velocity and pressure (considering the conservation of mass and an incompressible flow). The longer length of the upper surface means a higher velocity, and a lower pressure. Because of this occurrence, the profile tends to create lift.
This is seen in Figure 20.

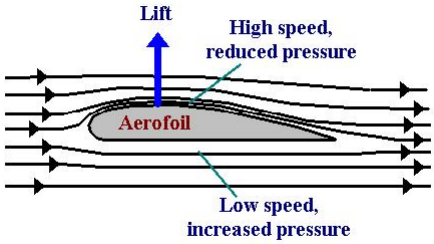

Figure 20: Simple explanation of the lift phenomena [18]

The foil creates two forces: a lift force and a drag force [35]. Those forces can be calculated with :

$$L = \frac{1}{2}\rho V^2 S C_L \tag{1}$$

and

$$D = \frac{1}{2}\rho V^2 S C_D \tag{2}$$

In equations 1 and 2: L is the lift,D is the drag, ρ is the density of the fluid, V is the velocity, S the projected surface, C_L the lift coefficient and C_D the drag coefficient
This is also shown in Figure 21:

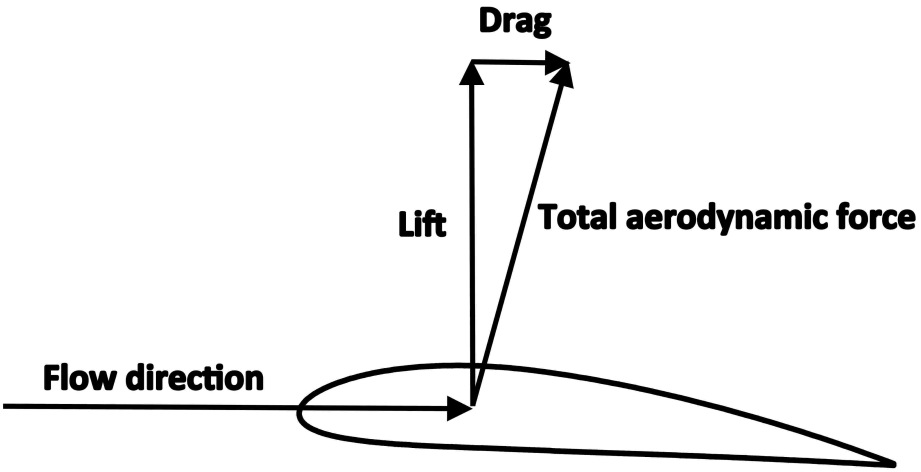

Figure 21: Visualization of the lift and drag on an foil section ([19])

Drag as many contributors :
Lift-induced drag which is the one of the main reason why Drag increases when the angle of attack increases. Lift induced drag comes from the deflection of the flow by the hydrofoil. Induced drag can be characterised by the following equation 3 :

$$D_i = \frac{L^2}{\frac{1}{2}\rho V^2 S \pi e AR} \tag{3}$$

Where in 3 : D_i is the induced drag and e the span efficiency value.

Form Drag which is directly dependent of the longitudinal section of the hydrofoil.

2 The need for experimental research in hydrofoil

Hydrofoils bring very interesting advantages to vessel design by reducing the drag forces, but this comes at the price of technical complexity that makes it difficult to implement in real life. After a first interest in the 50's, mostly driven by military research, the hydrofoils came again into light in recent years, driven this time by competitive sailing.
There are therefore two distinct corpuses of research, one that dates from the early 50s and 60s which had a lot of experimental procedures most importantly in the NACA research Facility in Langley (cite all papers from NACA) and the other more recently from the early 2000s at a time in which the hydrofoil came back to prominence via the sailing sphere.
Many tests were done 50 to 60 years ago in very expensive facilities. At that time there was no CFD, so experiments were key to understanding the foils effects.
Today on the contrary, a lot of research is done through CFD, and there is a lack of recent experimental research. Recent experiments remained mostly in the private sphere because most of the research was undertaken either by the military or by private design firms operating in a highly competitive market (Ocean racing, the America's Cup, etc.). There is no incentive to publish or make public their findings. CFD simulation is more difficult when hydrofoils operate in surface proximity because the physical effects are much more complex. The hydrofoils operate in surface proximity most of the time in real conditions.
Therefore; it is important to implement the means to test hydrofoils in a near surface environment, where CFD could be less accurate. These tests traditionally use very expensive facilities.
The main issue to perform these tests is the cost of experimental research. There is a need for cost effective experimental research on hydrofoils in a near surface environment.
Hence, the projects investigate the possibility to test hydrofoils experimentally in surface proximity at an affordable price and with relatively basic tooling.

3 Aims and objectives

The main objective was to put in place an experimental protocol/process to measure lift and drag generated by hydrofoils, that was:

1. Cost effective
2. That uses quick and simple tooling to enable quick verification of cost effective solutions and that enables agile testing to verify proofs of concepts.

A second objective was to perform a series of test on a NACA 4412 hydrofoil to extract Lift and Drag characteristics in surface proximity. To check if the results are coherent with the expectation and therefore validate the concept of this experimental test rig.

4 Literature review

As of today, the effects of the proximity to a surface on the efficiency of a hydrofoil have not yet been the subject of extensive investigation.
The aim of this literature review is to summarize the work that has already been done in this field.
This Literature review will be split up in two parts: The first part detailing the physics taking place, the second part dealing with the experimental set-up that were used in similar experiments.

4.1 Physics

4.1.1 Introduction

The basic physics acting on a submerged hydrofoil operating away from any boundaries can be characterized by fluid dynamics theories coming from the aeronautics field.
The main differences between an air-plane wing and a hydrofoil are the environment in which they operate: The hydrofoil acts in surface proximity and in a fluid that will boil as the pressure drops - this is called cavitation.

4.2 Lift

Lift occurs when a moving flow of gas is turned by a solid object. The flow is turned in one direction, and the lift is generated in the opposite direction, according to Newton's Third Law of action and reaction. Lift is a mechanical force. It is generated by the interaction and contact of a solid body with a fluid (liquid or gas). For lift to be generated, the solid body must be in contact with the fluid: no fluid, no lift. Lift is generated by the difference in velocity between the solid object and the fluid. There must be motion between the object and the fluid: no motion, no lift. It makes no difference whether the object moves through a static fluid, or the fluid moves past a static solid object. Lift acts perpendicular to the motion. Drag acts in the direction opposed to the motion.

4.2.1 Initial conditions

When calculating the forces on a submerged hydrofoil, it is safe to assume that the flow is inviscid and incompressible.

4.2.2 Free surface effects

Once the hydrofoil is moving in a fluid, a low pressure is generated on its upper surface. Inversely, a higher pressure is generated on its lower surface [35]. This pressure difference causes the foil to lift upwards. When studying the hydrofoil under the free surface and in surface proximity, the low pressure described previously acts to deform the free surface, which in turn reduces lift

generated. This surface is represented by a wave generated along the span of the hydrofoil. This curves the flow. This curving of the flow physically reduces the dynamic camber of the hydrofoils and because lift is a product of camber, it reduces lift.

4.2.3 Definition of the free surface

Here the free surface is at a constant pressure, which means that Bernoulli's theory states that the perturbation velocity of the plane of the free surface should be zero.
This can be solved by modelling the hydrofoil with the allotment of sources, sinks and vortices and then positioning those same things over the free surface so that the resulting perturbation are null along the 0 plane, as shown in Figure 22.

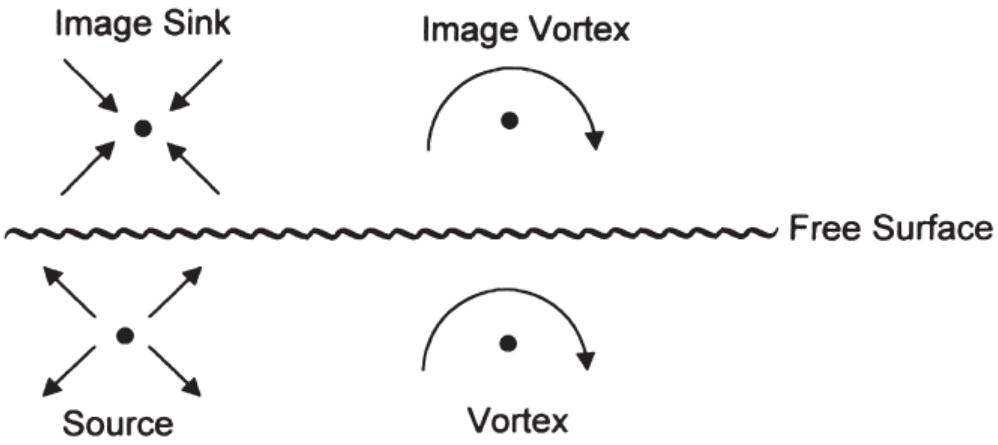

Figure 22: Images used to describe the effect of the free surface [20]

4.2.4 Biplane theory

The biplane theory basically states that the flow caused by a hydrofoil at a depth h underneath a free surface can be approximated by placing an image of that hydrofoil above the same free surface and summing the perturbation generated by the two hydrofoils. This was detailed by Max M. in 1923 ([36]). It is shown that the lift of a biplane is related to the lift of a monoplane at the same angle of attack by a factor B:

$$C_L = B(2\pi \sin \alpha) \tag{4}$$

In Equation 4, B is the 2D biplane correction factor, α the angle of attack. The conclusion here from the Biplane theory is that a hydrofoil needs a higher angle of attack than a monoplane. This increase in angle of attack was characterized by Munk (1923) [36] as:

$$\Delta\alpha = \beta_B C_L \tag{5}$$

$$\beta_B = \frac{1-\beta}{2\pi B} \tag{6}$$

4.2.5 Horseshoe vortex model

The horseshoe vortex is a model that implies the representation of a vortex around a wing. This model is not realistic because according to the Kutta-Joukowski ([37]) theorem it involves a continual circulation at all sections of the wingspan (in this case, the hydrofoil). A visualisation of the Horseshoes vortices is shown in Figure (23) below :

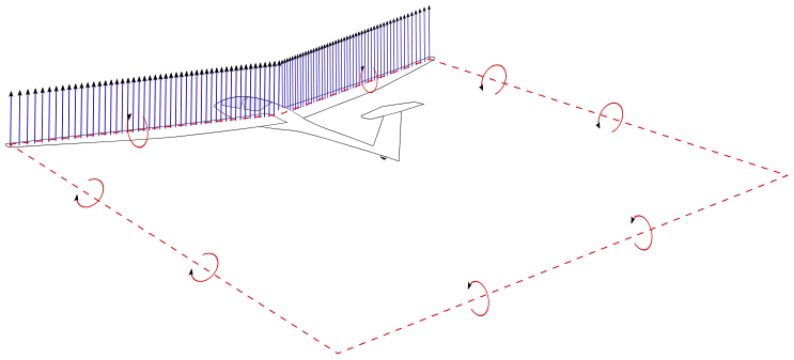

Figure 23: Horseshoe Vortices [21]

A way to apply the Horseshoe vortex model is to model the free surface as an image horseshoe vortex located at a distance from the foil. The formula

was given by Waldin ([22]):

$$W_{HV} = \frac{\Gamma}{2\pi}\left[\frac{2}{sc}\sqrt{\left(\frac{c}{2}\right)^2 + s^2} + \frac{1}{s}\right] \tag{7}$$

Where W_{HV} is the vertical velocity induced by horseshoe vortex, Γ the circulation, s the semi-span.

The vertical disturbance velocity due to the image vortex is :

$$W_{IHV} = \frac{\Gamma}{4\pi}\left\{\frac{c}{(\frac{c}{2})^2 + (2h)^2} \times \frac{s}{\sqrt{(\frac{c}{2})^2 + (2h)^2 + s^2}} + \frac{2s}{(2h)^2 + s^2}\left[1 + \frac{c}{2\sqrt{(\frac{c}{2}) + (2h)^2 + s^2}}\right]\right\} \tag{8}$$

Where W_{IHV} is the vertical velocity induced by the image horseshoe vortex.

It was then determined that the effect of the free surface on the flow is :

$$\frac{\Gamma}{\Gamma_\infty} = \frac{W_{HW}}{W_{HW} + W_{IHW}} \tag{9}$$

Where Γ_∞ is the infinite fluid circulation.

If we consider an infinite aspect ratio ($AR \to \infty$) 10 then this becomes the correction factor K put forth by Ducane (1972)([38]).

$$\frac{C_{L\alpha}}{C_{L\alpha^\infty}} = \frac{1 + 16(\frac{h}{c})^2}{2 + 16(\frac{h}{c})^2} \tag{10}$$

The tip effect, which is a produce of the end of the hydrofoil as described by the horseshoe model, tends to affect both the Lift and drag characteristics of the hydrofoil.

4.2.6 Momentum theory

W.J.M Rankine and Froude developed an alternative theory, which was the Momentum theory later used by Payne. The momentum theory is used to define an ideal model of a propeller or rotor.
Momentum theory suggests that in surface proximity, less fluid is available to be deflected downwards by the hydrofoil.
Unlike in the Biplane and Waldin models, the surface proximity effect in the Payne model is defined by depth to span ratio alone. The Biplane and Waldin model is mostly defined by depth to chord ratio h/c which is the submergence. This is shown in Figure 24 below. In his experiment, Waldin measured the lift and drag characteristic of an aspect ratio 10 hydrofoil at two towing tanks ([22]). The results are shown in Figure 24 below.

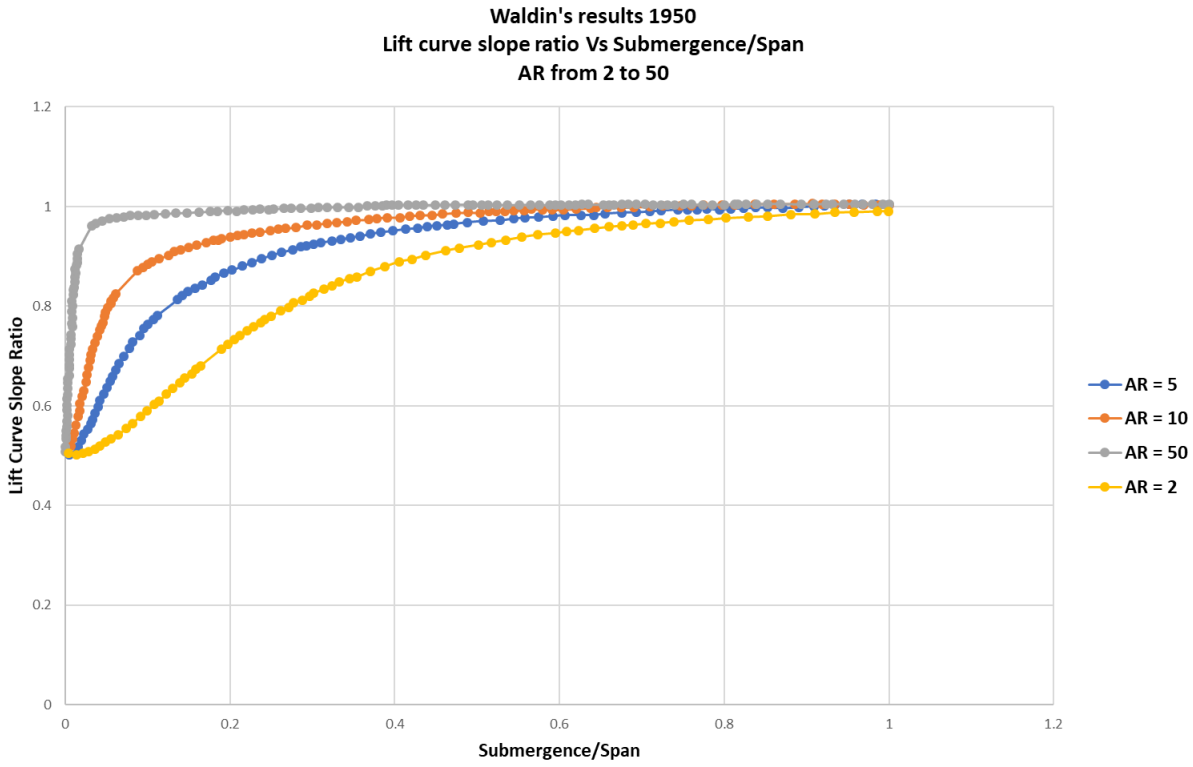

Figure 24: Lift curve Slope ratio plotted against the submergence over span from [22]

4.3 Froude Number

The Froude number comes from the English hydrodynamicist William Froude. The Froude number is a dimensionless number that characterises in a fluid the relative importance of its kinetic energy of its particles over its gravitational energy.
In naval architecture and in hydrodynamics the Froude number is used in a significant manner to determine the resistance of models moving through water. Models with the same Froude number are therefore easily comparable.

4.3.1 Cavitation

Cavitation is a process of vaporisation caused by the decrease in pressure in a fluid flow until the vapours saturation pressure is reached. It creates vapour cavities in a liquid. Those are liquid-free zones (bubbles). When a high enough pressure is reached these vapour cavities implode and create a shock wave. This is the main cause of wear on some machinery and boat appendages (pumps, propellers, rudders etc.). Cavitation is usually an undesirable occurrence. An example of cavitation caused by a propeller is shown in Figure 25.

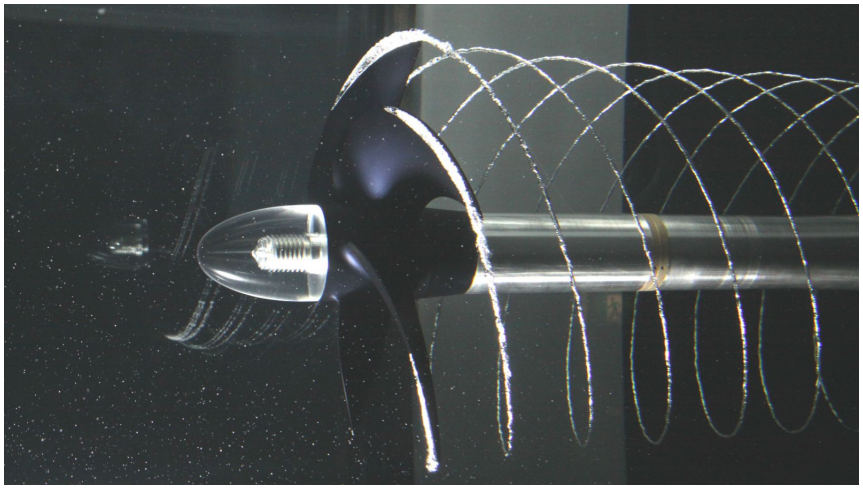

Figure 25: Cavitation caused by a propeller [23]

The formula below detailed by K. Ward and N. Land in 1940 [39] helps determine the speed at which the cavitation phenomenon can be expected.

$$(V)^2 = \frac{P_a + P_w - P_v}{(\frac{\rho}{2})(-P_{min})} \tag{11}$$

Where in equation 11 P_a is the atmospheric pressure, P_w the hydrostatic head at depth of point of minimum pressure, P_v the water vapour pressure and $-P_{min}$ the pressure coefficient at the point of minimum pressure. Values for $-P_{min}$ were found according to Pinkerton R. (1936) [40].

4.3.2 Ventilation

Hydrodynamic profiles (in this case hydrofoils) evolving near the surface tend to suffer from air entrainment. This phenomenon is called ventilation. Ventilation is the result of two major occurrences: the first is closeness to the surface; the second is the fact that the hydrodynamic depression on the extrados of the profile is below atmospheric pressure. Those factors make it so that air can find a passage and become aspirated into the zone of the extrados. This passage is possible if the hydrostatic load at the depression of the extrados is less than the depression generated by the lift of the extrados. This results in a sudden loss of lift.

4.3.3 Effects of Waves

As detailed earlier, the fact that the hydrofoil is travelling under the free surface creates a wave. This is in part due to using finite rather than infinite Froude numbers. This wave affects both the lift and drag as detailed by Daskovsky, Kotchin and Vladimorov ([20], [41] and [42]).
It as been shown ([20]) that the alteration in angle of attack required to achieve an infinite Froude number lift can be approached by:

$$\alpha_W = \frac{C_L}{2F_c^2} e^{-\left[\frac{(2\frac{h}{c})}{F_c^2}\right]} \tag{12}$$

Where α_W is the change in α due to wave effect and F_c is the Froude number on chord.
The wave drag can also be approximated by :

$$C_{DW} = \frac{C_L^2}{2F_c^2} e^{-\left[\frac{(2\frac{h}{c})}{F_c^2}\right]} \tag{13}$$

In 13 C_{DW} is the wave induced drag coefficient.
As seen in Figure (26), the effect of the wave generated is higher at lower froude numbers and lower submergence.

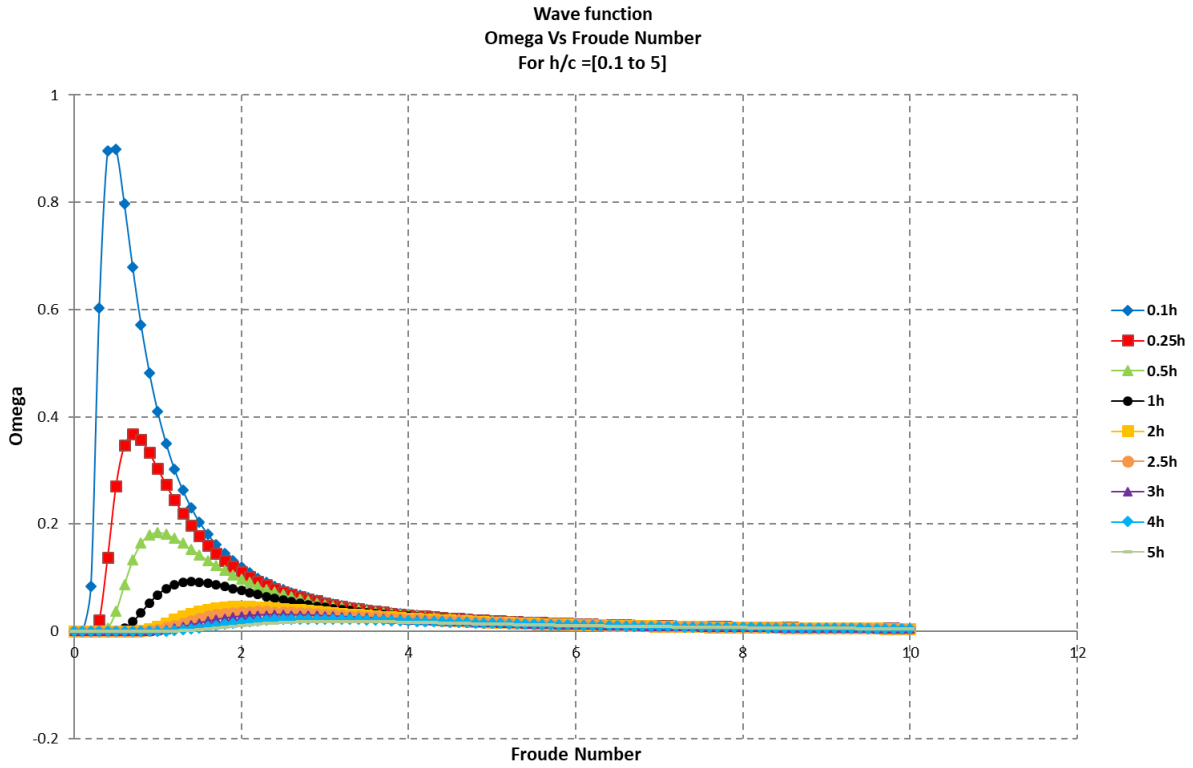

Figure 26: Omega plotted against Froude for the function taken in 13

4.4 Testing and experimental rigs

As of today, the way hydrofoils have been tested in a near surface come in three distinct categories : -Testing in a towing tank or more generally with a moving hydrofoil in a standing body of water -Testing in a cavitation tunnel where the wing is fixed and the flow moves around it -Using a numerical approach with CFD software.
This section discusses the first two methods presented above.

The first method is one where the hydrofoil moves in a standing body of water. Most of the time this will be done by towing a foil in a tank, but as seen below it can also be towed by a boat.
The Langley towing tank in the US was an experimental setup at NACA headquarters ([24], [43], [39], [22]). In most of those experiments, the profiles were constructed of a single piece of machined alloy. ([24], [39]).

The general way to study foils experimentally when not using a cavitation tunnel is the towing tank such as the one used by Harwood, Young and Ceccio ([44]). The tank used in this study is 110 m long by 6.7 m wide and 3.05 m deep. It is significantly larger than the tank used in Cranfield University, which is 30 m by 1.5 m by 1.5 m.
The tank used by Hardwood et al. ([44]) is equipped with a gantry-type carriage capable of speeds up to 6.1 m/s. The system used here is the same as the one in this study with the exception that the one used here can only achieve speeds of up to 3.5 m/s.
One other study that proved useful was the one done by K. Ward and N. Land in 1940 ([39]) in the Langley towing tank. The method used for testing is the following : hydrofoils were held by two struts not at the extremity, but at approximately 200 mm from the edges of the hydrofoils. The hydrofoils used in this study are NACA 16-509 and NACA 16-1009. The range of speeds used in this study is between 6.1 and 24.4 m/s (20 to 80 feet per second). The angles range from -2 to 18 degrees. The submergences tested are 1, 2 and 5 chords. In Ward and Land's work the principal emphasis is put on cavitation and this explains why the speeds are so high. The results show that cavitation happens from speeds of 10 m/s. This report can be a useful reference for the rig design and the general approach to the testing phase. An another experimental procedure, as detailed by Daskovsky M. in 2000 [20], here the hydrofoil is towed in front of a work boat in the upper Severn River. One of the problems with testing hydrofoils in a river is that the environment is less controlled than in a tank in a laboratory.

4.4.1 Measurement of Forces and Moments

One of the other aspects of experimentally testing hydrofoils, is the way the forces (Lift, Drag,...) are recorded. Hardwood uses a IP68 OMEGA 190 transducer ([44]) while Daskovsky uses load cells ([20]).

4.4.2 Cavitation tunnels

The other way to study hydrofoils is to use a cavitation tunnel as detailed by Longo, Chiapponi and Clavero in 2014 [45], by Sedlar, Ji, Kratky, Rebok and Huzlik in 2016 [46] and by Zhen, Beom-soo, Moo-rong and Ji-yuan in 2008 [47].

The concept of a cavitation tunnel is the following : it is very similar to a recirculating wind tunnel, but with water as the working fluid. Related phenomena are then investigated, such as measuring the forces on scale models of submarines or lift and drag on hydrofoils.
In those tunnels, the hydrofoils are relatively small compared to the towing tanks equivalents. This is mainly because of two factors : the actual size of the tunnel, and the fact that the speeds can be greater, making the model smaller for the same effective Reynolds number.
In this configuration, the forces can be measured in with : a transducer like seen above, Tap holes to measure pressure ([46]) and load cells.
Another common occurrence with the cavitation tunnel is the use of PIV (Particle image velocimetry) equipment. This is because in this case the foil is fixed and the PIV equipment does not need to move.
The basis of PIV is as follows: it is an optical method of flow visualization, and it is used to obtain instantaneous velocity measurements and related properties in fluids. The set-up uses a high speed camera and very specific lighting.
The PIV method was not be used here because of the specific tank method and, because having a PIV set-up working along a moving rig is burdensome.

Another important thing is the repeatability of the process to ensure confidence with the results. This is not detailed as much in the papers above. Because of the complicated nature of the tests and the fact that they are expensive to undertake, most of the time the runs in one configuration are repeated only once or twice. However, points in data sets are always the results of a high frequency of data collection (30Hz to 1kHz) and those values are averaged to give a single point. This is detailed by Daskovsky ([20]).

4.5 Ground interference

The effect of Ground interference have been detailed by Reid, Elliott in 1932 [48] and used by Kenneth, Waldin et al in 1950 [24].
The formula used for this ground correction is :

$$(C_D)_{corrected} = (C_D)_{measured} + \delta \frac{(C_L)^2}{\pi AR} \tag{14}$$

Where in equation δ is an interference coefficient that varies with the distance from the hydrofoil to the tank bottom. Values for δ are given By Reid. E (1932) [48] are presented in Figure 27 below :

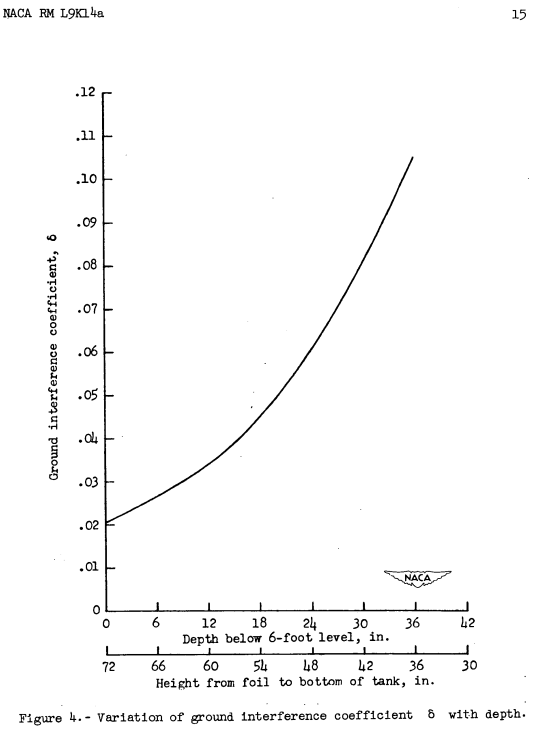

Figure 4.- Variation of ground interference coefficient δ with depth.

Figure 27: Variation of ground interference coefficient δ with depth [24]

All these previous examples give an overview of the different set-ups used in experiments similar to the one led in Cranfield university.

5 Methods and experimental setup

5.1 Introduction

This chapter details the design, the manufacture and set-up of the test rig. A previous rig is assessed for its use in our application close to the surface.

5.2 Design Goals

To be able to test in the Ocean Tests Laboratory in Cranfield it is important to consider the limitations either to comply to the stated aims and objectives or to comply with what is available to us in the laboratory. A trade-off shall be found between the possibilities of the test facility and its cost, which means mostly its size.
The size of the towing tank is the primary concern when designing the experiment. The tank is 30 meters long, 1.5 meters wide and 1.5 meters deep. Another concern is the speed of the towing carriage which has a top speed of 3.5 m/s. Those two parameters dictate a big part of the design aspect: primarily the size of the hydrofoil being tested. The depth of the tank also dictates the range in depth at which hydrofoils can be tested (maximum of 1.5 meters of range). The width of the tank also dictate the maximum span of the hydrofoils. As seen (before/after) the minimum span is dictated by two things, the aspect ratio of the hydrofoils and the maximum towing speed of the towing carriage.

5.3 Feasibility study and design

When I arrived in Cranfield to start my research, my colleague Mr Daniel James had already designed a similar test rig as seen in figure 28.

Figure 28: DHMTU 10-40.2-10.2-60.21.5 used in WIG crafts in the Cranfield towing tank.

As seen on figure 28, the wing is supported by three struts, the middle strut being used to change the angle of attack. This wing was designed by Mr James and built in the Cranfield workshop. This design was relatively simple but was not practical for this experiment for two main reasons :
- It was designed to work close to the bottom of the tank and therefore would interfere with the tank structure above if raised higher.
- Changing the angle of attack of the hydrofoil and its submergence was very complicated and time consuming

A NACA 4412 profile was ordered - it was made by Design Craft in Southampton. The profile was 1 meter long and made out of high density foam. The ends were printed with the 3d Printer 29 and then glued on. This was done so that bolts could be used to hold the hydrofoil. After this, fibreglass and epoxy resin were applied to strengthen the wing and to provide a smoother profile.The fibreglass and resin applied was very thin and uniform and did not change the profile of the wing. A lot of time was spent working on the surface texture in order achieve a very smooth surface. It was sanded and painted until completely smooth.
Work was done on the struts. The struts were made of wood and had a hole and slot, as seen on figure 30.

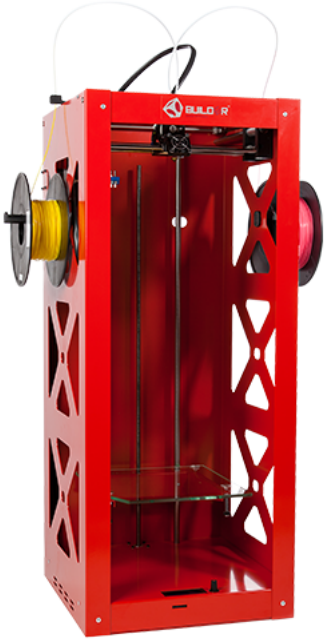

Figure 29: Big Builder Dual-Feed Red Edition 3D printer

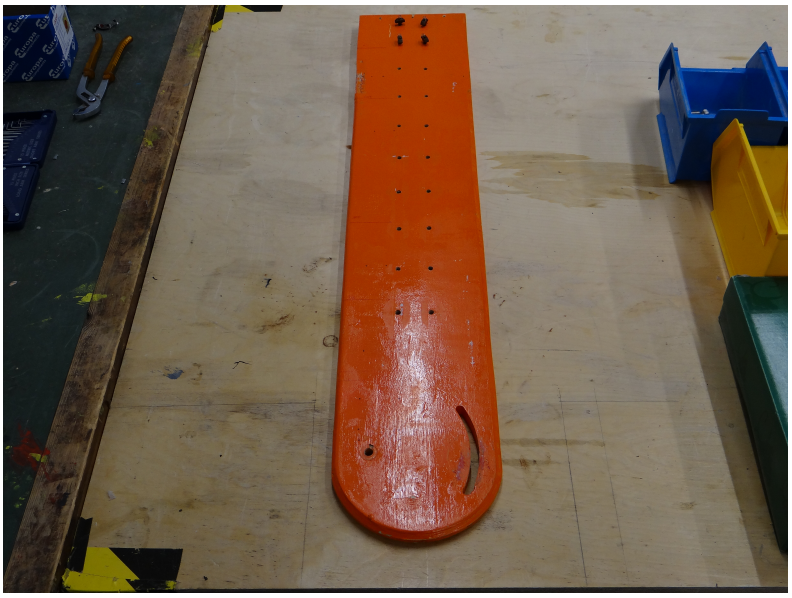

Figure 30: Starboard Strut

The slot enabled the change of the angle of attack.

6 Instrumentation and calibration of the test rig

6.1 Introduction

This chapter details the instrumentation and the calibration of the angles of the foil used. The main instrument used is a multi-axis balance that measures the outputting forces and torques from all three Cartesian coordinates (x, y, and z).

6.2 Instrumentation

To measure the lift of the foil, a multi –axis force and torque sensor is used. The lift and then the lift coefficient are extrapolated from the force and torque. The sensor that is used and that was already in the lab is the IP68 OMEGA160 Transducer as seen in Figure 31, it measures the outputting forces and torques from all three Cartesian coordinates (x, y, and z).

Figure 31: IP68 OMEGA160 Transducer

The sensor uses the DAQ F/T protocol to communicate. This is one of the most versatile protocols. It is in part because the sensor transmits the data from the six strain gauges as voltage which can be interpreted by an array of devices. A simpler method will be used, using the software given by the manufacturer. The output is a .CSV file which can be read on excel. The format is 6 columns representing the forces and the moments.
As seen in the chart below 32, there are two possible calibrations, giving different accuracies and ranges.

Calibration	Fx,Fy	Fz	Tx,Ty	Tz	Fx,Fy	Fz	Tx,Ty	Tz
~~SI-1000-120~~	~~1000 N~~	~~2500 N~~	~~120 Nm~~	~~120 Nm~~	~~1/4 N~~	~~1/4 N~~	~~1/40 Nm~~	~~1/80 Nm~~
SI-1500-240	1500 N	3750 N	240 Nm	240 Nm	1/4 N	1/2 N	1/20 Nm	1/40 Nm
SI-2500-400	2500 N	6250 N	400 Nm	400 Nm	1/2 N	3/4 N	1/20 Nm	1/20 Nm

Figure 32: Calibration table

In the Cranfield towing tank, X+ designates the direction to the right when facing the wave maker, Y+ is the direction from the wave maker to the beach

and Z+ is the upward direction, as seen in Figure 33.

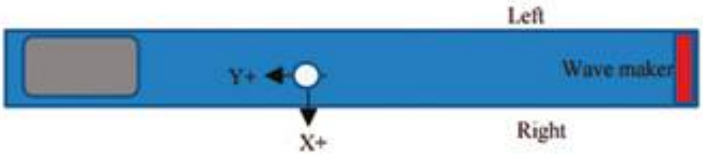

Figure 33: Orientation of the balance

6.3 Calibration of the test rig

To have a better precision when calibrating the angles the measures of those angles, will be taken 600mm from the point of rotation of the hydrofoil. To achieve this, the rig is positioned on a perfectly flat surface (Figure 35), which allows to position a vertical and straight bar at the exact distant needed. As seen on Figure 34 a laser level was used to ensure that the rig was perfectly level.

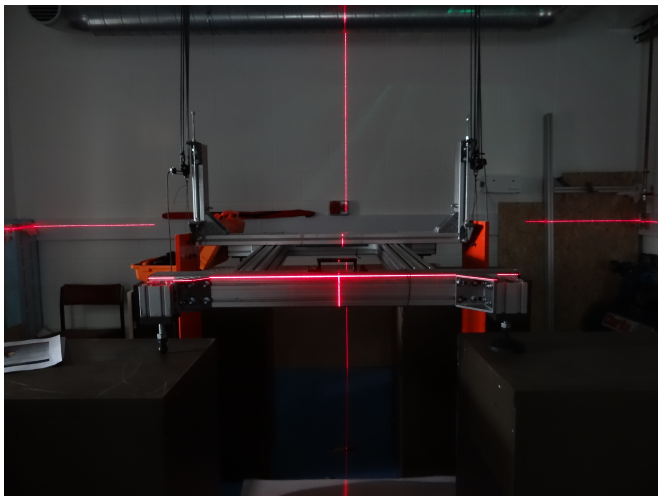

Figure 34: Laser level used to ensure the rig is perfectly level

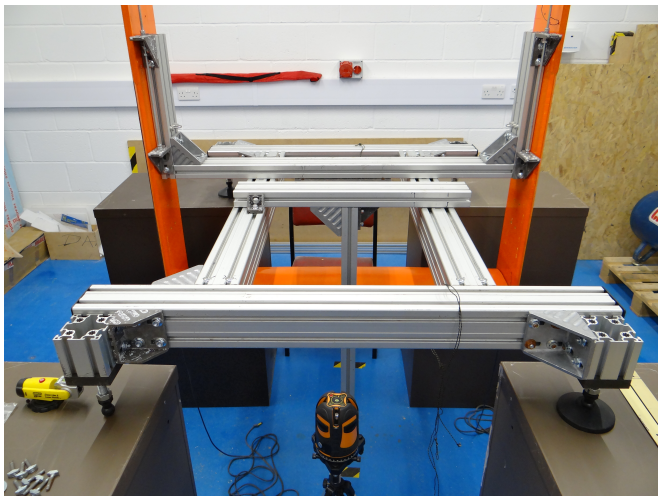

Figure 35: Hydrofoil and calibration rig on a level surface

The difference in length does not affect the angle but it ensures the measure is more precise as seen in Figure 36.

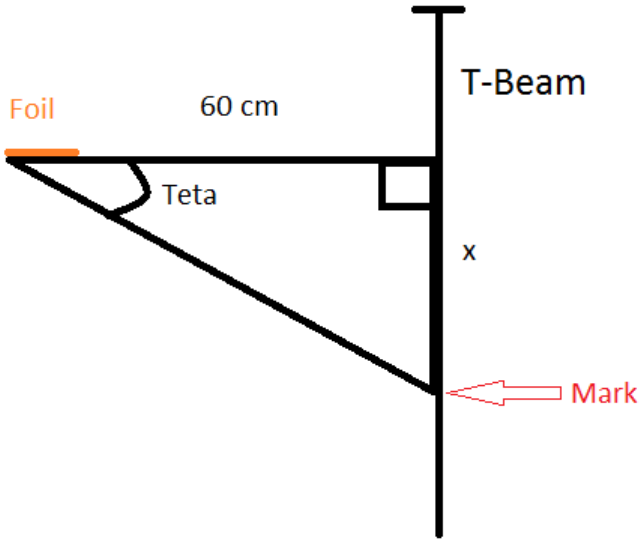

Figure 36: Trigonometry representation of the setup

A strut is attached to the underside of the foil and used as a reference along the vertical beam as seen in Figure 37.

Figure 37: Marks used to calibrate the angles of attacks in the workshop

A square section of aluminium was used temporarily, it was held down by double sided tape and clapms along the underside of the foil 38.

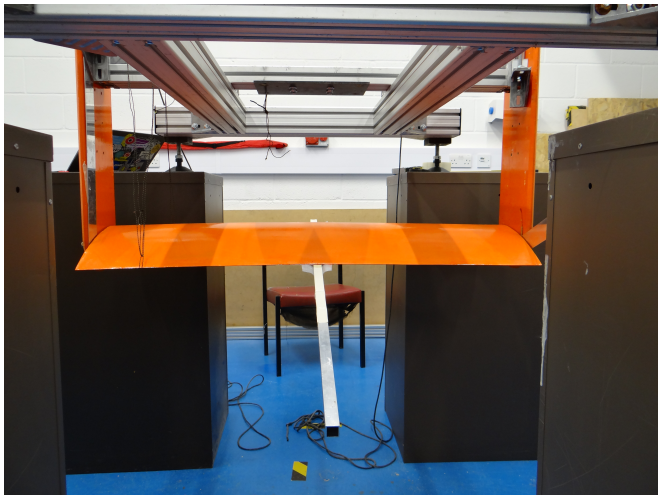

Figure 38: Square section used to calibrate the different angles of attack in the workshop

Because the angles change, the distance from the foil also changes. This enables the measures to be written down on the horizontal beam on which the vertical beam will slide.
By using the different measurements on each plane the angles, of the foils can be set accurately.
The first angle set was the zero angle so that the calculation could be checked with a greater efficiency - a horizontal plane is easy to check.
An inclinometer was used to double check the angles from the trigonometry calculations.
The purpose of the calibration was to allow the angle to be changed without removing the foil from the tank. The system of changing angle is as follows: two flat bars, which connected the foil to two beams, were fixed along the struts of each side. A long threaded bar connected to a flat strip made it possible to adjust the angle precisely; at each angle drawn on the fixed beam, a line is drawn on the beam along the struts as seen on Figure 39

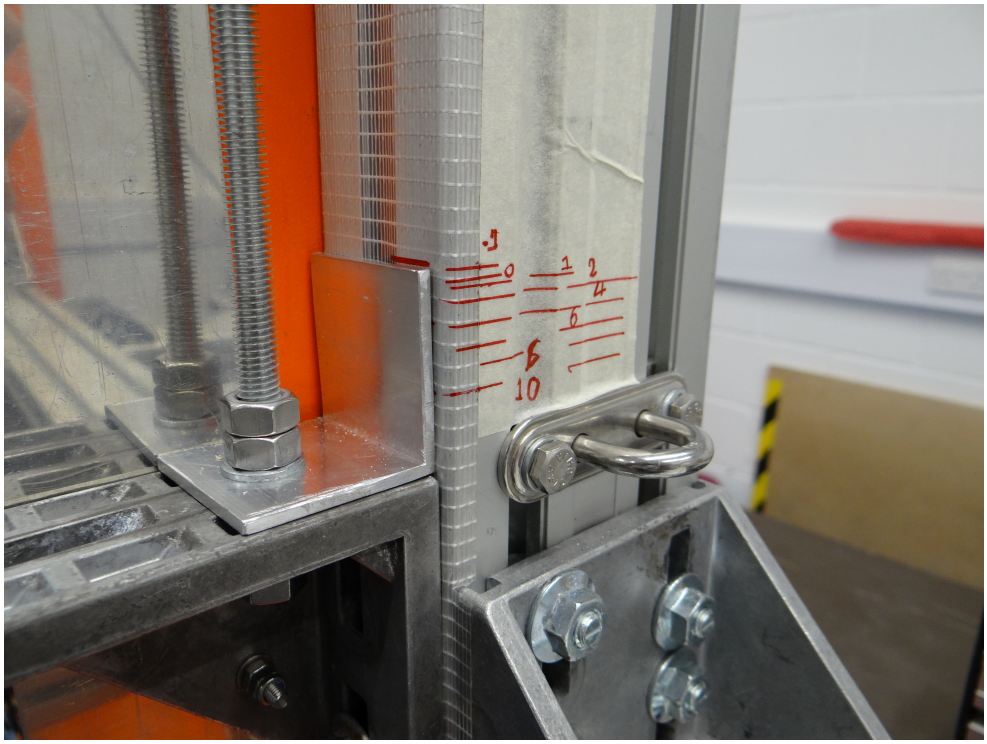

Figure 39: mechanism to change the angle once in the tank

Figure 40: Front view of the finished Hydrofoil

Figure 41: Side view of the finished hydrofoil

The rig was then fixed under the carriage inside the Cranfield towing tank as seen on Figure 42.

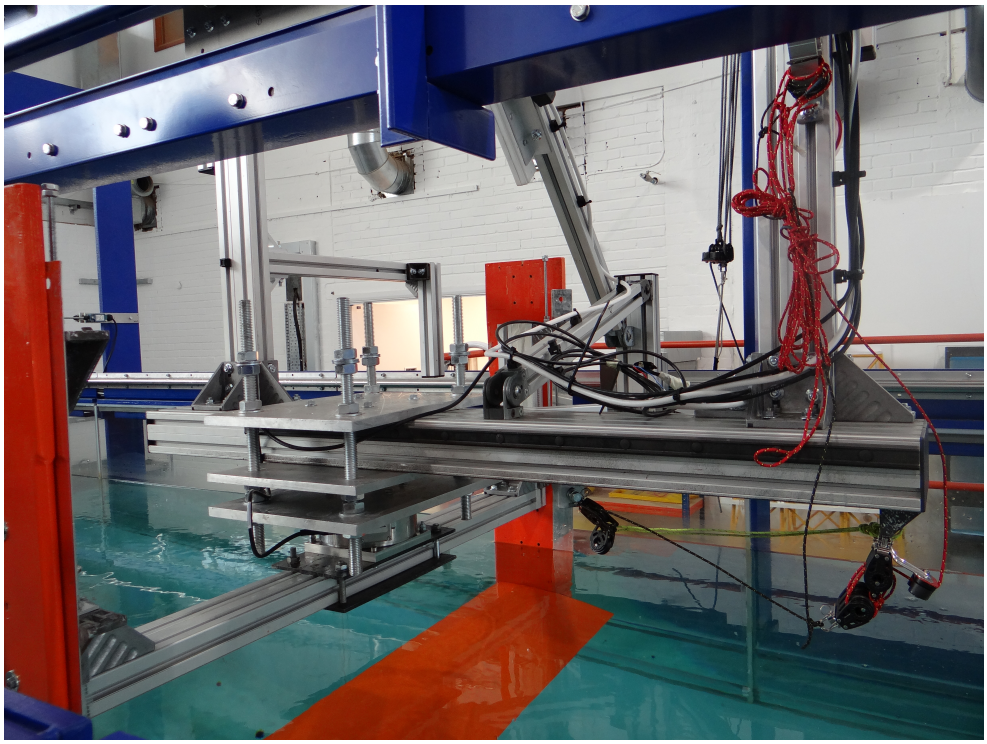

Figure 42: Hydrofoil and rig attached to the towing carriage inside the Ocean systems tank in Cranfield

6.4 Scaling

The problem is that in order to have a usable Reynolds number, the chord has to be has big as possible. This is limited by three factors: the size of the printing tools, the aspect ratio of the wing and the width of the towing tank in which the tests will be done. The chord could be longer than 300 mm but then the aspect ratio would be too low.
Because of a constant chord length, the aspect ratio can be given by:

$$Ar = \frac{b}{c} \tag{15}$$

In equation 15 : Ar is the Aspect ratio, b is the span of the wing and c the chord length.

The formula for scaling is:

$$Vp = \sqrt{Sc} * Vm \tag{16}$$

In equation 16: Vp is the scaled velocity, Sc is scale and Vm the real velocity.
The reynolds number is defined as such:

$$Re = \frac{\rho V L}{\mu} \tag{17}$$

In equation 17 : μ is the dynamic viscosity of the fluid.

In order to scale at 30 *kts* (a reasonable goal for some high performance sail boats), the scale should be around *1:20*. This would mean that in the experiment, the chord would be 6000 *mm*.
Unfortunately, the wing was designed at a *1:1* scale. This means that the scaled speed will only be of approximately 7 *kts* .
A smaller foil could have been designed and tested, but then the Reynolds number would not have been big enough. For example, if a speed of 30 *kts* was wanted then the foil would have a chord of 15 *mm* and a length of 60 *mm* (to keep the same aspect ratio). If that was the case then the Reynolds number would be around: 53,600.

7 Test Programme

7.1 Test plan

During the testing phase, different configurations will been run. The aim is to present a clear picture of what is happening.
The test plan is detailed in the tables beneath. Three parameters changed are: the angle of attack (AoA), the submergence (h/c) and the Reynolds number (Re).

1. The angle of attack is the angle at which the foil is presented in the incoming flow.
2. The submergence is the distance between the free surface and the foil. This distance is specified in 5.
3. The Reynolds number, Which is a component of velocity as detailed earlier in 17.

The most time consuming part of this test plan is setting an angle of attack at a fixed submergence. Once this is done then the rig can be run multiple times is short successions.

The table 1 gives an example of the test plan.
Here in 1 the three factors are clearly highlighted, the Velocity, the Angle of

Reynolds Number of 612638 (2.0 m/s)						
h/c / AoA	0.1	0.25	0.5	1	2	2.5
-1						
0						
1						
2						
4						
6						
8						
10						

Table 1: Test plan with a Reynolds number of 612638 (2.0 m/s)

attack and the submergence. A table like this will be needed for each of the different velocities.

7.2 Confidence interval

Ideally, the runs would be repeated at least 3 times but the time frame allotted would have to be reconsidered. The time used to set up the configuration (angle of attack and submergence) would also have to be considered.
Once a configuration has been set-up, running a number of tests will be relatively quick. Because D. James will be testing a very similar concept and tests, there will be better understanding of how much time is needed for each configuration set-up.
From then on, it is all about the confidence level that is aimed for. The confidence level is used to determine the margin of error and is as follows:
It is known that the results will be between a and b with $Z\%$ of certainty where a is the mean, b the size of half the confidence interval and $Z\%$ the level of confidence.
The choice of level of confidence is set as Z, most of the time 95% is taken, but it can be set higher or lower.
Once the level of confidence is set, b can be calculated:

$$b = T_\alpha * \sigma / \sqrt{nb} \tag{18}$$

In equation 18 : T_α is an elaborate formula that depends on Student's Distribution Law (that formula will not be detailed here), σ is the Standard deviation and nb is the number of points.
An approximation to remember is:

T_α	% of confidence
1	68 %
2	95 %
3	99.7 %

Table 2: % depending on T_α

To summarize: A certain numbers of value will be gathered , and the confidence interval will be worked out. If it is too big (for example 5 $\pm$ 200) more points will have to be gathered (b depends directly on the number of points). This will help achieve a high degree of confidence in the results.

The formula used in this section is the one mentioned earlier 18 .
The results are presented in the table below (3):

Submergence of 0.1 c and an AoA of 0 Degrees				
	1.0 m/s		2.5 m/s	
	Drag	Lift	Drag	Lift
Number of runs	1	1	1	1
Number of points	876	876	326	326
Average	7.41	79.06	21.14	15.05
Std Dev	0.10	0.47	0.15	1.41
B	0.06	0.30	0.055	0.51
Error %	0.88	0.39	0.26	3.4

Table 3: Results of repeatability for a fixed submergence and angle of attack

7.2.1 Observations:

It can be seen from the Table (3) that at lower speed, the same confidence interval is reached with less runs.
This can be explained in a few ways :
-At 2.5 m/s the the force is higher this skews the ratio .

-When the speed is 2.5m/s the runs last 6.5 seconds and when the speed is 1.0m/s the run lasts 17.5 seconds this means that we have ≈ 2.70 more points.

To account for this, a 6.5 second interval is taken within the 17.5 seconds of the 1.0m/s run. As shown in Figure 43 below :

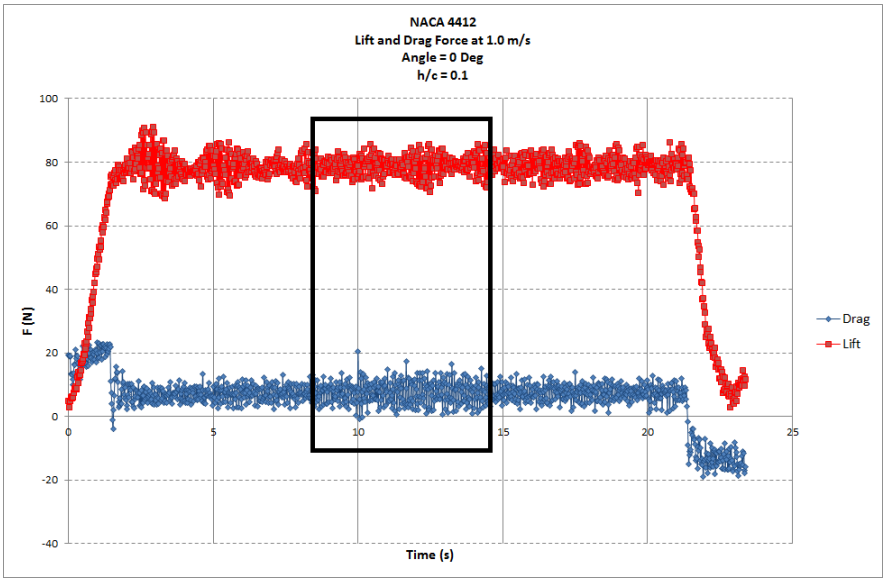

Figure 43: Fz (N) plotted against the time waited between each run at 1.0 m/s, Submergence of 0.1 and an angle of Attack of 0.0 Deg. The 6.5 second interval is shown here.

Table 4 below shows that this hypothesis does not hold up to testing. As shown here, the confidence interval stays relatively the same.

Submergence of 0.1 c and AoA of 0 Degrees				
	1.0 m/s (long run)		1.0 m/s (short run)	
	Drag	Lift	Drag	Lift
Number of runs	10	10	10	10
Number of points	876	876	326	326
Average	7.41	79.06	7.52	78.93
Std Dev	0.10	0.47	0.11	0.44
B	0.06	0.30	0.07	0.28
Error %	0.88	0.39	0.92	0.35

Table 4: Results of repeatability for a fixed submergence and angle of attack comparing the effect of the number of points.

There is no way of controlling for the force ratio and the problem arises from trying to account for speed.

7.3 Repeatability

7.3.1 Methods

The method used here is the following : A series of run are undertaken at a fixed speed, angle and submergence. The series were made up of 6 runs which were done at different fixed intervals. The intervals were determined by adding 1, 2, 5 and 10 minutes after the minimum waiting time (The minimum waited time here is 25 seconds due to the carriage coming back to the start point). This was repeated 3 times (Lift, Lift_2, Lift_3, Drag, Drag_2 and Drag_3 shown here in 44) This is shown in the Table beneath 5 :

Run number	Time waited
1	NA
2	1.25
3	2.25
4	3.25
5	6.25
6	11.25

Table 5: Time waited between each run in minutes

Here, 1.25 minute increment is the shortest time between runs. The results were then plotted out (44).

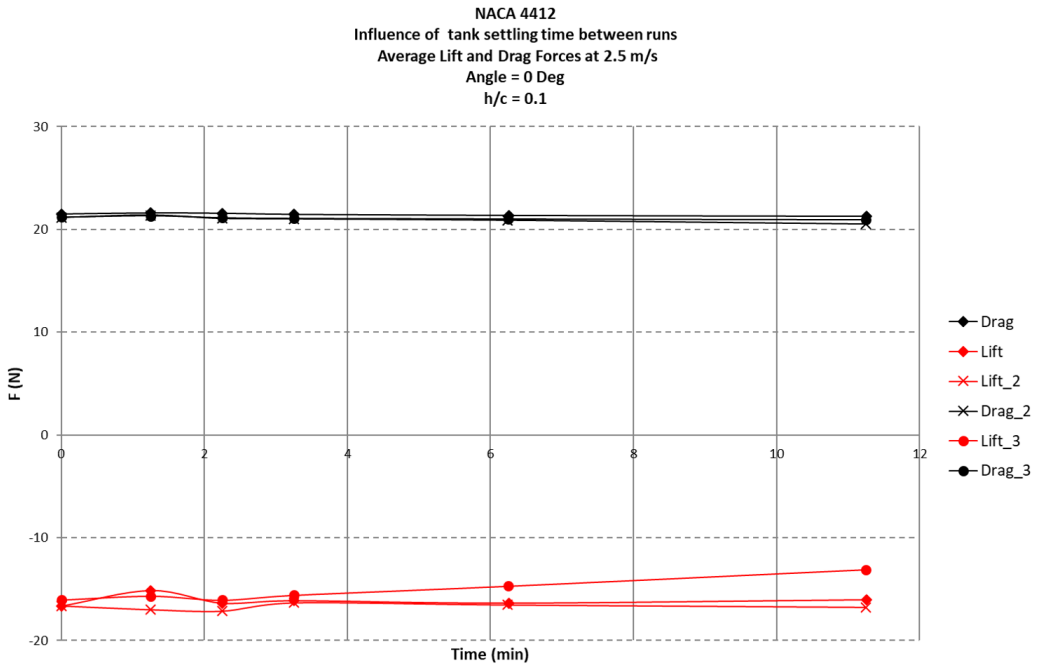

Figure 44: Fz (N) plotted against the time waited between each run at 2.5 m/s, Submergence of 0.1 and an angle of Attack of 0 Degrees.

It can be seen here that at 1.25 minutes waited, the deviation is higher than at other points. This supports the theory that the influence of settling water only matters if the time waited is under 2 minutes.
It was then concluded that the optimal time to wait between runs when testing and especially when testing for repeatability was 2 minutes.
It is also noticed that Lift_3 in 44 tends to deviate from Lift and Lift_2, this is thought to be due to calibration error of the balance.
This is also confirmed by plotting the Standard Deviation as shown below in Figure 45.

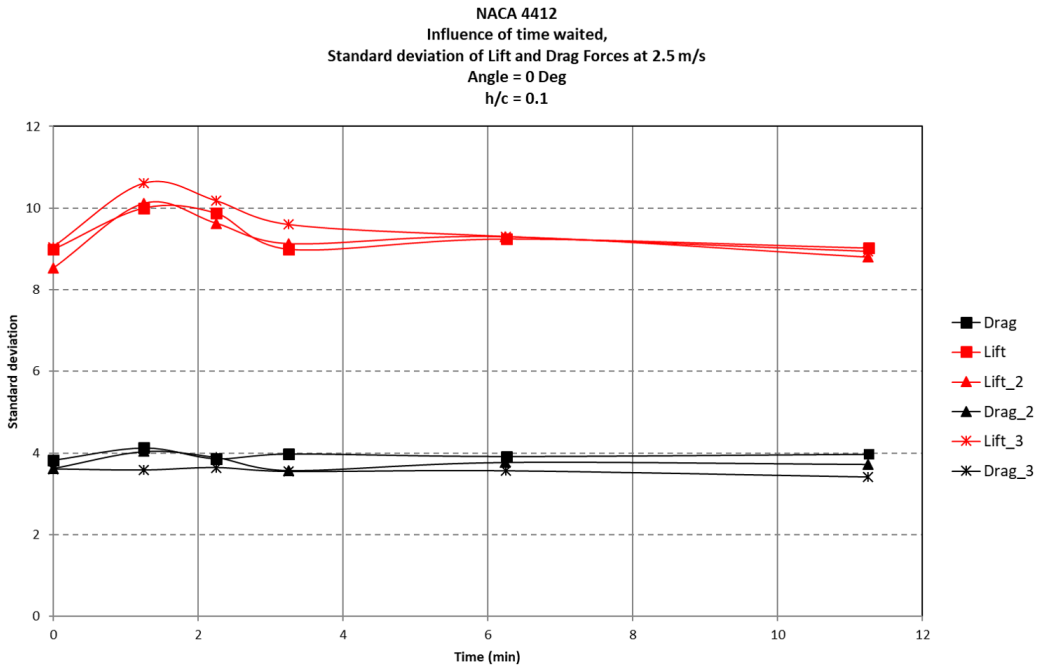

Figure 45: Standard deviation plotted against the time waited between each run at 2.5 m/s, Submergence of 0.1 and an angle of Attack of 0 Deg

During those tests, the entire run - including acceleration and deceleration phases - was recorded on the balance. To keep consistency in the results, the data used in the files was the average force between 1.5 seconds and 8 seconds. This period is shown in the figure below (46) in the black frame:

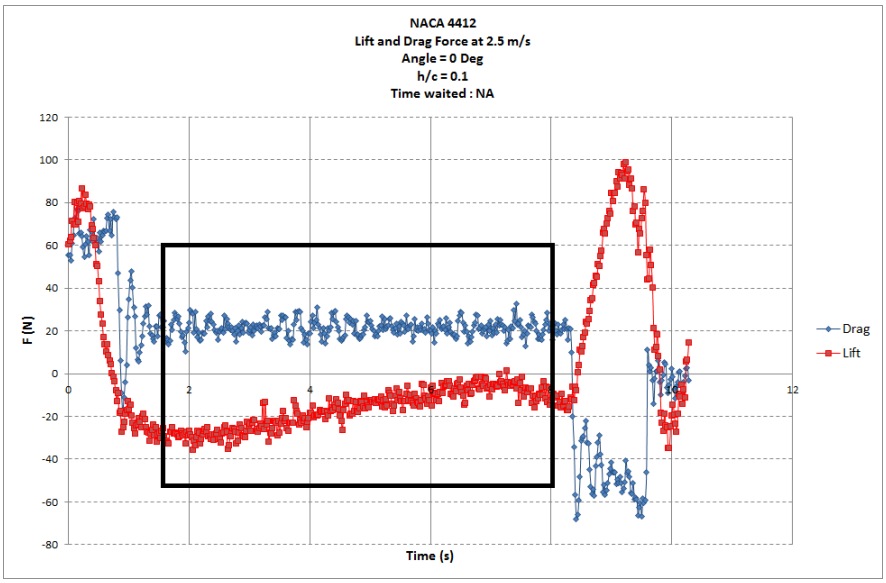

Figure 46: Total time series taken for a run at 2.5 m/s, Submergence of 0.1 and an angle of Attack of 0.0 Deg

This frame was determined by the acceleration and deceleration speed of the carriage, which for a speed of 2.5 m/s is 2.0 m/s^2.
Figure 46 clearly shows the acceleration and the deceleration of the hydrofoil in the tank. Here it can be noticed that the steady state is not reached in the lift component. It is assumed that the lift component follows a sin curve (This is seen at all speeds and it is noticed that as speed increase the length of the signal increases) and that if we take Half a period then the average is representative.

7.4 Test Procedure

The tests were carried out as follows:

- Determining of the depth of the foil in the workshop. It proved too complicated to adjust over water.
- Determining of the angle of attack. The first angle (here, 10 degrees) was set in the workshop just after the depth was set. The subsequent angles (10 to -1 degrees) could be set over the tank. This was done by tightening nuts on a threaded bar on either side. this is how a high degree of precision was achieved.
- Setting the speed of the carriage via the "carriage control panel". At the same time, acceleration and deceleration were also set. Inputs are detailed in Figure 6.

Reynolds Number	Acceleration (m/s^2)	speed (m/s)	deceleration (m/s^2)
153,159	0.5	0.5	0.5
229,739	0.5	0.75	0.5
306,319	0.5	1.0	0.5
382,899	1.0	1.25	1.0
459,479	1.0	1.5	1.0
536,058	1.5	1.75	1.5
612,638	1.5	2.0	1.5
689,218	2.0	2.25	2.0
765,798	2.0	2.5	2.0
842,378	2.5	2.75	2.5
918,958	2.5	3.0	2.5

Table 6: Acceleration and deceleration for different speeds

- The next step was to set the file name for the balance recording. This was done via the balance software (ATI DAQ). The files names were as follows: 0.0deg_1.0h_0.5v_500Hz_AVG_10.csv
- The run then started and the foil travelled the length of the tank.
- Once the file was recorded, it was opened in excel.
- The first thing that was done was to plot the average forces and calculating the standard deviation. The force was then plotted along the vertical axis (fz). This last step was simply a safety check to make sure nothing had gone wrong in the test.

- The next step was to copy the data over to my log file. In that file, the lift, drag and standard deviation were also plotted. This gave a clear view of the trends. It is important to do this after each run because the runs take time and the risk of making mistakes must be minimized.

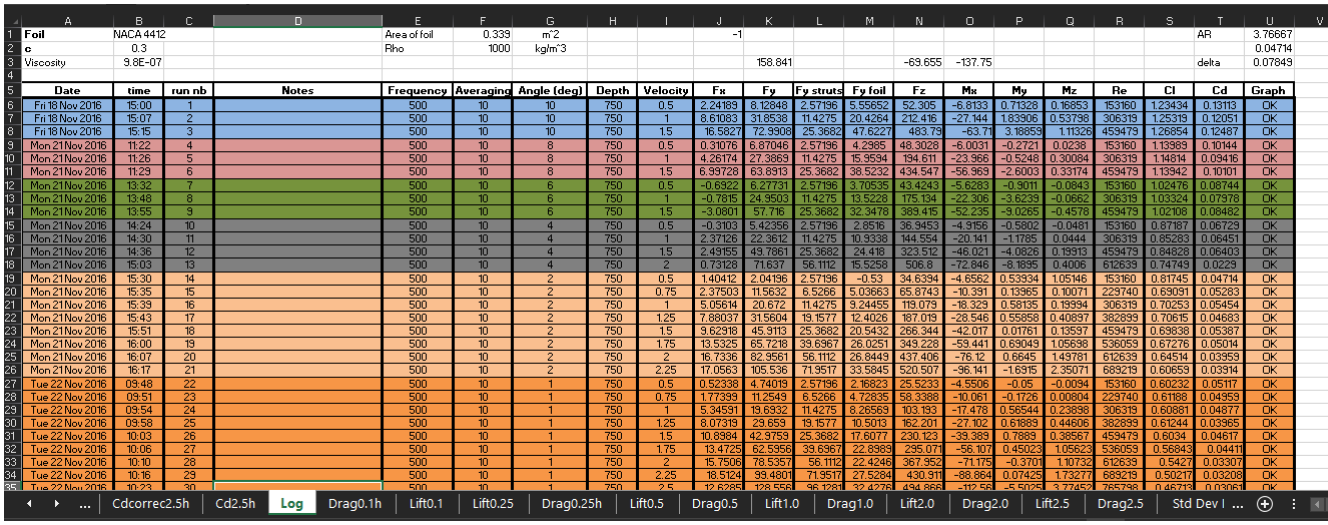

	A	B	C	D	E	F	G	H	I	J	K	L	M	N	O	P	Q	R	S	T	U
1	Foil	NACA 4412			Area of foil	0.339	m^2			-1										AR	3.76667
2	c	0.3			Rho	1000	kg/m^3														0.04714
3	Viscosity	9.8E-07									158.841			-69.655	-137.75					delta	0.07849
4																					
5	Date	time	run nb	Notes	Frequency	Averaging	Angle (deg)	Depth	Velocity	Fx	Fy	Fy struts	Fy foil	Fz	Mx	My	Mz	Re	Cl	Cd	Graph
6	Fri 18 Nov 2016	15:00	1		500	10	10	750	0.5	2.24189	8.12848	2.57196	5.55652	52.305	-6.8133	0.71328	0.16853	153160	1.23434	0.13113	OK
7	Fri 18 Nov 2016	15:07	2		500	10	10	750	1	8.61083	31.8538	11.4275	20.4264	212.416	-27.144	1.83906	0.53798	306319	1.25319	0.12051	OK
8	Fri 18 Nov 2016	15:15	3		500	10	10	750	1.5	16.5827	72.9908	25.3682	47.6227	483.79	-63.71	3.18859	1.11326	459479	1.26854	0.12487	OK
9	Mon 21 Nov 2016	11:22	4		500	10	8	750	0.5	0.31076	6.87046	2.57196	4.2985	48.3028	-6.0031	-0.2721	0.0238	153160	1.13989	0.10144	OK
10	Mon 21 Nov 2016	11:26	5		500	10	8	750	1	4.26174	27.3869	11.4275	15.9594	194.611	-23.966	-0.5248	0.30084	306319	1.14814	0.09416	OK
11	Mon 21 Nov 2016	11:29	6		500	10	8	750	1.5	6.99728	63.8913	25.3682	38.5232	434.547	-56.969	-2.6003	0.33174	459479	1.13942	0.10101	OK
12	Mon 21 Nov 2016	13:32	7		500	10	6	750	0.5	-0.6922	6.27731	2.57196	3.70535	43.4243	-5.6283	-0.9011	-0.0843	153160	1.02476	0.08744	OK
13	Mon 21 Nov 2016	13:48	8		500	10	6	750	1	-0.7815	24.9503	11.4275	13.5228	175.134	-22.306	-3.6239	-0.0662	306319	1.03324	0.07978	OK
14	Mon 21 Nov 2016	13:55	9		500	10	6	750	1.5	-3.0801	57.716	25.3682	32.3478	389.415	-52.235	-9.0265	-0.4578	459479	1.02108	0.08482	OK
15	Mon 21 Nov 2016	14:24	10		500	10	4	750	0.5	-0.3103	5.42356	2.57196	2.8516	36.9453	-4.9156	-0.5802	-0.0481	153160	0.87167	0.06729	OK
16	Mon 21 Nov 2016	14:30	11		500	10	4	750	1	2.37126	22.3612	11.4275	10.9338	144.554	-20.141	-1.1785	0.0444	306319	0.85283	0.06451	OK
17	Mon 21 Nov 2016	14:36	12		500	10	4	750	1.5	2.49155	49.7861	25.3682	24.418	323.512	-46.021	-4.0826	0.19313	459479	0.84828	0.06403	OK
18	Mon 21 Nov 2016	15:03	13		500	10	4	750	2	0.73128	71.637	56.1112	15.5258	506.8	-72.846	-8.1895	0.4006	612639	0.74749	0.0229	OK
19	Mon 21 Nov 2016	15:30	14		500	10	2	750	0.5	1.40412	2.04196	2.57196	-0.53	34.6394	-4.6562	0.53934	1.05146	153160	0.81745	0.04714	OK
20	Mon 21 Nov 2016	15:35	15		500	10	2	750	0.75	2.37503	11.5632	6.5266	5.03663	65.8743	-10.391	0.13965	0.10071	229740	0.69091	0.05283	OK
21	Mon 21 Nov 2016	15:39	16		500	10	2	750	1	5.05614	20.672	11.4275	9.24455	119.079	-18.323	0.58135	0.19394	306319	0.70253	0.05454	OK
22	Mon 21 Nov 2016	15:43	17		500	10	2	750	1.25	7.88037	31.5604	19.1577	12.4026	187.019	-28.546	0.55858	0.40697	382899	0.70615	0.04683	OK
23	Mon 21 Nov 2016	15:51	18		500	10	2	750	1.5	9.62316	45.3113	25.3682	20.5432	266.344	-42.017	0.01761	0.13597	459479	0.69838	0.05387	OK
24	Mon 21 Nov 2016	16:00	19		500	10	2	750	1.75	13.5325	65.7218	39.6967	26.0251	343.228	-59.441	0.69049	1.05698	536059	0.67276	0.05014	OK
25	Mon 21 Nov 2016	16:07	20		500	10	2	750	2	16.7336	82.9561	56.1112	26.8449	437.406	-76.12	0.6645	1.49781	612639	0.64514	0.03959	OK
26	Mon 21 Nov 2016	16:17	21		500	10	2	750	2.25	17.0563	105.536	71.3517	33.5845	520.507	-96.141	-1.6915	2.35071	689219	0.60659	0.03914	OK
27	Tue 22 Nov 2016	09:48	22		500	10	1	750	0.5	0.52338	4.74019	2.57196	2.16823	25.5233	-4.5506	-0.05	-0.0094	153160	0.60232	0.05117	OK
28	Tue 22 Nov 2016	09:51	23		500	10	1	750	0.75	1.77399	11.2549	6.5266	4.72835	58.3388	-10.061	-0.1726	0.00804	229740	0.61188	0.04959	OK
29	Tue 22 Nov 2016	09:54	24		500	10	1	750	1	5.34591	19.6932	11.4275	8.26569	103.193	-17.478	0.56544	0.23898	306319	0.60881	0.04877	OK
30	Tue 22 Nov 2016	09:58	25		500	10	1	750	1.25	8.07319	29.659	19.1577	10.5013	162.201	-27.102	0.61889	0.44606	382899	0.61244	0.03965	OK
31	Tue 22 Nov 2016	10:03	26		500	10	1	750	1.5	10.8984	42.9759	25.3682	17.6077	230.123	-39.389	0.7889	0.38567	459479	0.6034	0.04617	OK
32	Tue 22 Nov 2016	10:06	27		500	10	1	750	1.75	13.4725	62.5956	39.6967	22.8989	295.071	-56.107	0.45023	1.05623	536059	0.56843	0.04411	OK
33	Tue 22 Nov 2016	10:10	28		500	10	1	750	2	15.7506	78.5357	56.1112	22.4246	367.952	-71.175	-0.3701	1.10732	612639	0.5427	0.03307	OK
34	Tue 22 Nov 2016	10:16	29		500	10	1	750	2.25	18.5124	99.4801	71.3517	27.5284	430.911	-88.864	0.07425	1.73277	689219	0.50217	0.03208	OK
35	Tue 22 Nov 2016	10:23	30		500	10	1	750	2.5	12.6285	128.558	36.1281	32.4276	494.866	-112.58	-5.5025	2.77452	765738	0.46218	0.03061	OK

Cdcorrec2.5h | Cd2.5h | Log | Drag0.1h | Lift0.1 | Lift0.25 | Drag0.25h | Lift0.5 | Drag0.5 | Lift1.0 | Drag1.0 | Lift2.0 | Drag2.0 | Lift2.5 | Drag2.5 | Std Dev I

Figure 47: Log file with all the different recorded values : date and time, run number, notes, Frequency of acquisition of the balance, Averaging of the results from balance, Angle of attack, Depth, Velocity, Fx, Fy, Fz, Mx, My, Mz, Re, Cl and Cd.

- Runs without the foil were also done. This was used to calculate the drag and the drag coefficient (Cd). The formula for the drag coefficient is detailed above 2, and the formula can also be presented as follows:

$$C_D = \frac{D}{\frac{1}{2}\rho V^2 S} \tag{19}$$

Here D is the force recorded in the experiment. D can also be shown as :

$$D = F_y total - F_y struts \tag{20}$$

In equation 20 : $F_y total$ is the total Drag force generated by the hydrofoil and the struts supporting it and $F_y struts$ is the drag force generated by the struts only. Therefore, the formula used to calculate the drag coefficient of the hydrofoil (C_D) is :

$$C_D = \frac{(F_y total - F_y struts)}{\frac{1}{2}\rho V^2 S} \tag{21}$$

- Once the numbers were collected in 47 Graphs could be plotted.

8 Test results

8.1 Introduction

In this chapter, the results of the tests are presented as plots showing the lift and characteristics of the wing.
Here the buoyancy force is not taken into account because the balance is zeroed before each run.
The data presented here is also presented as timeseries in the appendices.

8.2 Experimental curves

Here is an analysis of the results from the experiments conducted in the Ocean System Test Laboratory in Cranfield.

8.2.1 Effect of angle of attack

8.2.1.1 Angle = -1 Degrees

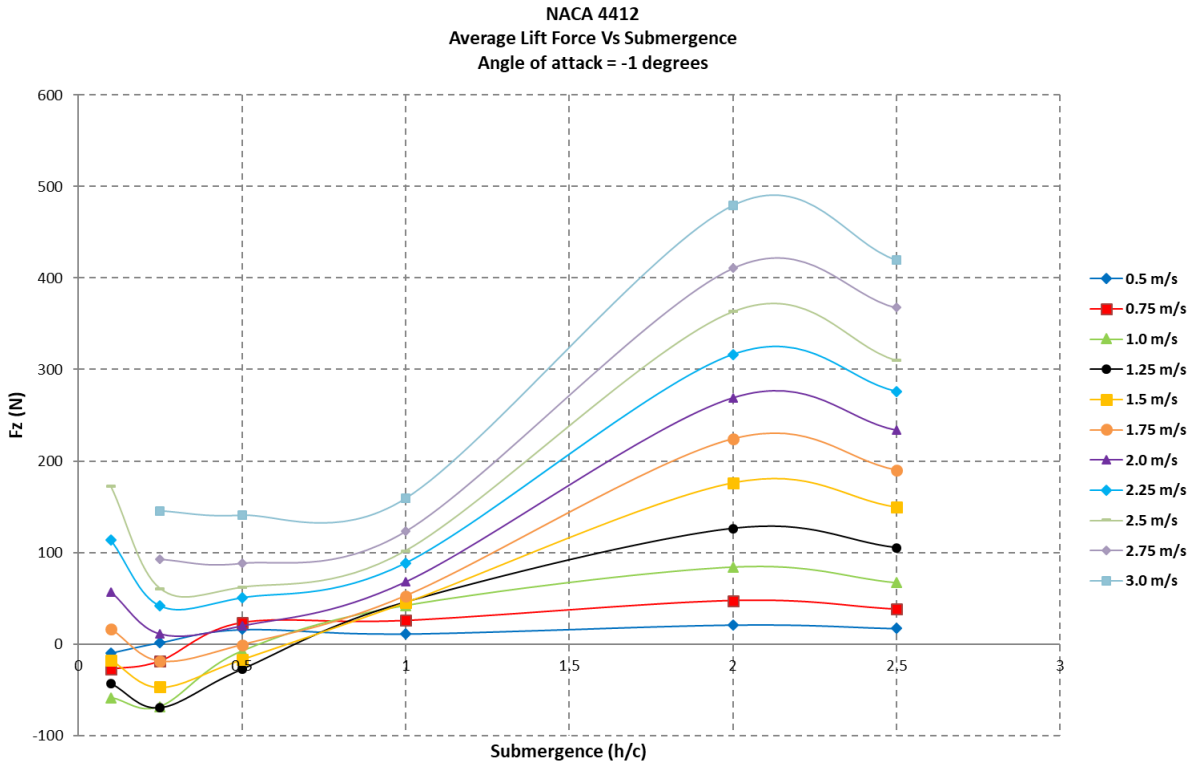

Figure 48: Lift generated plotted against the submergence for an angle of attack of -1 degrees for a range of velocities.

A linear progression is seen from a submergence of 0.5 c to a submergence

of 2.0 c, from a submergence of 2.0 c to 2.5 c a decrease can be seen. This reduction is higher when the velocity increases. At a speed of 2.75 m/s and 3.0 m/s, this effect is amplified.

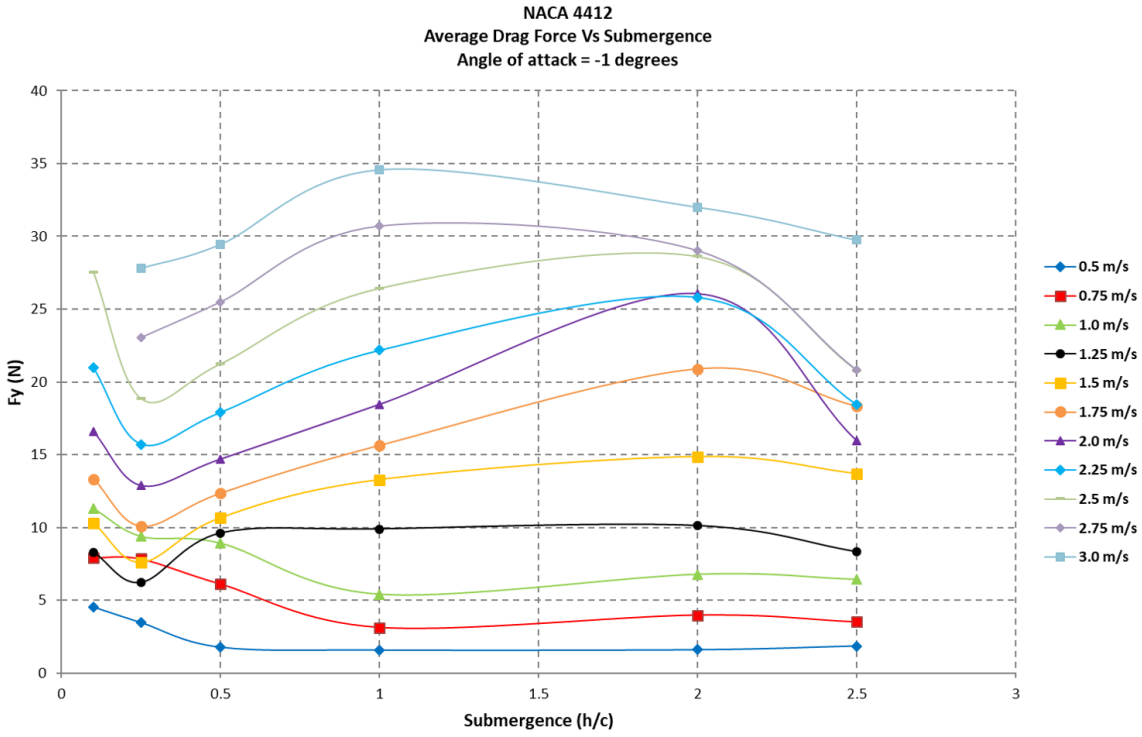

Figure 49: Drag generated plotted against the submergence for an angle of attack of -1 degrees for a range of velocities.

The average drag force can be seen here to increase from a lower speed to a higher velocity. This due the fact that Drag is a product of speed 2.

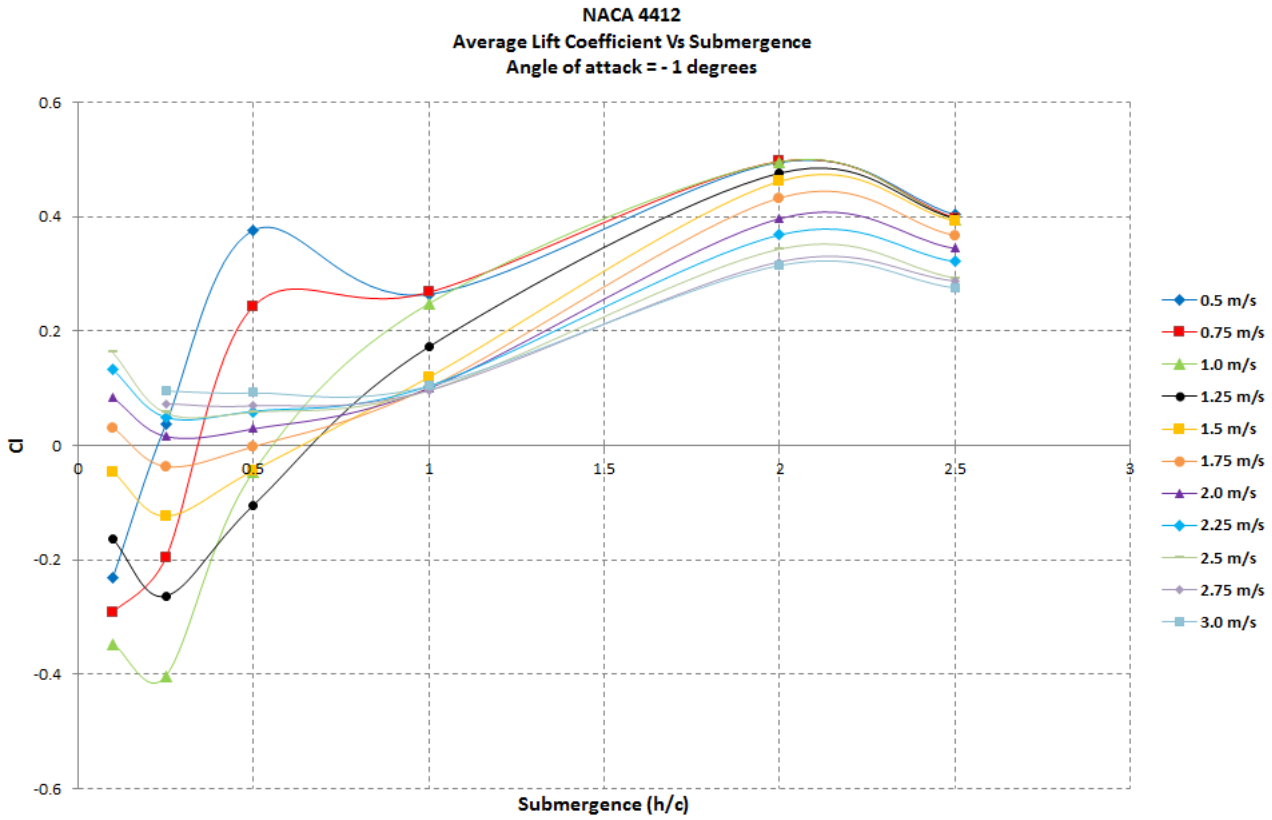

Figure 50: Lift coefficient generated plotted against the submergence for an angle of attack of -1 degrees for a range of velocities.

Here is presented the average lift coefficient plotted against the submergence for a range of velocities. A negative lift coefficient can be seen between a speed of 0.5 m/s to 1.75 m/s. A sharp increase can be seen for a speed of 0.5 and 0.75 m/s from a submergence of 0.25 c to 0.5 c. A regular increase can be seen between a submergence of 0.25 c and 2.0 c. Then a slight dip is seen from 2.0 c to 2.5 c at all speeds.

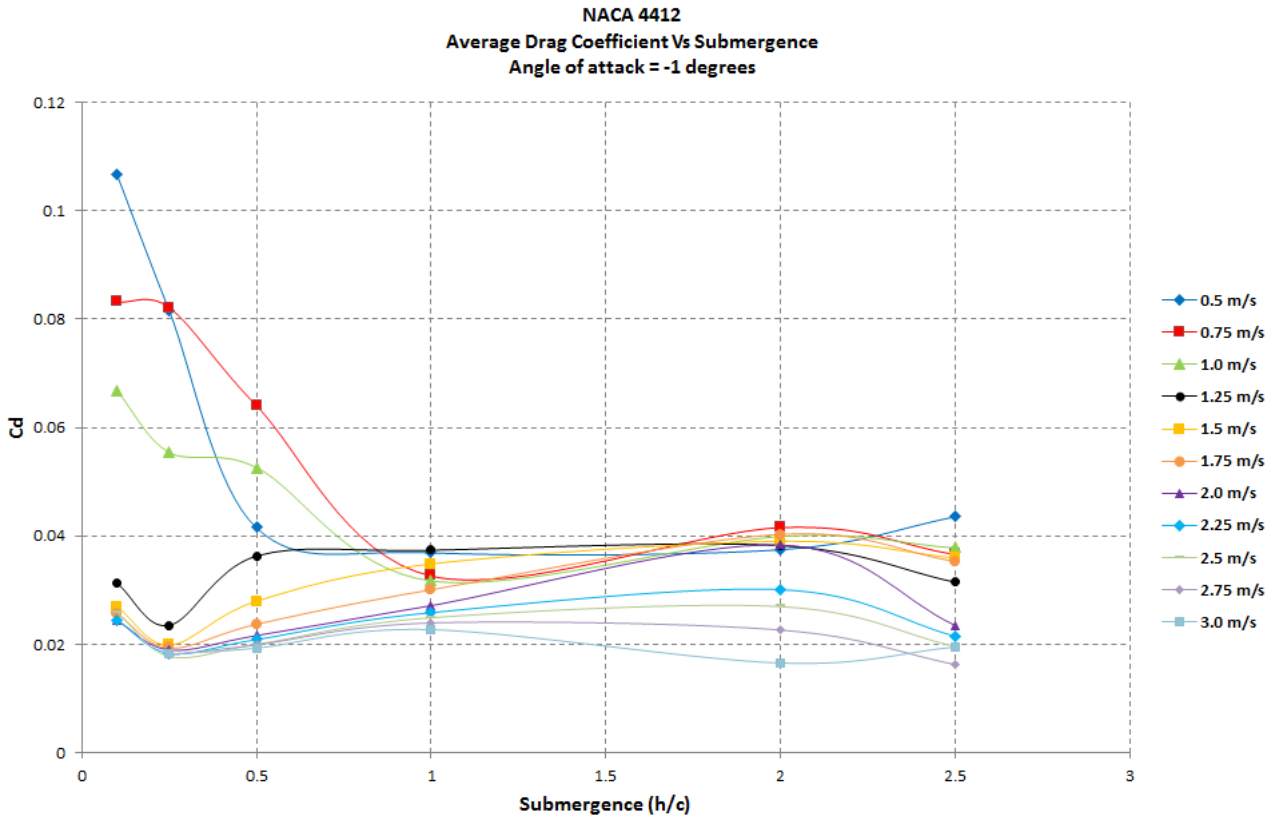

Figure 51: Drag coefficient generated plotted against the submergence for an angle of attack of -1 degrees for a range of velocities.

Here is presented the average drag coefficient plotted against the submergence for a a range of velocities. It can be seen that between 0.5 c and 2.5 c the change of drag coefficient is negligible. At lower speeds and lower submergences the drag increases nearly five folds, as seen for 0.5 and 0.75 m/s.

8.2.1.2 Angle = 0 Degrees

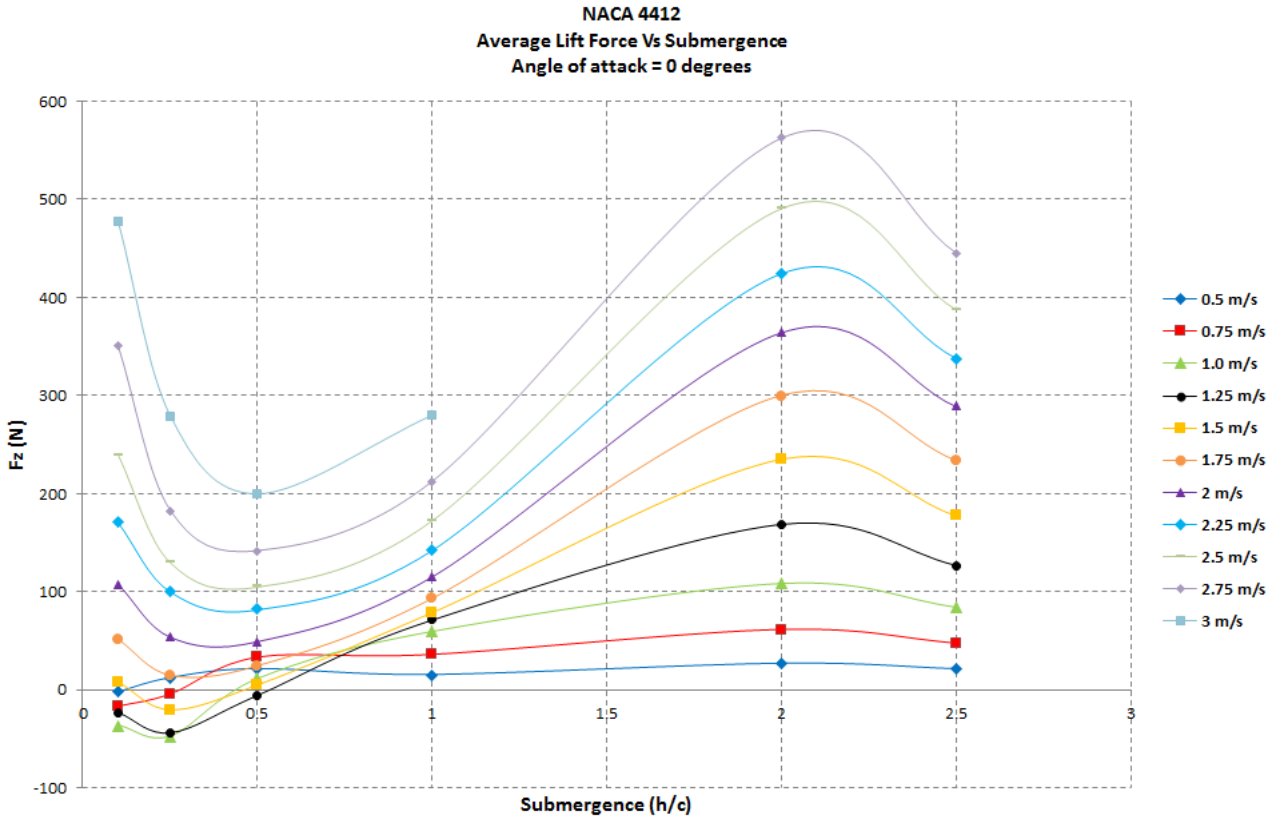

Figure 52: Lift generated plotted against the submergence for an angle of attack of 0 degrees for a range of velocities.

Here is presented the average lift force plotted against the submergence for an angle of attack of 0 degrees. All the curves follow the same trend, that trend is amplified at higher speeds. From 0.5 c to 2.0 c, the increase is linear, there is a dip after 2.0 c. At the other end of the curves, from a submergence of 0.1 c to 0.5 c the force generated by the hydrofoil is higher at shallower depths.

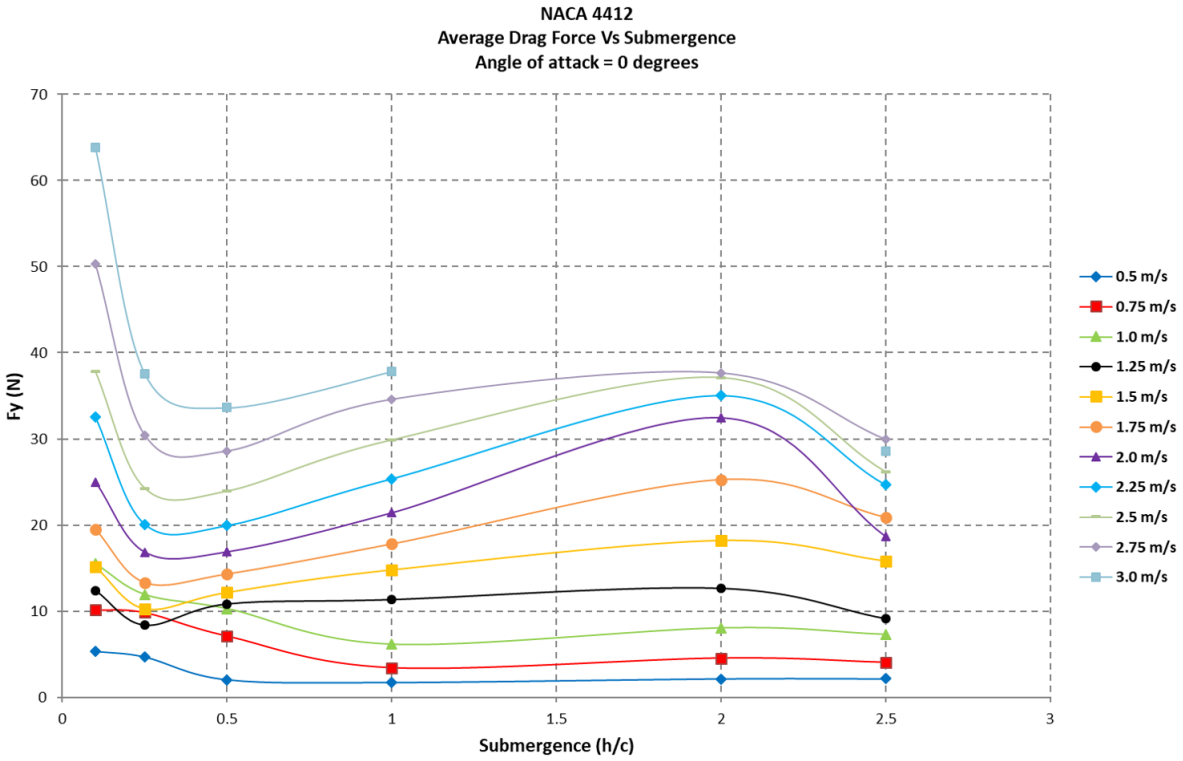

Figure 53: Drag generated plotted against the submergence for an angle of attack of 0 degrees for a range of velocities.

Here is presented the average drag force plotted against the submergence for an angle of attack of 0 degrees. It can be seen here that the drag forces increases with speed.

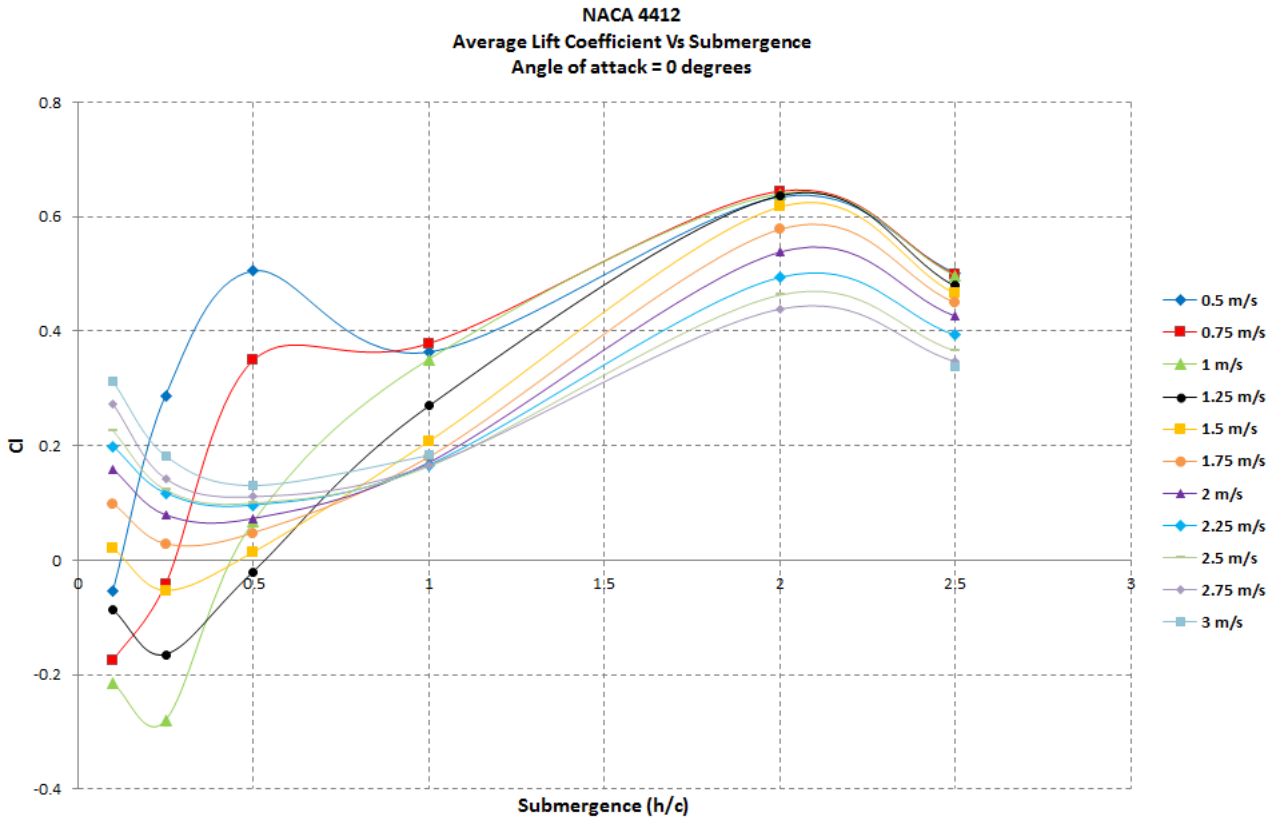

Figure 54: Lift coefficient generated plotted against the submergence for an angle of attack of 0 degrees for a range of velocities.

Here is presented the average lift coefficient plotted against the submergence for a range of velocities. A negative lift coefficient can be seen between a speed of 0.5 m/s to 1.5 m/s. A sharp increase can be seen for a speed of 0.5 and 0.75 m/s, from a submergence of 0.25 c to 0.5 c. A regular increase can be seen between a submergence of 0.25 c and 2.0 c. Then a slight dip is seen from 2.0 c to 2.5 c at all speeds.

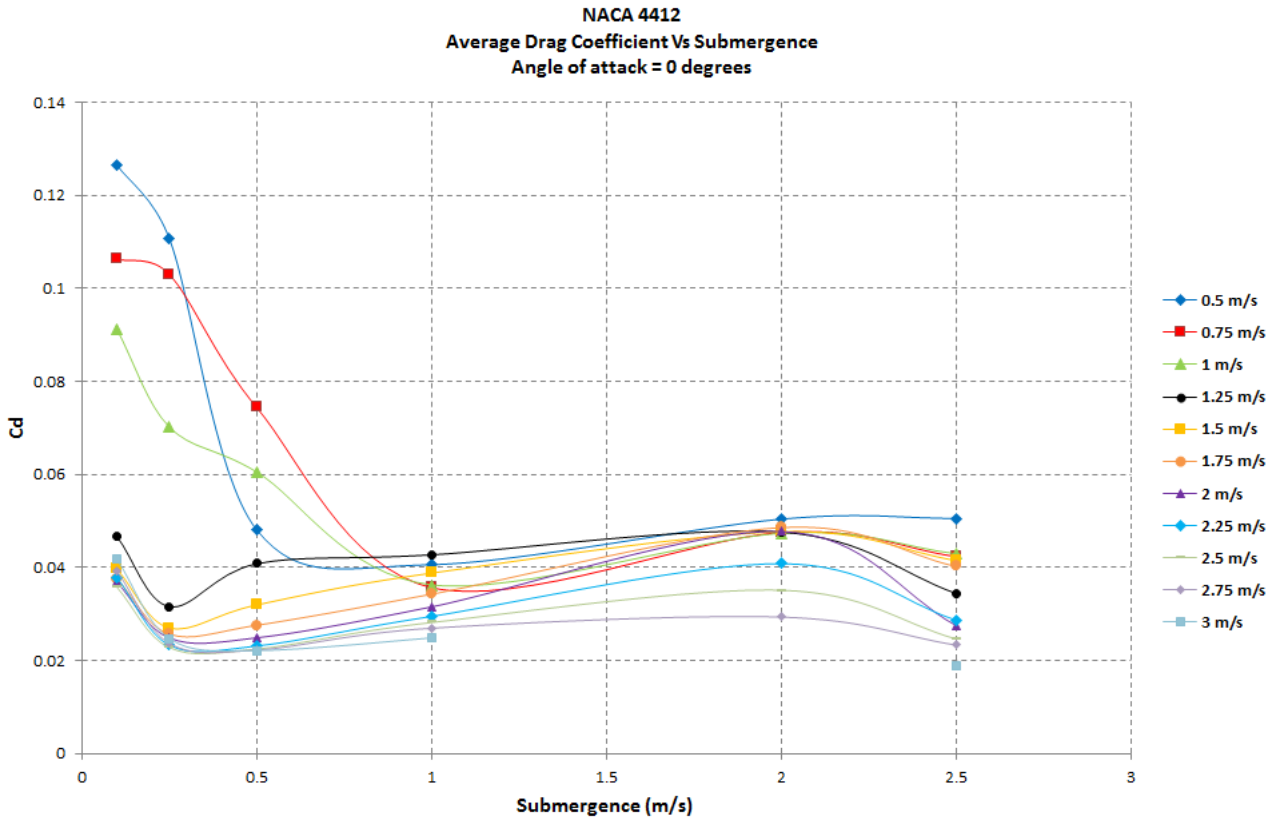

Figure 55: Drag coefficient generated plotted against the submergence for an angle of attack of 0 degrees for a range of velocities.

Here is presented the average drag coefficient plotted against the submergence for a a range of velocities. It can be seen that between 0.5 c and 2.5 c, the change of drag coefficient is negligible. At lower speeds and lower submergence the drag increases nearly five folds, as seen for 0.5, 0.75 m/s and 1.0 m/s.

8.2.1.3 Angle = 1 Degree

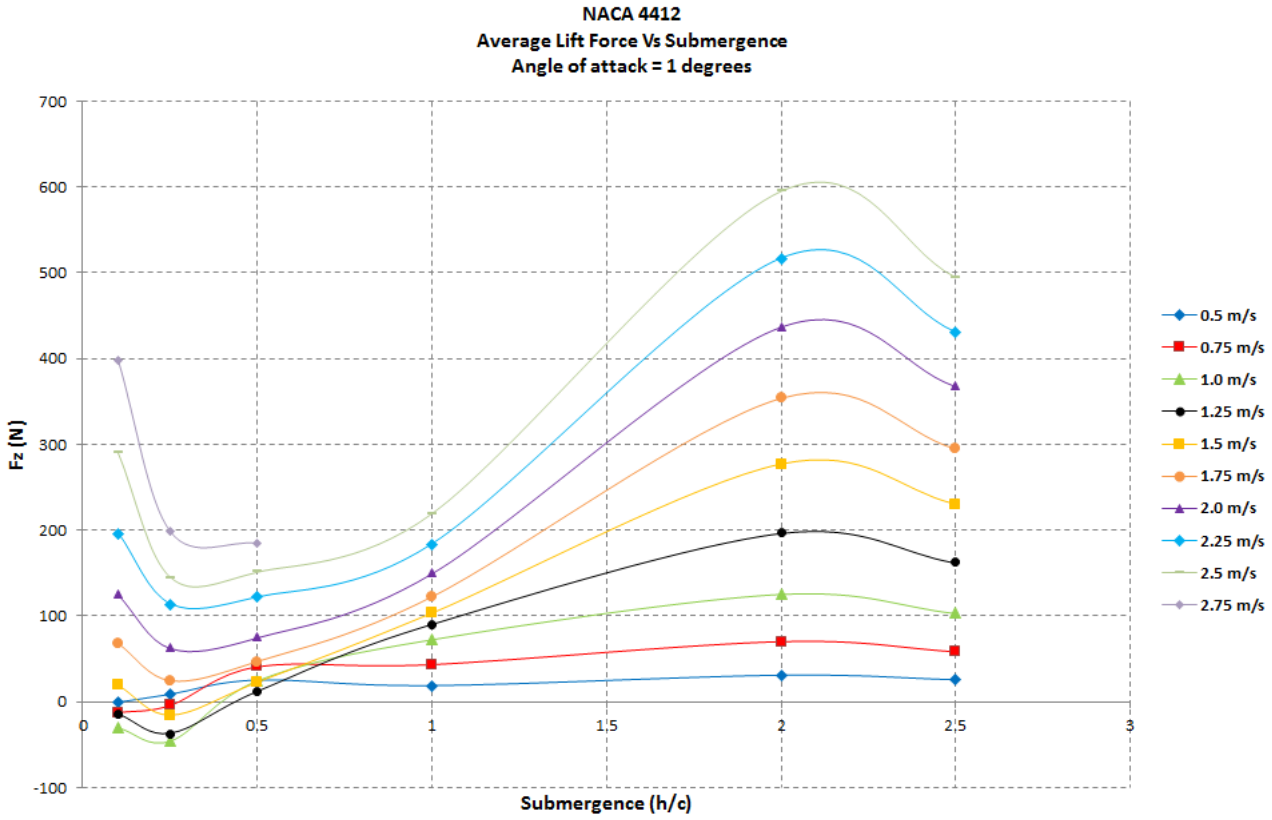

Figure 56: Lift generated plotted against the submergence for an angle of attack of 1 degrees for a range of velocities.

Here is presented the average lift force plotted against the submergence for an angle of attack of 1 degrees. All the curves follow the same trend, that trend is amplified at higher speeds. From 0.5 c to 2.0 c, the increase is stable, there is a dip after 2.0 c. At the other end of the curves, from a submergence of 0.1 c to 0.5 c, the force generated by the hydrofoil is higher at shallower depths.

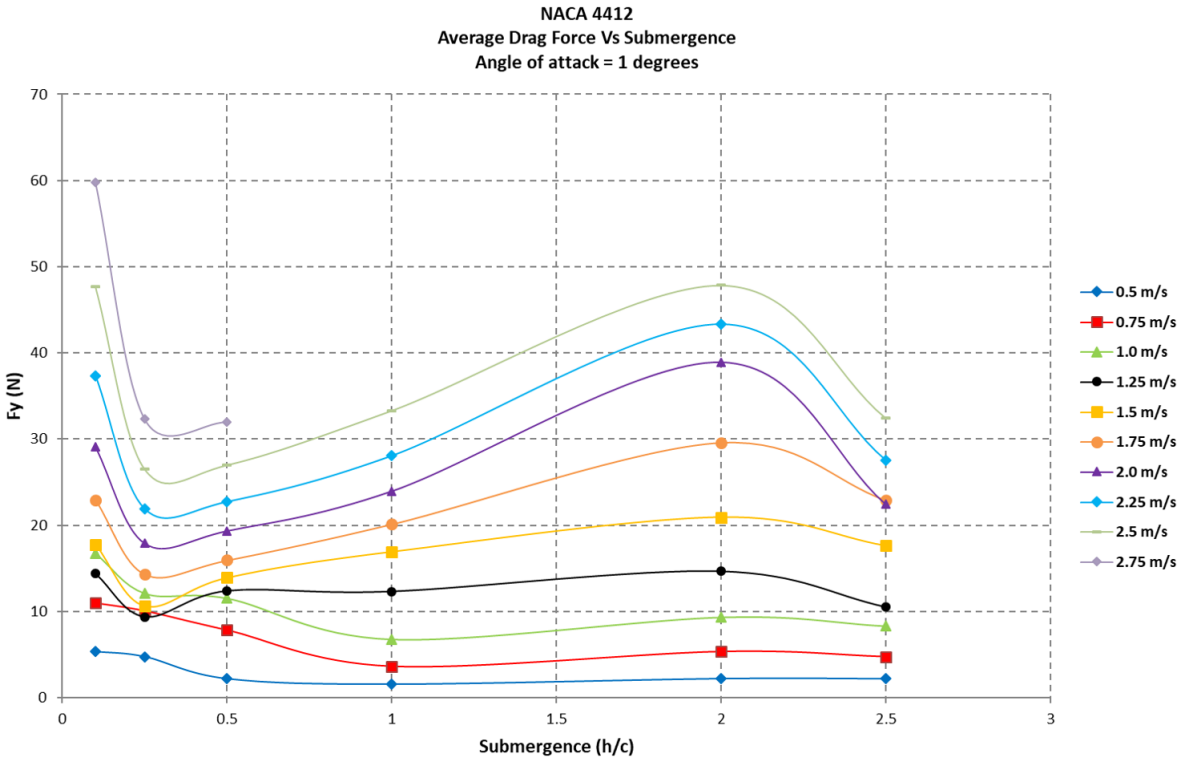

Figure 57: Drag generated plotted against the submergence for an angle of attack of 1 degrees for a range of velocities.

Here is presented the average drag force plotted against the submergence for an angle of attack of 1 degrees. It can be seen here that the drag force increases with speed.

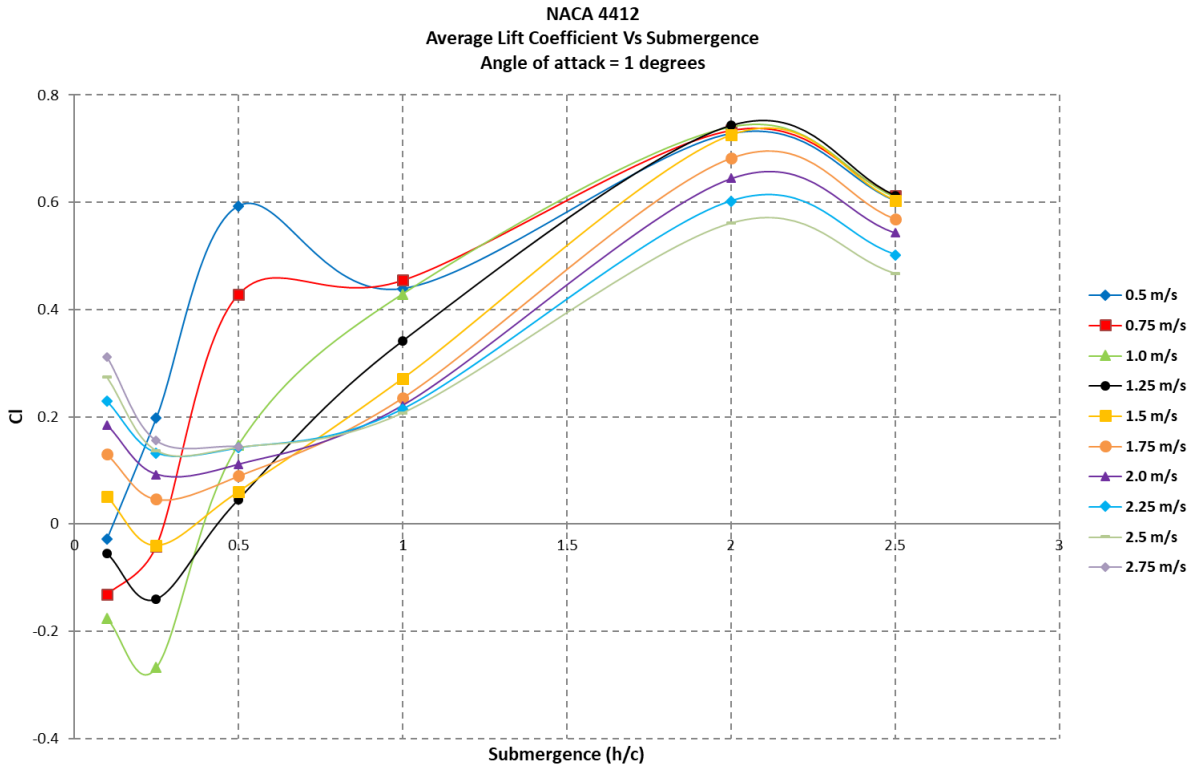

Figure 58: Lift coefficient generated plotted against the submergence for an angle of attack of 1 degrees for a range of velocities.

Here is presented the average lift coefficient plotted against the submergence for a range of velocities. A negative lift coefficient can be seen between a speed of 0.5 m/s to 1.5 m/s. A sharp increase can be seen for a speed of 0.5, 0.75 and 1.0 m/s, from a submergence of 0.25 c to 0.5 c. A regular increase can then be seen between a submergence of 0.25 c to 2.0 c. Then a slight dip is seen from 2.0 c to 2.5 c at all speeds.

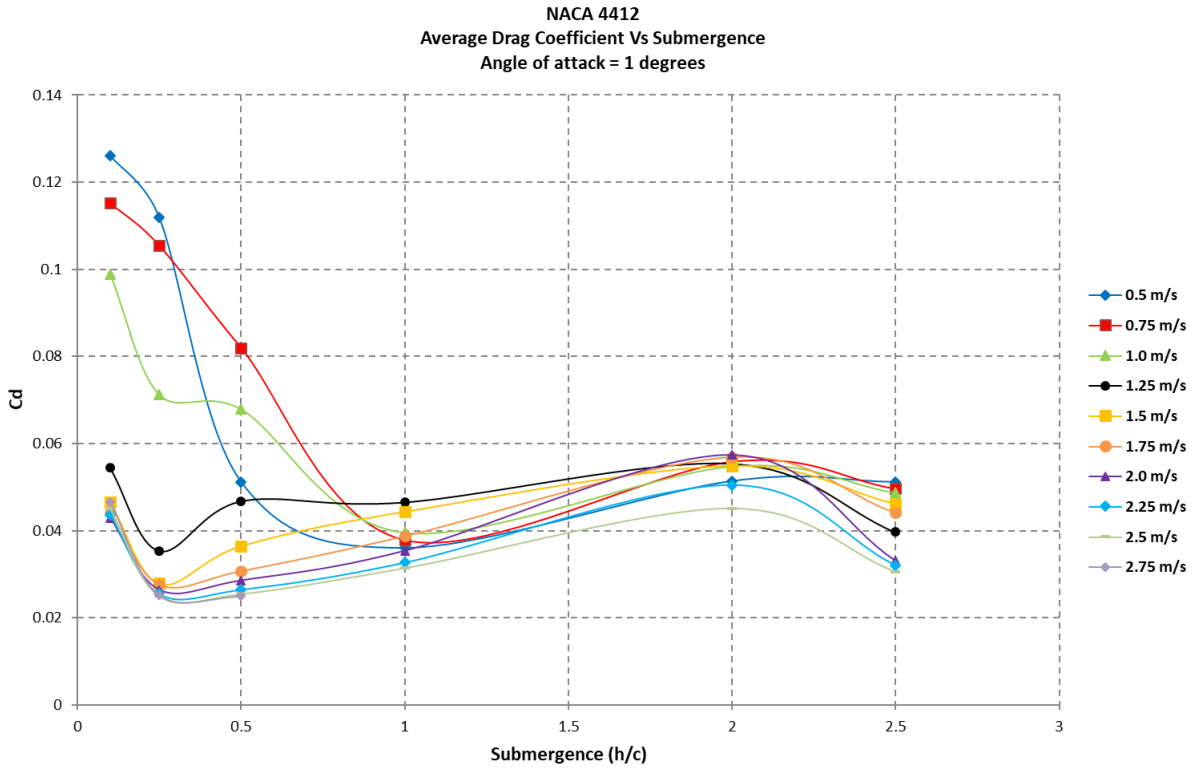

Figure 59: Drag coefficient generated plotted against the submergence for an angle of attack of 1 degrees for a range of velocities.

Here is presented the average drag coefficient plotted against the submergence for a a range of velocities. It can be seen that between 0.5 c and 2.0 c, the drag coefficient increases slightly with both speed and submergence. From 2.0 c to 2.5 c, a slight dip is seen at all speeds. At lower speeds and submergence the drag increases nearly five folds, as seen for 0.5, 0.75 and 1.0 m/s. There is also a slight dip in Drag coefficient at a submergence of 0.25 c.

8.2.1.4 Angle = 2 Degrees

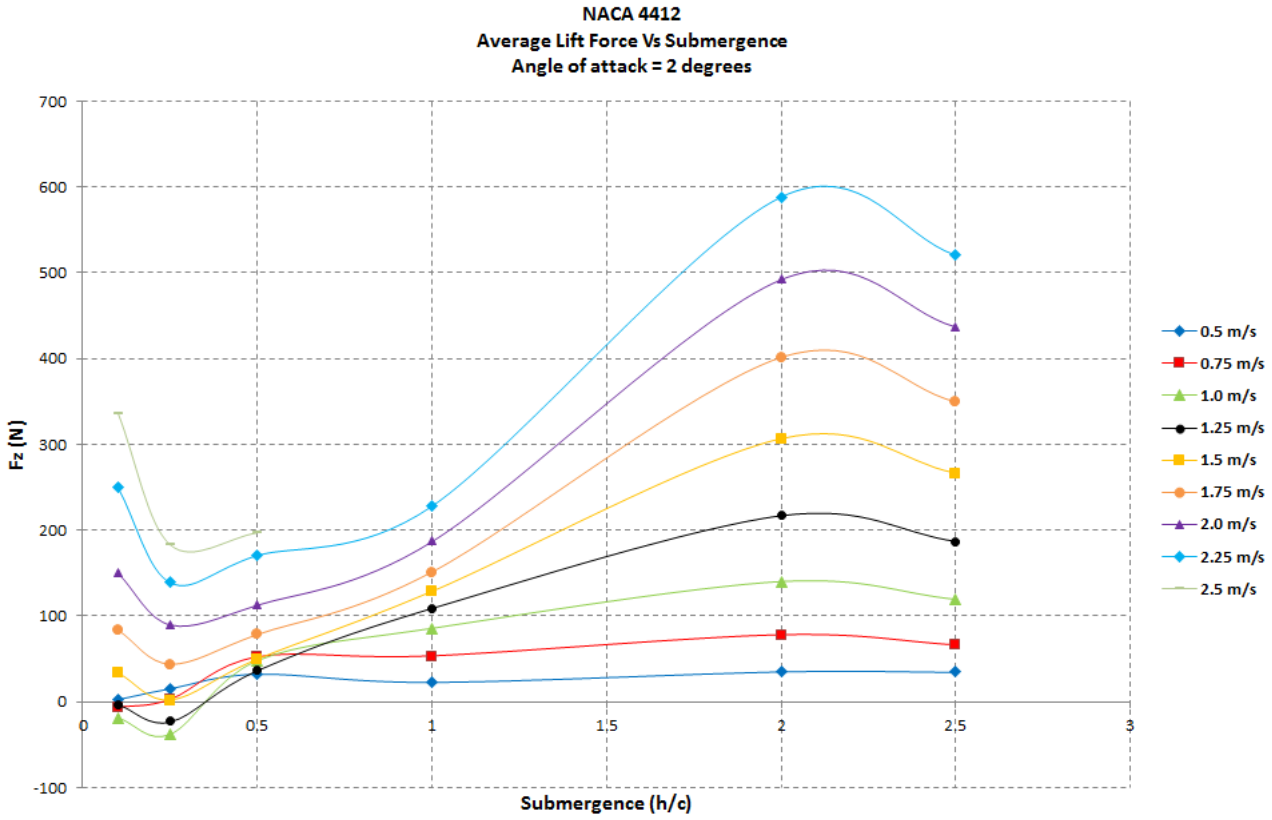

Figure 60: Lift generated plotted against the submergence for an angle of attack of 2 degrees for a range of velocities.

Here is presented the average lift force plotted against the submergence for an angle of attack of 2 degrees. All the curves follow the same trend, that trend is amplified at higher speeds. From 0.5 c to 2.0 c, the increase is linear, there is a dip after 2.0 c. At the other end of the curves, a dip in force and be seen at 0.25 c.

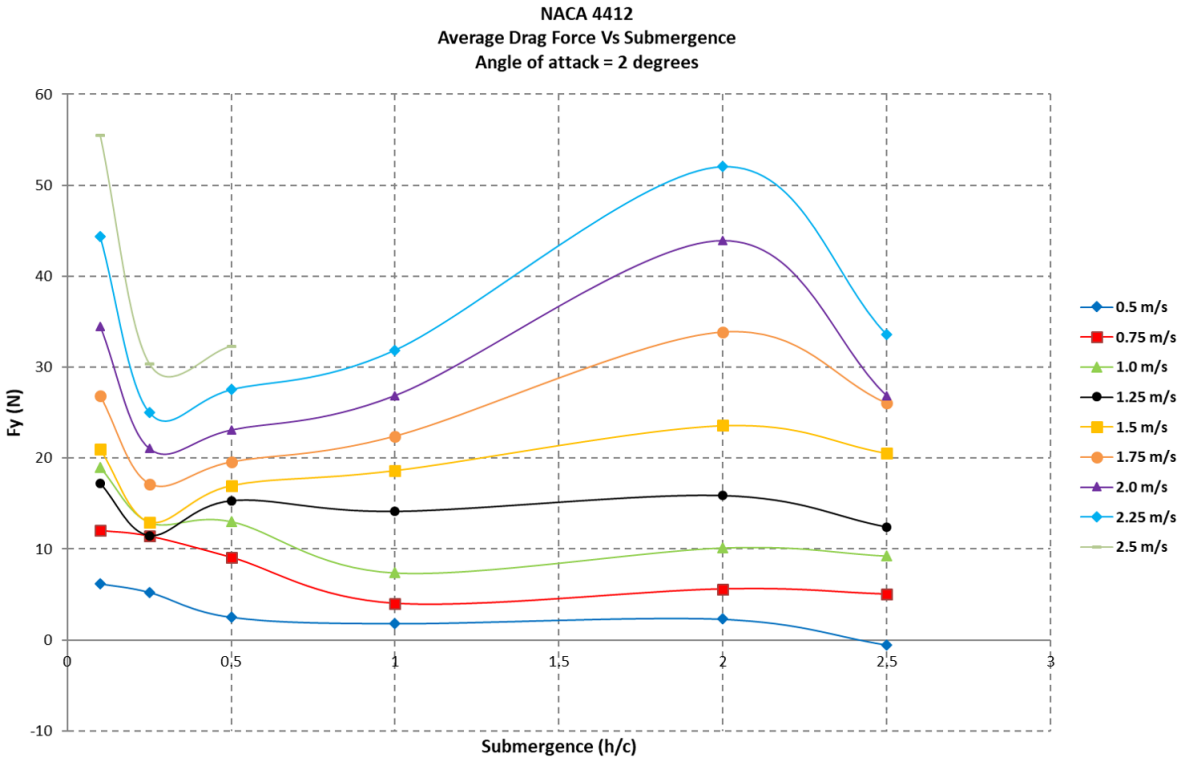

Figure 61: Drag generated plotted against the submergence for an angle of attack of 2 degrees for a range of velocities.

Here is presented the average drag force plotted against the submergence for an angle of attack of 2 degrees. All the curves follow the same trend, that trend is amplified at higher speeds. From 0.5 c to 2.0 c, the curves are relatively stable, after 2.0 c the drag forces tend to fall. At the other end of the curves, a dip in force and be seen at 0.25 c.

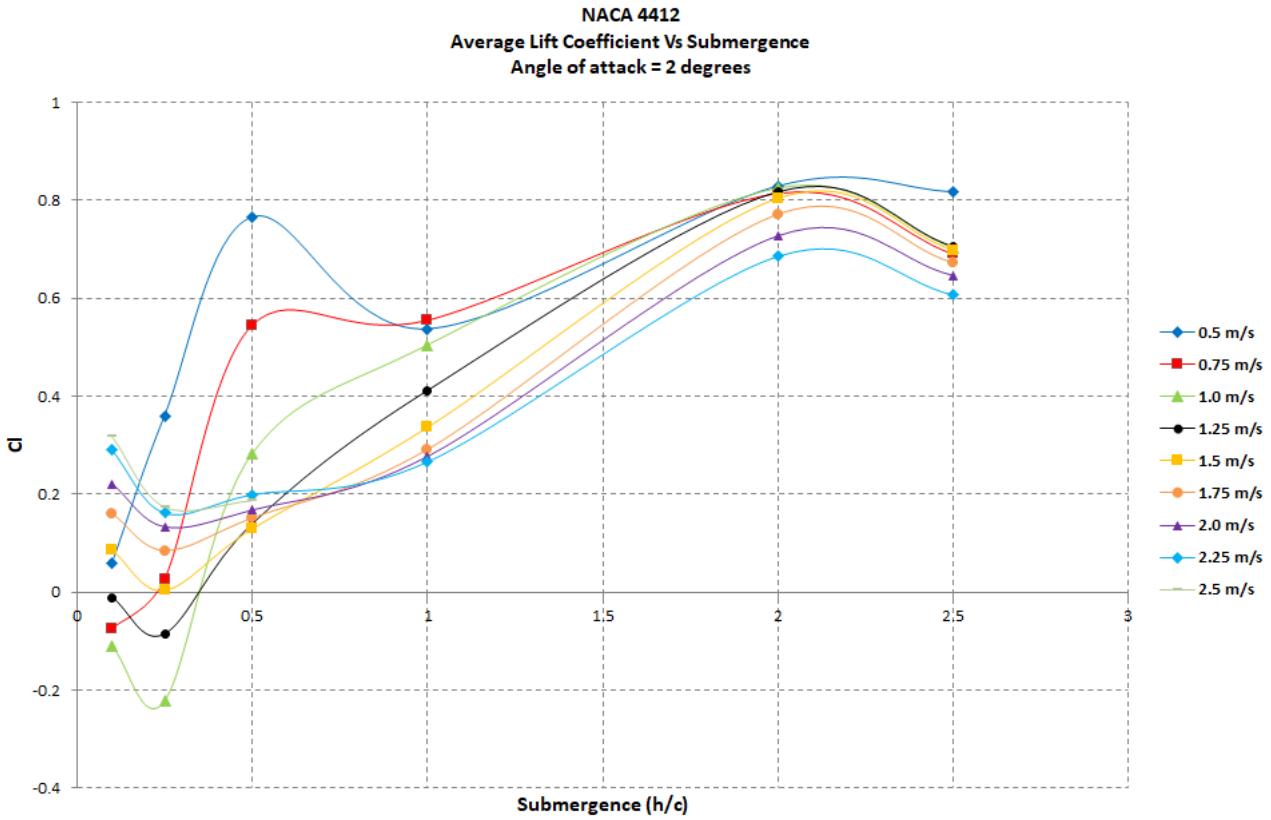

Figure 62: Lift coefficient generated plotted against the submergence for an angle of attack of 2 degrees for a range of velocities.

Here is presented the average lift coefficient plotted against the submergence for a range of velocities. A negative lift coefficient can be seen between a speed of 0.75 m/s to 1.25 m/s. A sharp increase can be seen for a speed of 0.5, 0.75 and 1.0 m/s from a submergence of 0.25 c to 0.5 c. A regular increase can then be seen between a submergence of 0.25 c and 2.0 c, after that a slight dip is seen from 2.0 c to 2.5 c at all speeds.

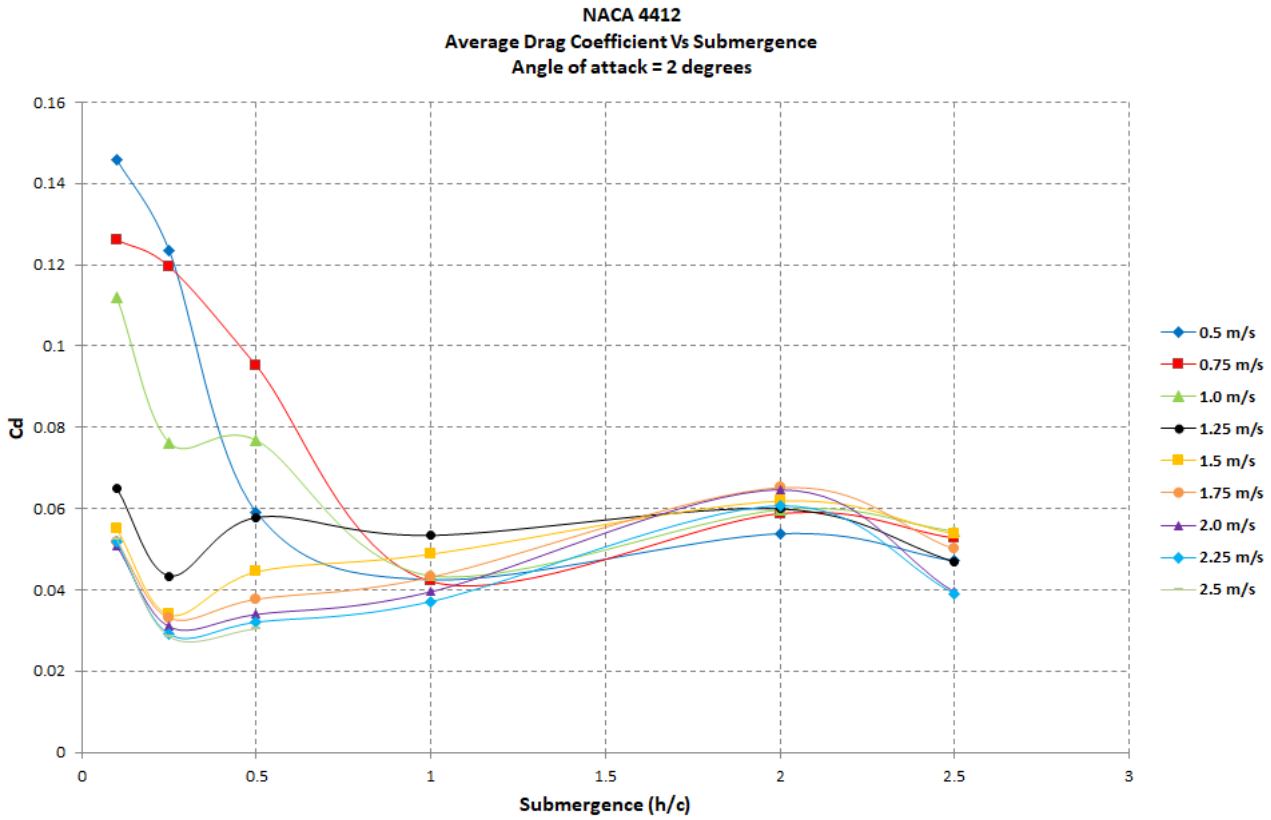

Figure 63: Drag coefficient generated plotted against the submergence for an angle of attack of 2 degrees for a range of velocities.

Here is presented the average drag coefficient plotted against the submergence for a a range of velocities. It can be seen that between 0.5 c and 2.0 c the drag coefficient increases slightly with both speed and submergence, from 2.0 c to 2.5 c a slight dip is seen at all speeds. At lower speeds and submergence the drag increases nearly five folds, as seen for 0.5, 0.75 and 1.0 m/s. There is also a slight dip in Drag coefficient at a submergence of 0.25 c.

8.2.1.5 Angle = 4 Degrees

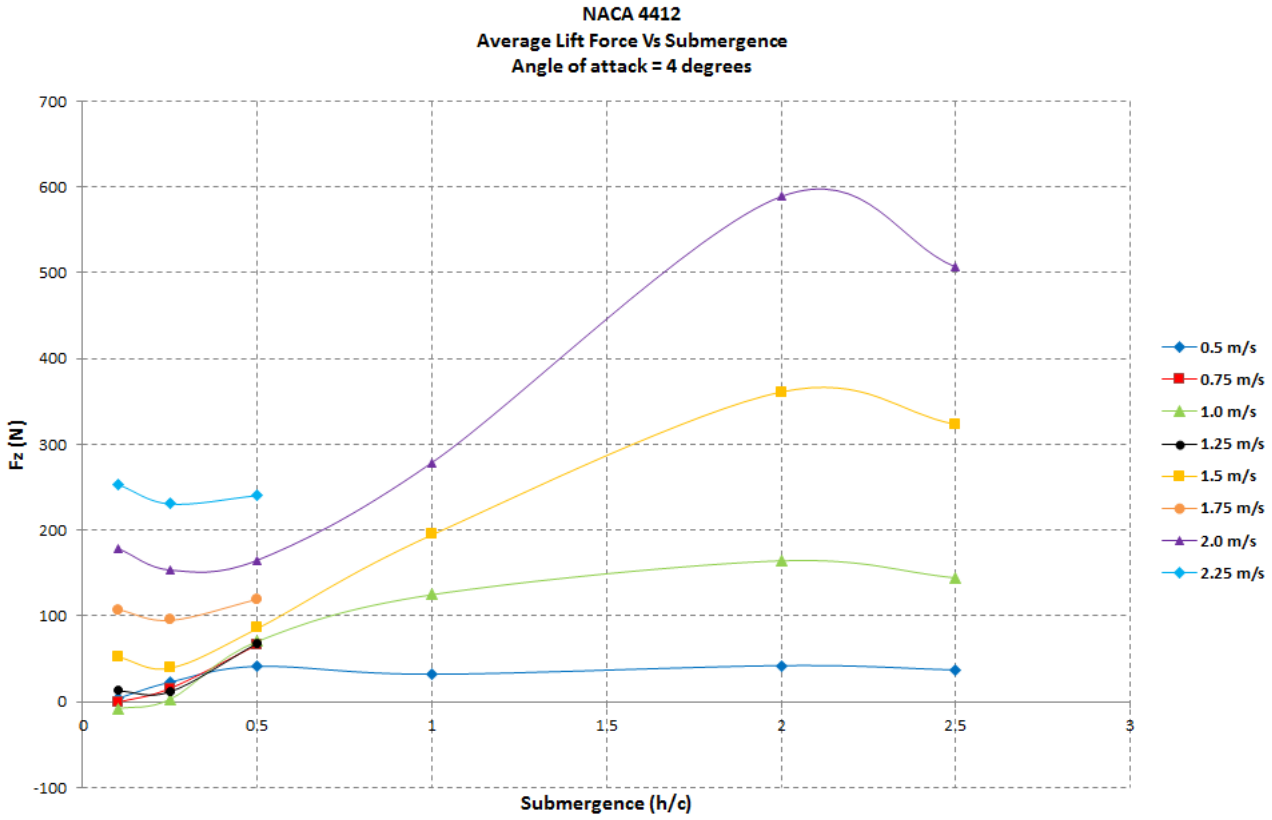

Figure 64: Lift generated plotted against the submergence for an angle of attack of 4 degrees for a range of velocities.

Here is presented the average lift force plotted against the submergence for an angle of attack of 4 degrees. For speeds of 0.5, 1.0, 1.5 and 2.0 m/s, the whole range of submergence is covered at other speeds only the shallow depths are covered. The same trend is shown as before with a slight dip at 0.25 c and then again from 2.0 c to 2.5 c.

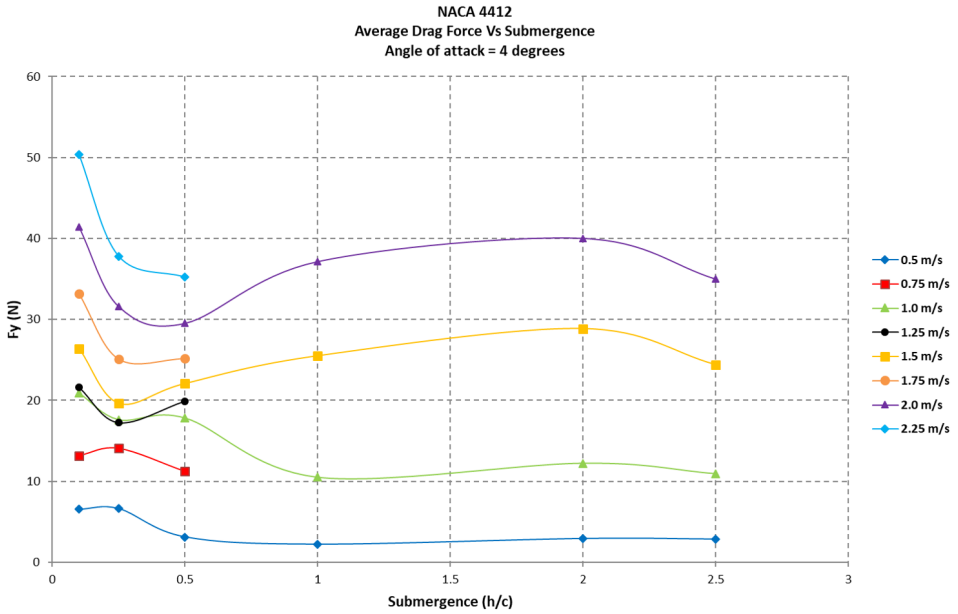

Figure 65: Drag generated plotted against the submergence for an angle of attack of 4 degrees for a range of velocities.

Here is presented the average drag force plotted against the submergence for an angle of attack of 4 degrees. For speeds of 0.5, 1.0, 1.5 and 2.0 m/s, the whole range of submergence is covered at other speeds only the shallow depths are covered. The same trend is shown as before with a slight dip at 0.25 c and then again from 2.0 c to 2.5 c.

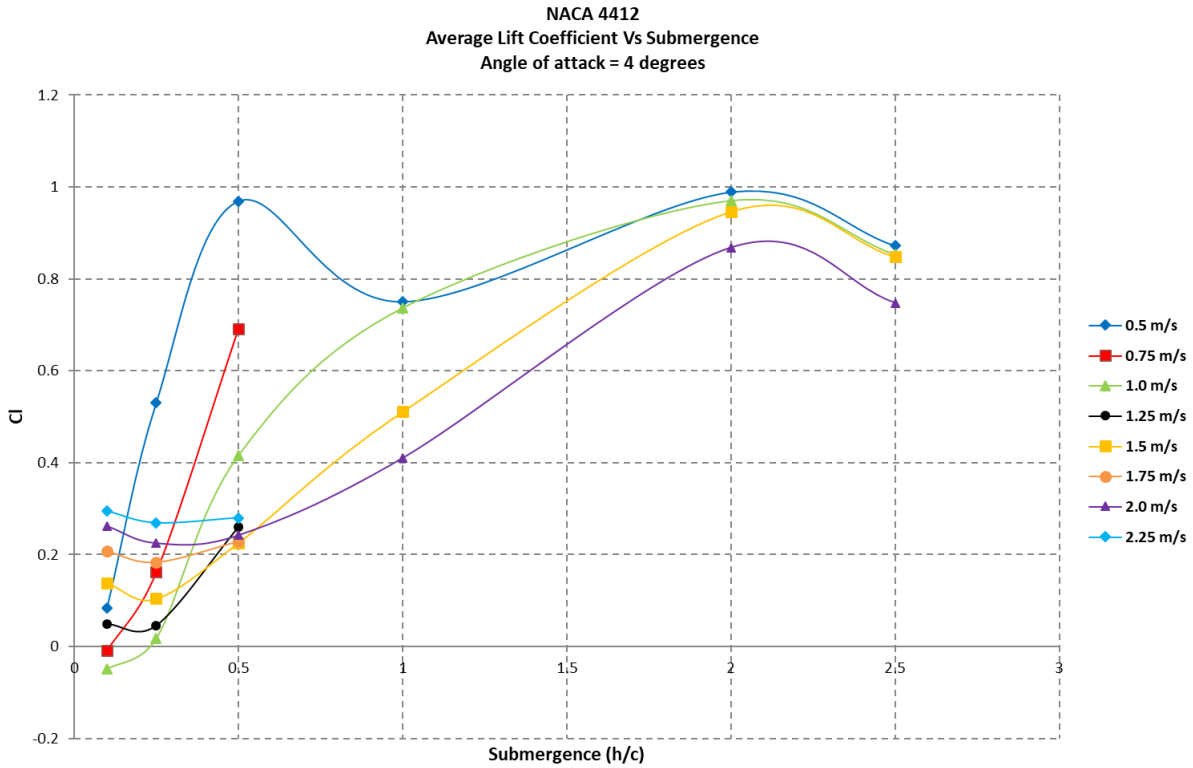

Figure 66: Lift coefficient generated plotted against the submergence for an angle of attack of 4 degrees for a range of velocities.

Here is presented the average lift coefficient plotted against the submergence for a range of velocities. A negative lift coefficient can be seen for a speed of 1.0 m/s. A sharp increase can be seen for a speed of 0.5 and 1.0 m/s between a submergence of 0.1 c to 0.5 c. A regular increase can then be seen between a submergence of 0.25 c and 2.0 c, after that a slight dip is seen from 2.0 c to 2.5 c at all speeds.

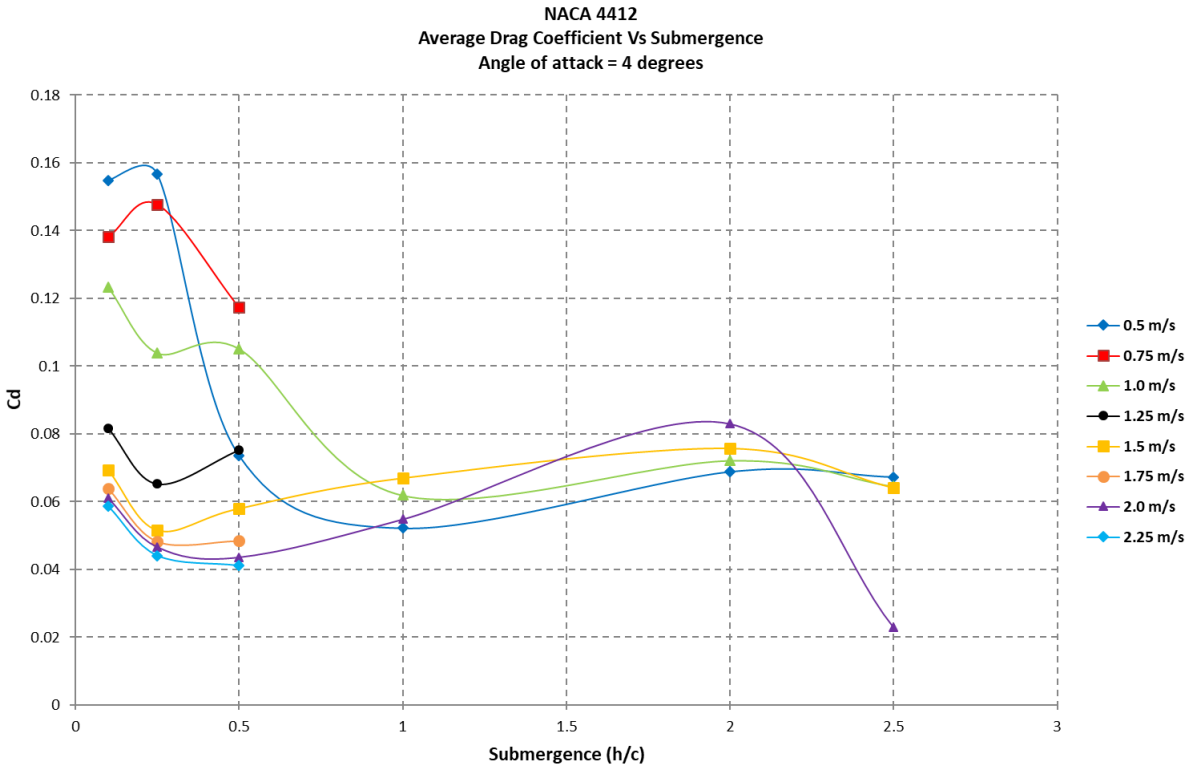

Figure 67: Drag coefficient generated plotted against the submergence for an angle of attack of 4 degrees for a range of velocities.

Here is presented the average drag coefficient plotted against the submergence for a a range of velocities. Between a submergence of 1.0 c and 2.5 c, the trend is mostly stable except for 2.0 m/s between 2.0 c and 2.5 c, as it decreases sharply.

8.2.1.6 Angle = 6 Degrees

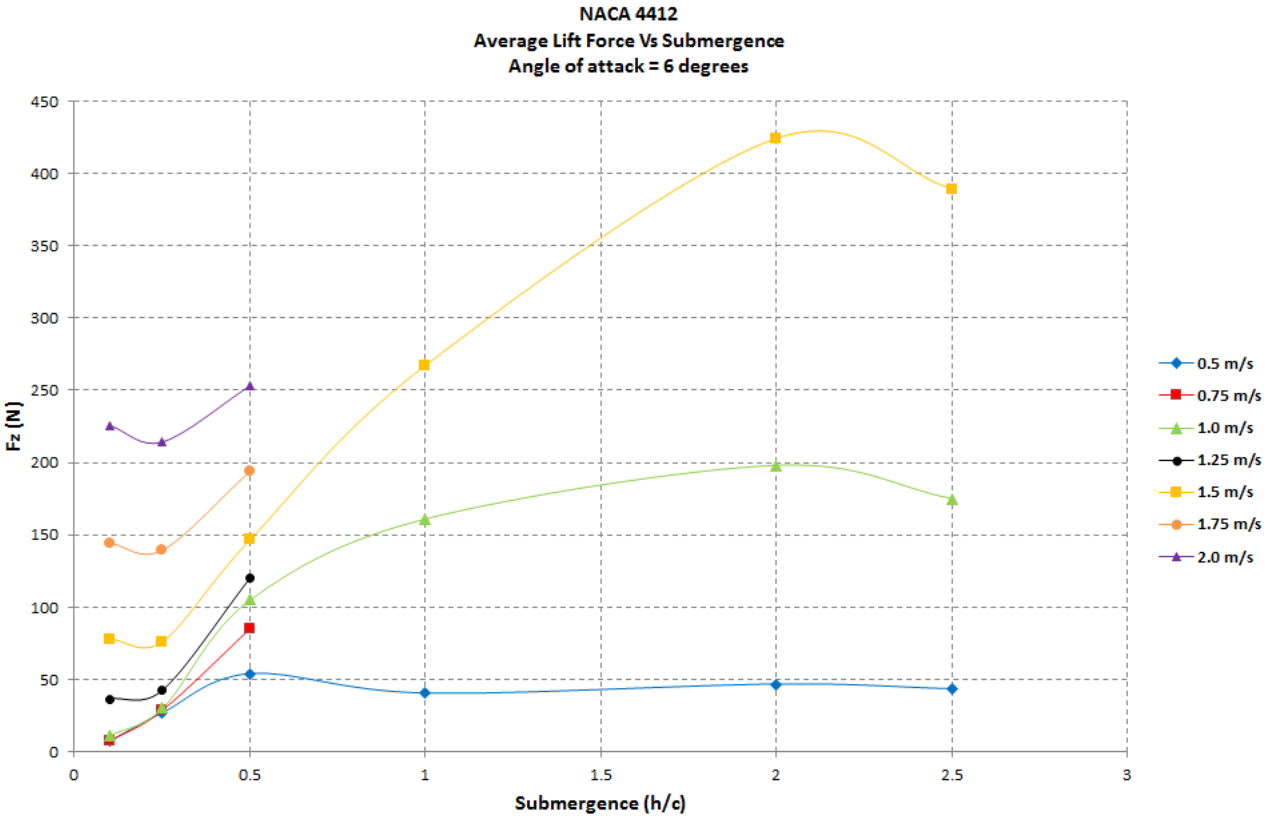

Figure 68: Lift generated plotted against the submergence for an angle of attack of 6 degrees for a range of velocities.

Here is presented the average lift force plotted against the submergence for an angle of attack of 6 degrees. For speeds of 0.5, 1.0 and 1.5 m/s the whole range of submergence is covered, at other speeds only the shallow depths are covered. The same trend is shown as before with a slight dip at 0.25 c and then again from 2.0 c to 2.5 c.

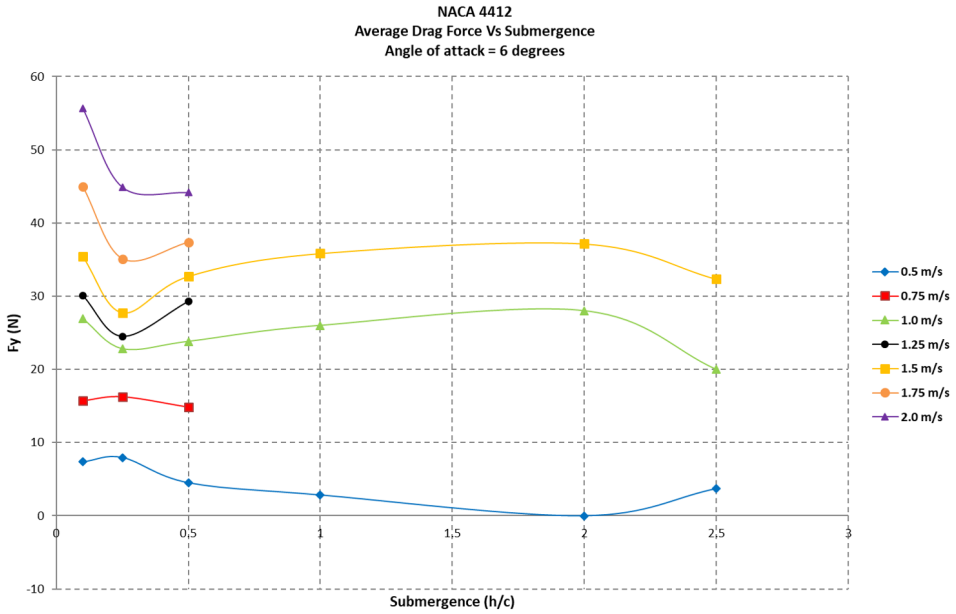

Figure 69: Drag generated plotted against the submergence for an angle of attack of 6 degrees for a range of velocities.

Here is presented the average drag force plotted against the submergence for an angle of attack of 6 degrees. For speeds of 0.5, 1.0, 1.5 and 2.0 m/s the whole range of submergence is covered at other speeds only the shallow depths are covered. The same trend is shown as before with a slight dip at 0.25 c and then again from 2.0 c to 2.5 c.

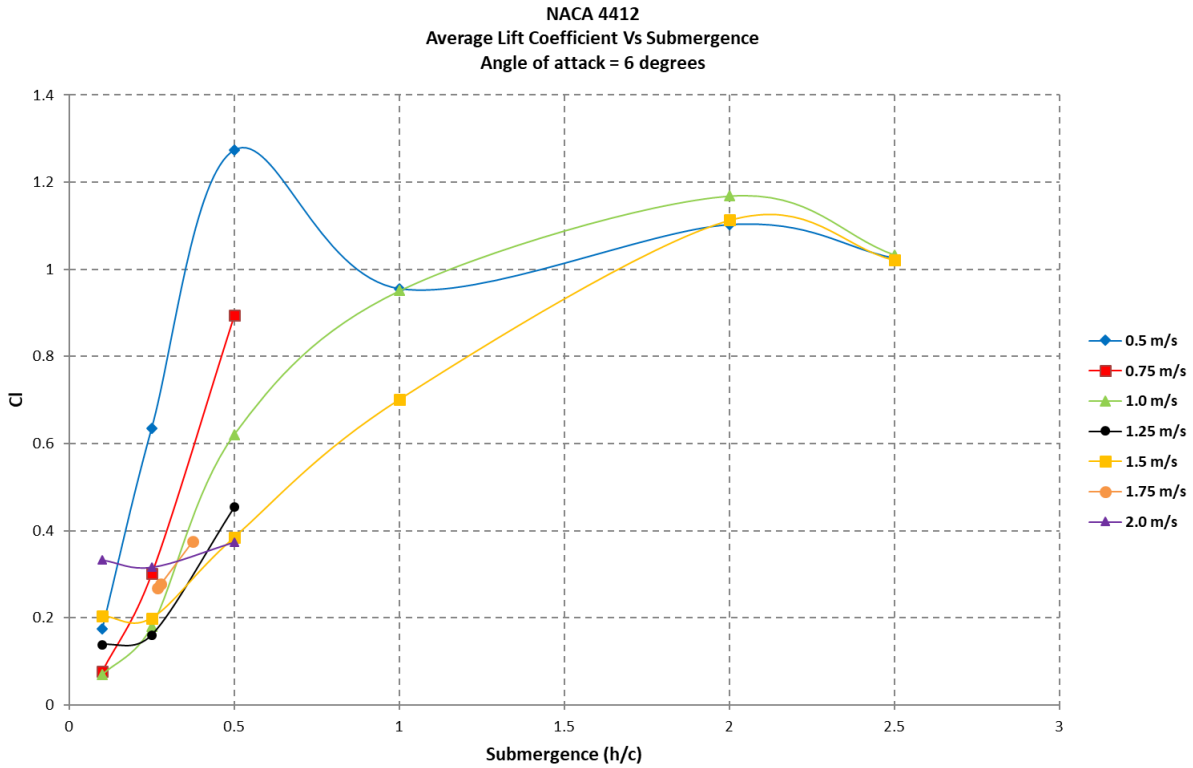

Figure 70: Lift coefficient generated plotted against the submergence for an angle of attack of 6 degrees for a range of velocities.

Here is presented the average lift coefficient plotted against the submergence for a range of velocities. A trend is presented in this figure : for a speed of 0.5 m/s, 1.0 m/s and 1.5 m/s the lift coefficient can be seen increasing with the submergence. There is also a increase for 0.5 m/s at 0.5 c.

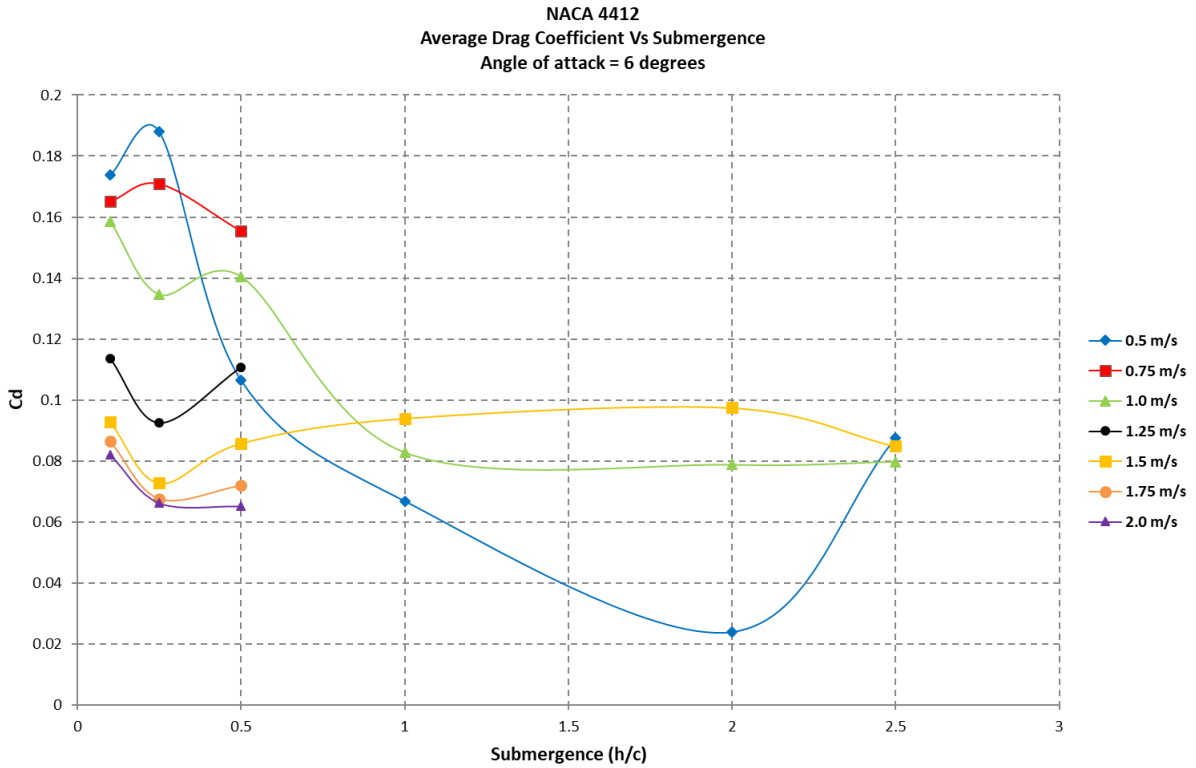

Figure 71: Drag coefficient generated plotted against the submergence for an angle of attack of 6 degrees for a range of velocities.

Here is presented the average drag coefficient plotted against the submergence for a a range of velocities. Between a submergence of 1.0 c and 2.5 c the trend is mostly linear except for a speed of 0.5 m/s which decreases sharply from 0.25 c to 2.0 c and also 1.0 m/s which decreases from 0.5 c to 1.0 c and then straighten outs.

8.2.1.7 Angle = 8 Degrees

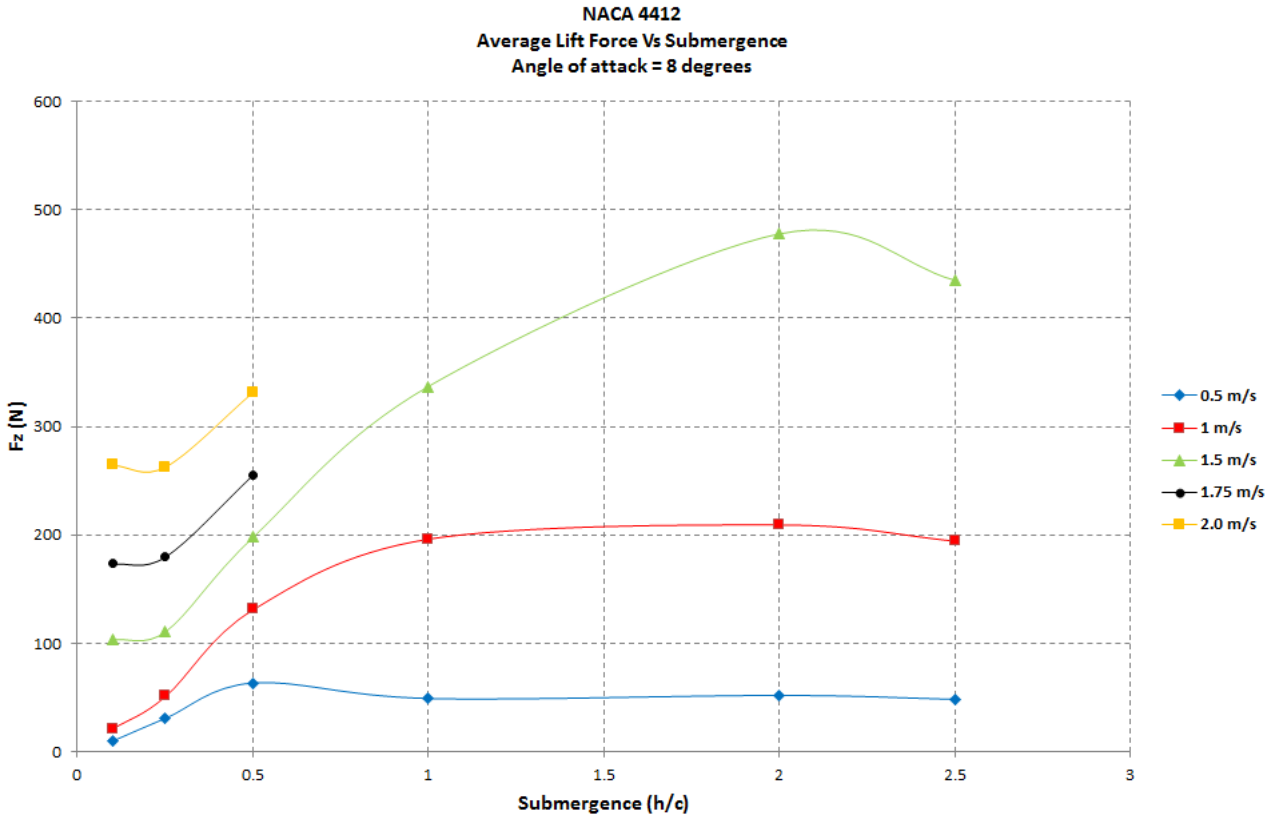

Figure 72: Lift generated plotted against the submergence for an angle of attack of 8 degrees for a range of velocities.

Here is presented the average lift force plotted against the submergence for an angle of attack of 8 degrees. For speeds of 0.5, 1.0 and 1.5 m/s the whole range of submergence is covered, at other speeds only the shallow depths are covered. There is an noticeable increase between 0.1 to 0.5 c. Then at 0.5 m/s and 1.0 m/s the lift force flatten out until 2.5 c. At a velocity of 1.5 m/s the lift force continues to grow until a submergence of 2.0 c after which it dips slightly.

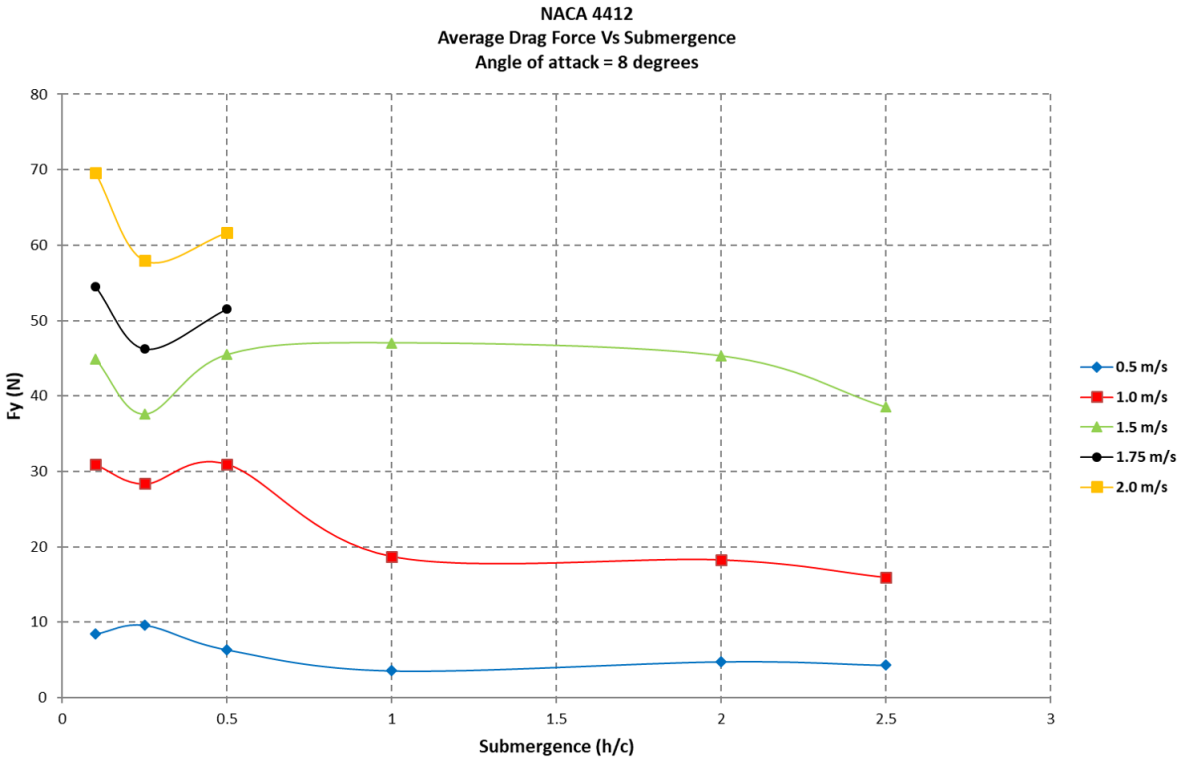

Figure 73: Drag generated plotted against the submergence for an angle of attack of 8 degrees for a range of velocities.

Here is presented the average drag force plotted against the submergence for an angle of attack of 8 degrees. For speeds of 0.5, 1.0 and 1.5 m/s the whole range of submergence is covered, at other speeds only the shallow depths are covered. The same trend is shown as before with a slight dip at 0.25c .

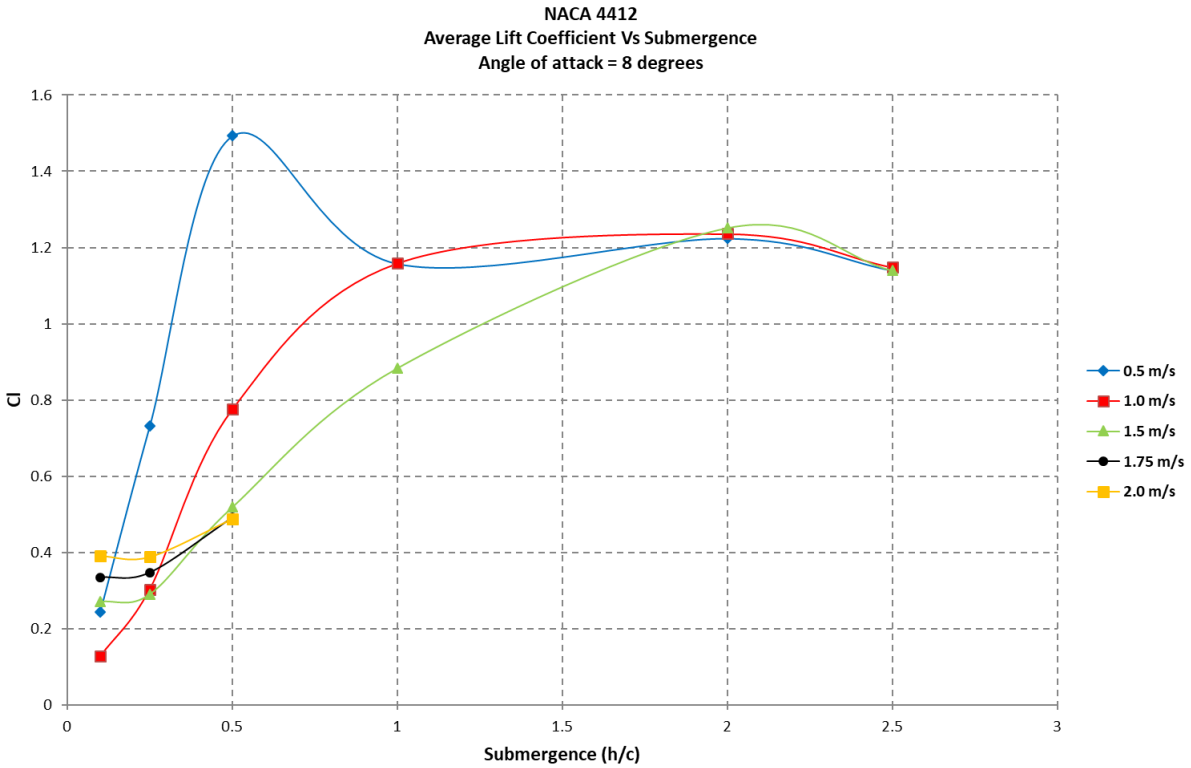

Figure 74: Lift coefficient generated plotted against the submergence for an angle of attack of 8 degrees for a range of velocities.

Here is presented the average lift coefficient plotted against the submergence for a range of velocities. A trend is presented in this figure : for a speed of 0.5 m/s, 1.0 m/s and 1.5 m/s the lift coefficient can be seen increasing with the submergence. There is also a increase for 0.5 m/s at 0.5 c.

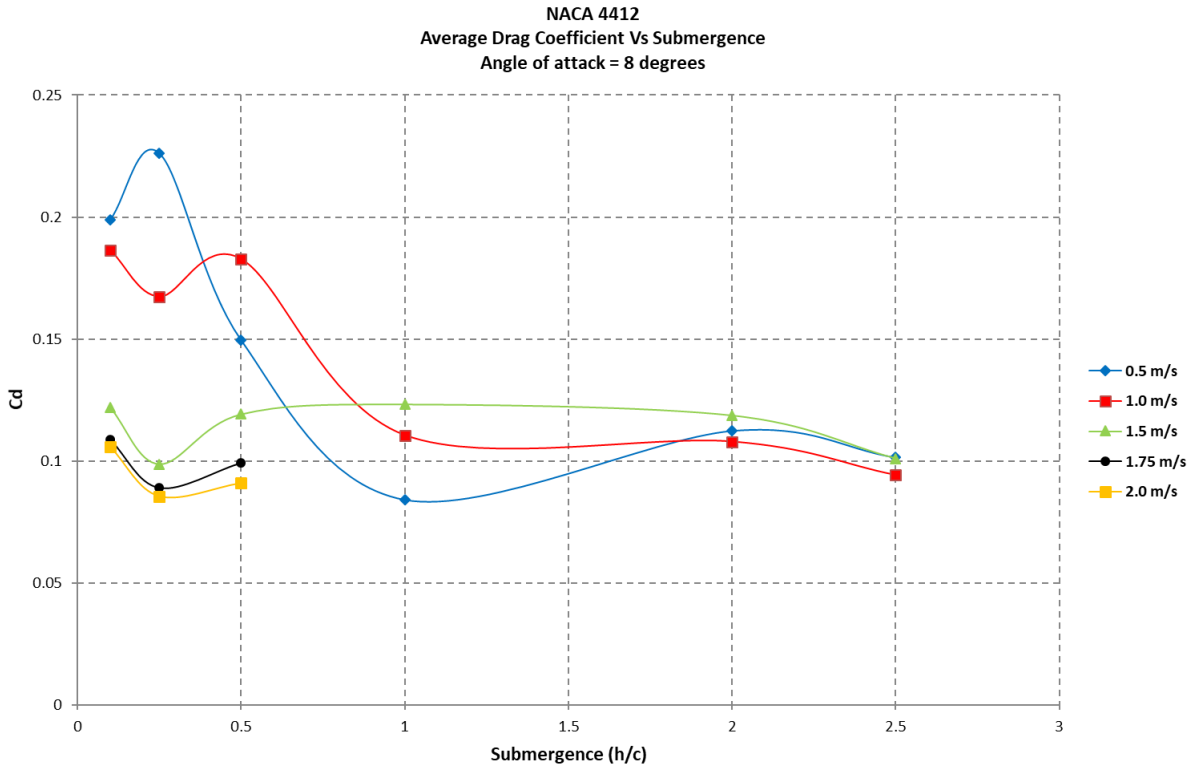

Figure 75: Drag coefficient generated plotted against the submergence for an angle of attack of 8 degrees for a range of velocities.

Here is presented the average drag coefficient plotted against the submergence for a a range of velocities. Between a submergence of 1.0 c and 2.5 c the trend is mostly linear.At a speed of 0.5 m/s and 1.0 m/s there is a sharp decrease until a submergence of 1.0 c.

8.2.1.8 Angle = 10 Degrees

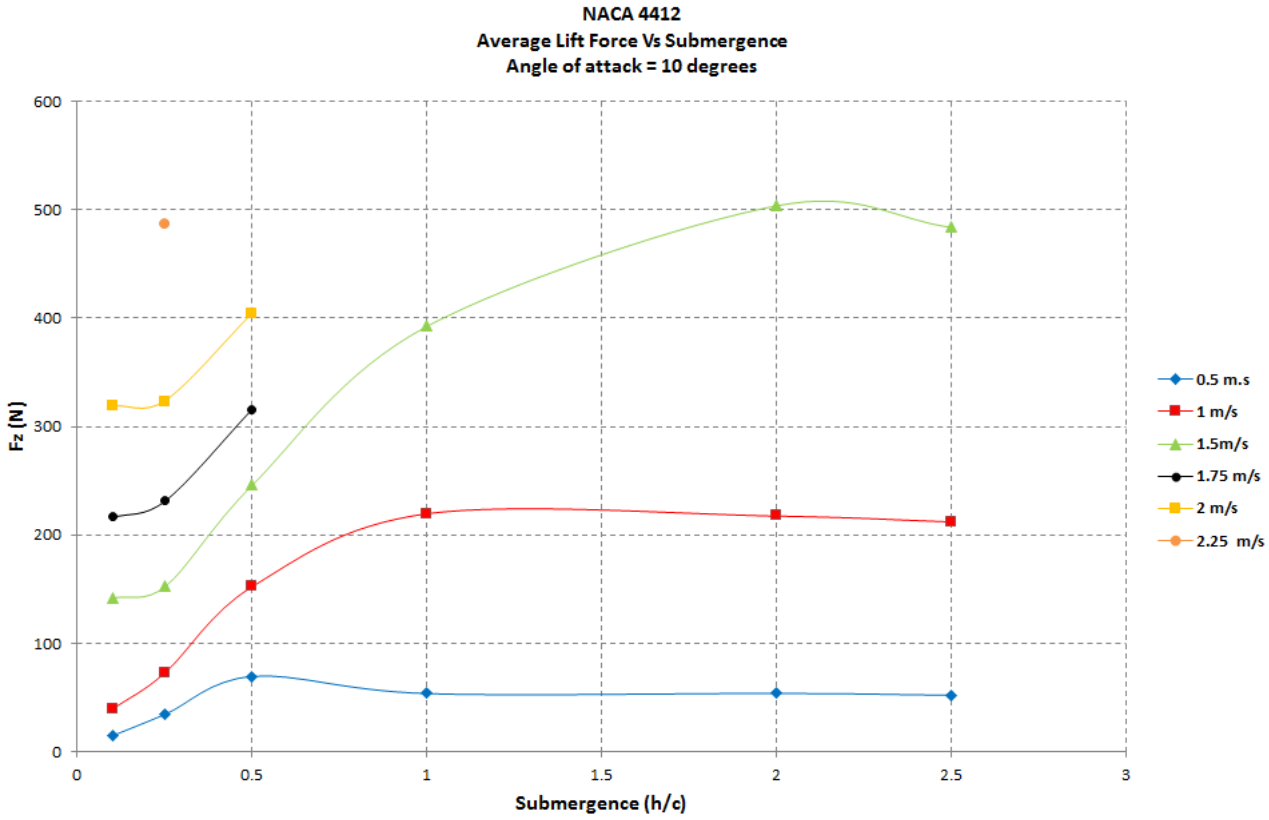

Figure 76: Lift generated plotted against the submergence for an angle of attack of 10 degrees for a range of velocities.

Here is presented the average lift force plotted against the submergence for an angle of attack of 10 degrees. For speeds of 0.5, 1.0 and 1.5 m/s the whole range of submergence is covered, at other speeds only the shallow depths are covered. There is an noticeable increase between 0.1 c to 0.5 c. Then at 0.5 m/s and 1.0 m/s the lift force flatten out until 2.5 c. At a velocity of 1.5 m/s the lift force continues to grow until a submergence of 2.0 c after which it dips slightly.

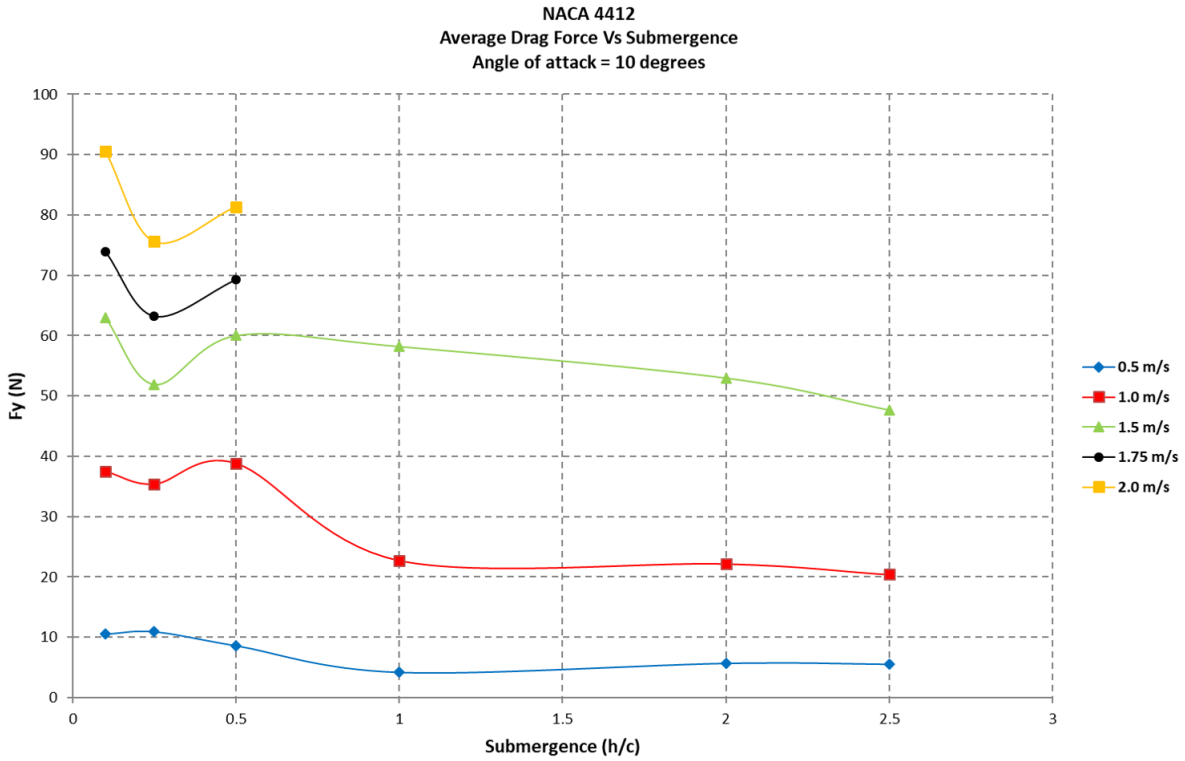

Figure 77: Drag generated plotted against the submergence for an angle of attack of 10 degrees for a range of velocities.

Here is presented the average drag force plotted against the submergence for an angle of attack of 10 degrees. For speeds of 0.5, 1.0 and 1.5 m/s the whole range of submergence is covered, at other speeds only the shallow depths are covered. The same trend is shown as before with a slight dip at 0.25 c.

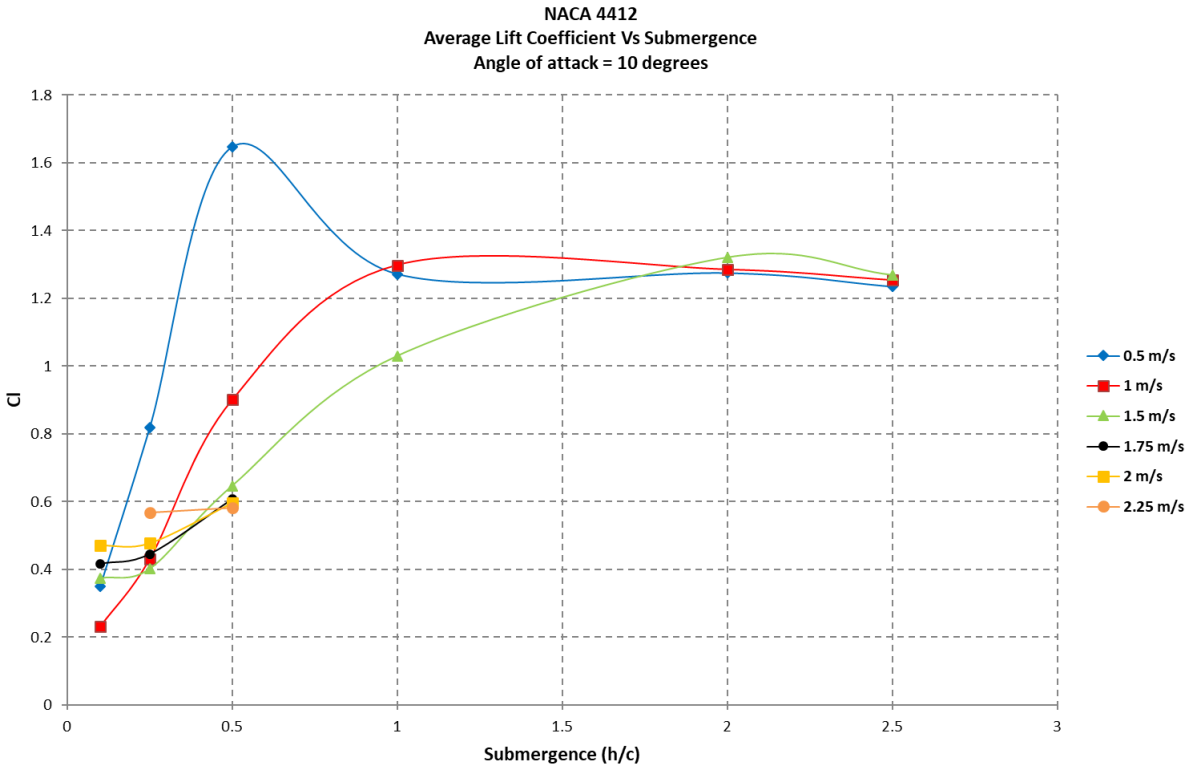

Figure 78: Lift coefficient generated plotted against the submergence for an angle of attack of 10 degrees for a range of velocities.

Here is presented the average lift coefficient plotted against the submergence for a range of velocities. A trend is presented in this figure : for a speed of 0.5 m/s, 1.0 m/s and 1.5 m/s the lift coefficient can be seen increasing with the submergence. There is also a increase for 0.5 m/s at 0.5 c.

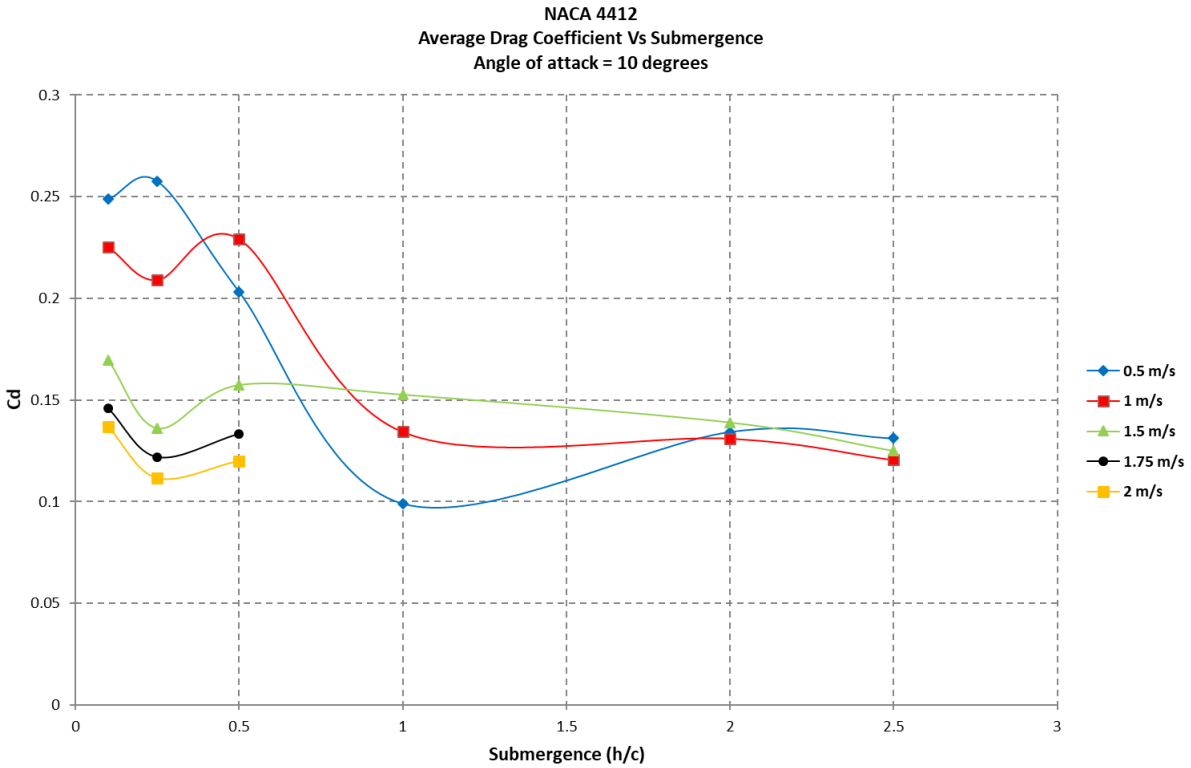

Figure 79: Drag coefficient generated plotted against the submergence for an angle of attack of 10 degrees for a range of velocities.

Here is presented the average drag coefficient plotted against the submergence for a a range of velocities. Between a submergence of 1.0 c and 2.5 c the trend is mostly linear. At a speed of 0.5 m/s and 1.0 m/s there is a sharp decrease until a submergence of 1.0 c. A slight dip at a submergence of 0.25 c for all speeds except 0.5 m/s can also be seen.

8.2.1.9 Conclusions

At all angles, two dips are seen one at 0.25c and another from 2.0c. There is no data point for a submergence greater than 2.5 c, making an extrapolation on the trend of the curves is impossible. The dip in lift forces and lift coefficient could be due to the effect of the tank floor.

8.2.2 Effect of depth

8.2.2.1 h/c = 2.5

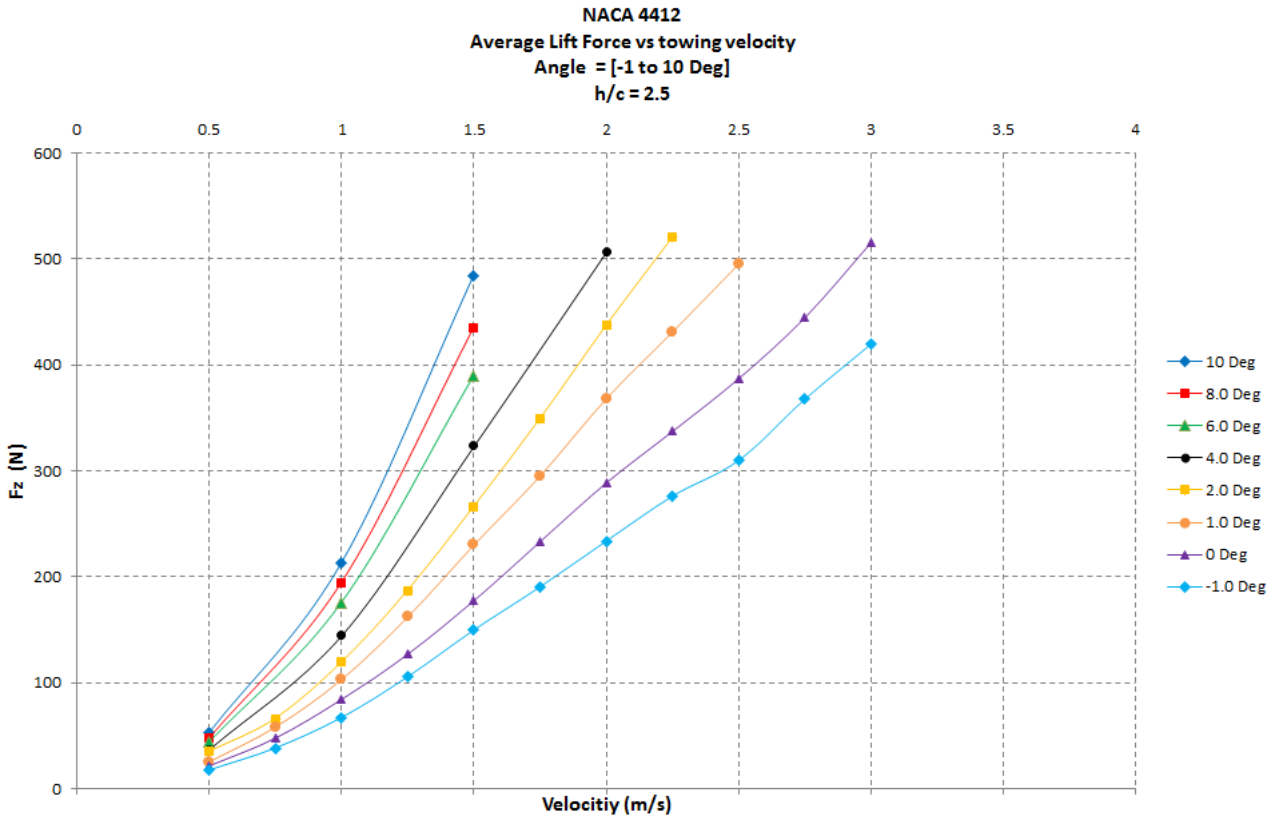

Figure 80: Lift generated plotted against the velocity for a submergence of 2.5 c for a range of angles of attack.

Here is presented the average lift force plotted against the velocity for a range of angles of attack. Here the curves follow the same trend of what is expected. A higher force for higher angles of attack and greater speed.

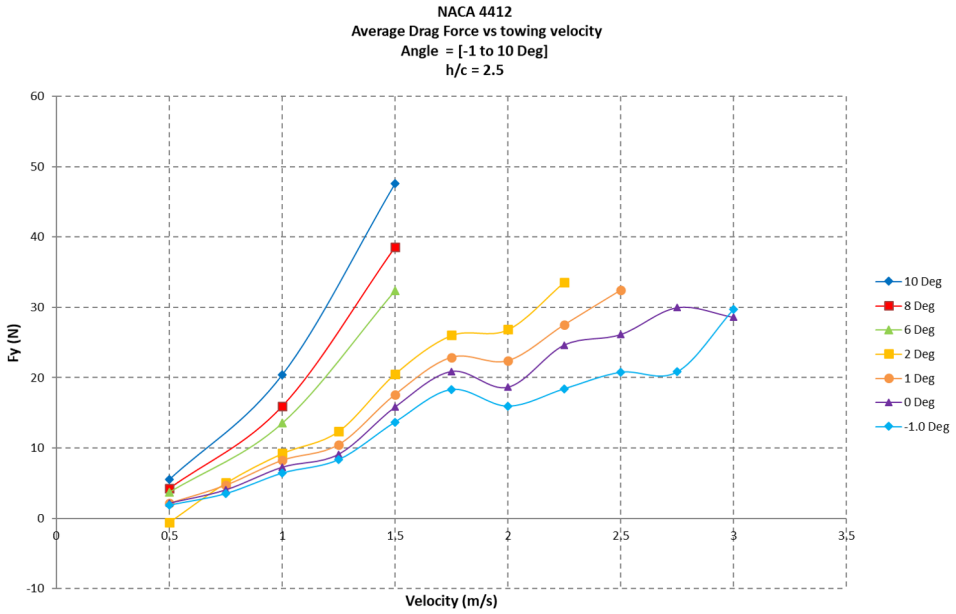

Figure 81: Drag generated plotted against the velocity for a submergence of 2.5 c for a range of angles of attack.

Here is presented the average drag force plotted against the velocity for a range of angles of attack. Here the curves follow the same trend, the separation between the angles of attack of -1, 0 and 1 degrees is minimal, the separation is clearer from an angle of attack of 2 degrees. It can also be seen that the drag forces generated are higher at greater angles of attack and velocity.

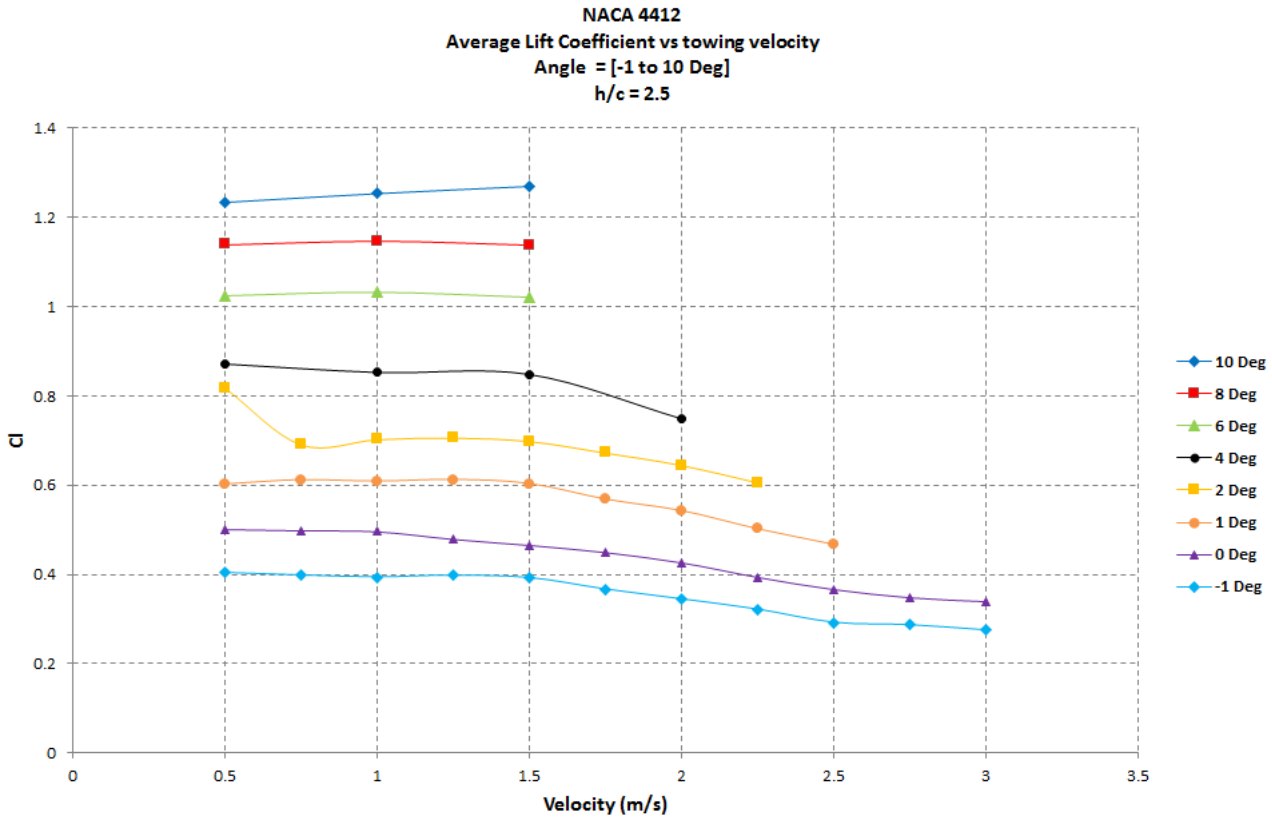

Figure 82: Lift coefficient generated plotted against the velocity for a submergence of 2.5 c for a range of angles of attack.

The figure above presents the average lift coefficient plotted against the velocity for a range of angles of attack. The trend here is that at lower angles and higher velocities the lift coefficient stays reasonably stable.

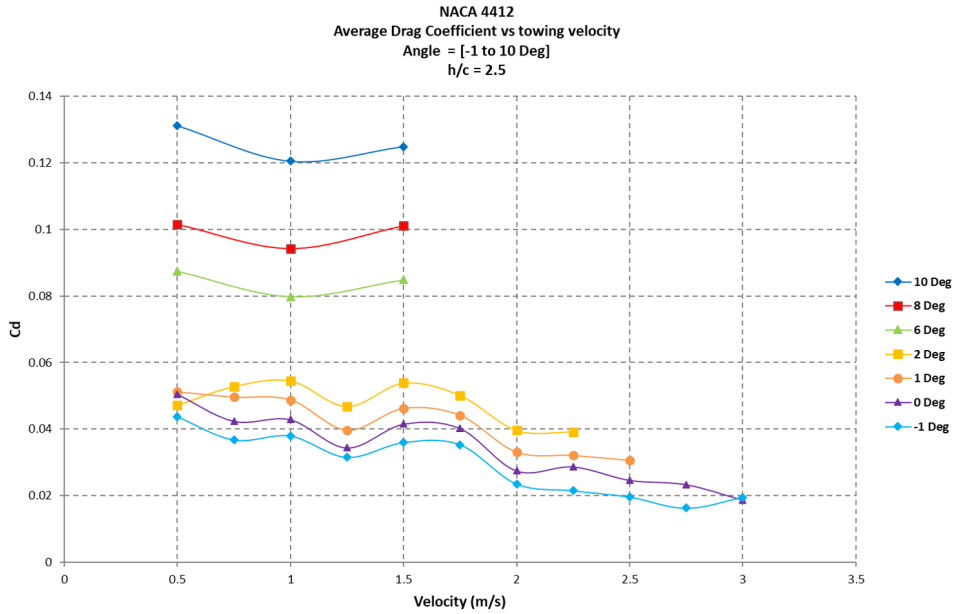

Figure 83: Drag coefficient generated plotted against the velocity for a submergence of 2.5 c for a range of angles of attack.

The figure above presents the average drag coefficient plotted against the velocity for a range of angles of attack. At higher angles (10, 8 and 6 degrees), a slight dip is seen for a velocity of 1 m/s. At angles from 2 degrees, a slight decrease is seen at a velocity of 1.25 m/s, this could be due to the fact that a run was done at that velocity and angle and not at higher angles. After 1.5 m/s the Drag coefficient decreases across all angles of attack represented.

8.2.2.2 h/c = 2

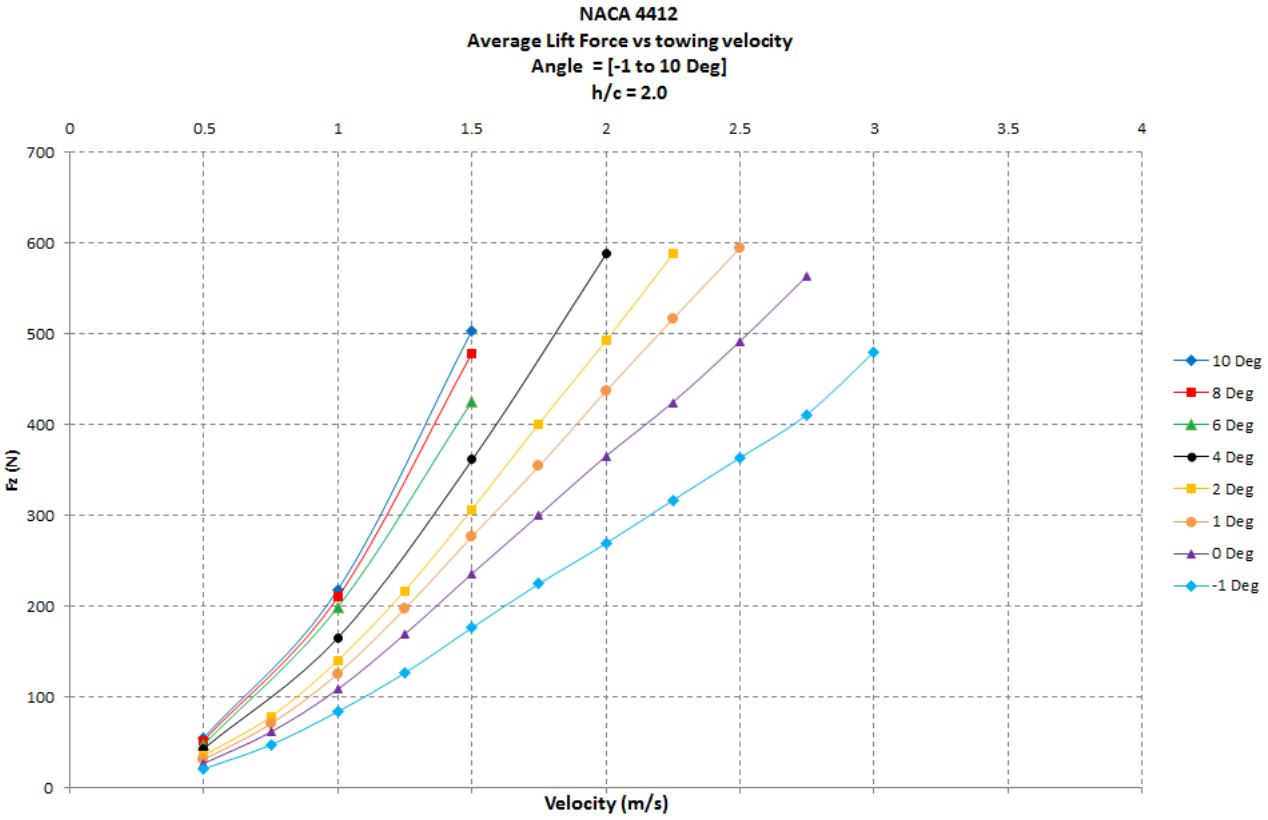

Figure 84: Lift generated plotted against the velocity for a submergence of 2.0 c for a range of angles of attack.

Here is presented the average lift force plotted against the velocity for a range of angles of attack. Here the curves follow the same trend of what is expected. A higher force for higher angles of attack and greater speed.

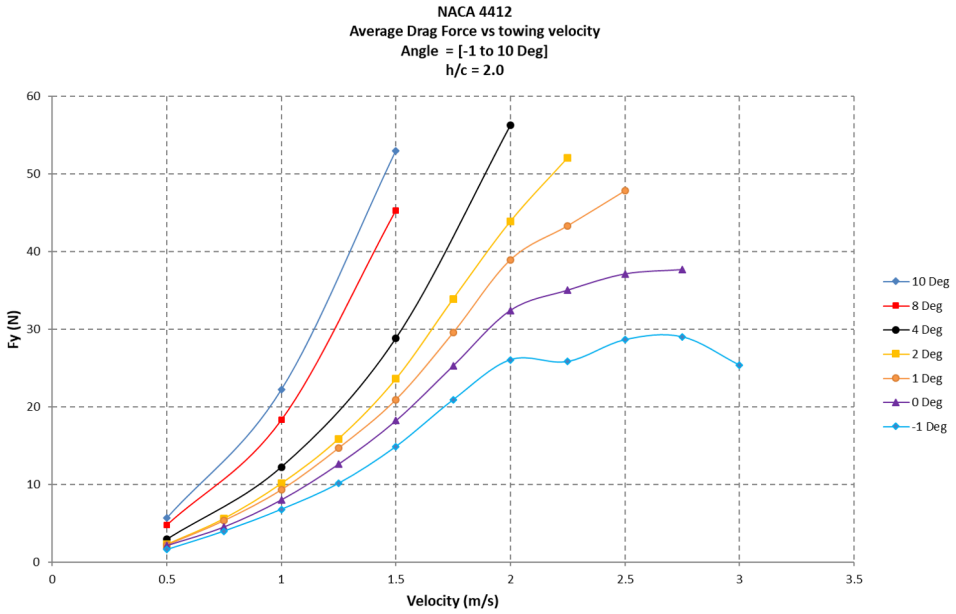

Figure 85: Drag generated plotted against the velocity for a submergence of 2.0 c for a range of angles of attack.

Here is presented the average drag force plotted against the velocity for a range of angles of attack. Here the curves follow the same trend, drag forces generated are higher at greater angles of attack and velocity.

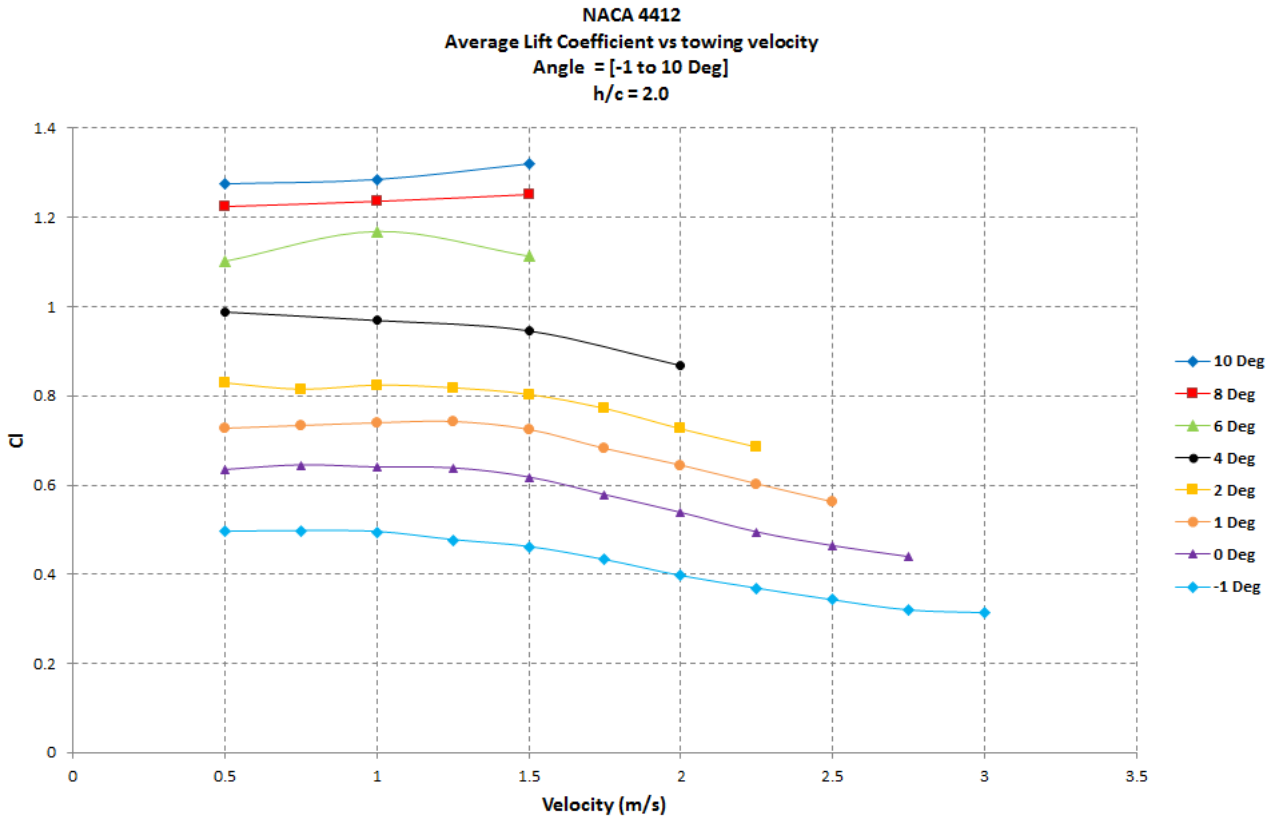

Figure 86: Lift coefficient generated plotted against the velocity for a submergence of 2.0 c for a range of angles of attack.

The figure above presents the average lift coefficient plotted against the velocity for a range of angles of attack. The trend here is that at lower angles and higher velocities, the lift coefficient decreases.

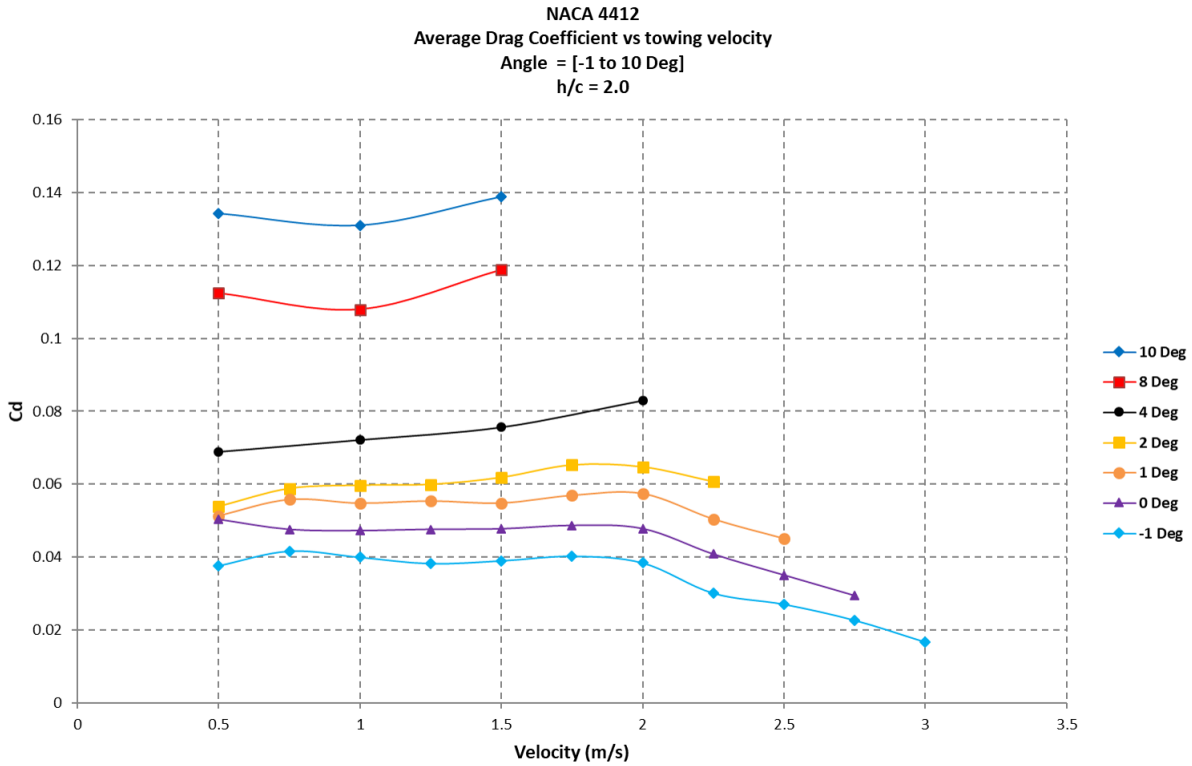

Figure 87: Drag coefficient generated plotted against the velocity for a submergence of 2.0 c for a range of angles of attack.

The figure above presents the average drag coefficient plotted against the velocity for a range of angles of attack. At higher angles (10 and 8 degrees), a slight dip is seen for a velocity of 1 m/s. At angles from 2 degrees from 2.0 m/s the drag coefficient decreases across all angles of attack represented. The outlier of the 6 degrees previously mentioned 85 is also represented.

8.2.2.3 h/c = 1

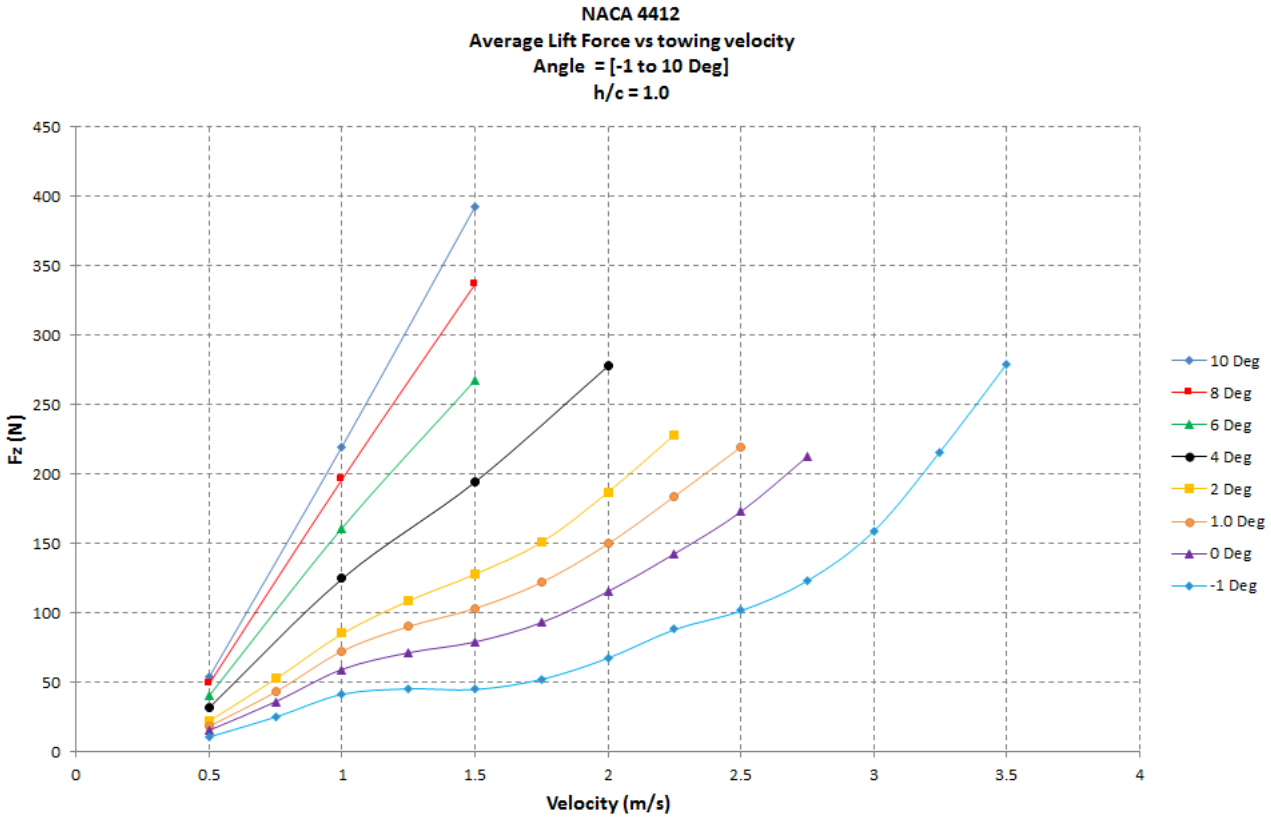

Figure 88: Lift generated plotted against the velocity for a submergence of 1.0 c for a range of angles of attack.

Here is presented the average lift force plotted against the velocity for a range of angles of attack. Tthe curves follow the same trend of what is expected.A higher force for higher angles of attack and greater speed. At smaller angles (-1 and 0 degrees), after a speed of 1.0 m/s the force rises slower than at lower angles.

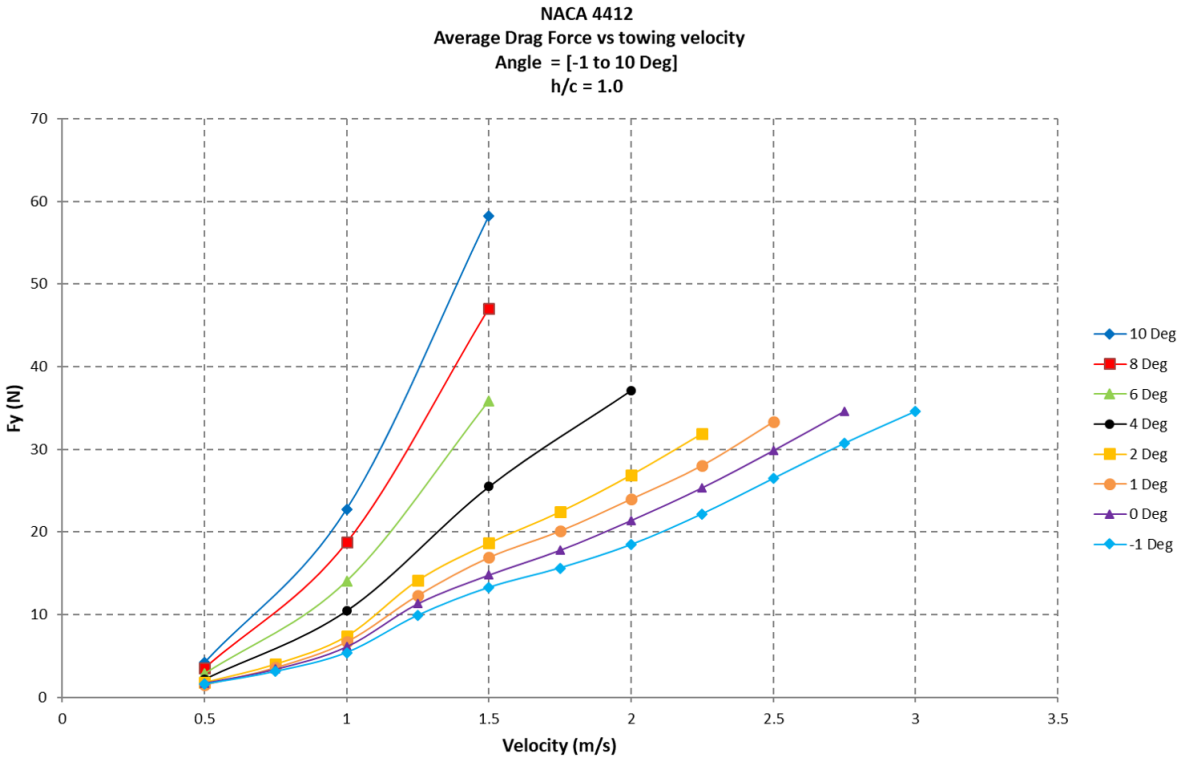

Figure 89: Drag generated plotted against the velocity for a submergence of 1.0 c for a range of angles of attack.

Here is presented the average drag force plotted against the velocity for a range of angles of attack. Here the curves follow the same trend, drag forces generated are higher at greater angles of attack and velocity.

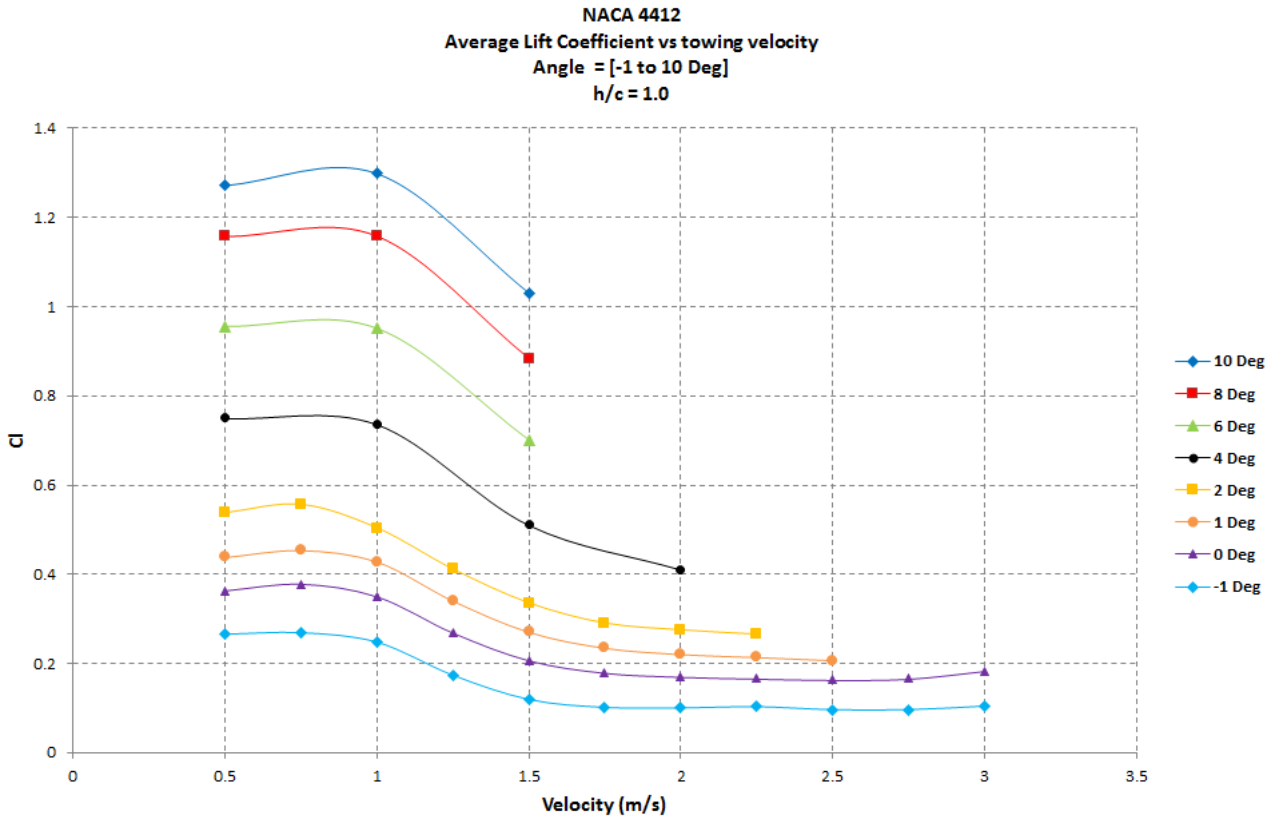

Figure 90: Lift coefficient generated plotted against the velocity for a submergence of 1.0 c for a range of angles of attack.

The figure above presents the average lift coefficient plotted against the velocity for a range of angles of attack. The trend here is that at lower angles and higher velocities, the drag coefficient decreases. A sharp decrease between 1.o and 1.5 m/s.

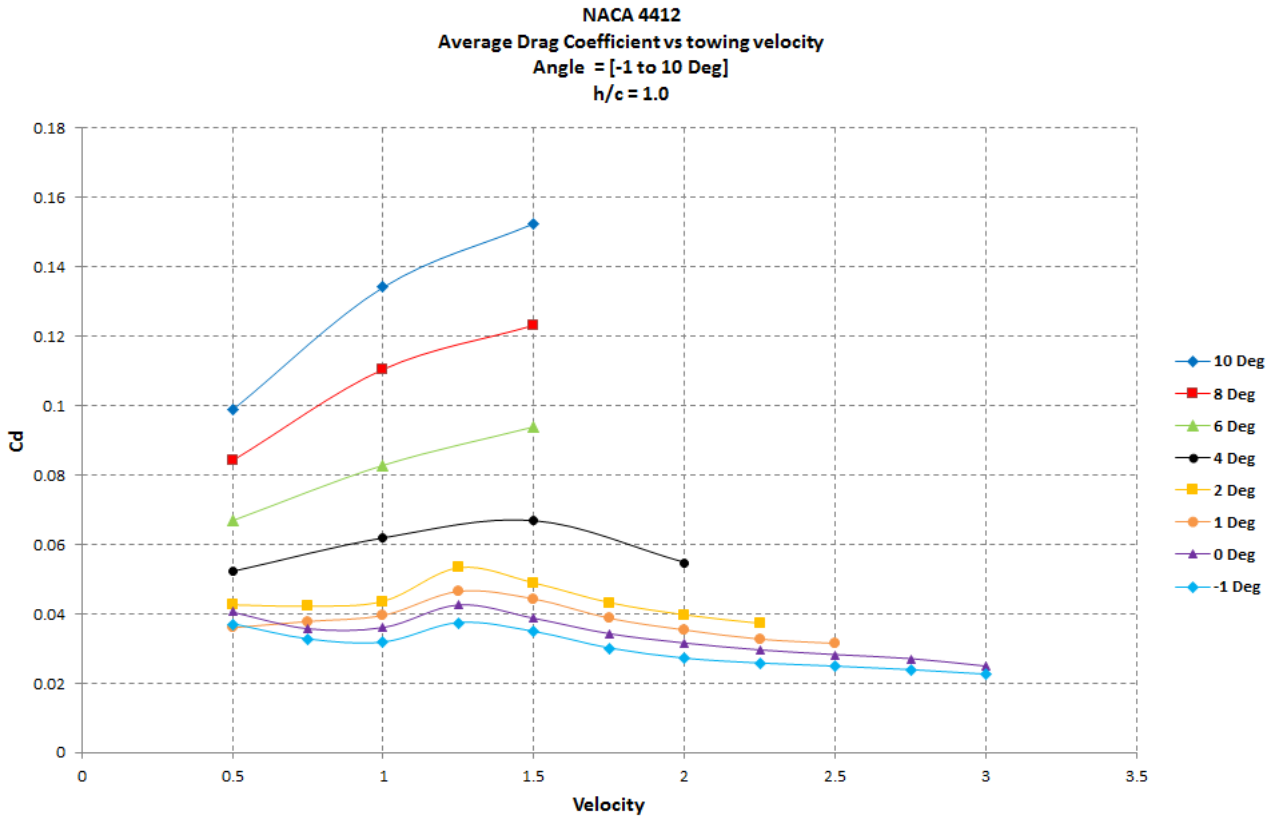

Figure 91: Drag coefficient generated plotted against the velocity for a submergence of 1.0 c for a range of angles of attack.

The figure above presents the average drag coefficient plotted against the velocity for a range of angles of attack. At angles from 2 degrees, the curves peak at 1.25 m/s and then decline.

8.2.2.4 h/c = 0.5

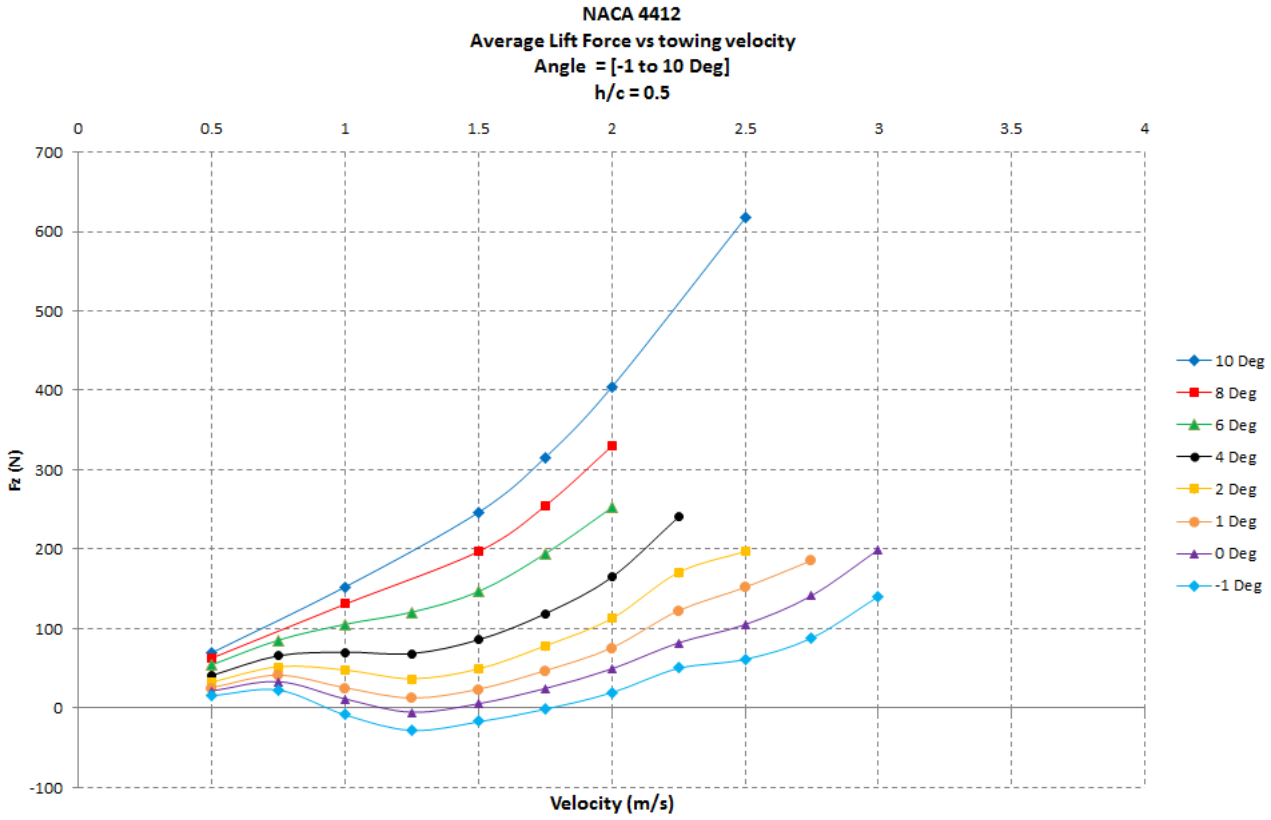

Figure 92: Lift generated plotted against the velocity for a submergence of 0.5 c for a range of angles of attack.

Here is presented the average lift force plotted against the velocity for a range of angles of attack. Here the curves follow the same trend. A higher force for higher angles of attack and greater speed. From an angle of 4 degrees we see a slight dip at 1.25 m/s, then the forces continue to be greater. At smaller angles (-1 and 0 degrees), between a speed of 1.0 and 1.75 m/s negative lift forces are produced.

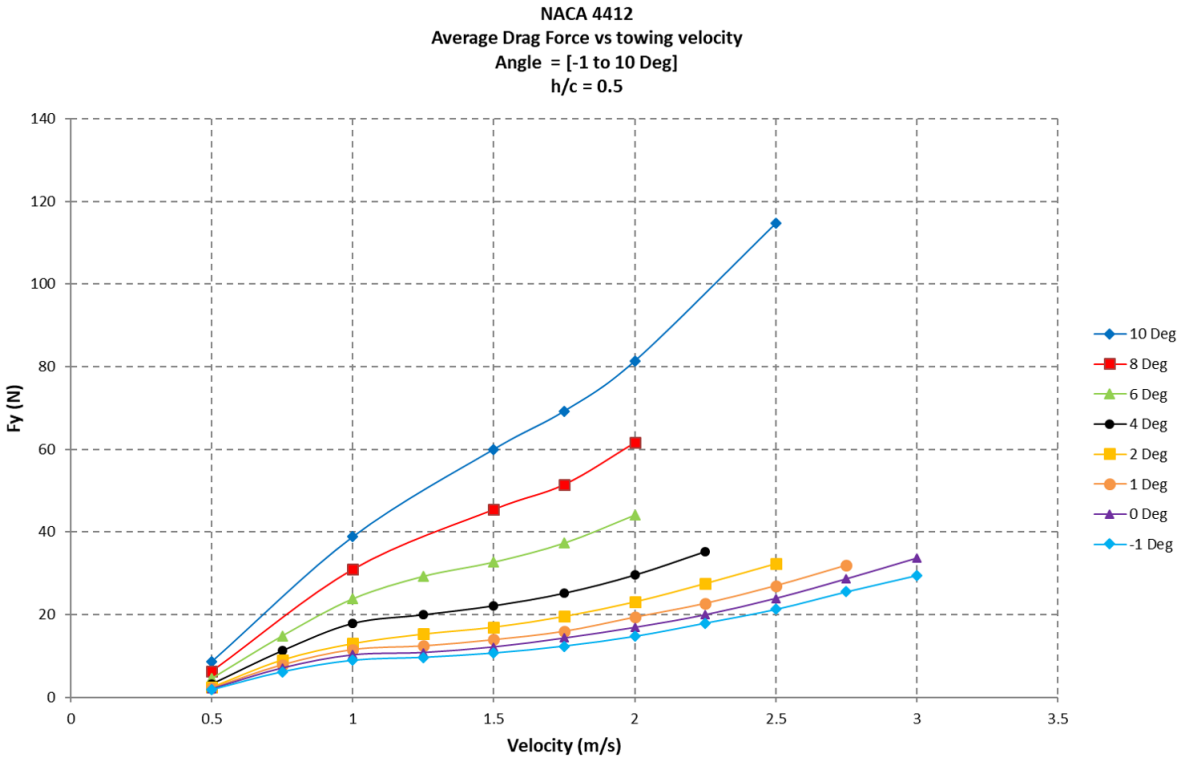

Figure 93: Drag generated plotted against the velocity for a submergence of 0.5 c for a range of angles of attack.

Here is presented the average drag force plotted against the velocity for a range of angles of attack. Here the curves follow the same trend, the separation between the angles of attack of -1, 0 and 1 degrees is minimal, the separation is clearer from an angle of attack of 2 degrees. It can also be seen that the drag forces generated are higher at greater angles of attack and velocity.

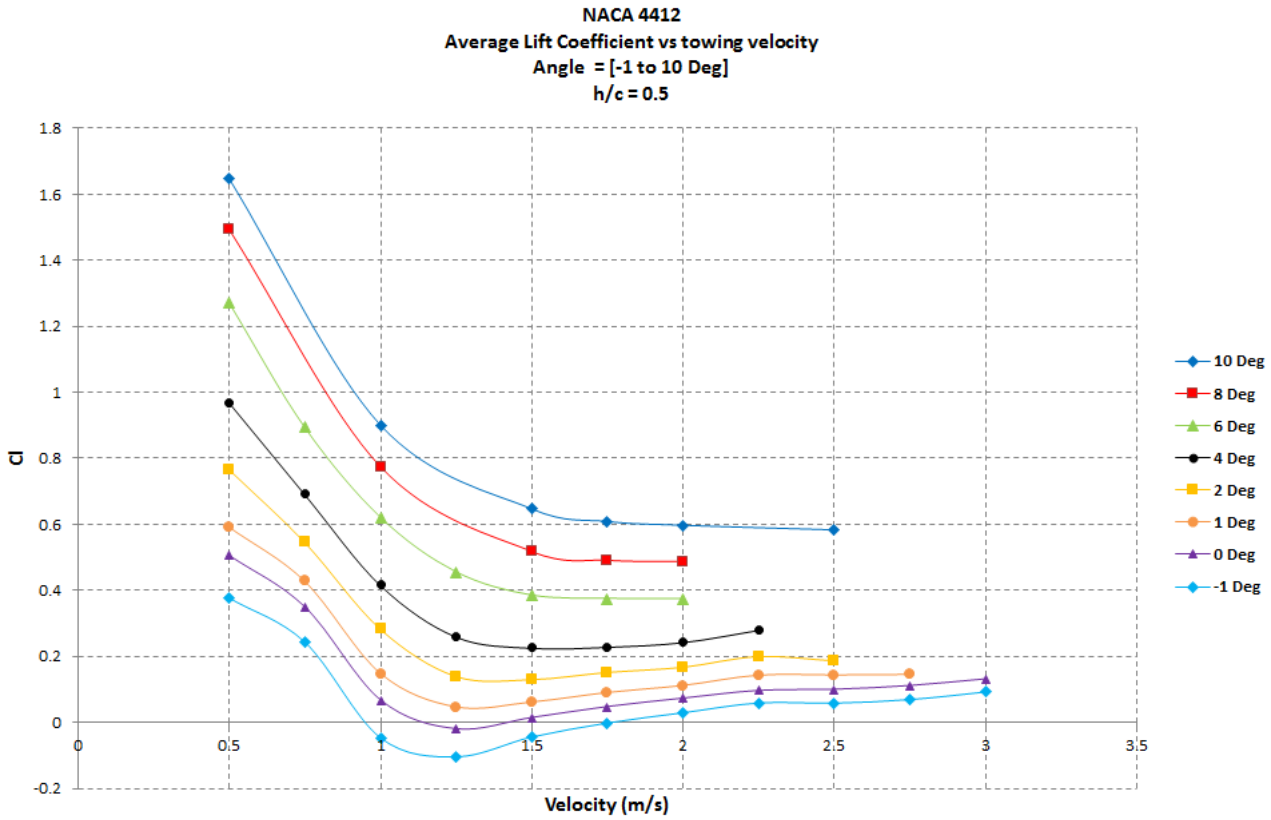

Figure 94: Lift coefficient generated plotted against the velocity for a submergence of 0.5 c for a range of angles of attack.

The figure above presents the average lift coefficient plotted against the velocity for a range of angles of attack. What is seen here is a sharp decline from a maximum value at 0.5 m/s. It declines rapidly until a speed of 1.5 m/s, where it straighten outs. The negative lifts seen in Figure 92 are also seen here.

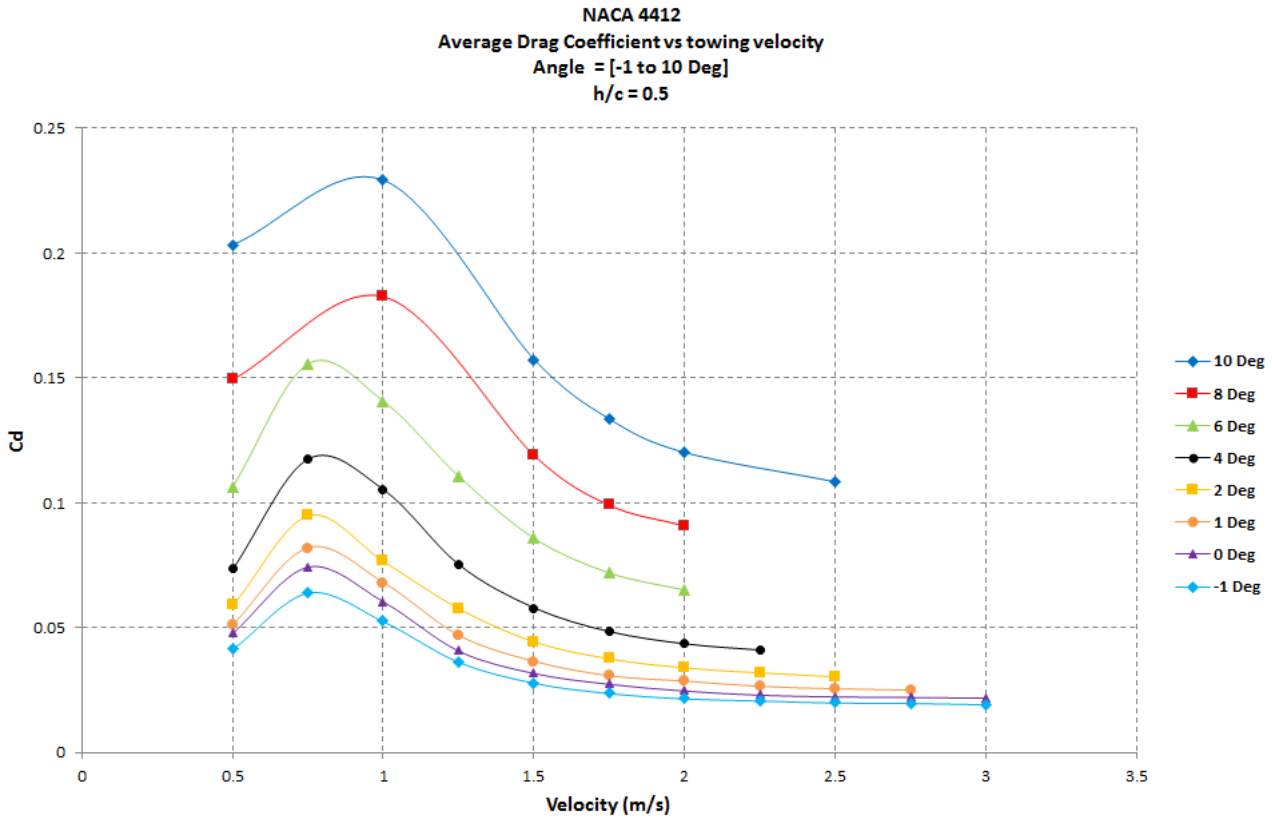

Figure 95: Drag coefficient generated plotted against the velocity for a submergence of 0.5 c for a range of angles of attack.

The figure above presents the average drag coefficient plotted against the velocity for a range of angles of attack. At all angles there is rise between 0.5 and 0.75 m/s, after which they decline.

8.2.2.5 h/c = 0.25

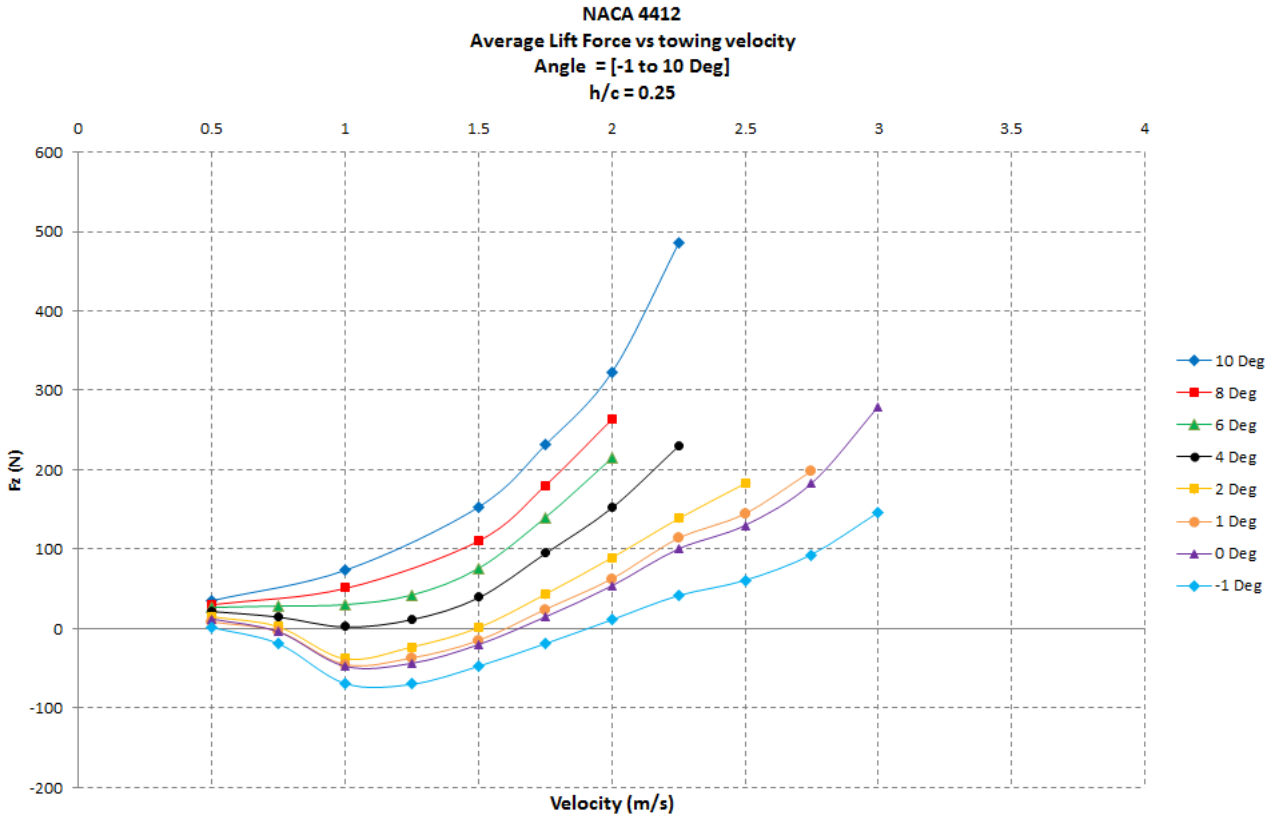

Figure 96: Lift generated plotted against the velocity for a submergence of 0.25 c for a range of angles of attack.

Here is presented the average lift force plotted against the velocity for a range of angles of attack. Here the curves follow the same trend. A higher force for higher angles of attack and greater speed. From an angle of 4 degrees we see a slight dip at 1.0 m/s, then the forces continue to be greater. At smaller angles (-1, 0, 1 and 2 degrees), between a speed of 0.75 and 1.75 m/s, negative lift forces are produced.

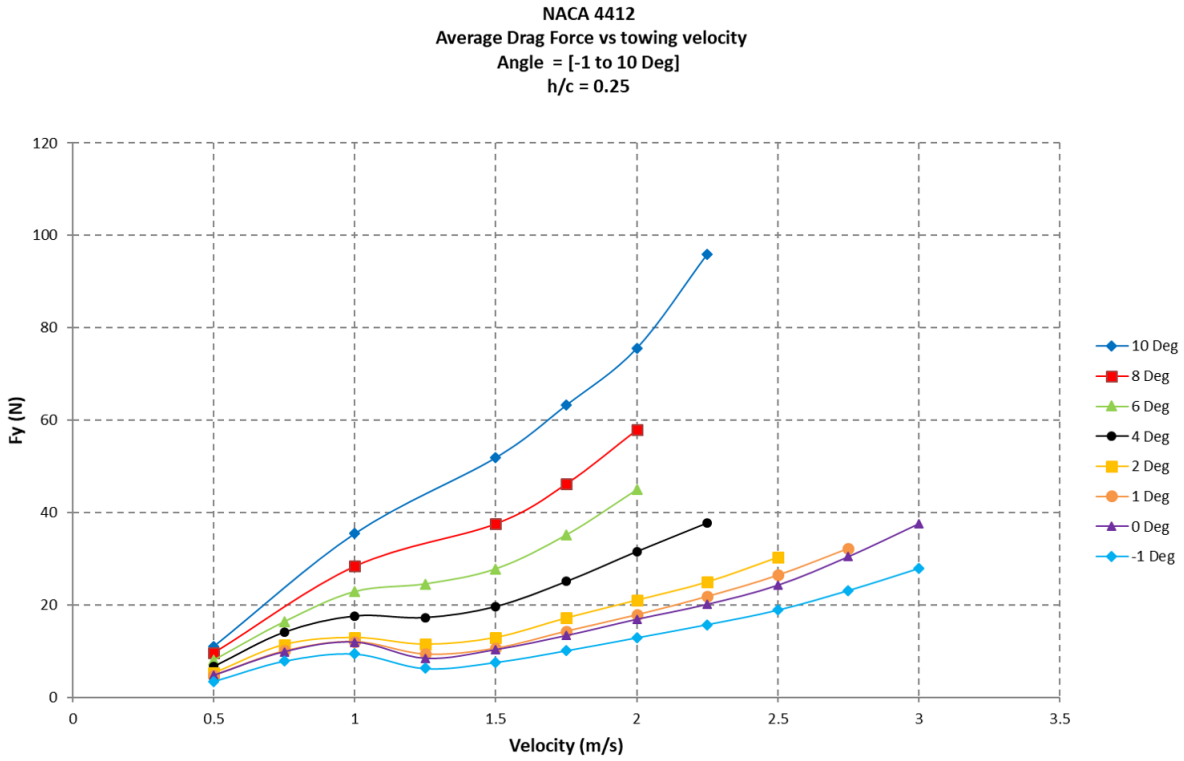

Figure 97: Drag generated plotted against the velocity for a submergence of 0.25 c for a range of angles of attack.

Here is presented the average drag force plotted against the velocity for a range of angles of attack. Here the curves follow the same trend, the separation between the angles of attack of 0, 1 and 2 degrees is minimal, the separation is clearer from an angle of attack of 4 degrees. It can also be seen that the drag forces generated are higher at greater angles of attack and velocity. a slight dip is seen at 1.25 m/s, for most angles of attack.

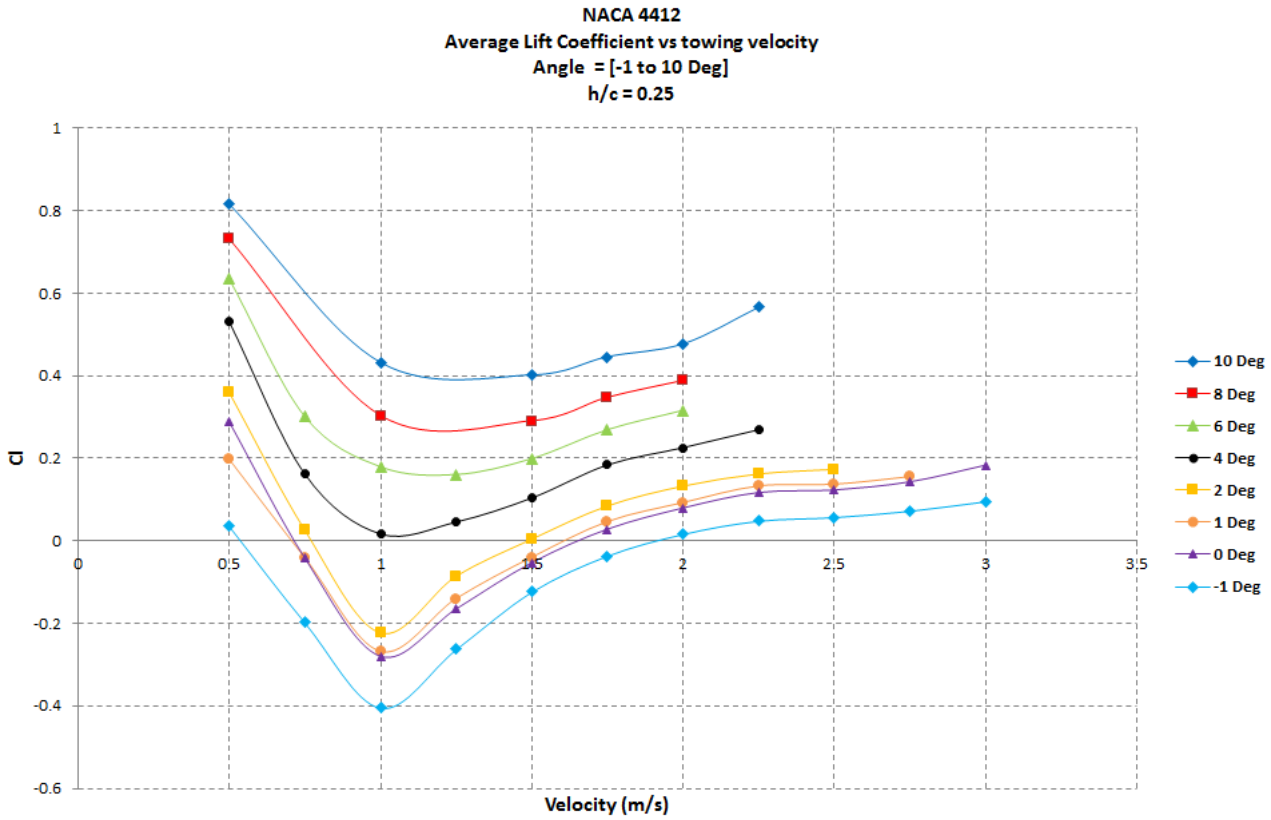

Figure 98: Lift coefficient generated plotted against the velocity for a submergence of 0.25 c for a range of angles of attack.

The figure above presents the average lift coefficient plotted against the velocity for a range of angles of attack. What is seen here is a sharp decline from a maximum value at 0.5 m/s. It declines rapidly until a speed of 1.0 m/s, where the values pick up. The negative lifts seen in Figure 96 are also seen here.

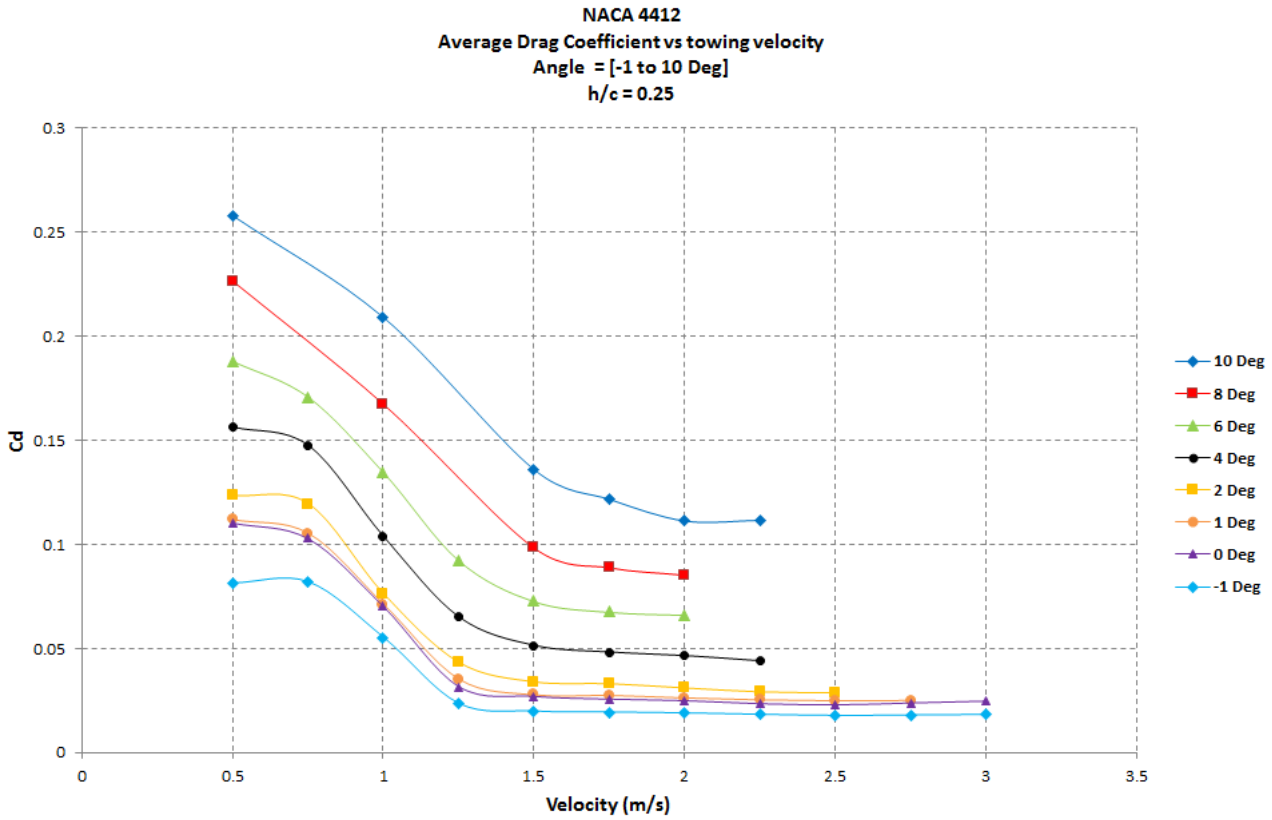

Figure 99: Drag coefficient generated plotted against the velocity for a submergence of 0.25 c for a range of angles of attack.

The figure above presents the average drag coefficient plotted against the velocity for a range of angles of attack. At most angles there is a slow decline between 0.5 and 0.75 m/s, then a decline until 1.25 m/s where it flattens out.

8.2.2.6 h/c = 0.1

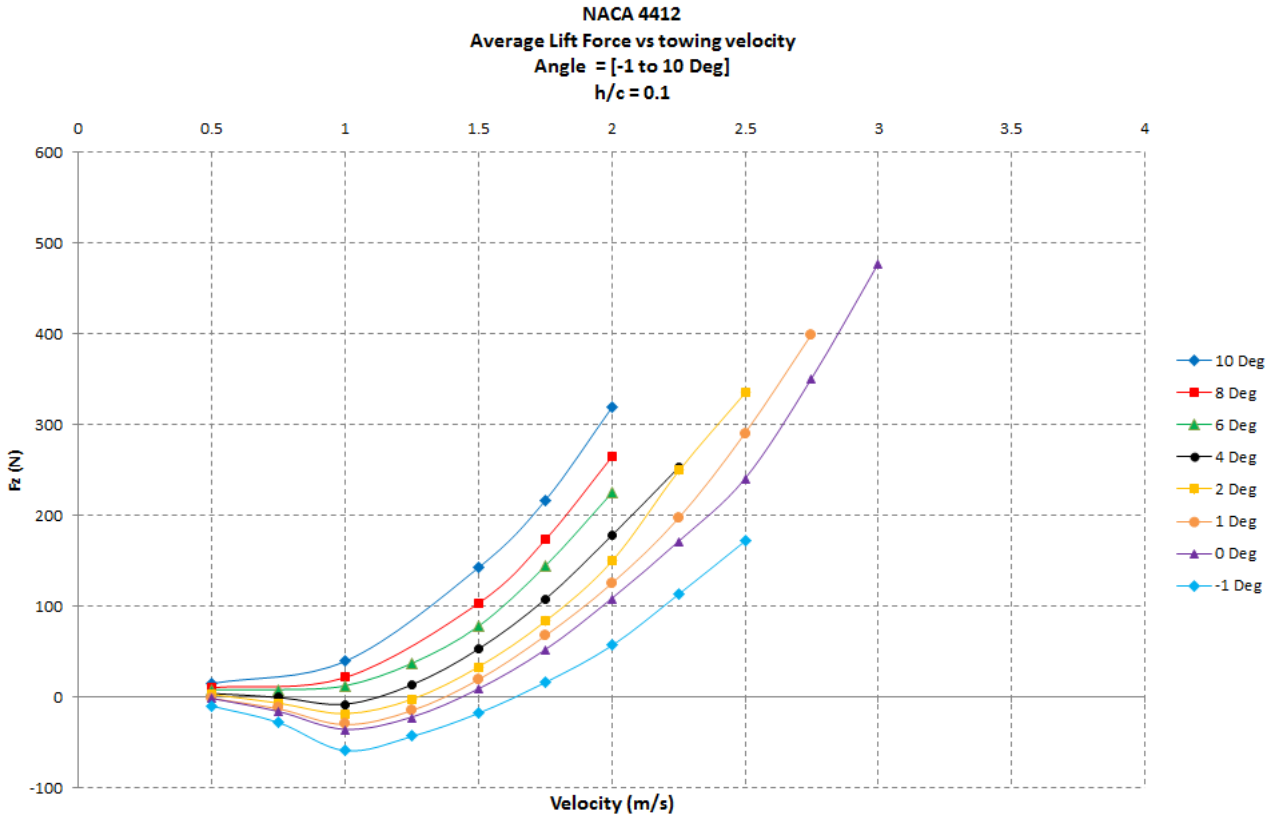

Figure 100: Lift generated plotted against the velocity for a submergence of 0.1 c for a range of angles of attack.

Here is presented the average lift force plotted against the velocity for a range of angles of attack. Here the curves follow the same trend, a higher force for higher angles of attack and greater speed. From an angle of 4 degrees, a slight dip at 1.0 m/s is seen and then the forces continue to be greater. At smaller angles (-1, 0, 1, 2 and 4 degrees), between a speed of 0.75 and 1.75 m/s negative lift forces are produced.

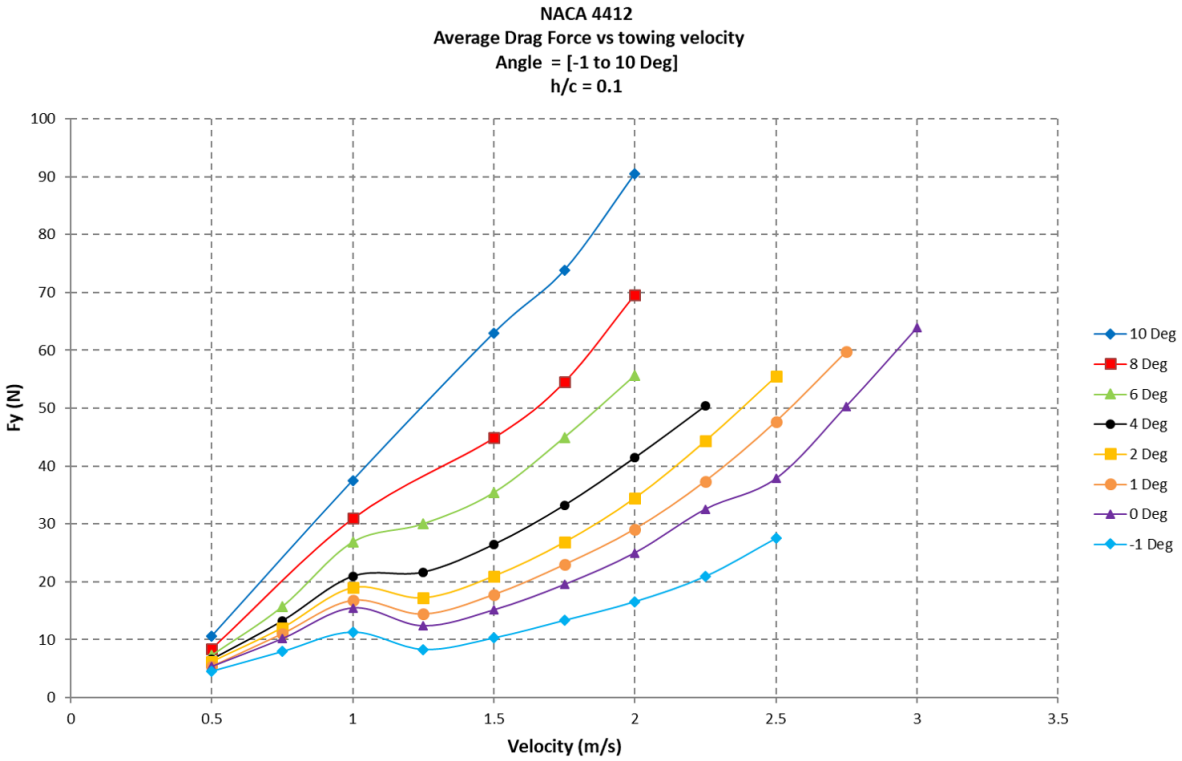

Figure 101: Drag generated plotted against the velocity for a submergence of 0.1 c for a range of angles of attack.

Here is presented the average drag force plotted against the velocity for a range of angles of attack. Here the curves follow the same trend. It can also be seen that the drag forces generated are higher at greater angles of attack and velocity. a slight dip is seen at 1.25 m/s, for angles of -1, 0, 1, 2,4 and 6 degrees.

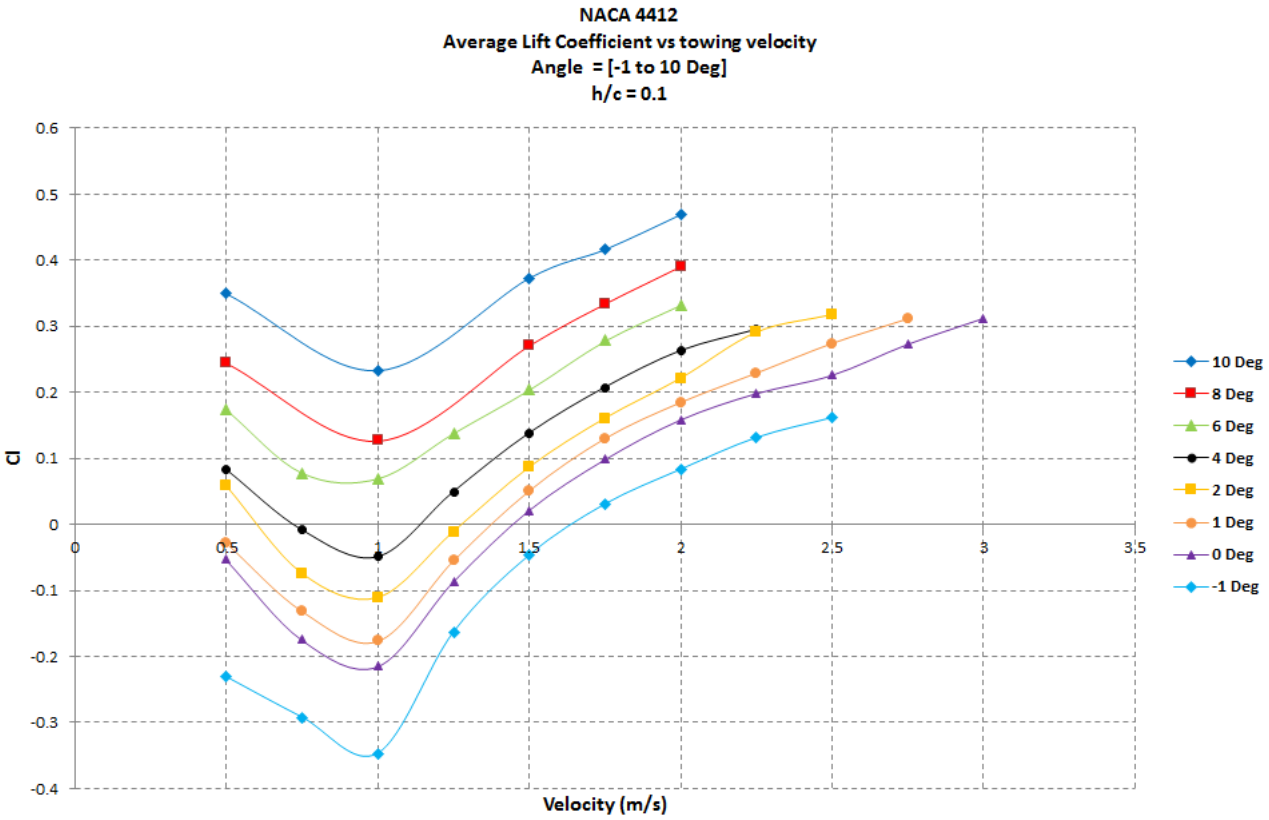

Figure 102: Lift coefficient generated plotted against the velocity for a submergence of 0.1 c for a range of angles of attack.

The figure above presents the average lift coefficient plotted against the velocity for a range of angles of attack. What is seen here is a sharp decline from a value at 0.5 m/s to 1.0 m/s, then a rise over the range of speed. The negative lifts seen in Figure 100 are also seen here.

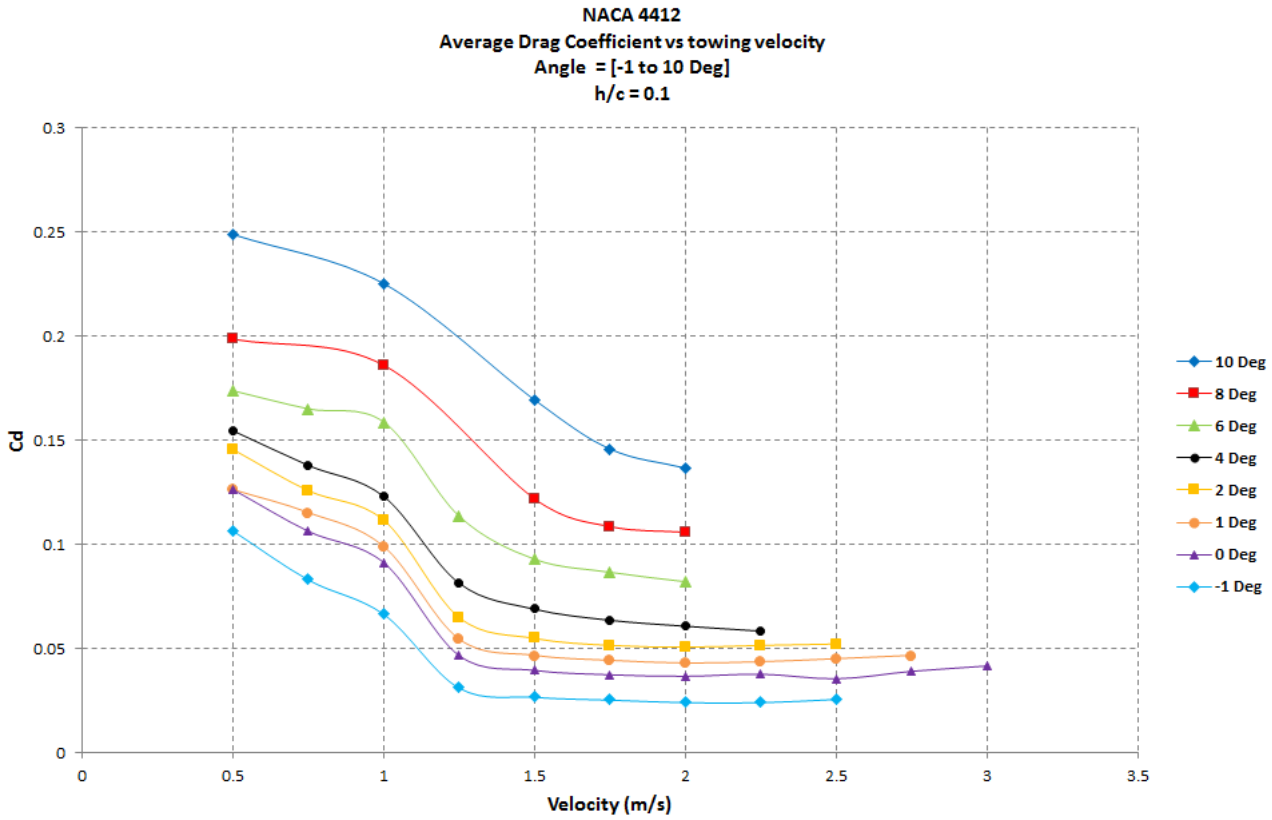

Figure 103: Drag coefficient generated plotted against the velocity for a submergence of 0.1 c for a range of angles of attack.

The figure above presents the average drag coefficient plotted against the velocity for a range of angles of attack. At most angles there is a slow decline between 0.5 and 1.25 m/s, after which it flattens out.

8.2.2.7 Conclusion

The effect of depth is seen particularly form a submergence of 1.0 chord. Negative lift forces are seen at low angles and low submergences. This could be due to ventilation.

8.2.3 Effect of towing velocity

8.2.3.1 velocity = 0.5 m/s

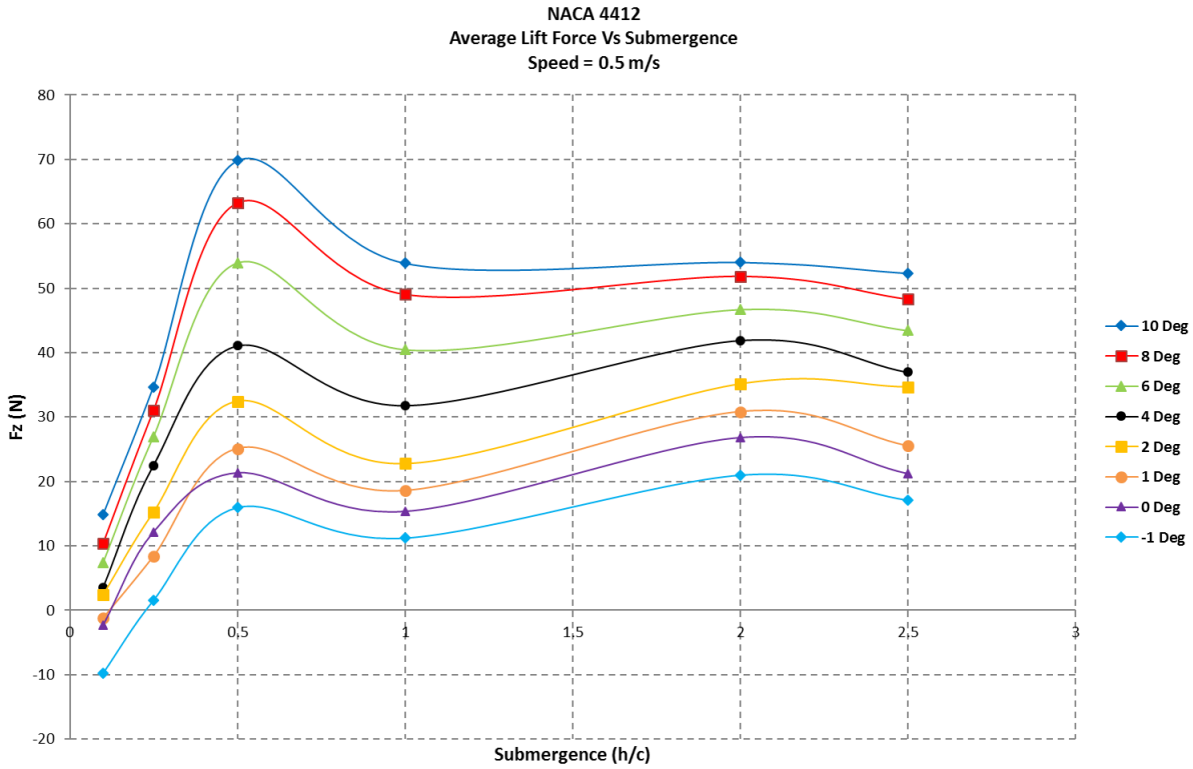

Figure 104: Lift generated plotted against the submergence (h/c) for a velocity of 0.5 m/s for a range of angles of attack.

Here is presented the average Lift force (Fz (N)), plotted against the submergence (h/c), at a speed of 0.5 m/s for a range of angles of attack. It can be seen here that there is a sharp increase between the lowest value at submergence of 0.1 c and 0.5 c. There is then a sharp decline from 0.5 c to 1.0 c, after which it become fairly regular until 2.5 c. A slight increase can be seen at 2.0 m/s.

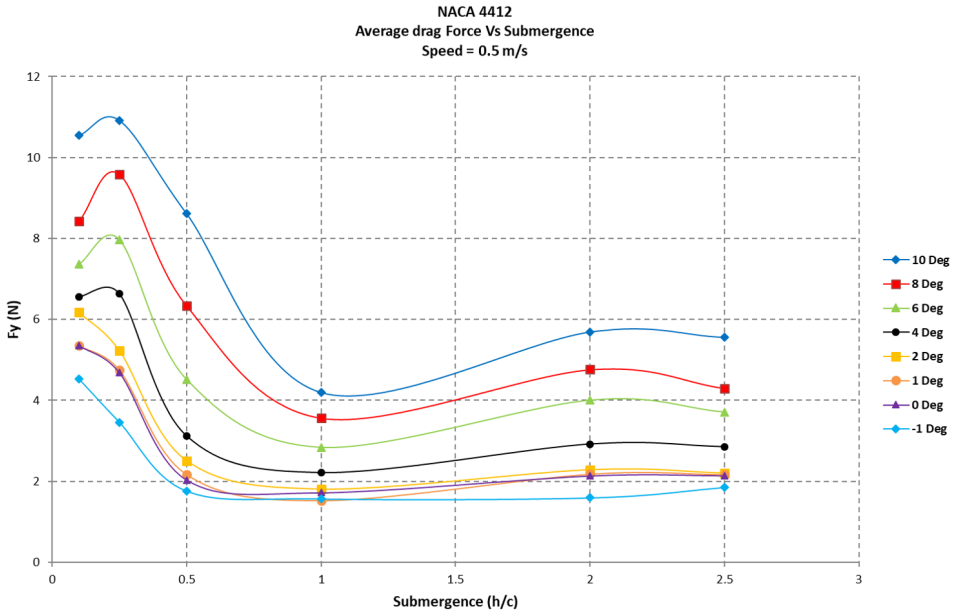

Figure 105: Drag generated plotted against the submergence (h/c) for a velocity of 0.5 m/s for a range of angles of attack.

Here is presented the average Drag force (Fy (N)), plotted against the submergence (h/c), at a speed of 0.5 m/s for a range of angles of attack. It can be seen that at a higher angles (4 to 10 degrees), there is a slight increase in value at 0.25 c. It then dips down back to a minimum value for a submergence of 1.0 c. There is also a slight dip from 2.0 to 2.5 c. At smaller angles (2 to -1 degrees), the curves go down until 0.5 c and then rise steadily until 2.5 c.

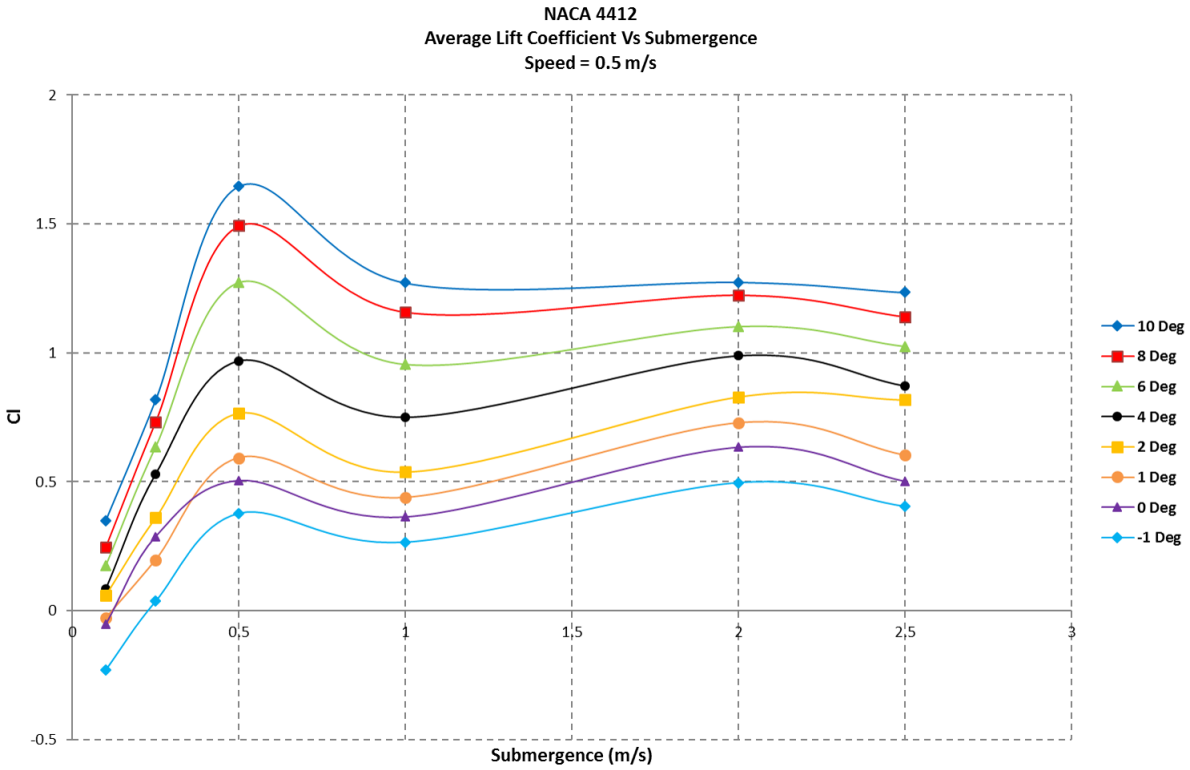

Figure 106: Lift coefficient generated plotted against the submergence (h/c) for a velocity of 0.5 m/s for a range of angles of attack.

Here is presented the average Lift coefficient (Cl), plotted against the submergence (h/c), at a speed of 0.5 m/s for a range of angles of attack. It can be seen here that there is a sharp increase between the lowest value at submergence of 0.1 c and 0.5 c. There is then a sharp decline from 0.5 c to 1.0 c. It become fairly regular until 2.5 c. A slight increase can be seen at 2.0 m/s. This echoes the values in Figure 104.

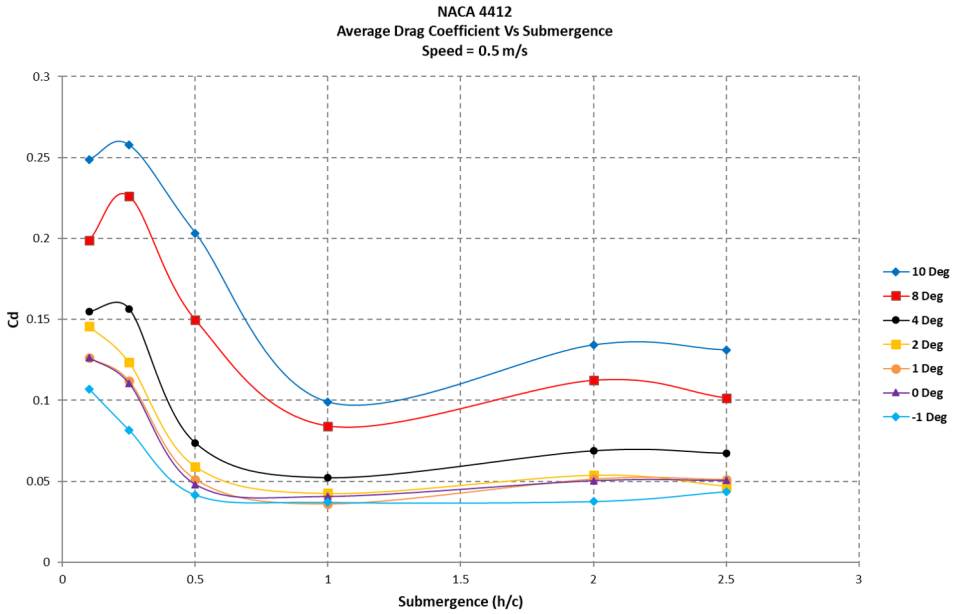

Figure 107: Drag coefficient generated plotted against the submergence (h/c) for a velocity of 0.5 m/s for a range of angles of attack.

Here is presented the average Drag coefficient (Cd), plotted against the submergence (h/c), at a speed of 0.5 m/s for a range of angles of attack. It can be seen that at a higher angles (4 to 10 degrees), there is a slight increase in value at 0.25 c. It then dips down back to a minimum value for a submergence of 1.0 c. A slight dip from 2.0 to 2.5 c is shown. At smaller angles (2 to -1 degrees), the curves go down until 0.5 c and then rise steadily until 2.5 c. This echoes the values in Figure 105.

8.2.3.2 velocity = 0.75 m/s

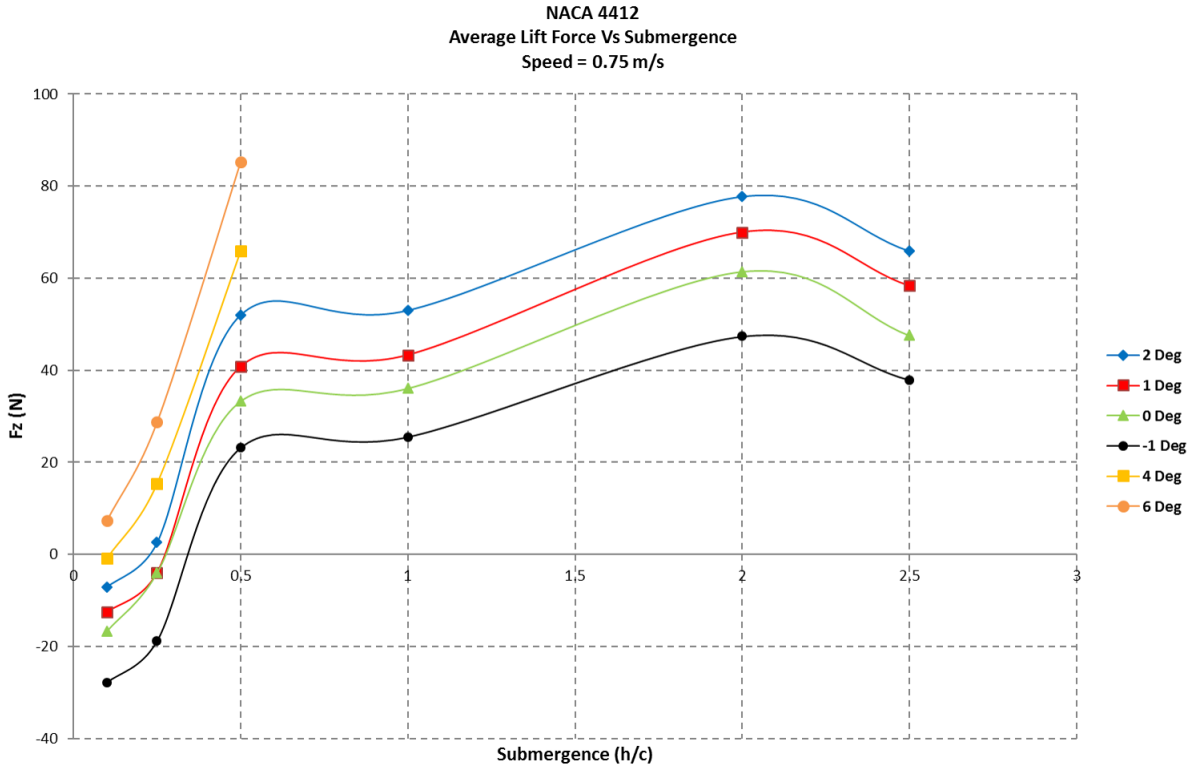

Figure 108: Lift generated plotted against the submergence (h/c) for a velocity of 0.75 m/s for a range of angles of attack.

Here is presented the average Lift force (Fz (N)), plotted against the submergence (h/c), at a speed of 0.75 m/s for a range of angles of attack. It can be seen here that there is a sharp increase between the lowest value at submergence of 0.1 c, and 0.5 c. It can be seen that the difference in value between 0.5 c and 1.0 c is negligible. The value then rise until 2.0 c to come down until 2.5 c.

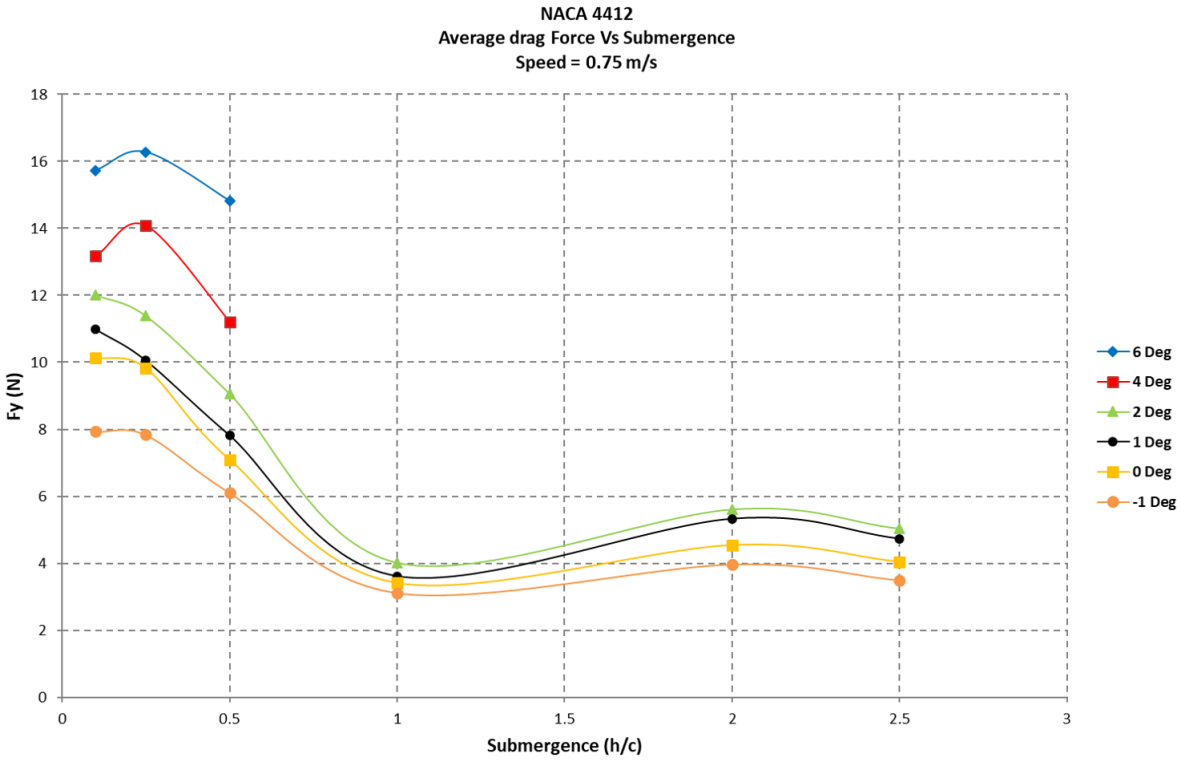

Figure 109: Drag generated plotted against the submergence (h/c) for a velocity of 0.75 m/s for a range of angles of attack.

Here is presented the average Drag force (Fy (N)), plotted against the submergence (h/c), at a speed of 0.75 m/s for a range of angles of attack. For smaller angles (2 to -1 degrees), the trend is a dip in drag forces at a submergence of 1.0 c. At 4 and 6 degrees, a small increase is seen at 0.25 c.

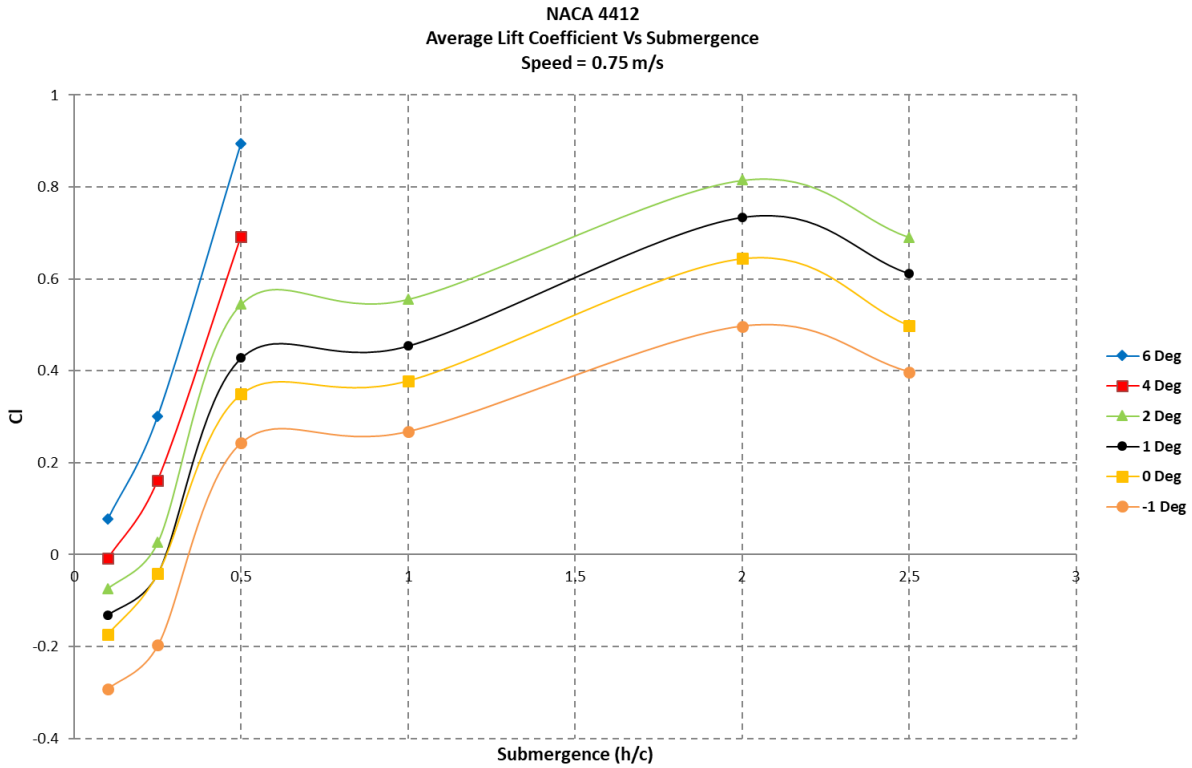

Figure 110: Lift coefficient generated plotted against the submergence (h/c) for a velocity of 0.75 m/s for a range of angles of attack.

Here is presented the average Lift coefficient (Cl), plotted against the submergence (h/c), at a speed of 0.75 m/s for a range of angles of attack. In this instance the lift coefficient follows the lift forces as shown in Figure 108.

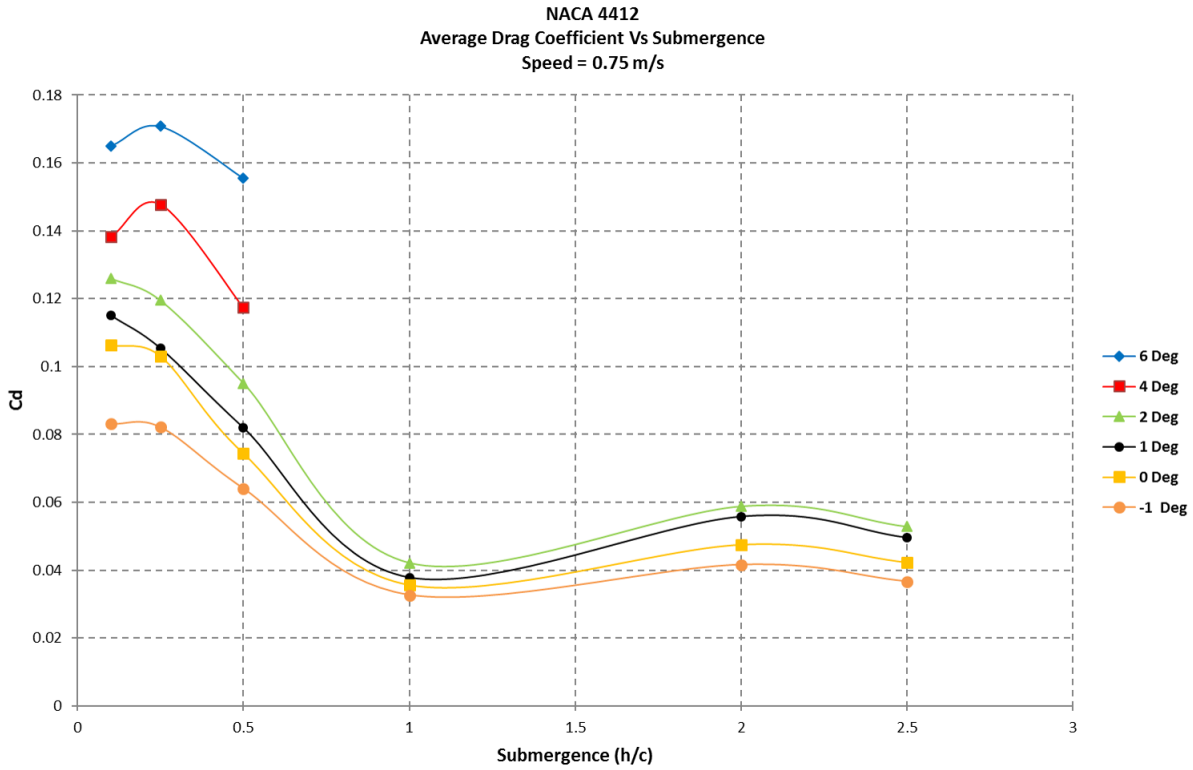

Figure 111: Drag coefficient generated plotted against the submergence (h/c) for a velocity of 0.75 m/s for a range of angles of attack.

Here is presented the average Drag coefficient (Cd), plotted against the submergence (h/c), at a speed of 0.75 m/s for a range of angles of attack. In this instance the drag coefficient follows the drag forces as shown in Figure 109.

8.2.3.3 velocity = 1.0 m/s

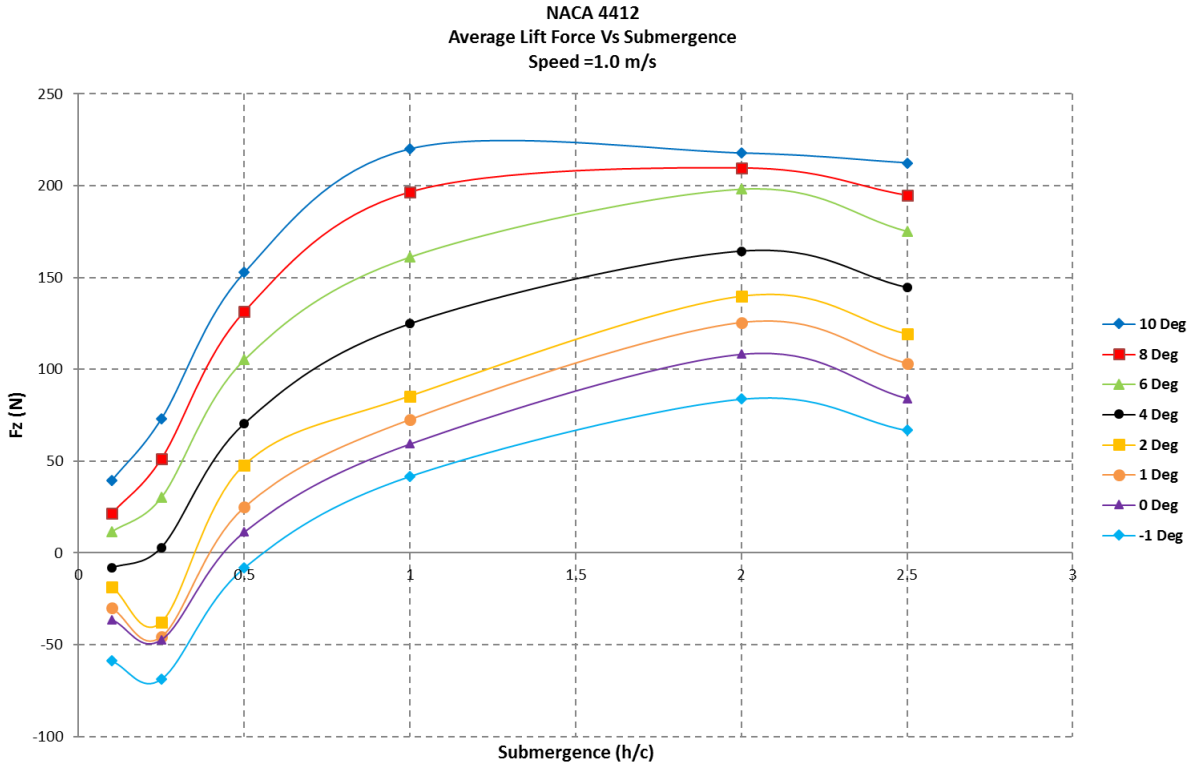

Figure 112: Lift generated plotted against the submergence (h/c) for a velocity of 1.0 m/s for a range of angles of attack.

Here is presented the average Lift force (Fz (N)), plotted against the submergence (h/c), at a speed of 1.0 m/s for a range of angles of attack. It can be seen that at higher angles (from 4 to 10 degrees) the values rise from a submergence of 0.1 c to 1.0 c. After 2.0 c a slight decrease can be seen. For lower angles (from 2 to -1 degrees), a decrease can be seen from 0.1 c to 0.25 c, then a steady rise until a submergence of 2.0 c, after which the values decrease.

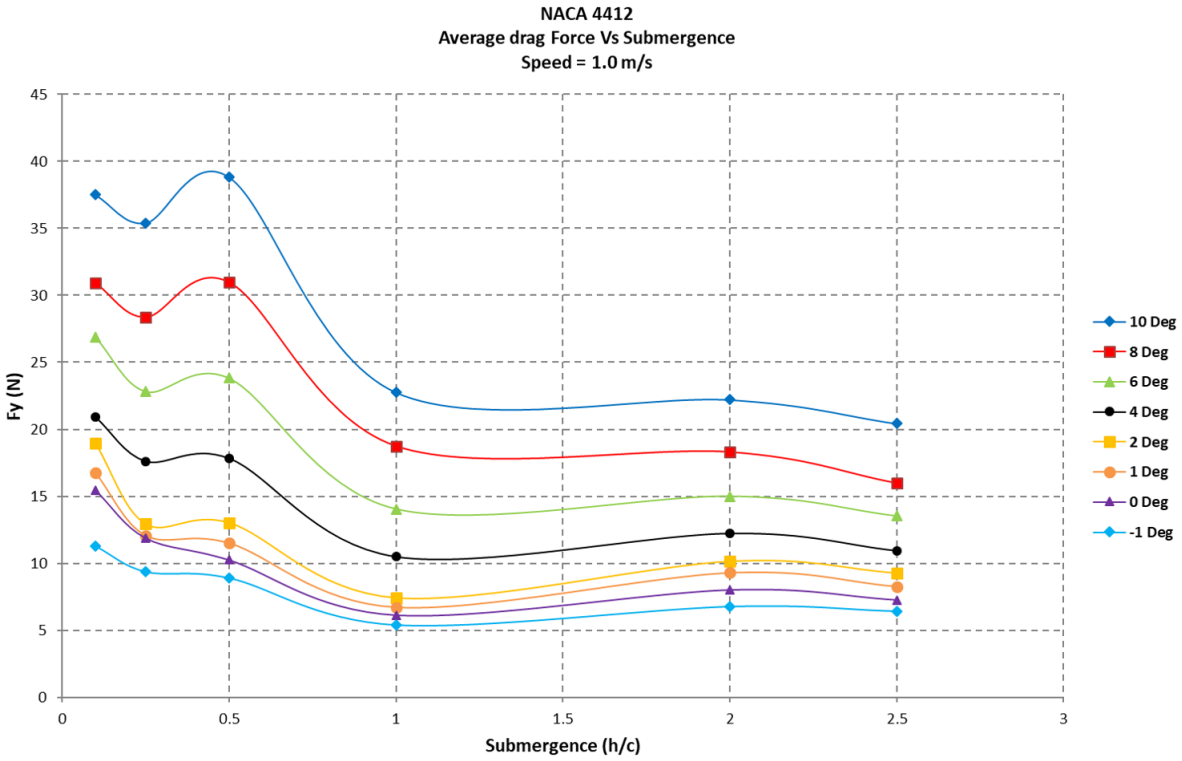

Figure 113: Drag generated plotted against the submergence (h/c) for a velocity of 1.0 m/s for a range of angles of attack.

Here is presented the average Drag force (Fy (N)), plotted against the submergence (h/c), at a speed of 1.0 m/s for a range of angles of attack. It can be seen that at all angles there is a slight decrease in value at 0.25 c. It then goes back up for a submergence of 0.5 c. Also a slight dip from 2.0 to 2.5 c can then be seen for all angles.

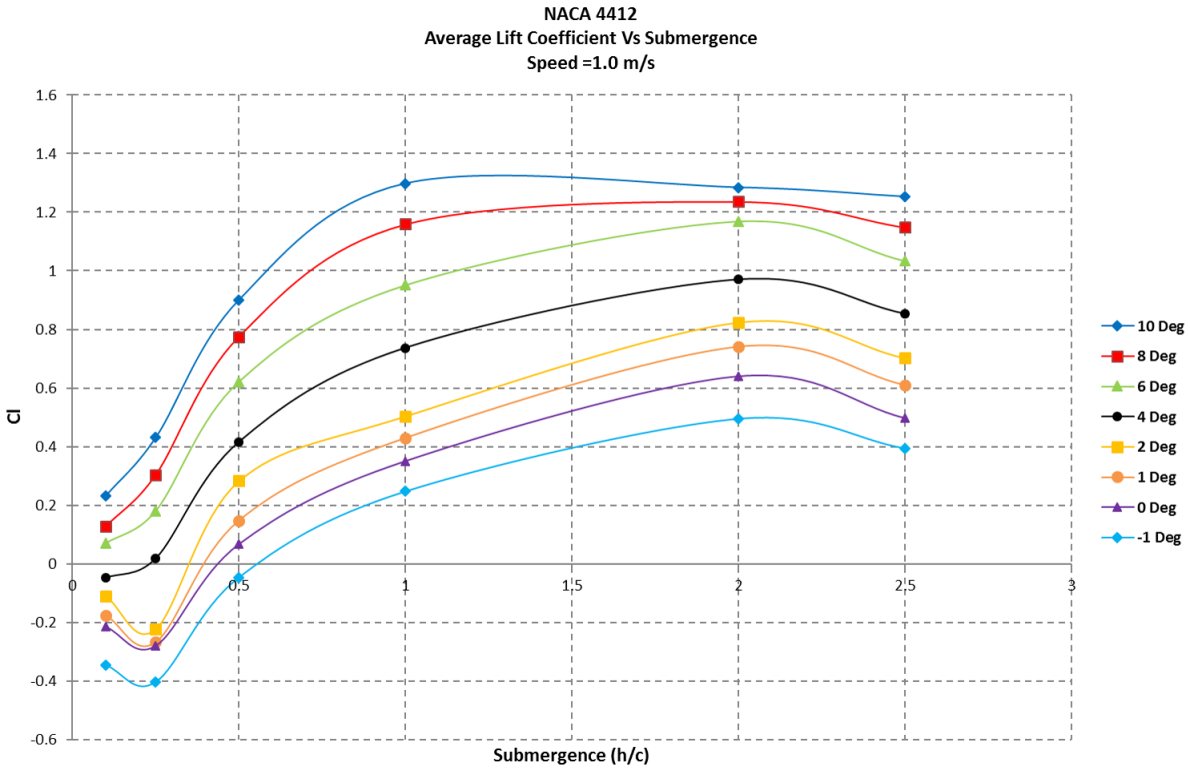

Figure 114: Lift coefficient generated plotted against the submergence (h/c) for a velocity of 1.0 m/s for a range of angles of attack.

Here is presented the average Lift coefficient (Cl), plotted against the submergence (h/c), at a speed of 1.0 m/s for a range of angles of attack. In this instance the lift coefficient follows the lift forces as shown in Figure 112.

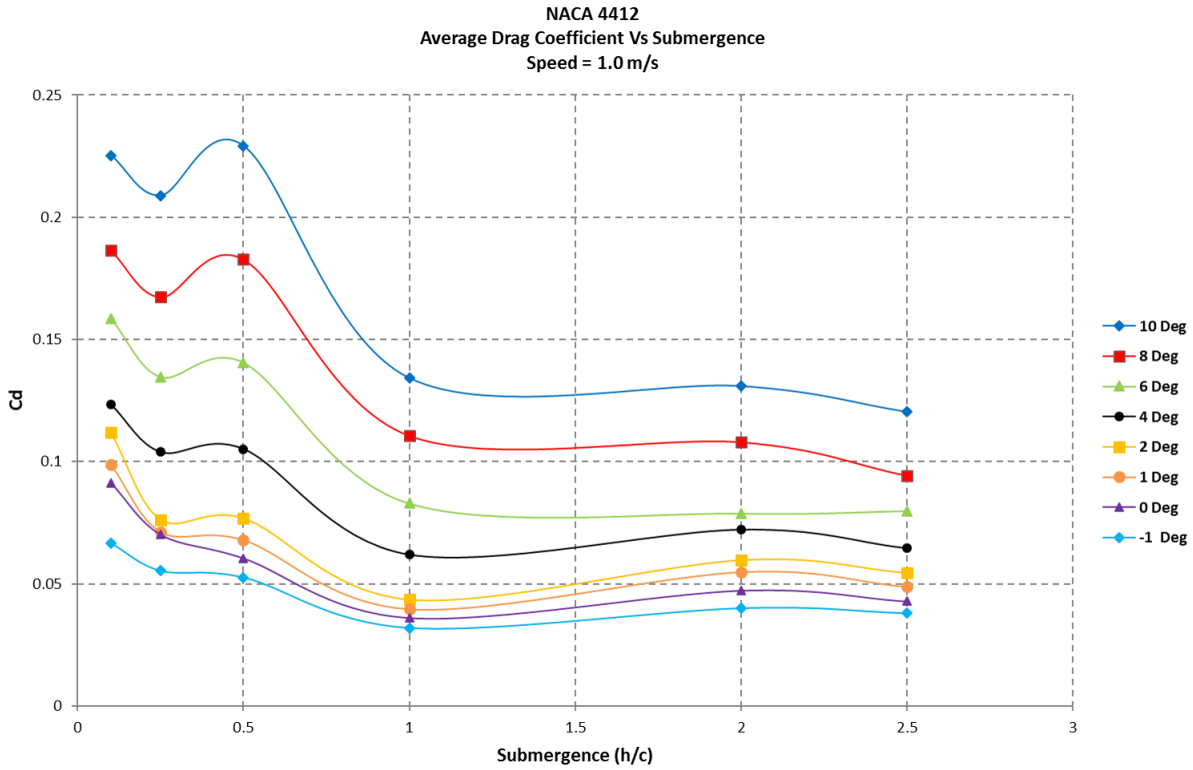

Figure 115: Drag coefficient generated plotted against the submergence (h/c) for a velocity of 1.0 m/s for a range of angles of attack.

Here is presented the average Drag coefficient (Cd), plotted against the submergence (h/c), at a speed of 1.0 m/s for a range of angles of attack. In this instance the drag coefficient follows the drag forces as shown in Figure 113.

8.2.3.4 velocity = 1.25 m/s

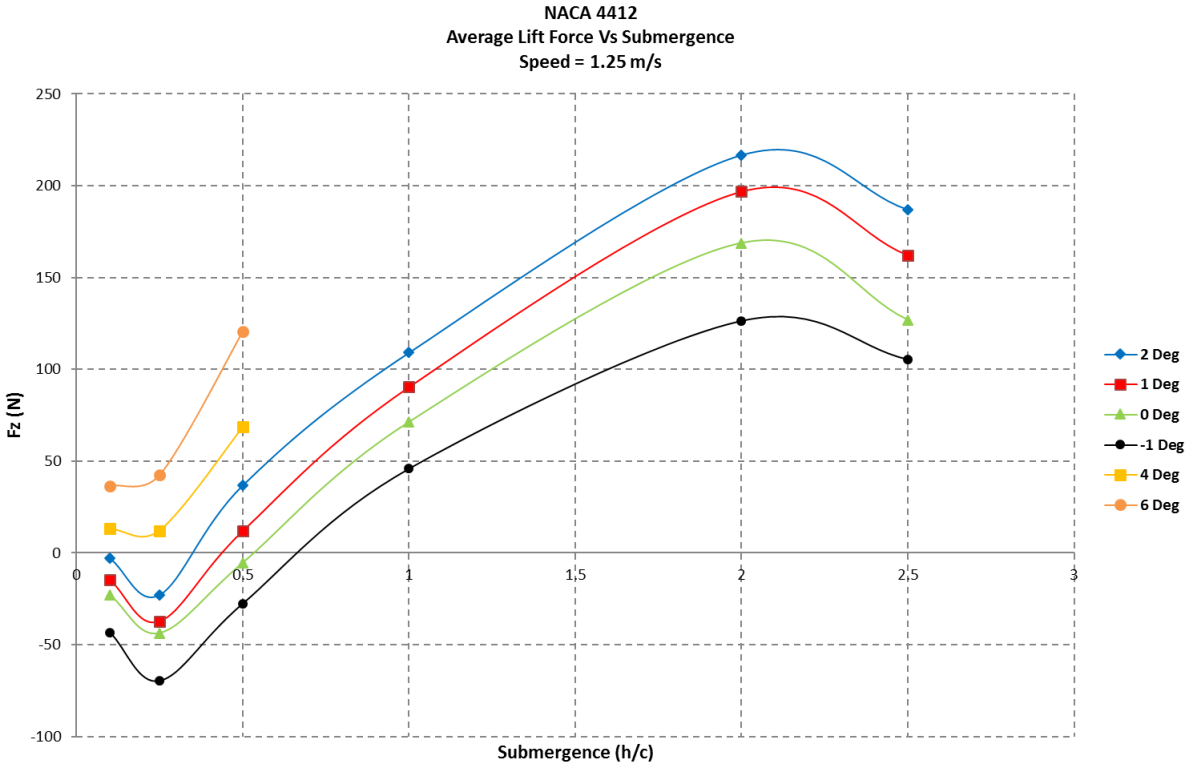

Figure 116: Lift generated plotted against the submergence (h/c) for a velocity of 1.25 m/s for a range of angles of attack.

Here is presented the average Lift force (Fz (N)), plotted against the submergence (h/c), at a speed of 1.25 m/s for a range of angles of attack. For all angles a decrease can be seen from 0.1 c to 0.25 c, a steady rise until a submergence of 2.0 c, after which the values decrease.

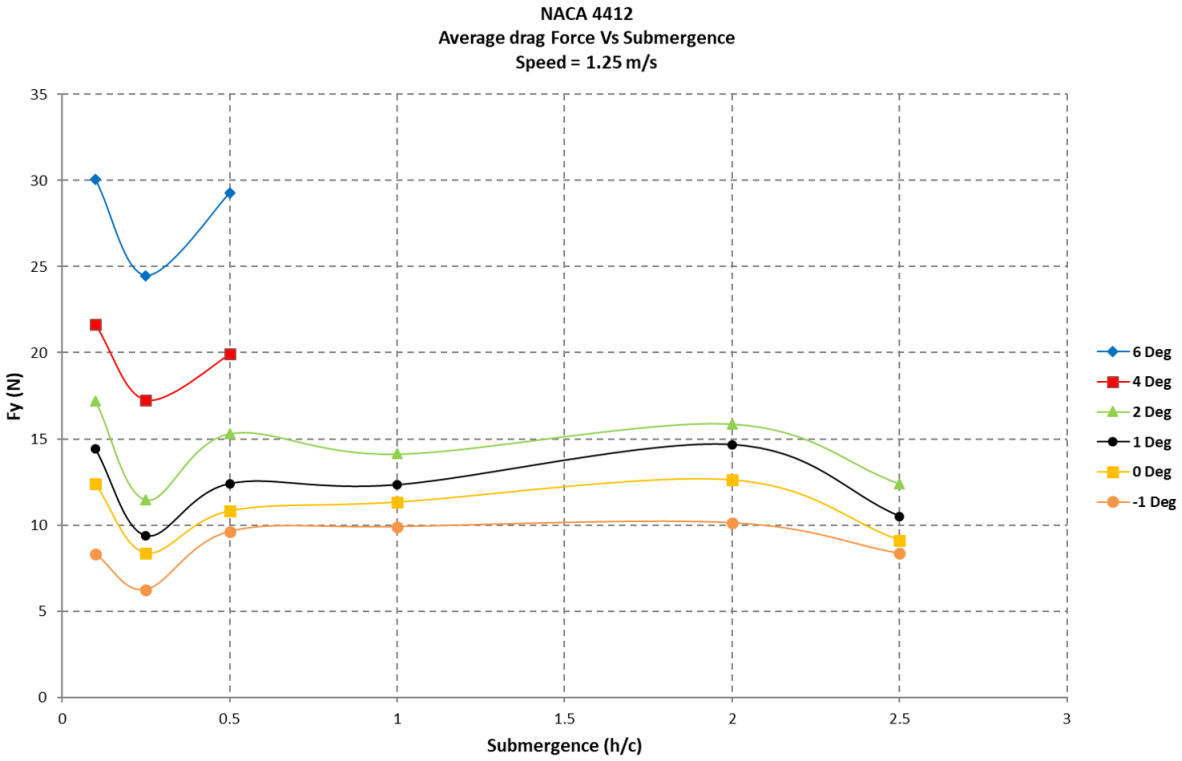

Figure 117: Drag generated plotted against the submergence (h/c) for a velocity of 1.25 m/s for a range of angles of attack.

Here is presented the average Drag force (Fy (N)), plotted against the submergence (h/c), at a speed of 1.25 m/s for a range of angles of attack. It can be seen that at all angles there is a slight decrease in value at 0.25 c, it then goes back up until 2.0 c.

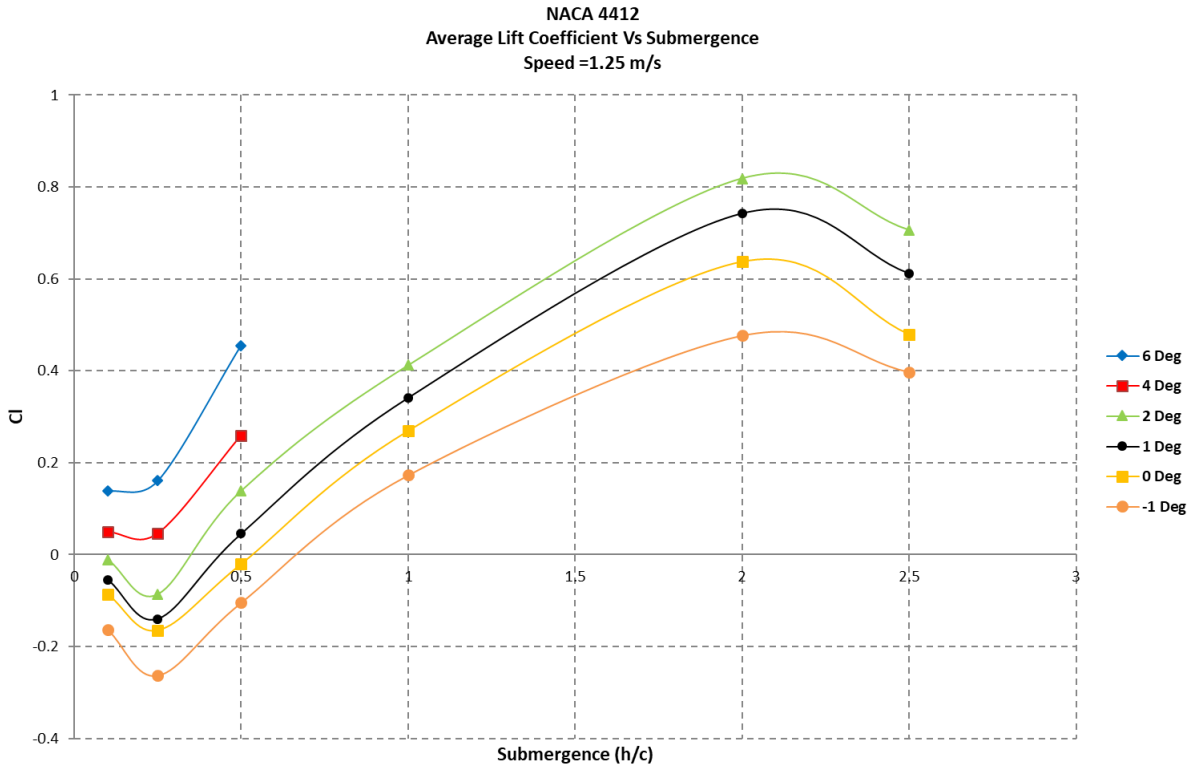

Figure 118: Lift coefficient generated plotted against the submergence (h/c) for a velocity of 1.25 m/s for a range of angles of attack.

Here is presented the average Lift coefficient (Cl), plotted against the submergence (h/c), at a speed of 1.25 m/s for a range of angles of attack. In this instance the lift coefficient follows the lift forces as shown in Figure 116.

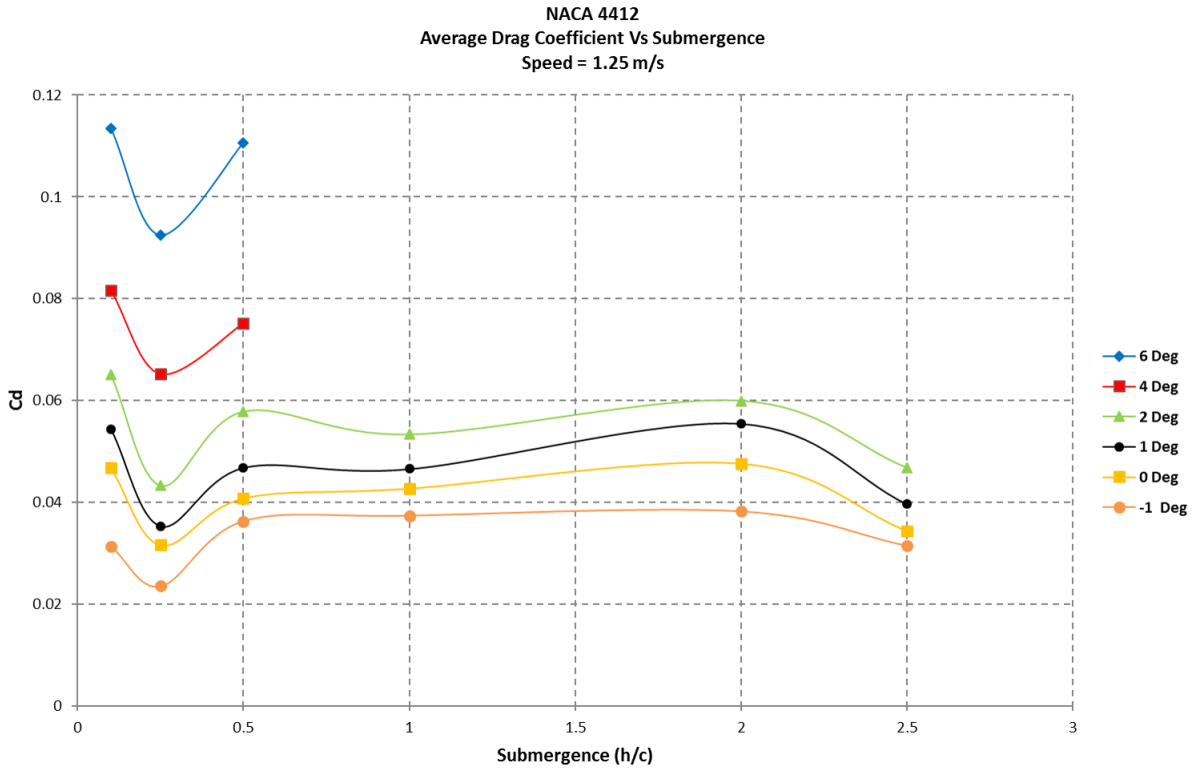

Figure 119: Drag coefficient generated plotted against the submergence (h/c) for a velocity of 1.25 m/s for a range of angles of attack.

Here is presented the average Drag coefficient (Cd), plotted against the submergence (h/c), at a speed of 1.25 m/s for a range of angles of attack. A decrease in value can be seen of a submergence of 0.25 c. The values then stay level until a submergence of 2.0 c is reached, after which they dip slightly.

8.2.3.5 velocity = 1.5 m/s

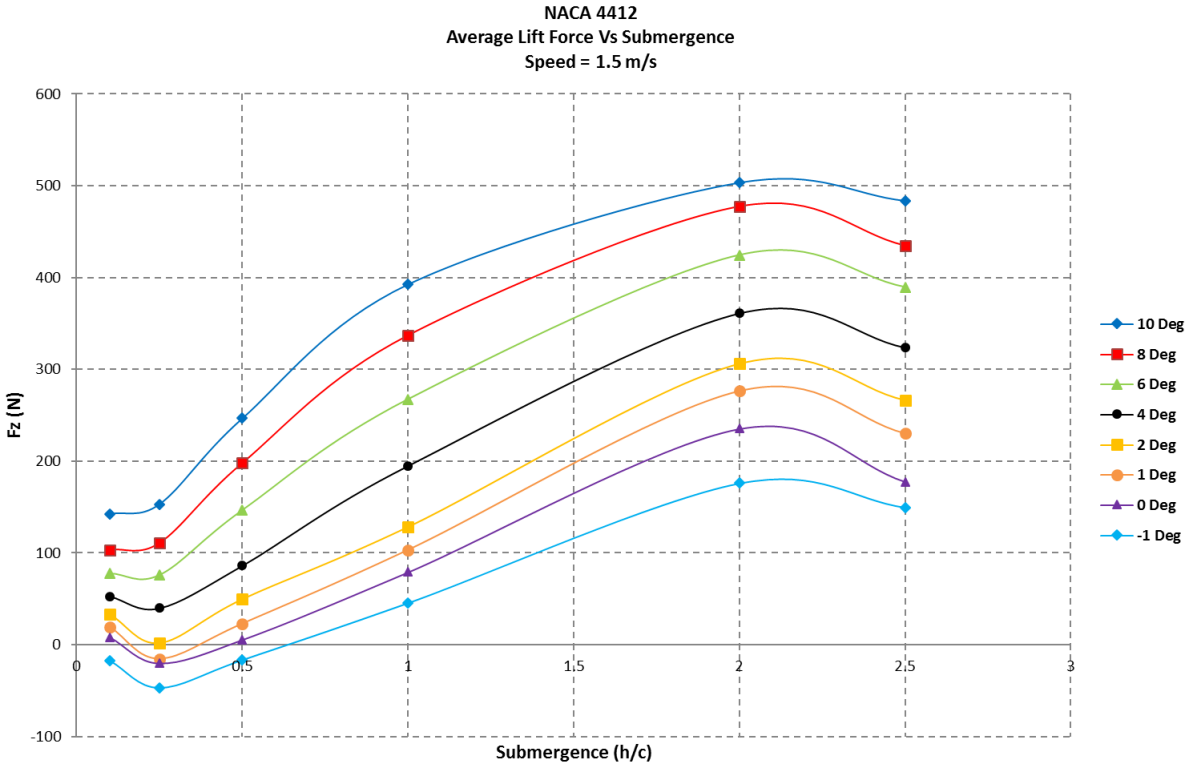

Figure 120: Lift generated plotted against the submergence (h/c) for a velocity of 1.5 m/s for a range of angles of attack.

Here is presented the average Lift force (Fz (N)), plotted against the submergence (h/c), at a speed of 1.5 m/s for a range of angles of attack. For all angles (except 10 and 8 degrees), a decrease can be seen from 0.1 c to 0.25 c, a steady rise until a submergence of 2.0 c after which the values decrease can then be seen.

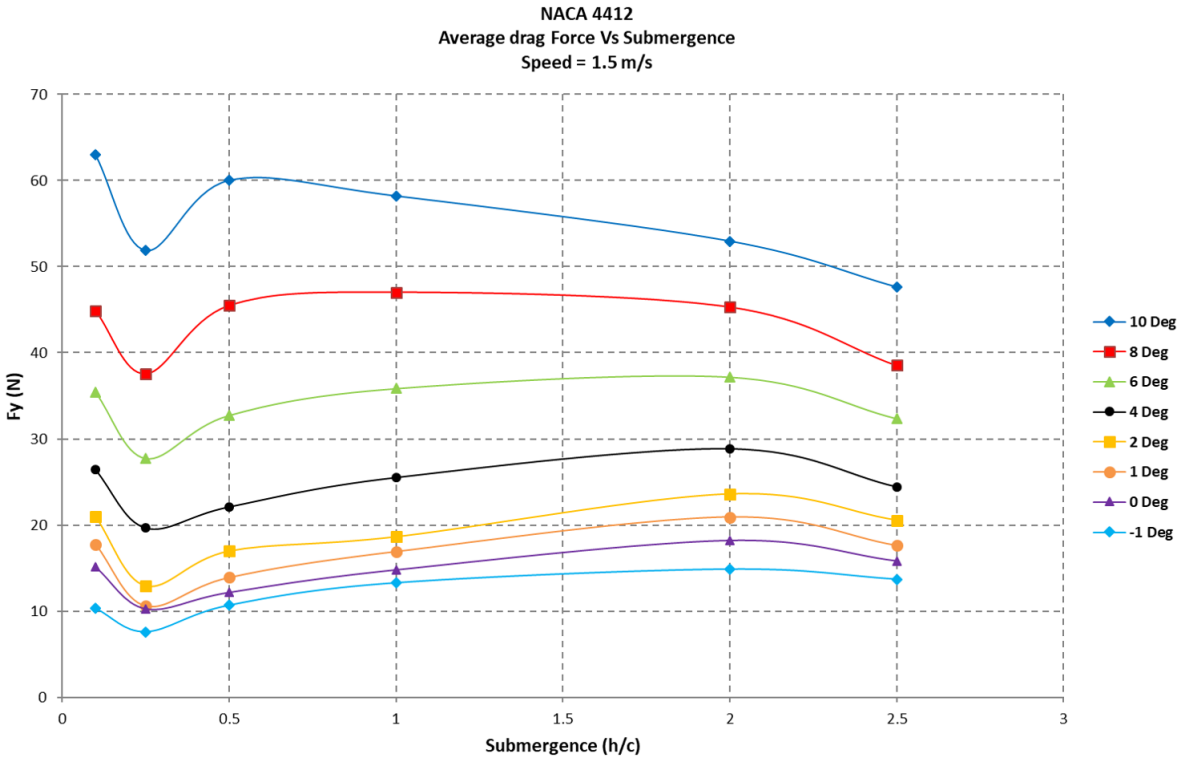

Figure 121: Drag generated plotted against the submergence (h/c) for a velocity of 1.5 m/s for a range of angles of attack.

Here is presented the average Drag force (Fy (N)), plotted against the submergence (h/c), at a speed of 1.5 m/s for a range of angles of attack. It can be seen that at all angles there is a slight decrease in value at 0.25 c, it then goes back up until 2.0 c.

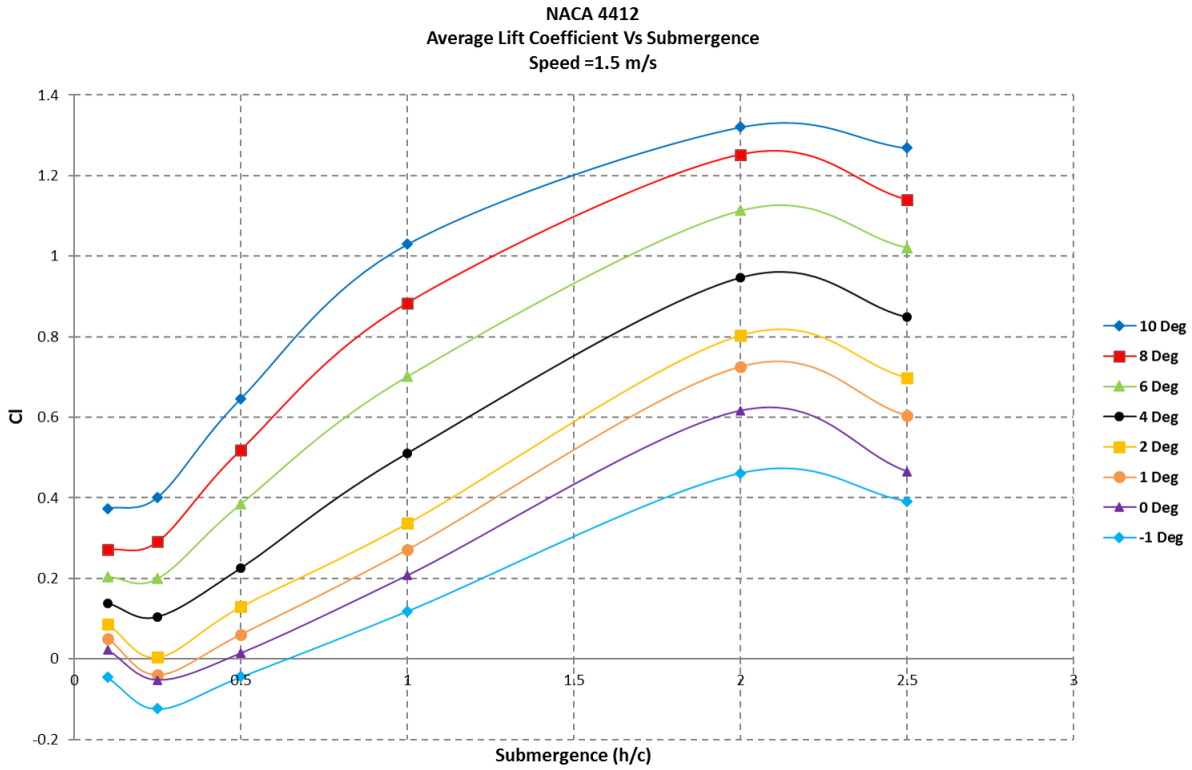

Figure 122: Lift coefficient generated plotted against the submergence (h/c) for a velocity of 1.5 m/s for a range of angles of attack.

Here is presented the average Lift coefficient (Cl), plotted against the submergence (h/c), at a speed of 1.5 m/s for a range of angles of attack. In this instance the lift coefficient follows the lift forces as shown in Figure 120.

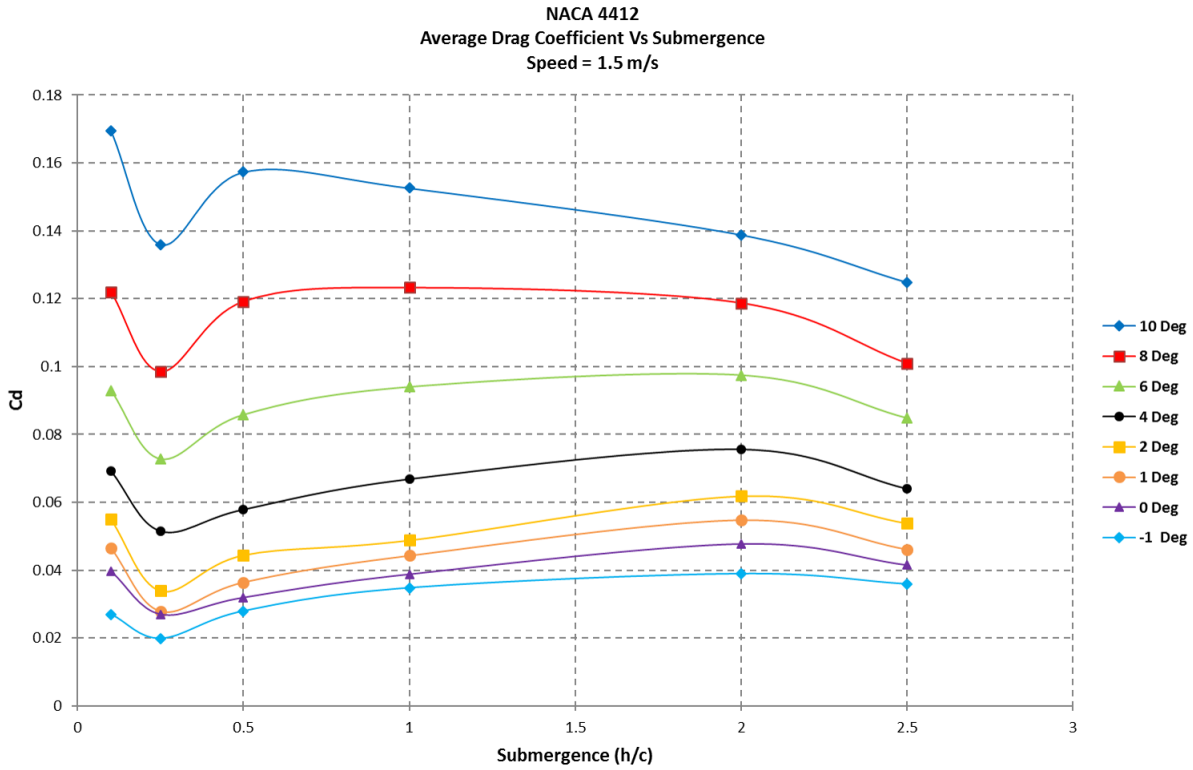

Figure 123: Drag coefficient generated plotted against the submergence (h/c) for a velocity of 1.5 m/s for a range of angles of attack.

Here is presented the average Drag coefficient (Cd), plotted against the submergence (h/c), at a speed of 1.5 m/s for a range of angles of attack. A decrease in value can be seen of a submergence of 0.25 c. The values then stay level until a submergence of 2.0 c is reached, after which they dip slightly.

8.2.3.6 velocity = 1.75 m/s

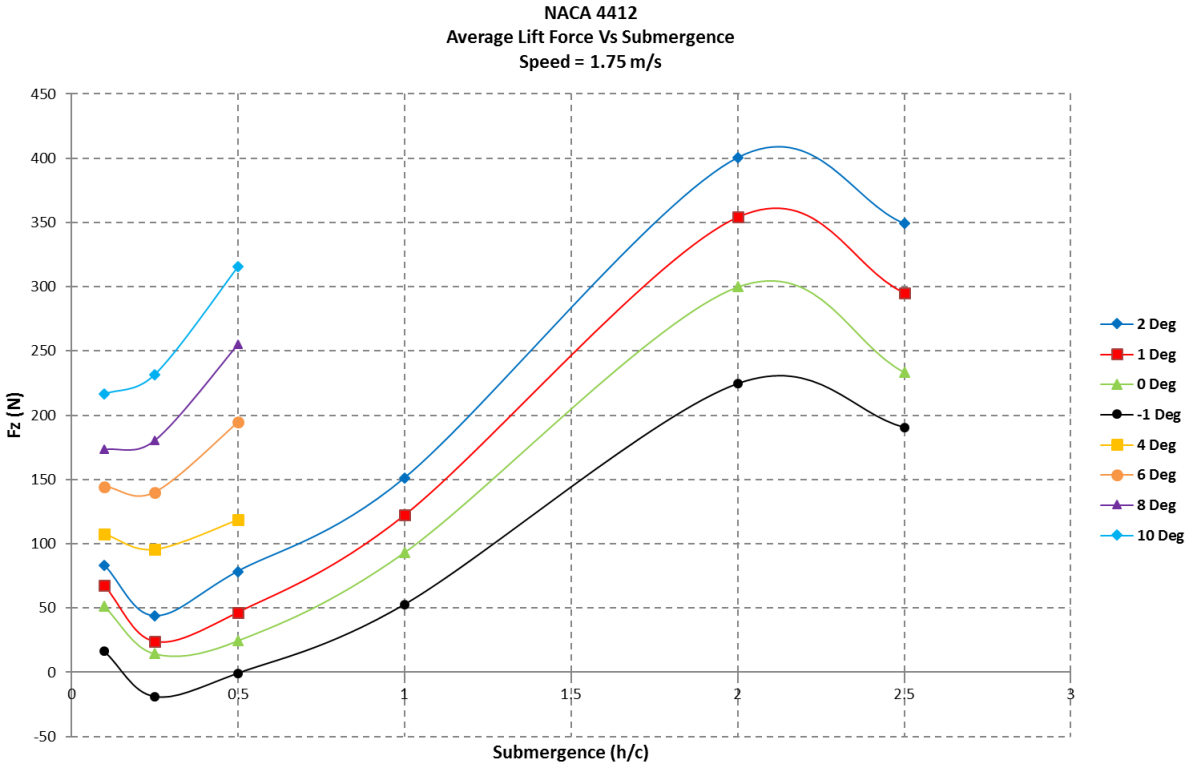

Figure 124: Lift generated plotted against the submergence (h/c) for a velocity of 1.75 m/s for a range of angles of attack.

Here is presented the average Lift force (Fz (N)), plotted against the submergence (h/c), at a speed of 1.75 m/s for a range of angles of attack. For all angles (except 10 and 8 degrees), a decrease can be seen from 0.1 c to 0.25 c. Then a steady rise until a submergence of 2.0 c, after which the values decrease.

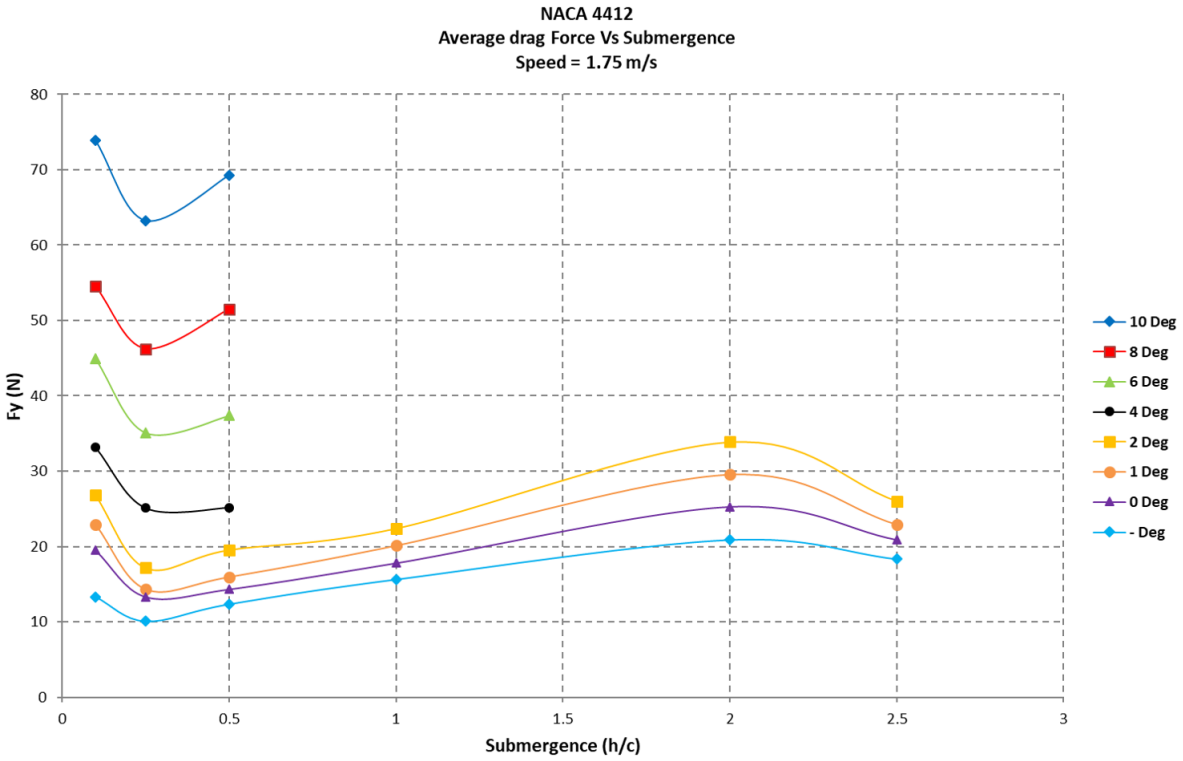

Figure 125: Drag generated plotted against the submergence (h/c) for a velocity of 1.75 m/s for a range of angles of attack.

Here is presented the average Drag force (Fy (N)), plotted against the submergence (h/c), at a speed of 1.75 m/s for a range of angles of attack. the values dip at a submergence of 0.25 c, rise steadily until a submergence of 2.0 c is reached. This trend is followed at all angles of attack.

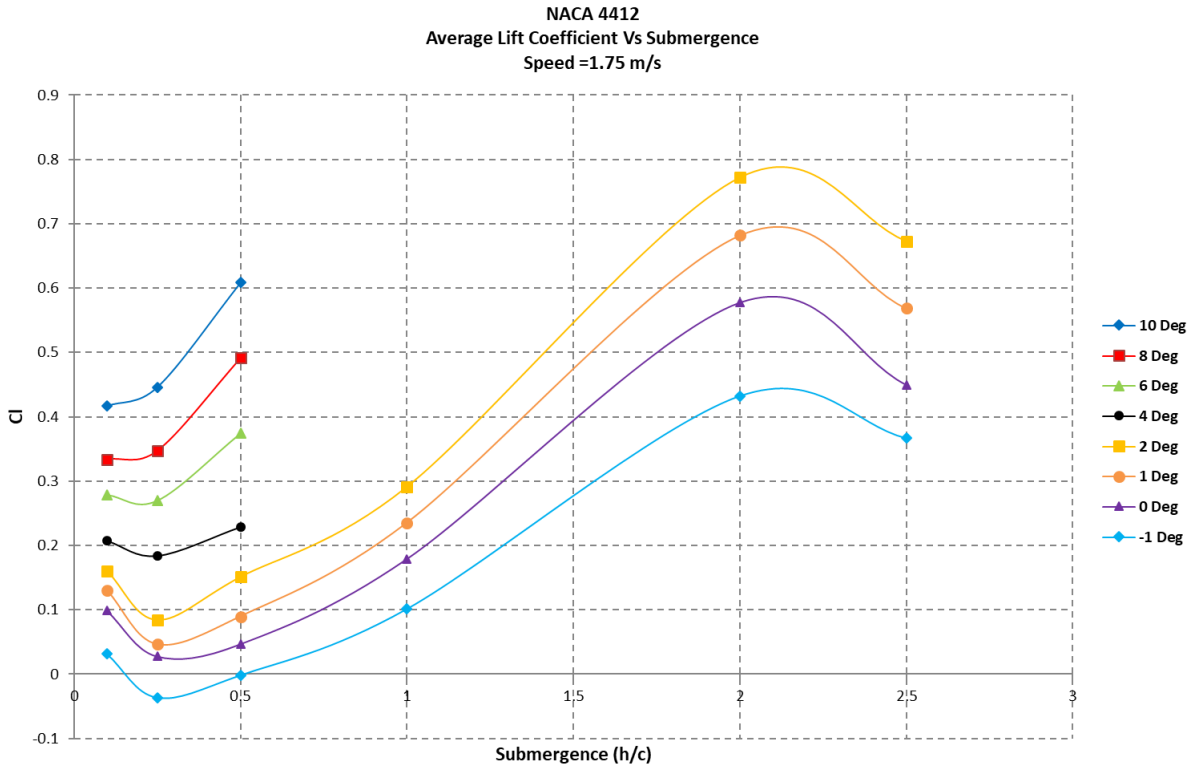

Figure 126: Lift coefficient generated plotted against the submergence (h/c) for a velocity of 1.75 m/s for a range of angles of attack.

Here is presented the average Lift coefficient (Cl), plotted against the submergence (h/c), at a speed of 1.75 m/s for a range of angles of attack. In this instance the lift coefficient follows the lift forces as shown in Figure 124.

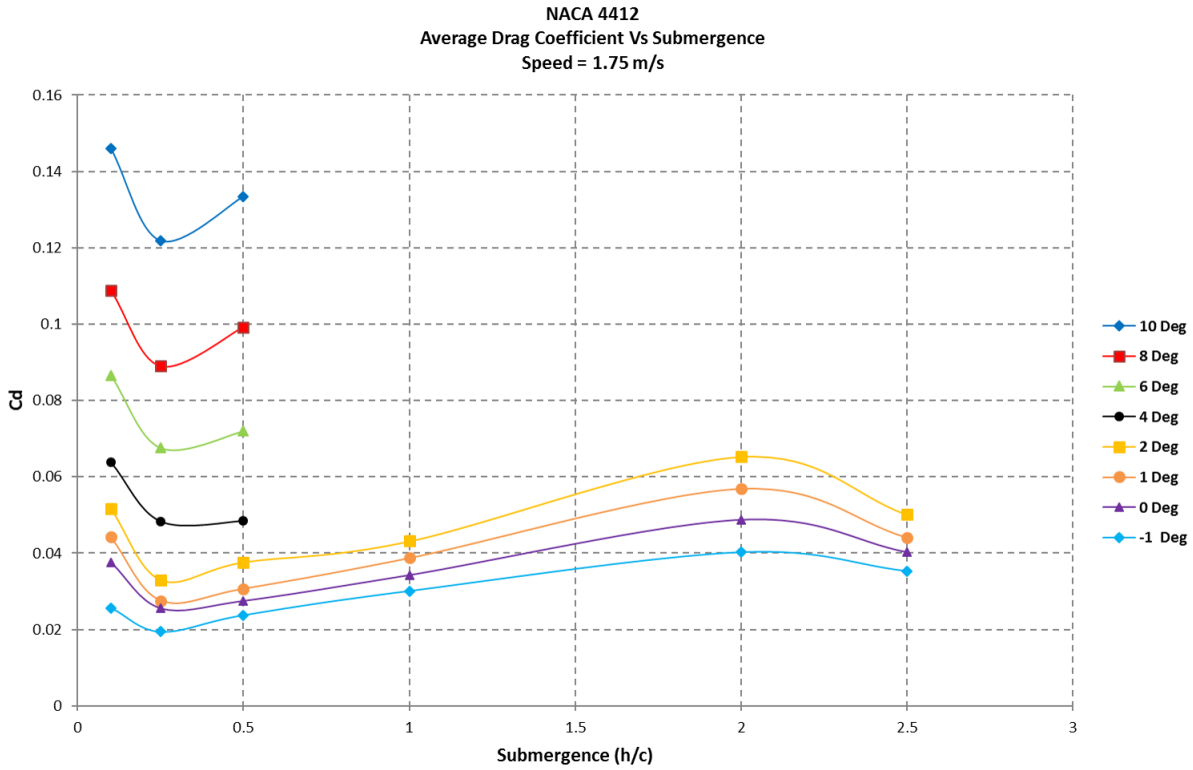

Figure 127: Drag coefficient generated plotted against the submergence (h/c) for a velocity of 1.75 m/s for a range of angles of attack.

Here is presented the average Drag coefficient (Cd), plotted against the submergence (h/c), at a speed of 1.75 m/s for a range of angles of attack. A decrease in value can be seen of a submergence of 0.25 c. The values then rise moderately until a submergence of 2.0 c is reached, after which they dip slightly.

8.2.3.7 velocity = 2.0 m/s

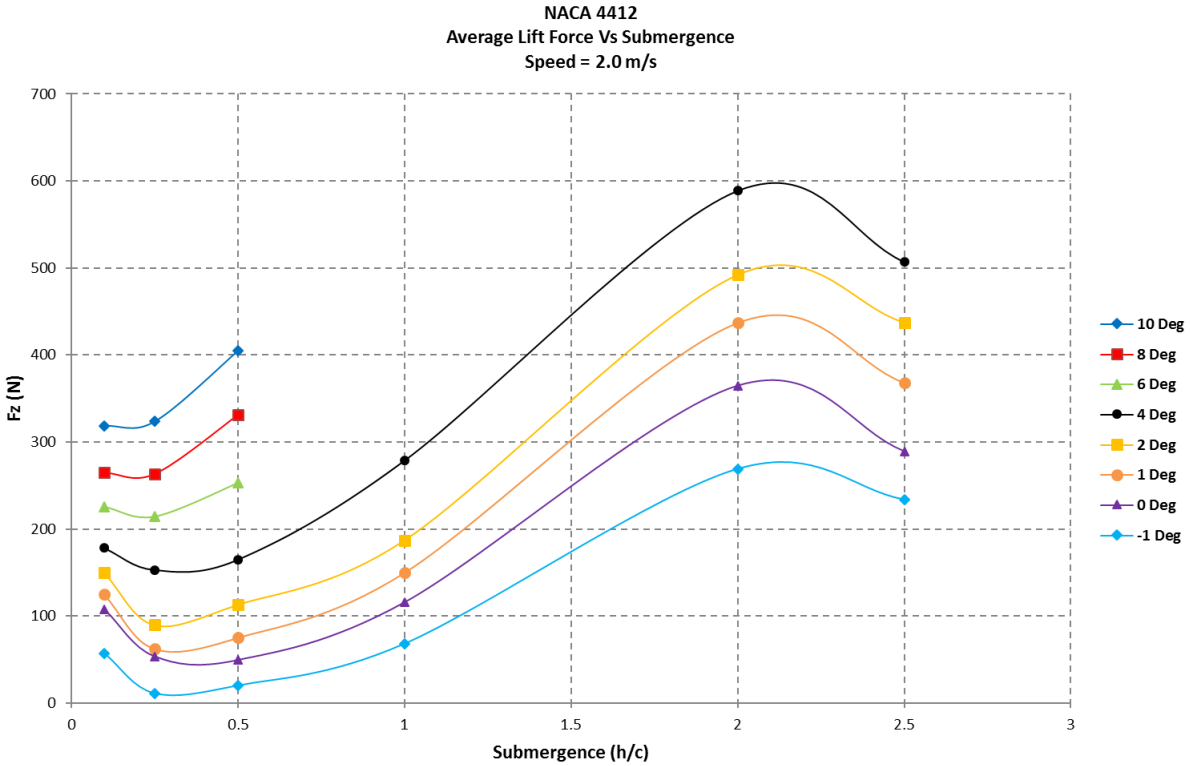

Figure 128: Lift generated plotted against the submergence (h/c) for a velocity of 2.0 m/s for a range of angles of attack.

Here is presented the average Lift force (Fz (N)), plotted against the submergence (h/c), at a speed of 2.0 m/s for a range of angles of attack. For all angles (except 10 degrees), a decrease can be seen from 0.1 c to 0.25 c, a rise until a submergence of 2.0 c after which the value decreases.

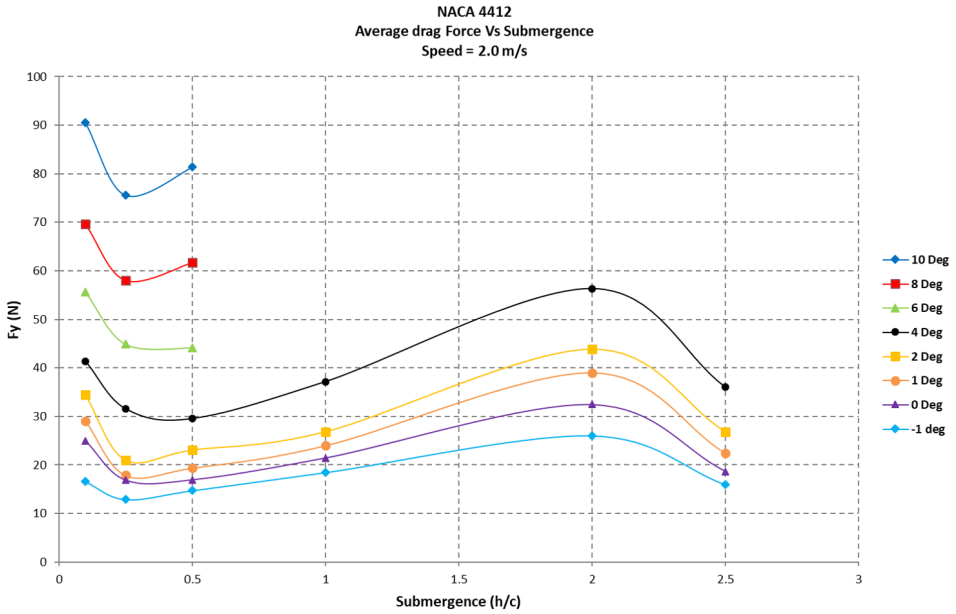

Figure 129: Drag generated plotted against the submergence (h/c) for a velocity of 2.0 m/s for a range of angles of attack.

Here is presented the average Drag force (Fy (N)), plotted against the submergence (h/c), at a speed of 2.0 m/s for a range of angles of attack. the values dip at a submergence of 0.25 c, rise steadily until a submergence of 2.0 c is reached. This trend is followed at all angles of attack.

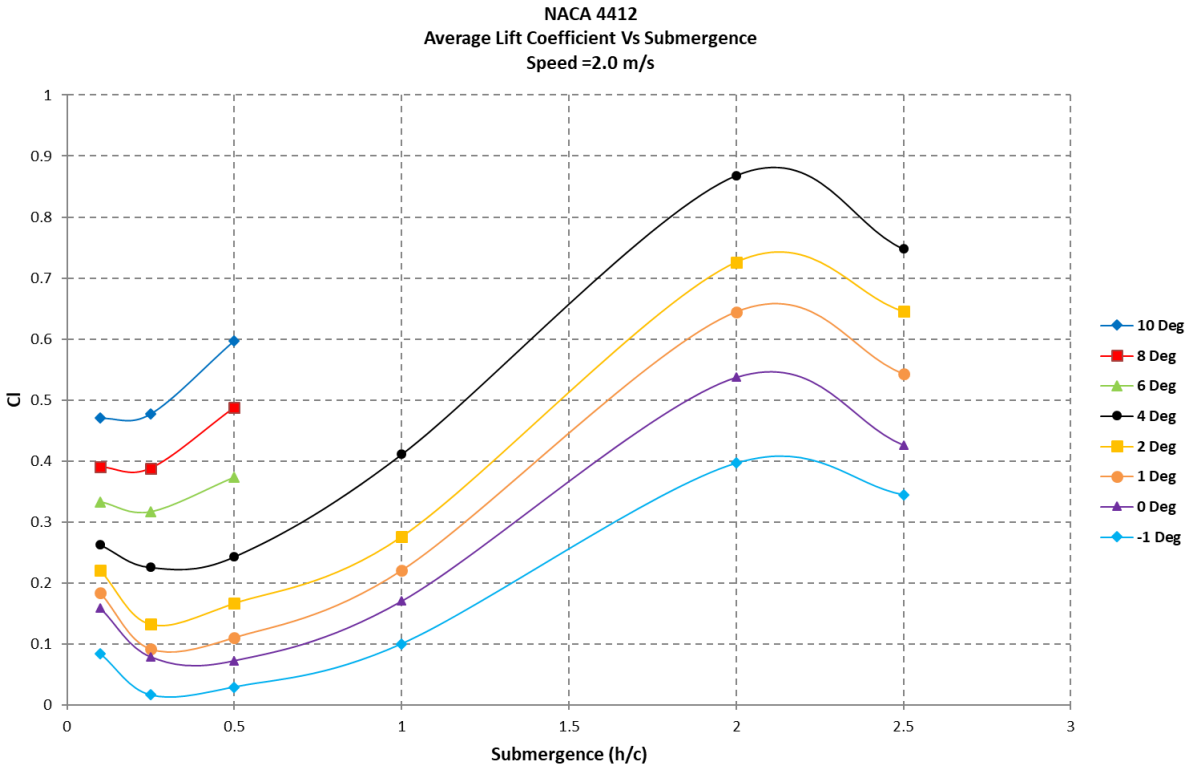

Figure 130: Lift coefficient generated plotted against the submergence (h/c) for a velocity of 2.0 m/s for a range of angles of attack.

Here is presented the average Lift coefficient (Cl), plotted against the submergence (h/c), at a speed of 2.0 m/s for a range of angles of attack. In this instance the lift coefficient follows the lift forces as shown in Figure 128.

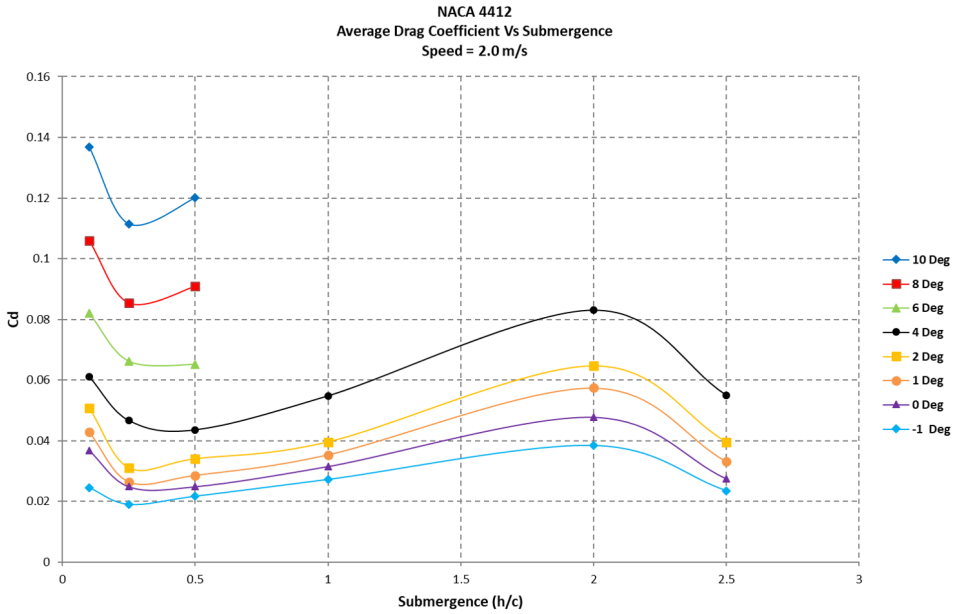

Figure 131: Drag coefficient generated plotted against the submergence (h/c) for a velocity of 2.0 m/s for a range of angles of attack.

Here is presented the average Drag coefficient (Cd), plotted against the submergence (h/c), at a speed of 2.0 m/s for a range of angles of attack. A decrease in value can be seen at a submergence of 0.25 c. The values then rise moderately until a submergence of 2.0 c is reached, after which they dip slightly.

8.2.3.8 velocity = 2.25 m/s

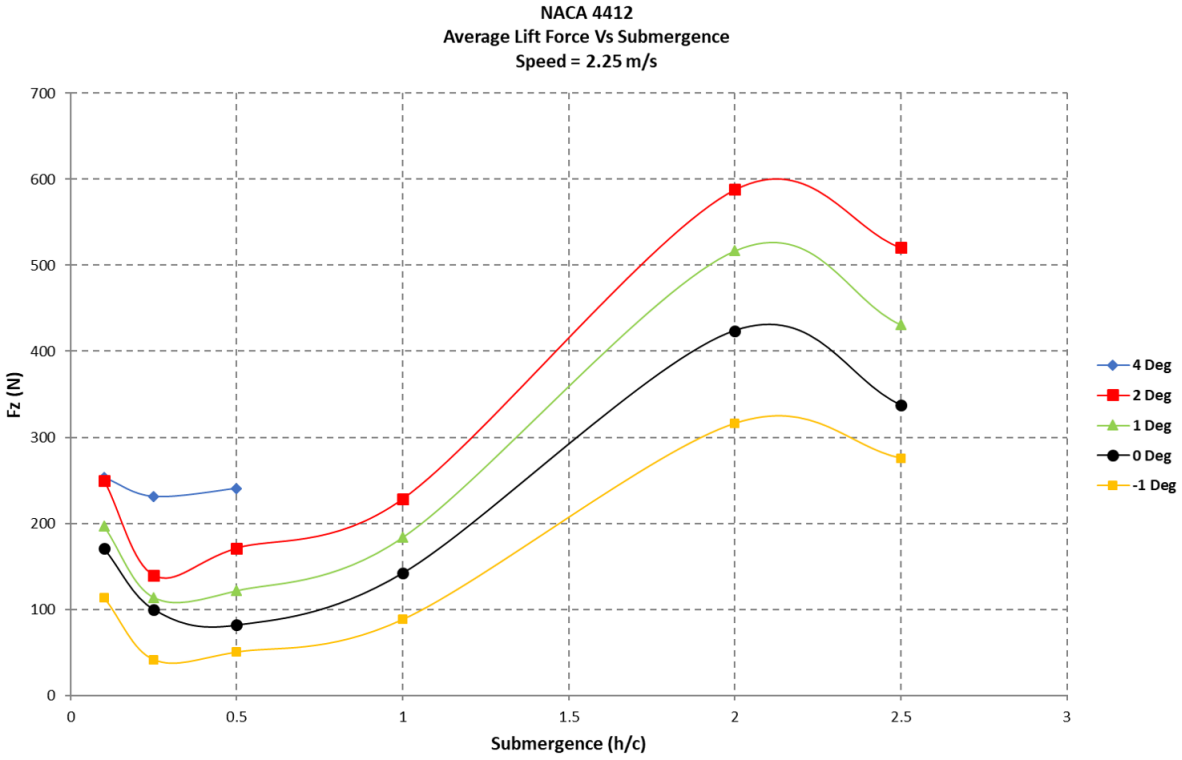

Figure 132: Lift generated plotted against the submergence (h/c) for a velocity of 2.25 m/s for a range of angles of attack.

Here is presented the average Lift force (Fz (N)), plotted against the submergence (h/c), at a speed of 2.25 m/s for a range of angles of attack. For all angles a decrease can be seen from 0.1 c to 0.25 c, a steady rise until a submergence of 2.0 c, after which the values decrease.

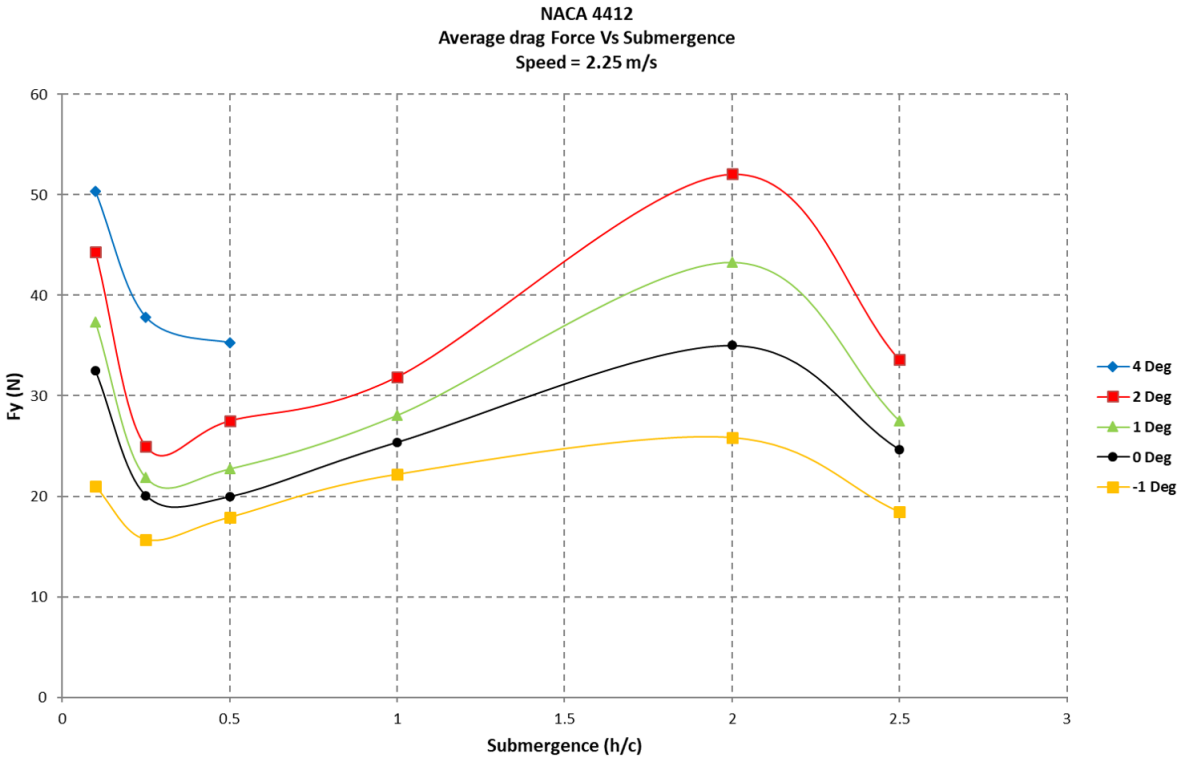

Figure 133: Drag generated plotted against the submergence (h/c) for a velocity of 2.25 m/s for a range of angles of attack.

Here is presented the average Drag force (Fy (N)), plotted against the submergence (h/c), at a speed of 2.25 m/s for a range of angles of attack. the values dip at a submergence of 0.25 c, rise steadily until a submergence of 2.0 c is reached. This trend is followed at all angles of attack.

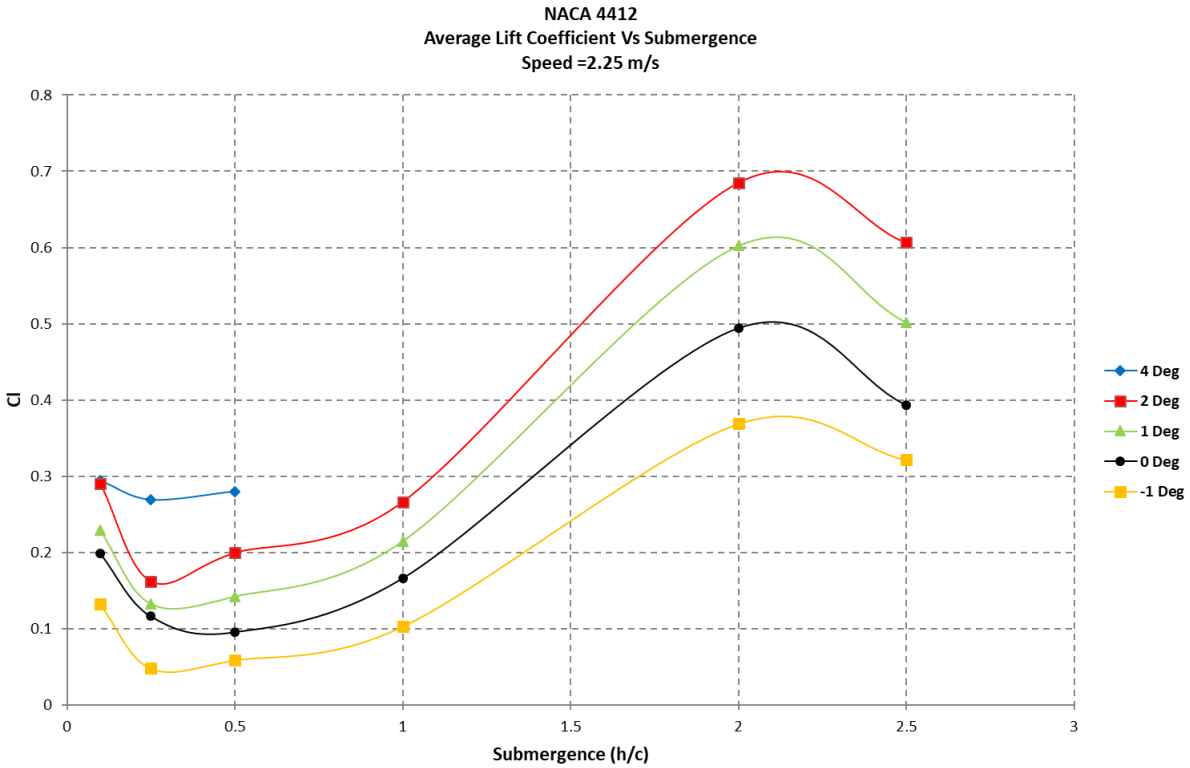

Figure 134: Lift coefficient generated plotted against the submergence (h/c) for a velocity of 2.25 m/s for a range of angles of attack.

Here is presented the average Lift coefficient (Cl), plotted against the submergence (h/c), at a speed of 2.25 m/s for a range of angles of attack. In this instance the lift coefficient follows the lift forces as shown in Figure 132.

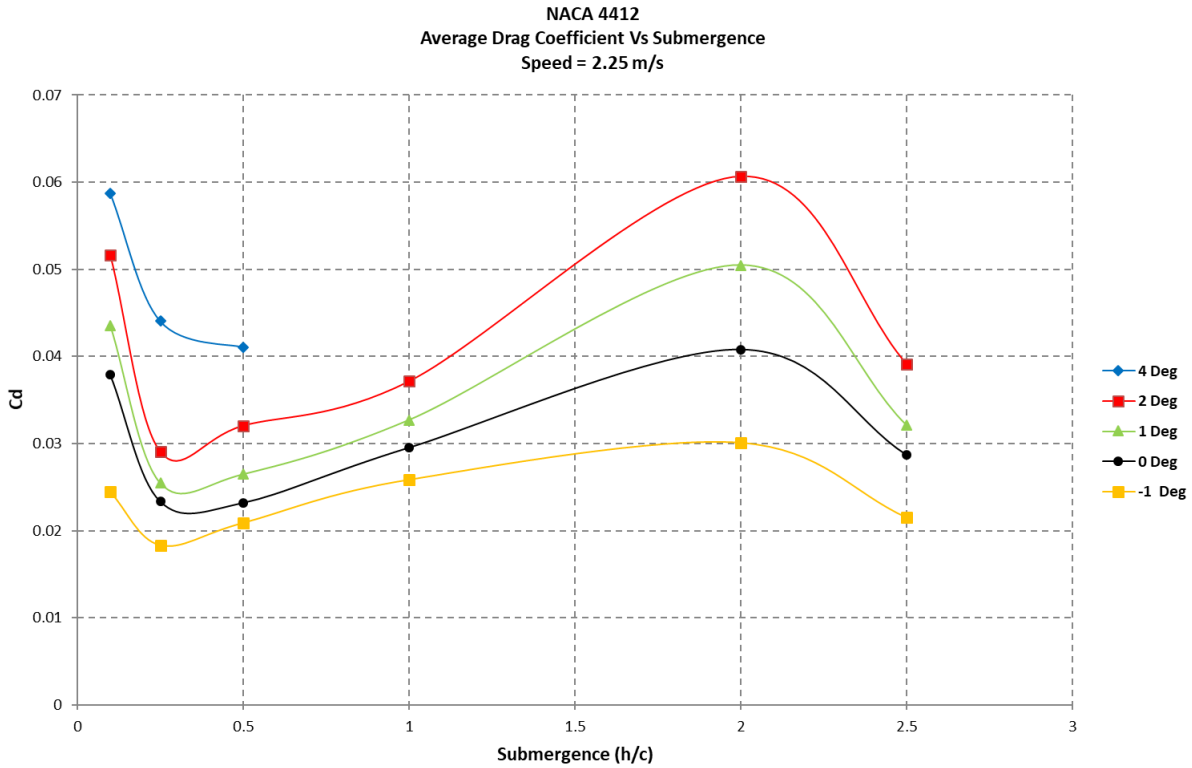

Figure 135: Drag coefficient generated plotted against the submergence (h/c) for a velocity of 2.25 m/s for a range of angles of attack.

Here is presented the average Drag coefficient (Cd), plotted against the submergence (h/c), at a speed of 2.25 m/s for a range of angles of attack. A decrease in value can be seen of a submergence of 0.25 c. The values then rise moderately until a submergence of 2.0 c is reached, after which they dip slightly.

8.2.3.9 velocity = 2.5 m/s

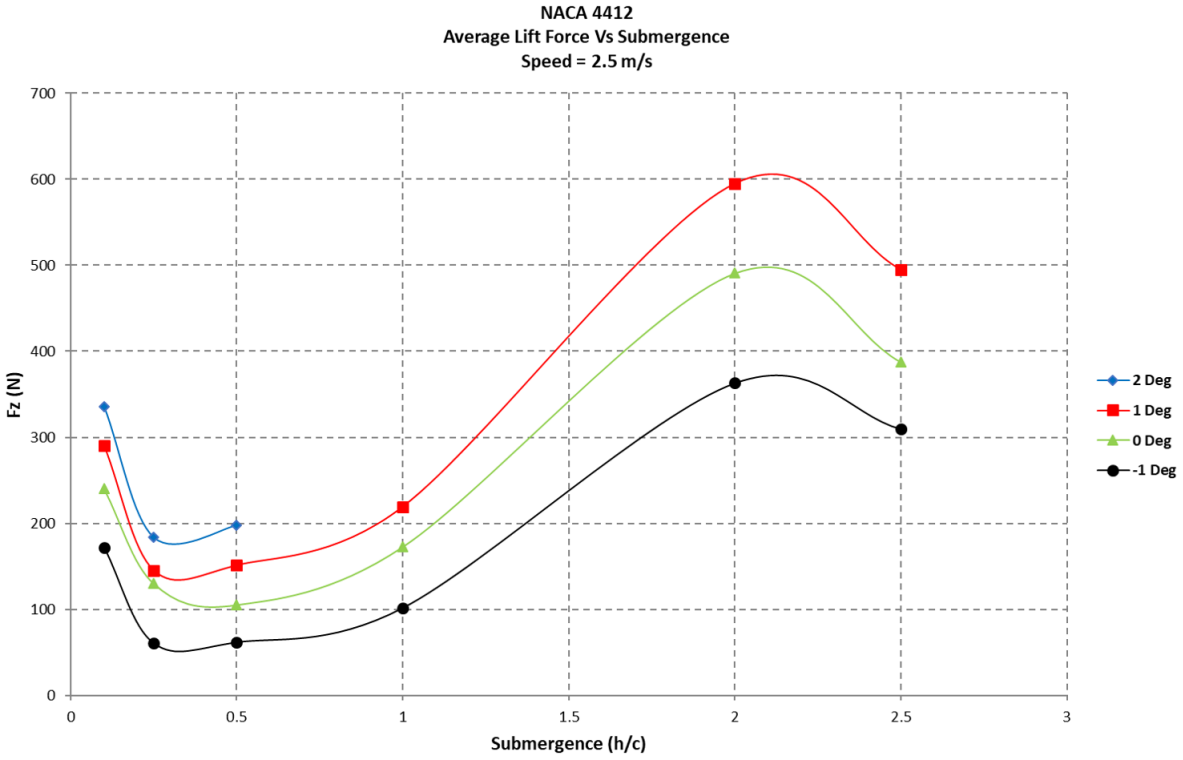

Figure 136: Lift generated plotted against the submergence (h/c) for a velocity of 2.5 m/s for a range of angles of attack.

Here is presented the average Lift force (Fz (N)), plotted against the submergence (h/c), at a speed of 2.5 m/s for a range of angles of attack. For all angles a decrease can be seen from 0.1 c to 0.25 c, a steady rise until a submergence of 2.0 c, after which the values decrease.

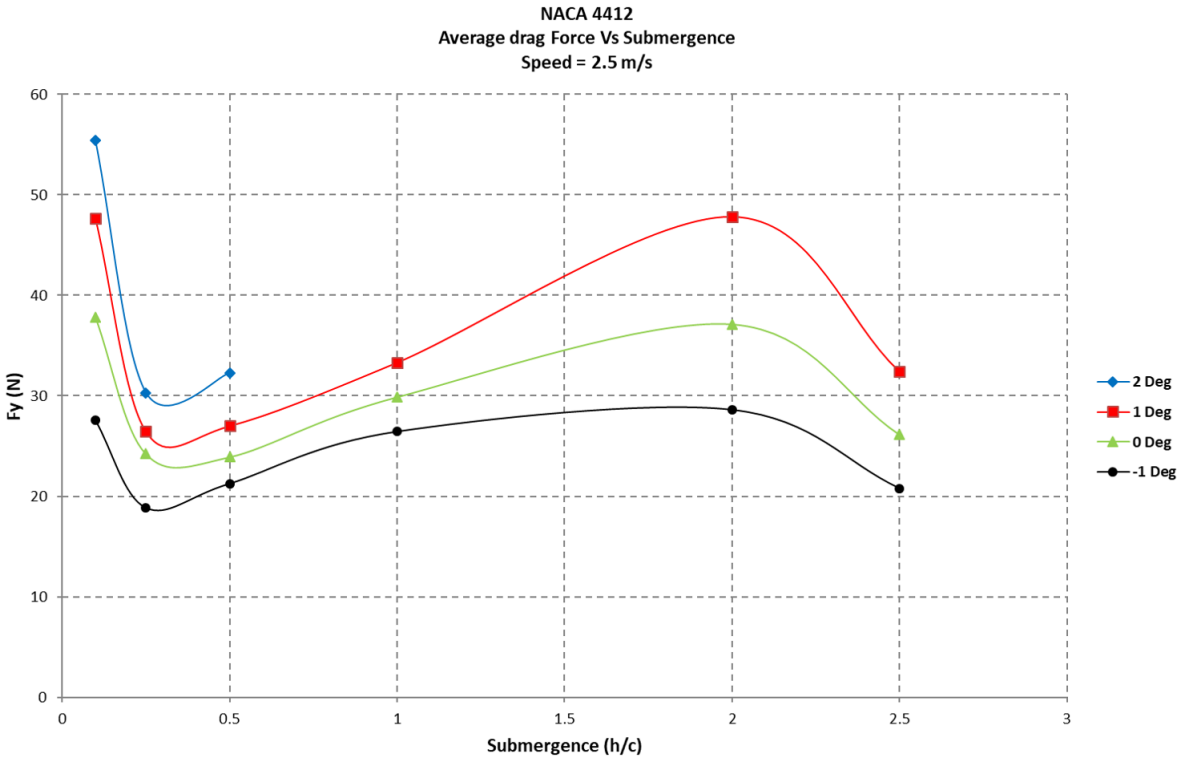

Figure 137: Drag generated plotted against the submergence (h/c) for a velocity of 2.5 m/s for a range of angles of attack.

Here is presented the average Drag force (Fy (N)), plotted against the submergence (h/c), at a speed of 2.5 m/s for a range of angles of attack. The values dip at a submergence of 0.25 c and then rise steadily until a submergence of 2.0 c is reached. This trend is followed at all angles of attack.

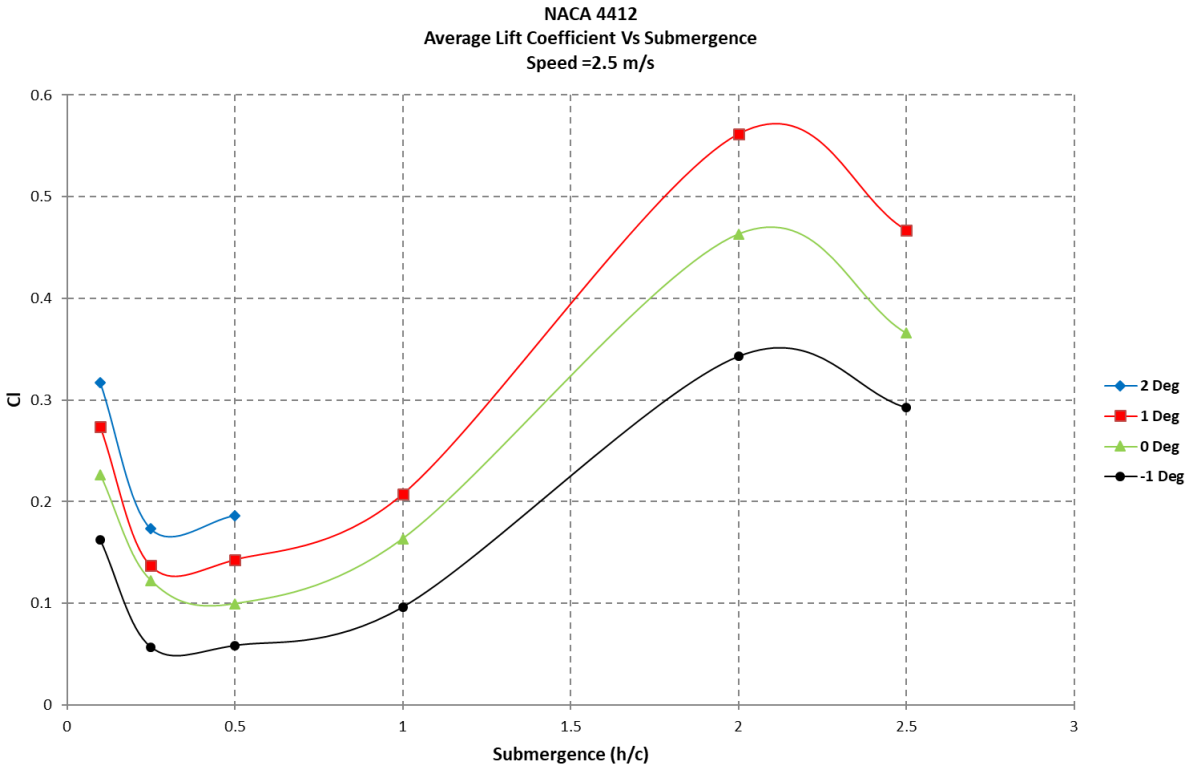

Figure 138: Lift coefficient generated plotted against the submergence (h/c) for a velocity of 2.5 m/s for a range of angles of attack.

Here is presented the average Lift coefficient (Cl), plotted against the submergence (h/c), at a speed of 2.5 m/s for a range of angles of attack. In this instance the lift coefficient follows the lift forces as shown in Figure 136.

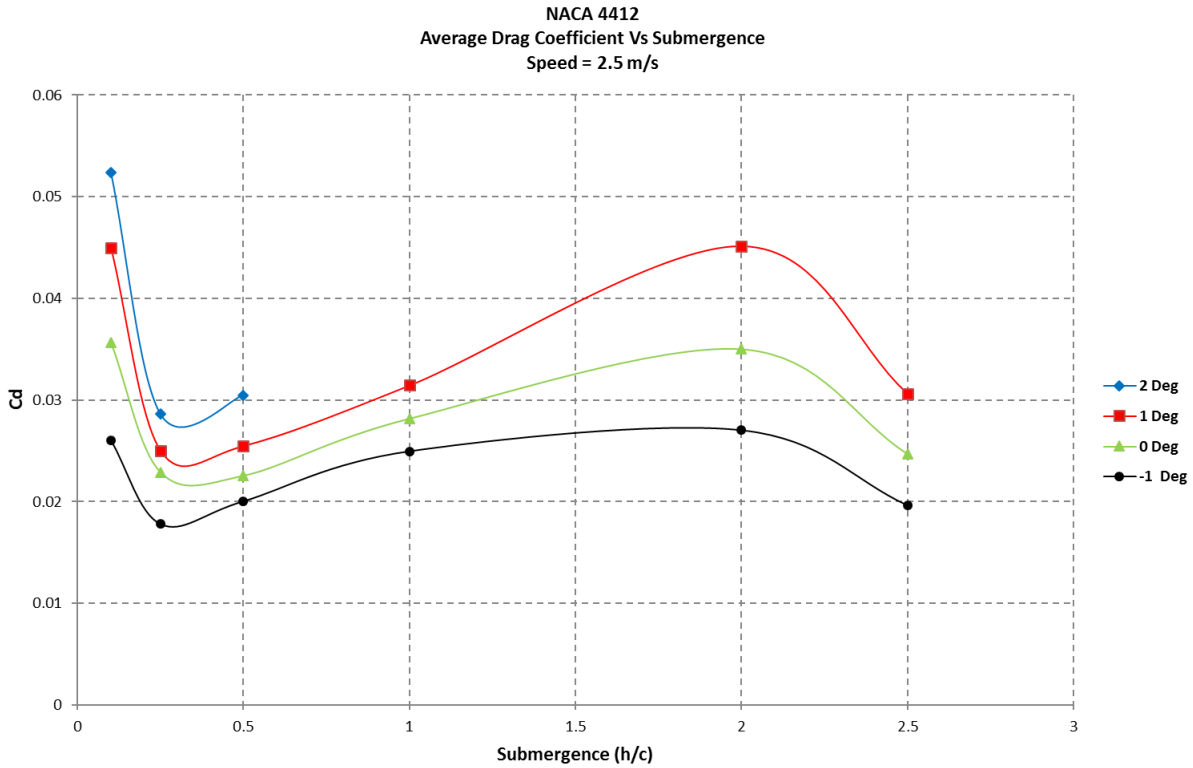

Figure 139: Drag coefficient generated plotted against the submergence (h/c) for a velocity of 2.5 m/s for a range of angles of attack.

Here is presented the average Drag coefficient (Cd), plotted against the submergence (h/c), at a speed of 2.5 m/s for a range of angles of attack. A decrease in value can be seen of a submergence of 0.25 c. The values then rise moderately until a submergence of 2.0 c is reached, after which they dip significantly.

8.2.3.10 velocity = 2.75 m/s

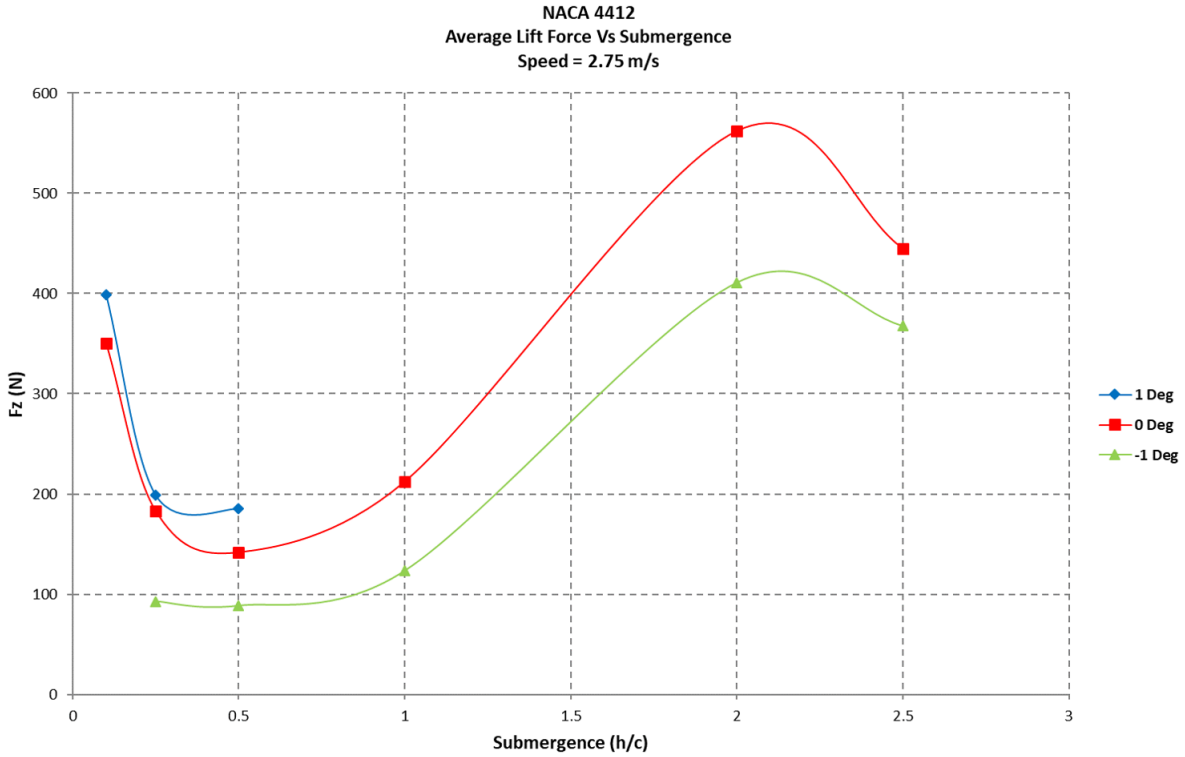

Figure 140: Lift generated plotted against the submergence (h/c) for a velocity of 2.75 m/s for a range of angles of attack.

Here is presented the average Lift force (Fz (N)), plotted against the submergence (h/c), at a speed of 2.75 m/s for 3angles of attack (1, 0 and -1 degrees). For all angles a decrease can be seen from 0.1 c to 0.25 c, a steady rise from 0.5 c until a submergence of 2.0 c, after which the values decrease.

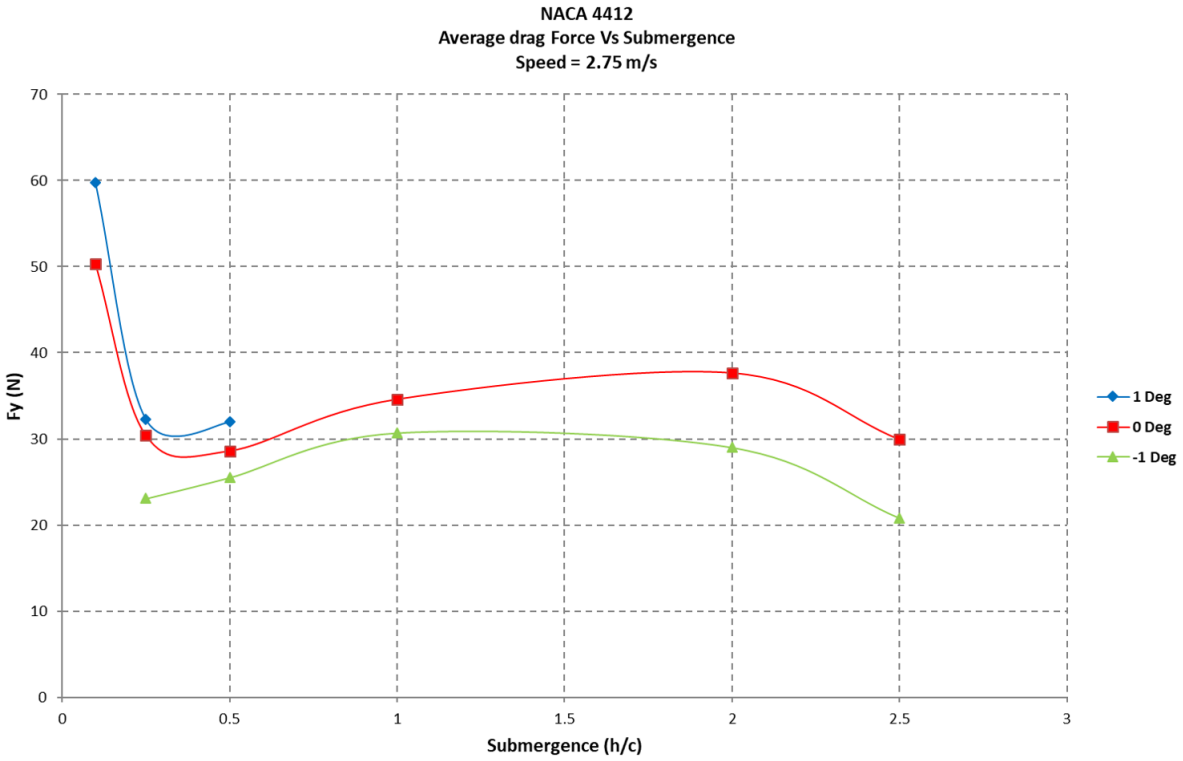

Figure 141: Drag generated plotted against the submergence (h/c) for a velocity of 2.75 m/s for a range of angles of attack.

Here is presented the average Drag force (Fy (N)), plotted against the submergence (h/c), at a speed of 2.75 m/s for a range of angles of attack. The values dip at a submergence of 0.25 c, rise steadily until a submergence of 2.0 c is reached. This trend is followed at all angles of attack.

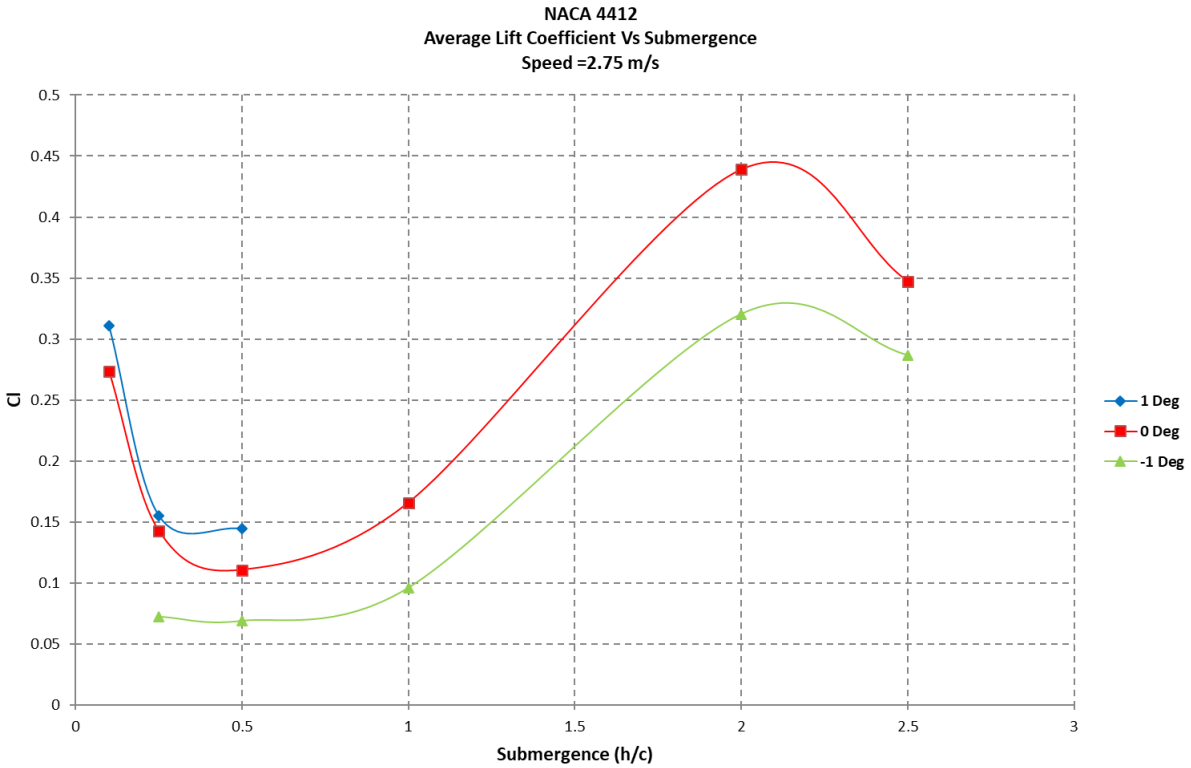

Figure 142: Lift coefficient generated plotted against the submergence (h/c) for a velocity of 2.75 m/s for a range of angles of attack.

Here is presented the average Lift coefficient (Cl), plotted against the submergence (h/c), at a speed of 2.75 m/s for a range of angles of attack. In this instance the lift coefficient follows the lift forces as shown in Figure 140.

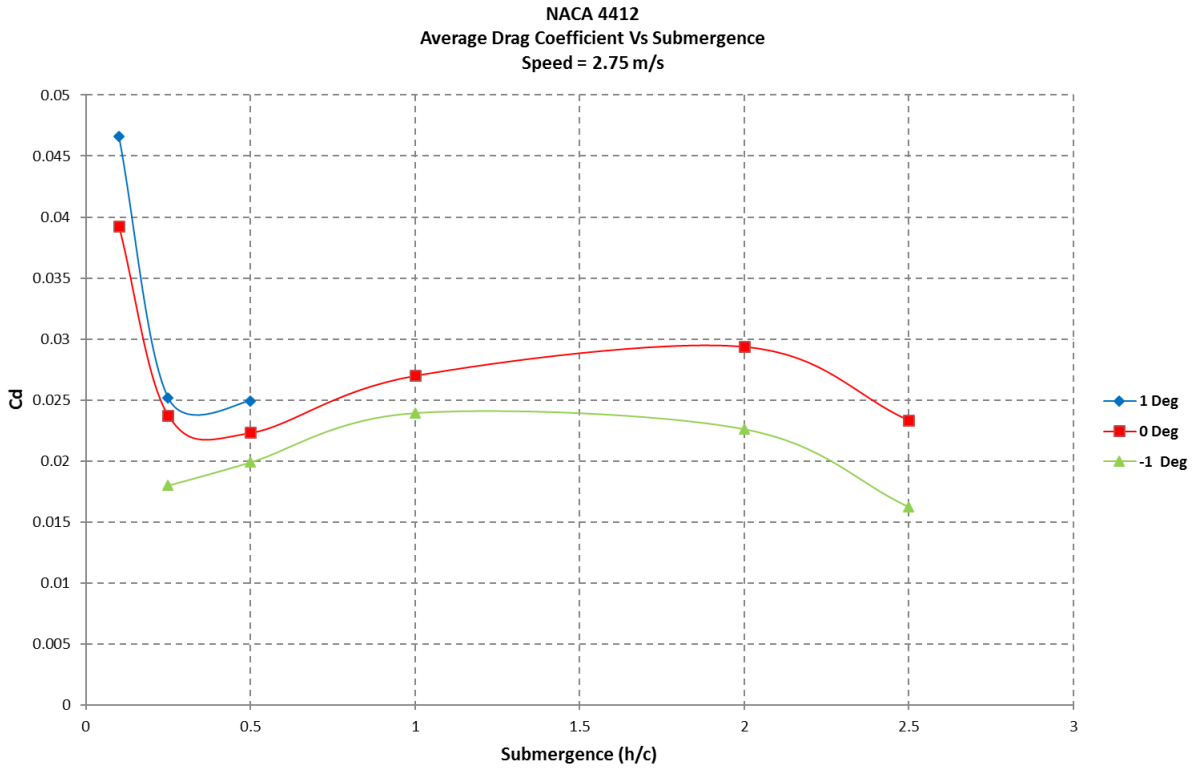

Figure 143: Drag coefficient generated plotted against the submergence (h/c) for a velocity of 2.75 m/s for a range of angles of attack.

Here is presented the average Drag coefficient (Cd), plotted against the submergence (h/c), at a speed of 2.75 m/s for a range of angles of attack. A decrease in value can be seen of a submergence of 0.25 c. The values then rise moderately until a submergence of 2.0 c is reached, after which they dip slightly.

8.2.3.11 velocity = 3.0 m/s

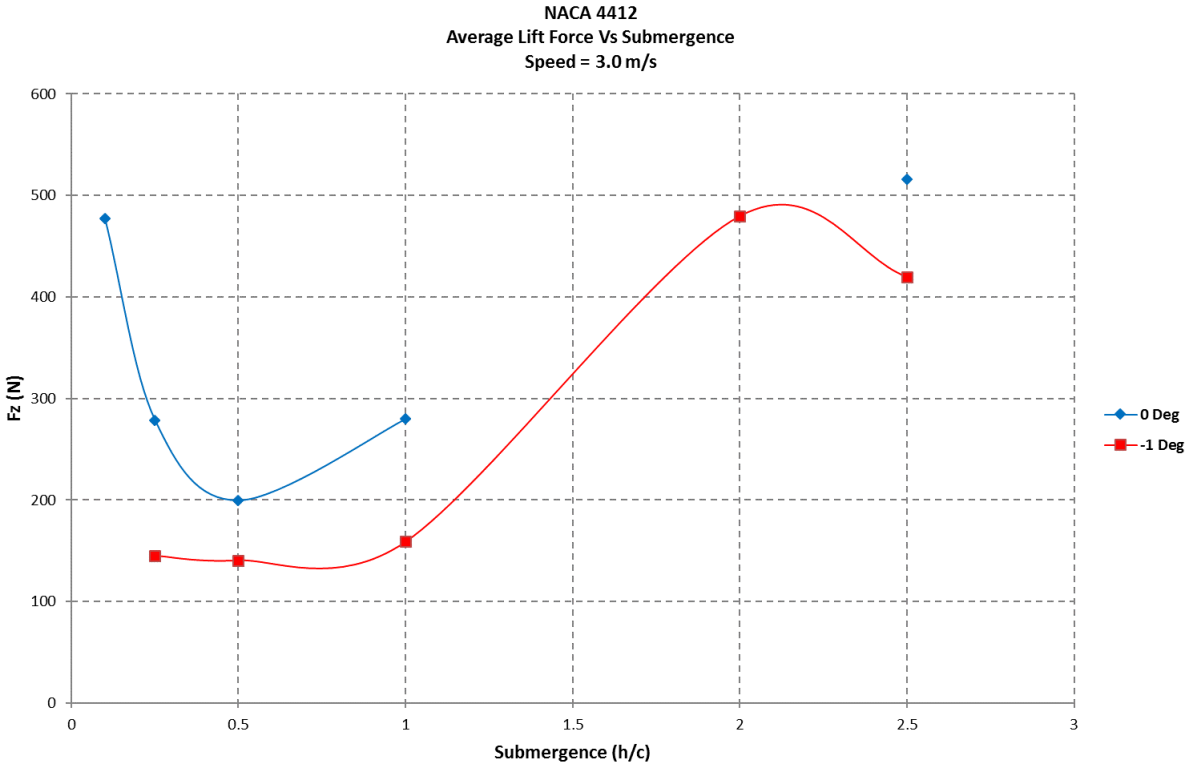

Figure 144: Lift generated plotted against the submergence (h/c) for a velocity of 3.0 m/s for a range of angles of attack.

Here is presented the average Lift force (Fz (N)), plotted against the submergence (h/c), at a speed of 3.0 m/s for 0 and -1 degrees. For these angles a decrease can be seen from 0.1 c to 0.25 c, a steady rise until a submergence of 2.0 c after which the values decrease.

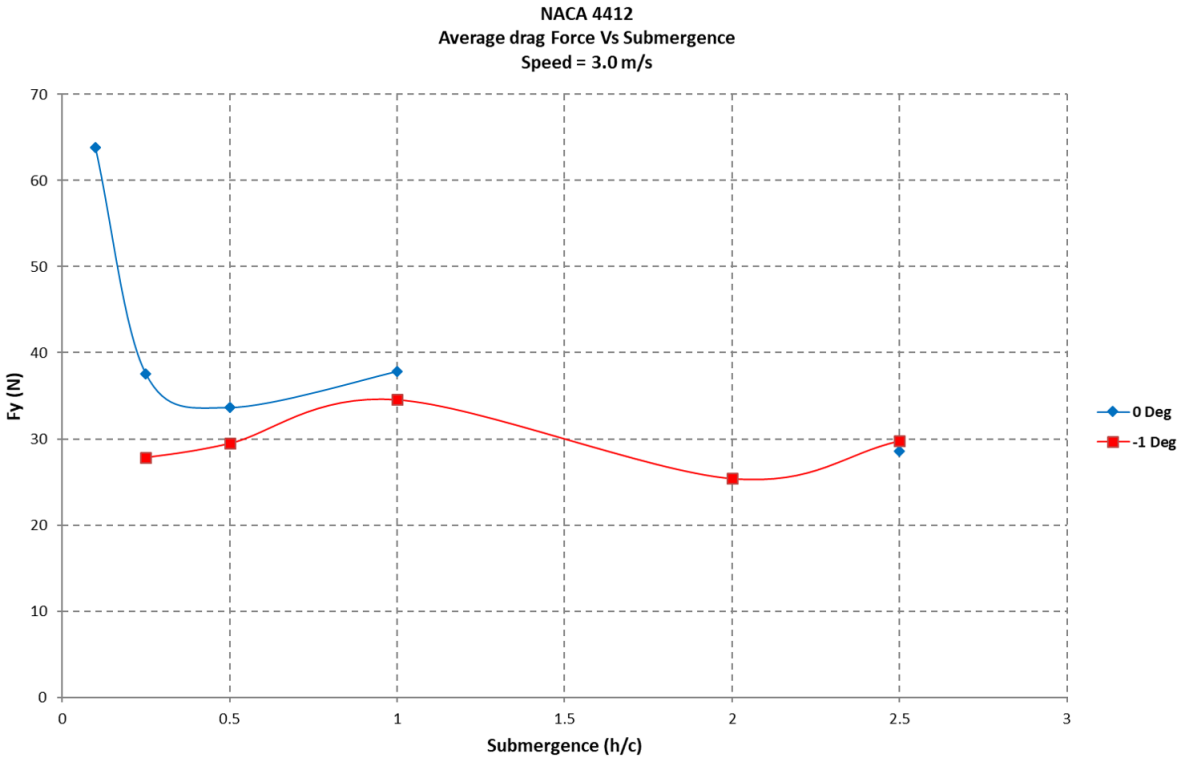

Figure 145: Drag generated plotted against the submergence (h/c) for a velocity of 3.0 m/s for a range of angles of attack.

Here is presented the average Drag force (Fy (N)), plotted against the submergence (h/c), at a speed of 3.0 m/s for a range of angles of attack. For an angle of attack of -1 degrees, the values fluctuate from depending on submergences. A high value is reached at a submergence of 1.0 c. At an angle of 0 degrees a dip in force is seen at a submergence of 0.25 c.

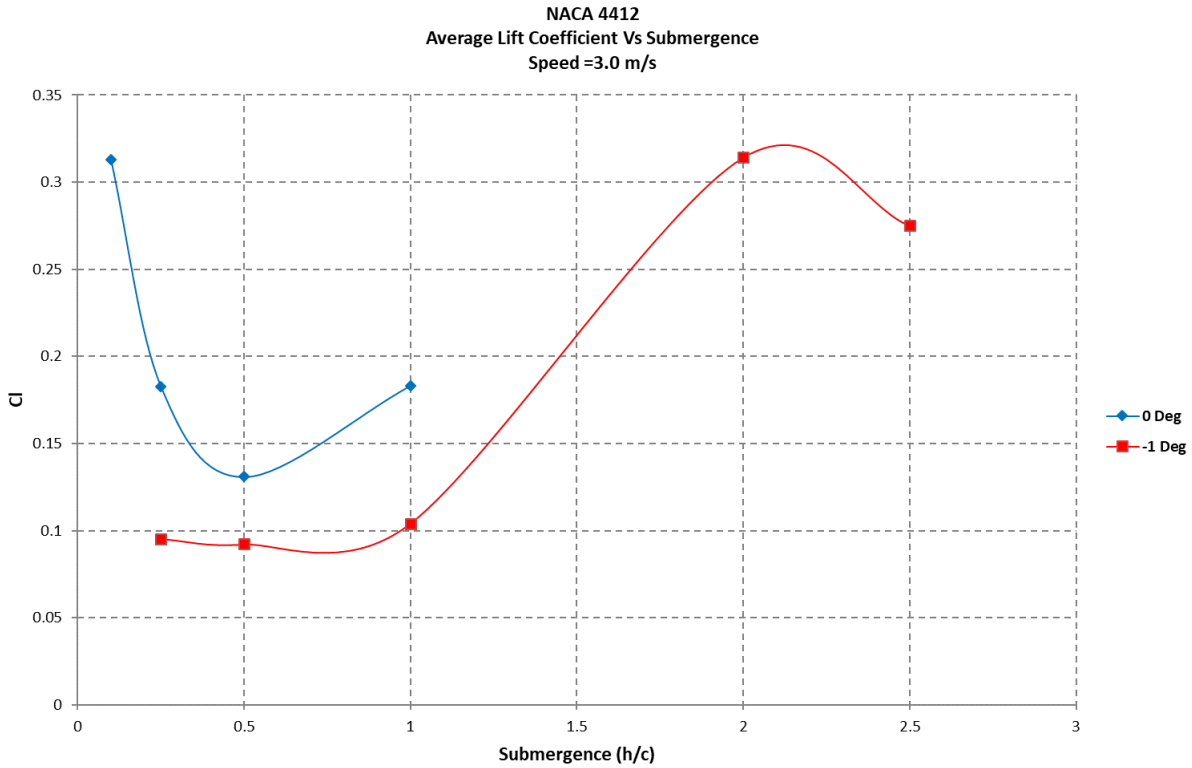

Figure 146: Lift coefficient generated plotted against the submergence (h/c) for a velocity of 3.0 m/s for a range of angles of attack.

Here is presented the average Lift coefficient (Cl), plotted against the submergence (h/c), at a speed of 3.0 m/s for a range of angles of attack. In this instance the lift coefficient follows the lift forces as shown in Figure 144.

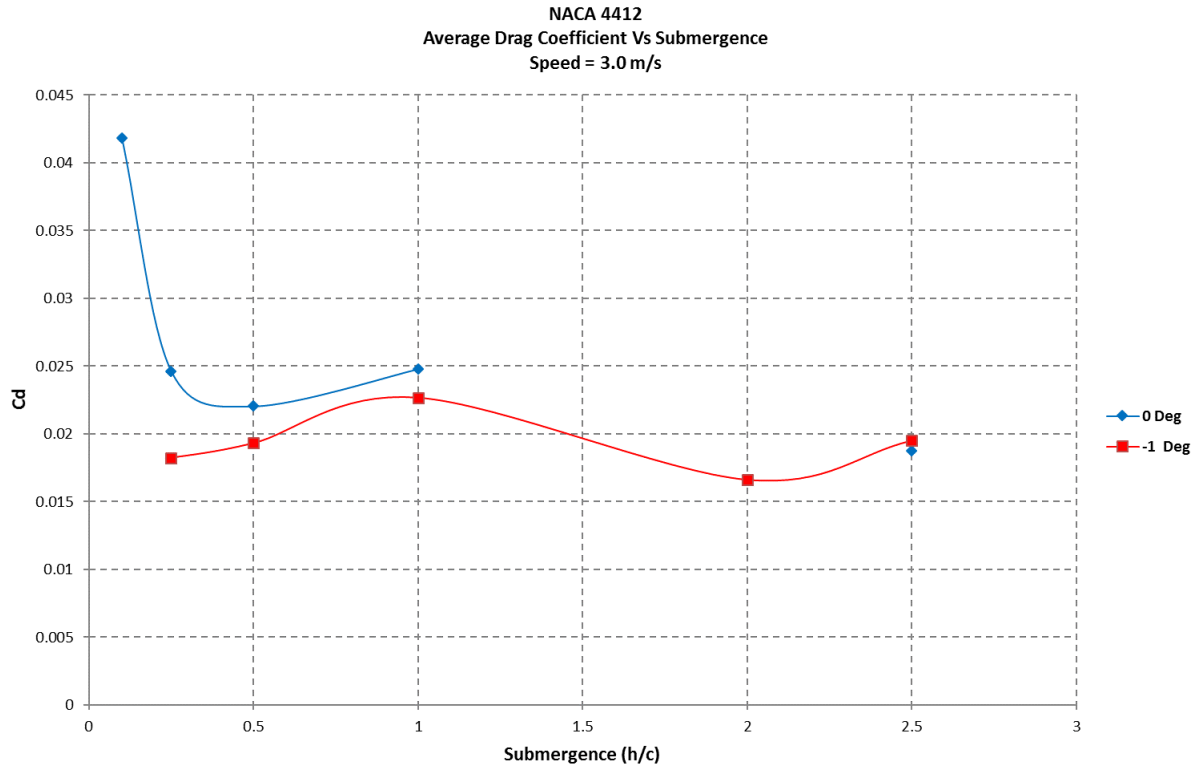

Figure 147: Drag coefficient generated plotted against the submergence (h/c) for a velocity of 3.0 m/s for a range of angles of attack.

Here is presented the average Drag coefficient (Cd), plotted against the submergence (h/c), at a speed of 3.0 m/s for a range of angles of attack. For an angle of attack of 0 degrees, there is a sharp decline between a submergence of 0.1 and 0.5 c, it then increases moderately for a submergence of 1.0 c. At an angle of -1 degrees, a slight increase in value for a submergence of 1.0 c, the value then dips at 2.0 c, before coming back up at 2.5 c.

8.2.3.12 Conclusion

The effects of the variation of velocity are only seen at low velocities. The combination with shallow submergence and small angles, creates negative lift.

8.3 Struts only

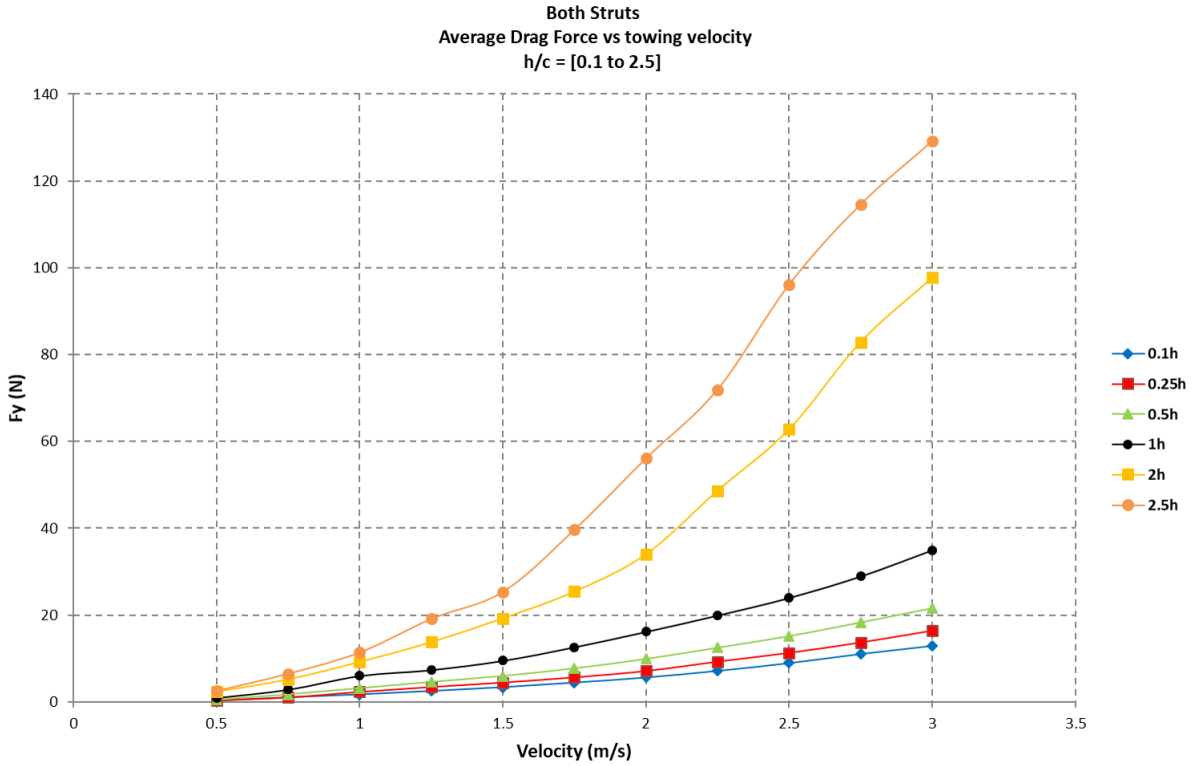

Figure 148: Drag forces (Fy (N)) generated by the struts without the foil at different towing velocities and different submergences.

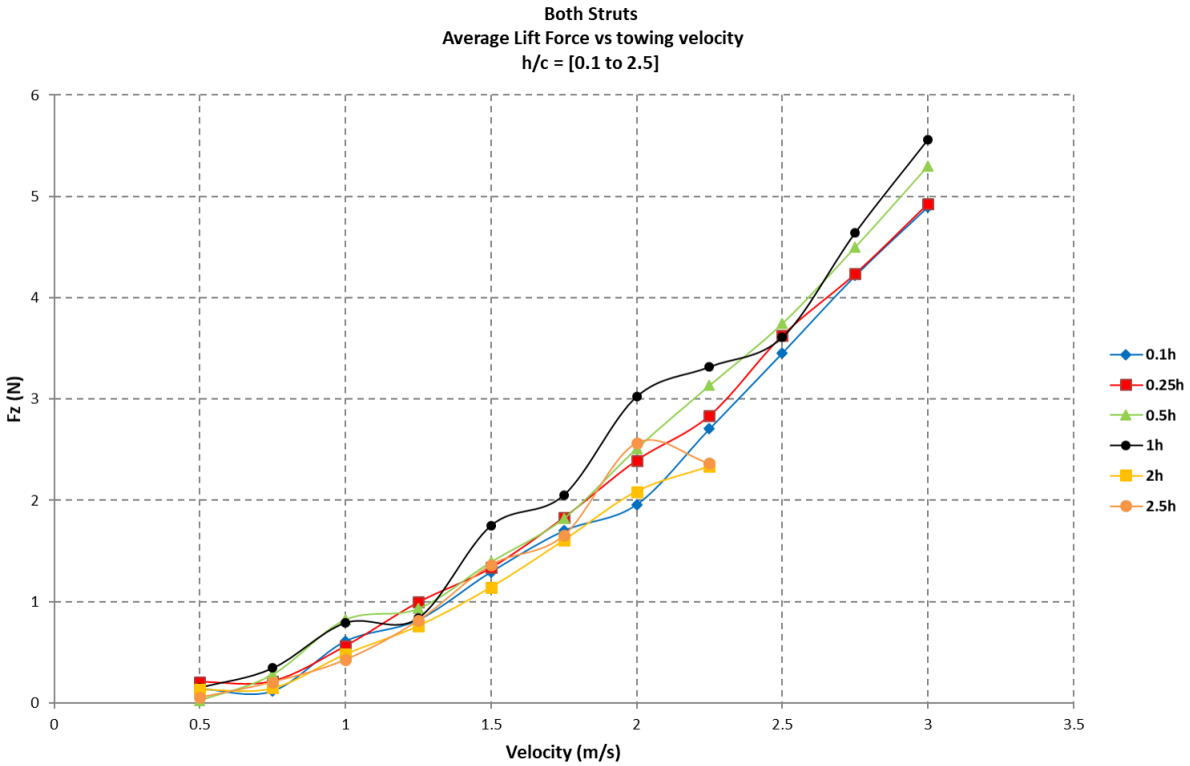

Figure 149: Lift forces(Fz (N)) generated by the struts without the foil at different towing velocities and different submergences.

It can be seen on Figures 148 and 149 the effects of the struts on the results gathered show it is mainly a drag component that is created. It is also shown that the lift component of the struts on their own is negligible.

9 Analysis of experimental data

9.1 Case of low submergence

9.1.1 Introduction

The following pages analyse the experimental data gathered at shallower submergences. The submergences studied here range from 0.1 chord to 1.0 chord.

9.1.2 Analysis of lift

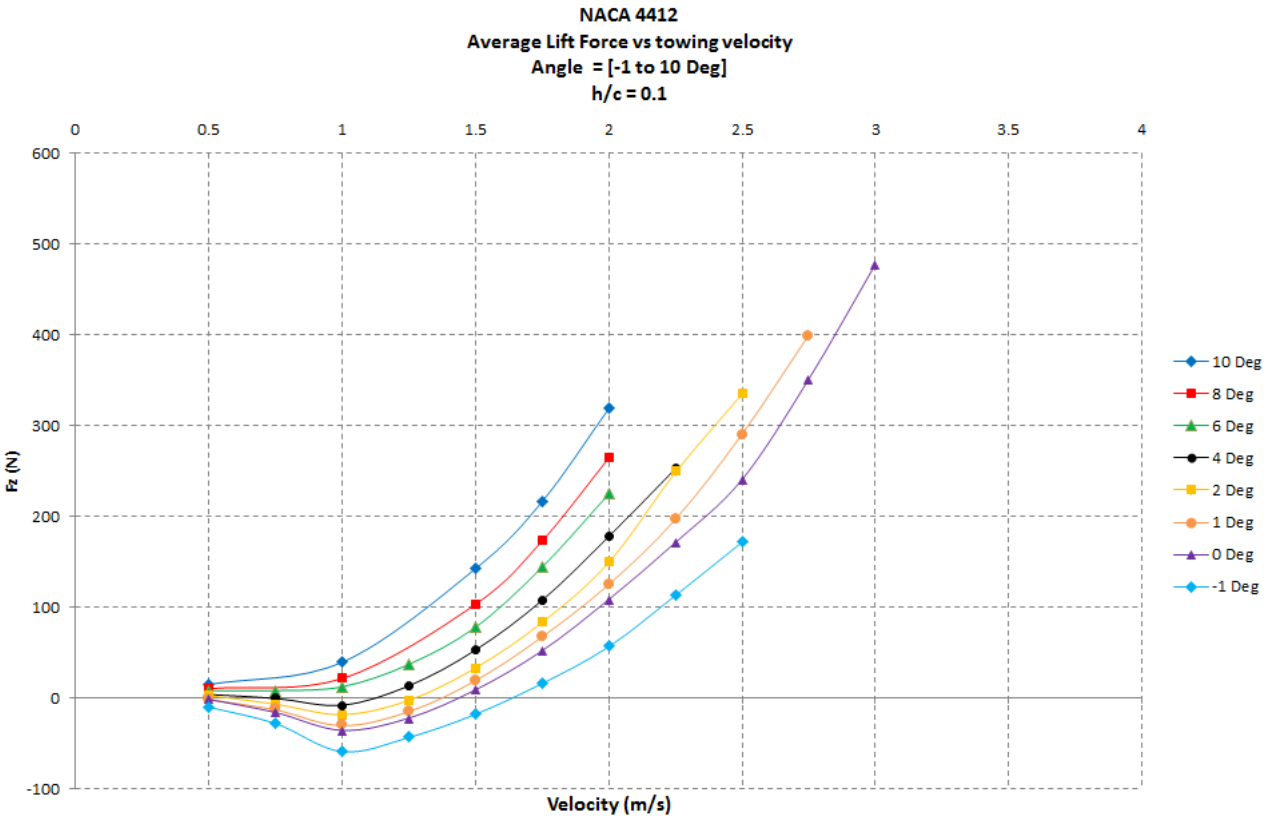

Figure 150: Lift forces (N) generated at different towing velocities and different angles for a submergence of 0.1 c.

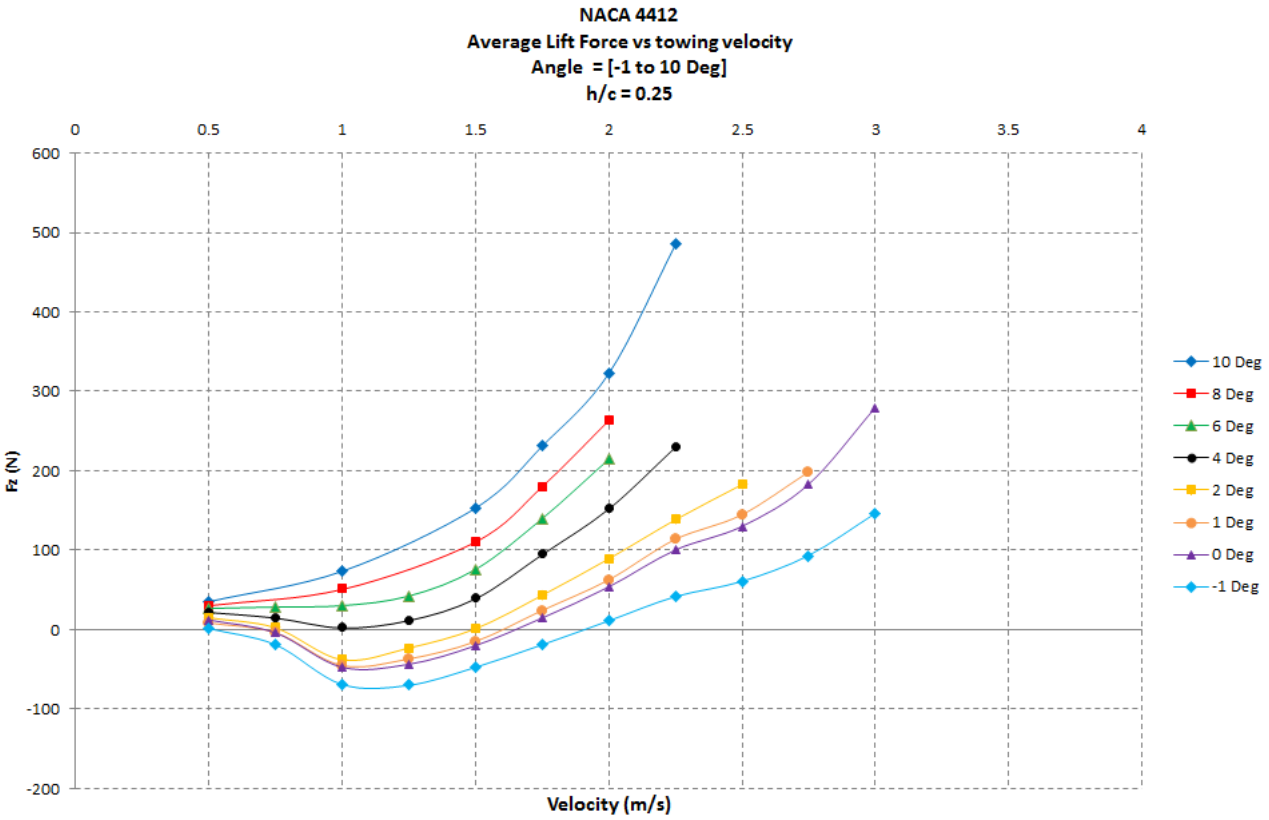

Figure 151: Lift forces (N) generated at different towing velocities and different angles for a submergence of 0.25 c.

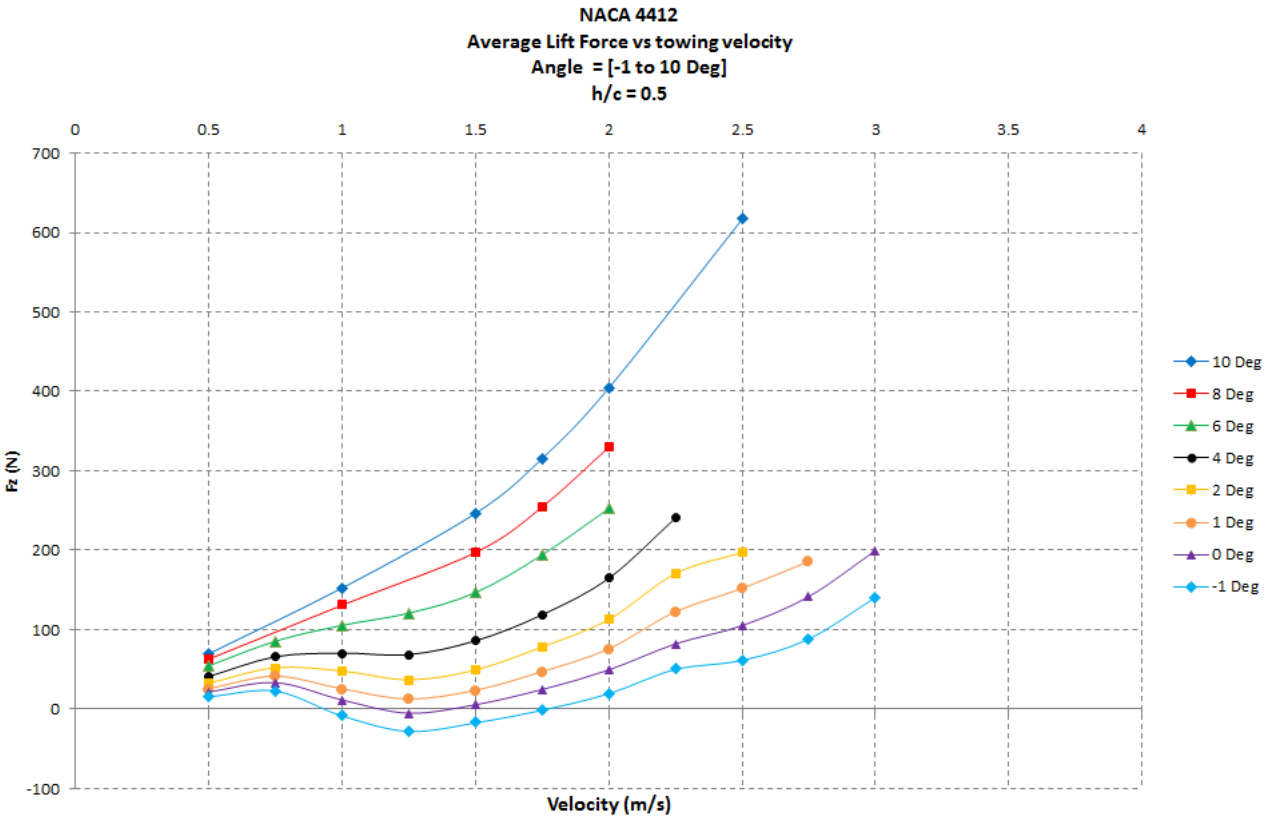

Figure 152: Lift forces (N) generated at different towing velocities and different angles for a submergence of 0.50 c.

As seen in Figures 151 and 152, negative lift forces are created at certain speeds for some angles.
This phenomenon happens until a submergence of 1.0 is reached. At a submergence of 0.5, only 0 and -1 degrees generate negative lift forces. At a submergence of 0.25, negative lift forces are created for angles 2, 1, 0 and -1 degrees. At a submergence of 0.1, a 4 degree angle of incidence also generates negative lift forces.
At higher angles of incidence, lift forces generated are not negative.
As a reminder, a NACA 4412 profile in free flow has a null lift for an angle of attack of -4 degrees.
As proven by Daskovsky's work in 2000 [20], it is possible to generate negative lift coefficients - see Figure 153.

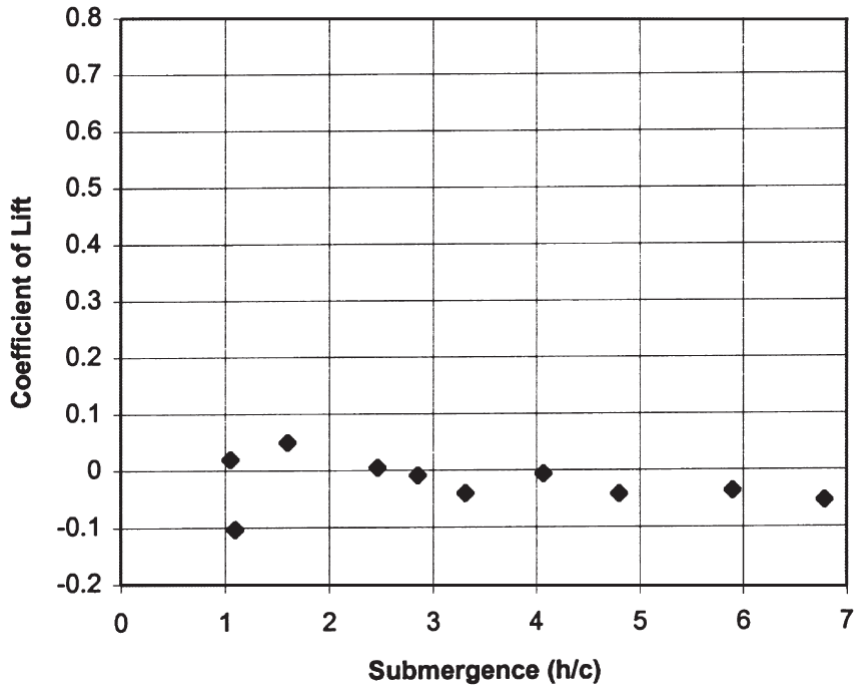

Figure 153: Coefficient of lift of a NACA 0012 Profile at 0 degrees Angle of Attack of zero degrees at a velocity of 3.0 m/s [20]

9.1.2.1 Ventilation

As detailed in 4.3.2, ventilation occurs when foils are used close to the surface. This explanation can be confirmed using the results of the video recording of the runs - see Figure 154.

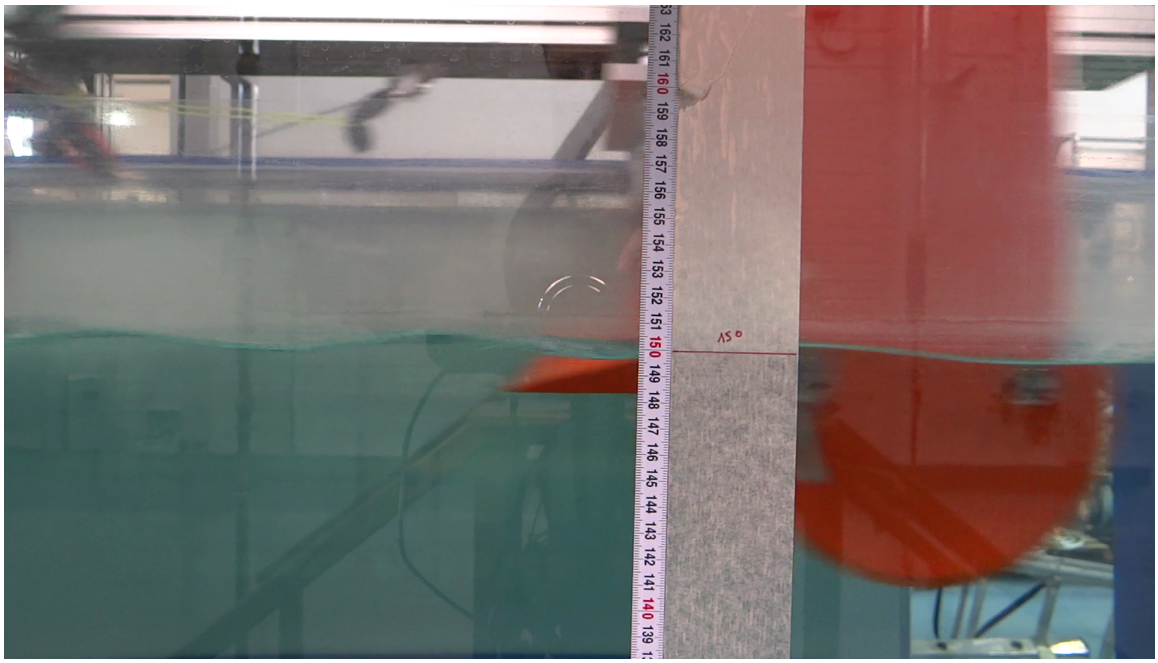

Figure 154: Flow visualisation at a speed of 0.5 m/s, a submergence of 0.1 chords and a angle of attack of 0 degrees

It is important to remember that the submergence was set in standing water, the hydrofoil displaces water as it goes along, This means that the submergence at the leading edge stays constant. The waves measured here are formed by the moving hydrofoil and occur behind it.

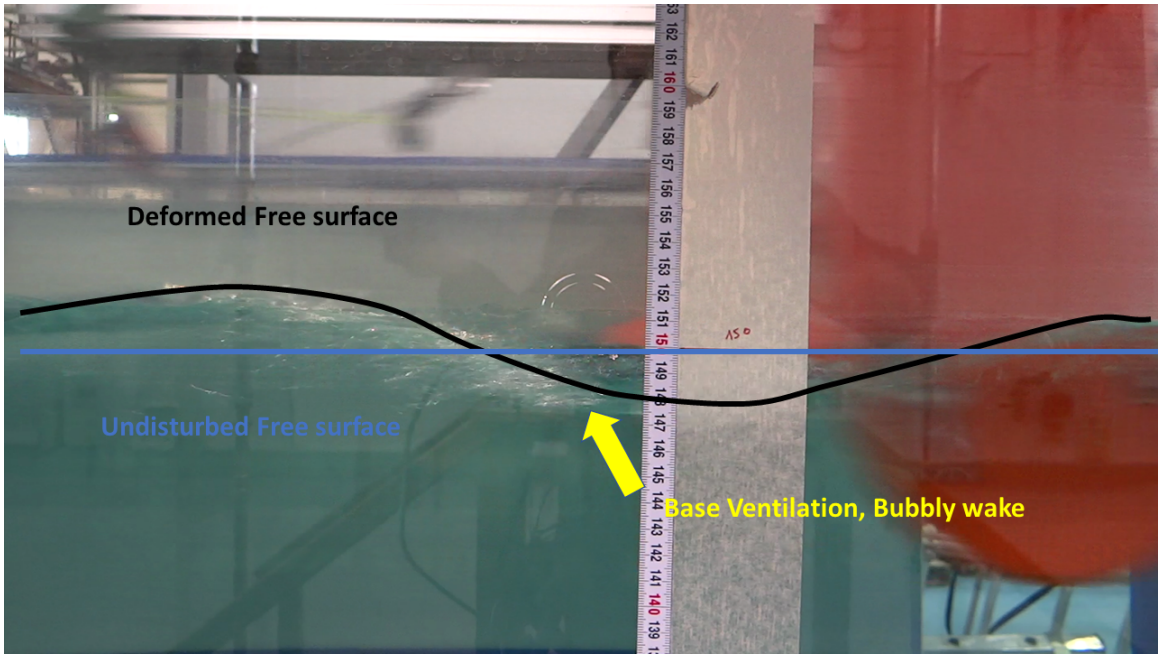

Figure 155: Flow visualisation at a speed of 1.0 m/s, a submergence of 0.1 chords and a angle of attack of 0 degrees

As seen in Figure 155 bubbles appear at a submergence of 0.1 chord and a speed of 1.0 m/s. This could indicates that air is in limited supply (but this is not the case here), or that it is sucked for a brief period.

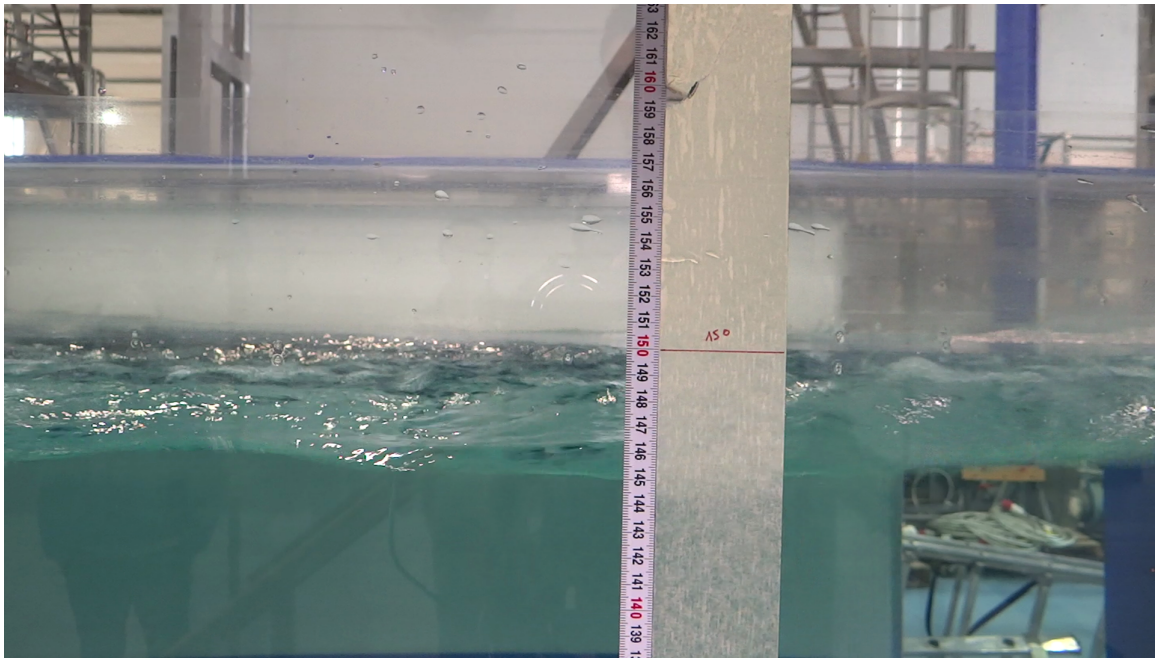

Figure 156: Flow visualisation at a speed of 3.0 m/s, a submergence of 0.1 chords and a angle of attack of 0 degrees

As shown in Figure 156, this phenomenon disappears when speed increases.

This indicates that in low speeds and low submergences, water has difficulties moving over the foil and air gets entrained. This in turn creates the negative lift observed at low speeds. At higher velocities, there is no ventilation and no negative lift is seen.

9.1.2.2 Cavitation

As seen in the Literature review 4, cavitation can come into play under certain conditions. by using the equation 11, it is possible to obtain speed metrics at which cavitation should start appearing. Those values are presented for an angle of attack of 0 Degrees at different submergences in Table 7 below :

Cavitation speed for a NACA 4412 hydrofoil at an angle of Attack of 0 degrees	
Submergence (h/c)	Velocity (m/s)
2.5	21.4
2	21.3
1	21
0.5	20.8
0.25	20.7
0.1	20.7

Table 7: Results of speeds at which the cavitation phenomenon can be expected.

As seen above, the results for this hydrofoil in those configurations, the speeds at which cavitation is expected is at least 20 m/s. Those speeds are not reached in this experiment. The experiment conducted here also shows that lift losses happen at lower speeds, and especially between 0.5 and 1.25 m/s It can be concluded that cavitation does not play a major role this experiment.

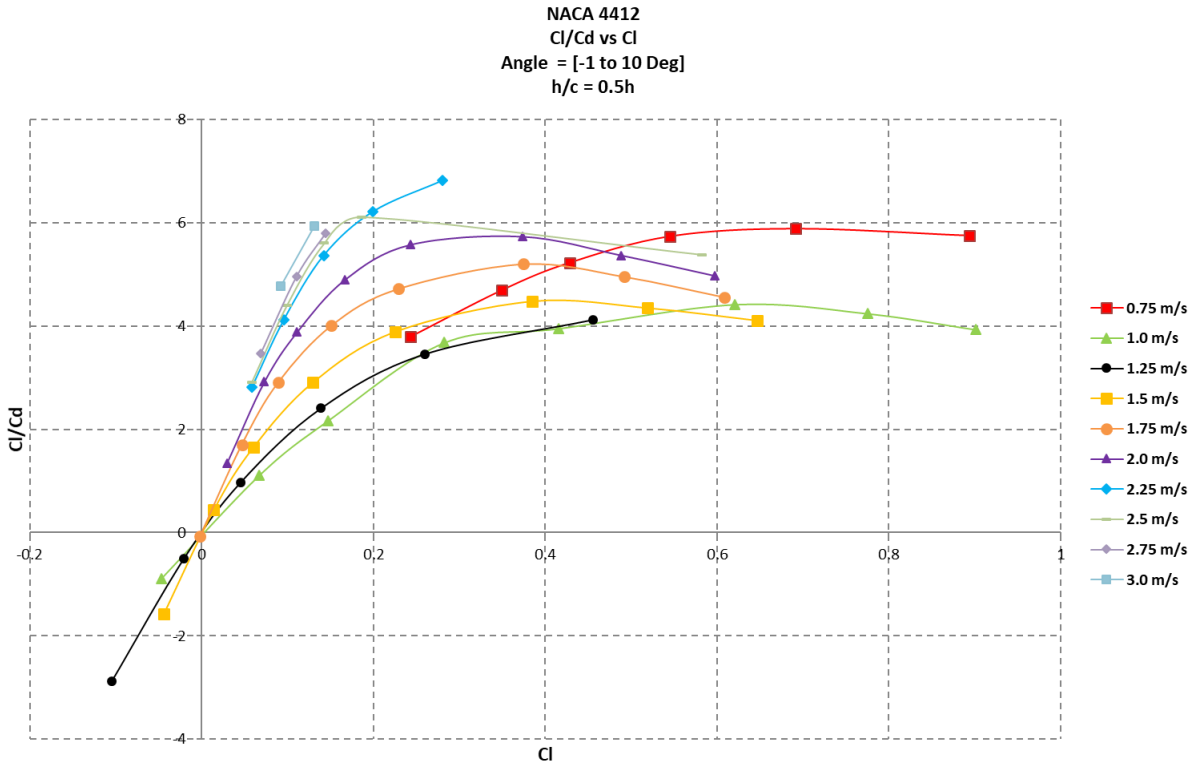

Figure 157: Average Lift coefficient over average Drag coefficient plotted against average lift coefficient, at different speeds for a submergence of 0.5 chords.

The results shown in figure 157 are comparable to those presented by Macks, N. Z.N., A. W.J. in 1951 [24].Those results are presented in Figure 158 below .

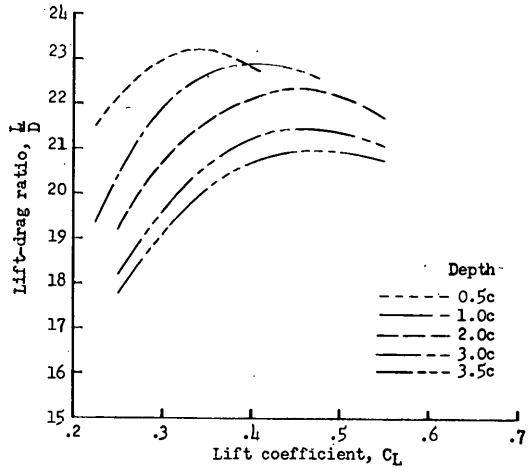

(a) 15 feet per second.

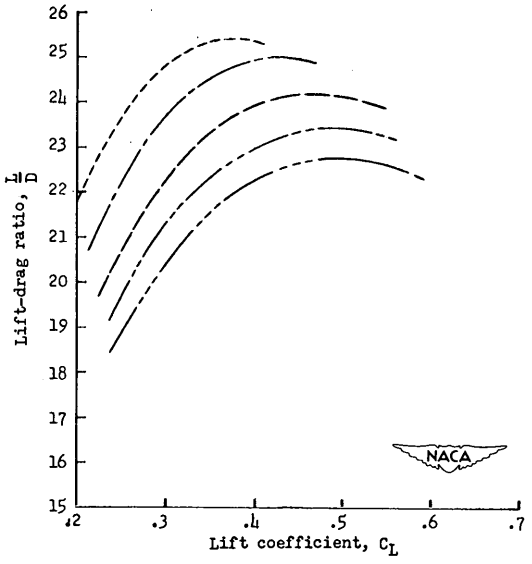

(b) 35 feet per second.

Figure 8.- Variation of lift-drag ratio with lift coefficient and depth of submersion. (Hydrofoil-strut configuration)

Figure 158: Results presented by Macks, N. Z.N., A. W.J. in 1951 [24] at different submergences for speeds of 4.6 m/s and 10.7 m/s

This further proves the point that cavitation is not a factor in this experiment.

9.1.3 Analysis of drag

As seen in Figure 159 below, differences in submergence do not have much of an impact on drag forces: :

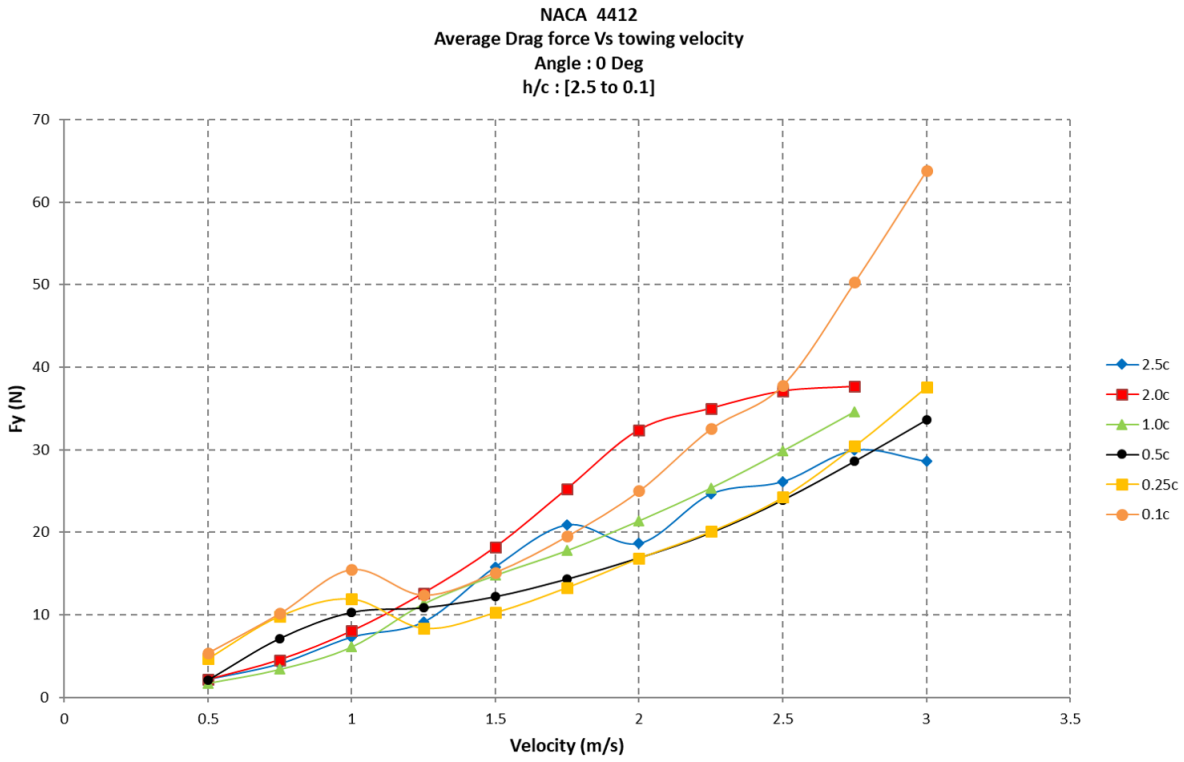

Figure 159: Drag force (F (N)) plotted against velocity for an angle of attack of 0 Degrees for the whole range of submergences.

This figure shows that the trend are relatively similar for different submergences except for a submergence of 0.1 c for which the drag grows a high rate from a velocity of 2.5 m/s. This can be seen in Figure 159 above and 171 below (except for the tendency at 0.1 c).
On the other hand, at lower angles of attack (-1, 0, 1 and 2 degrees), a slight dip in value can be seen for a speed of 1.25 m/s as seen in Figures 170, 159, 169 and 168. It is hard to know how to approach this because the experiment did not produce results for this speed (1.25 m/s) at higher angles.

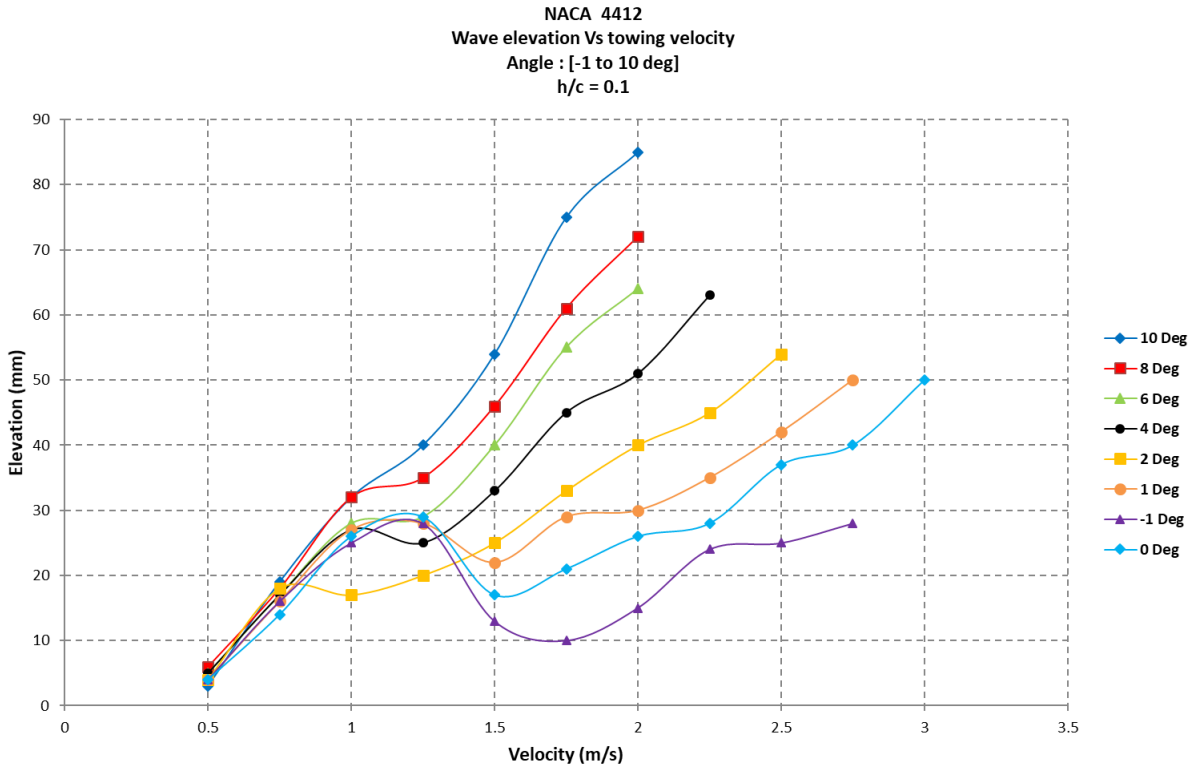

Figure 160: Wave elevation plotted against velocity for a range of angles of attack at a submergence of 0.1 chord.

The Data shown in Figure 160 seems to correlate with the data shown in Figure 26 [20]. The wave function detailed earlier effects the drag characteristics of the shallowly submerged Hydrofoil. It can be noted that because of tank effects the wave characteristics may not be representative. The results can also explain how smaller angles are affected as seen previously in Figures 170, 159, 169 and 168. This is also consistent with what is shown in Figure 161 :

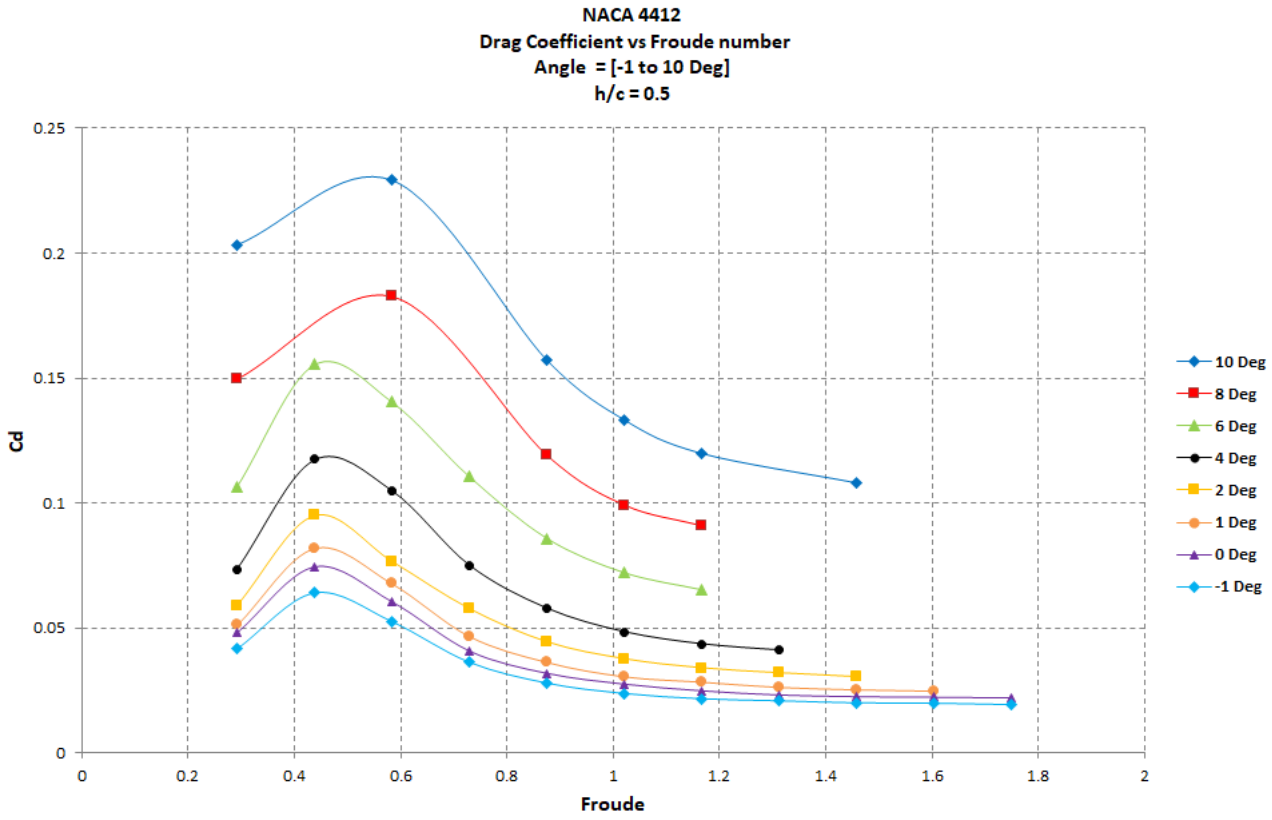

Figure 161: Average Drag coefficient plotted against Froude number, at different angles for a submergence of 0.5 chords

Here it can be seen that the surface effect is significant. High velocity results are relevant here because they are the real conditions at which hydrofoils are used.

9.1.4 conclusion

It has been shown that at lower angles and at shallow submergence (0.1, 0.25 and 0.5 chords), negative lift is created. Also shown here is that drag is affected by the shallower submergences from a speed of 1.0 m/s. The help of wave elevation in the wake of the foil also contributes to this analysis.

9.2 Case of higher submergence from mid-water depth

9.2.1 Introduction

The following pages examine experimental data gathered from tests conducted in mid-water depth. Focus is placed on results for a submergence of 2.0 and 2.5 chords.

9.2.2 Lift analysis

As shown in the results presented in section above 8, the values for Drag and Lift forces are systematically higher for submergences of 2.0 and 2.5 c.
This is well illustrated in Figure 162 below :

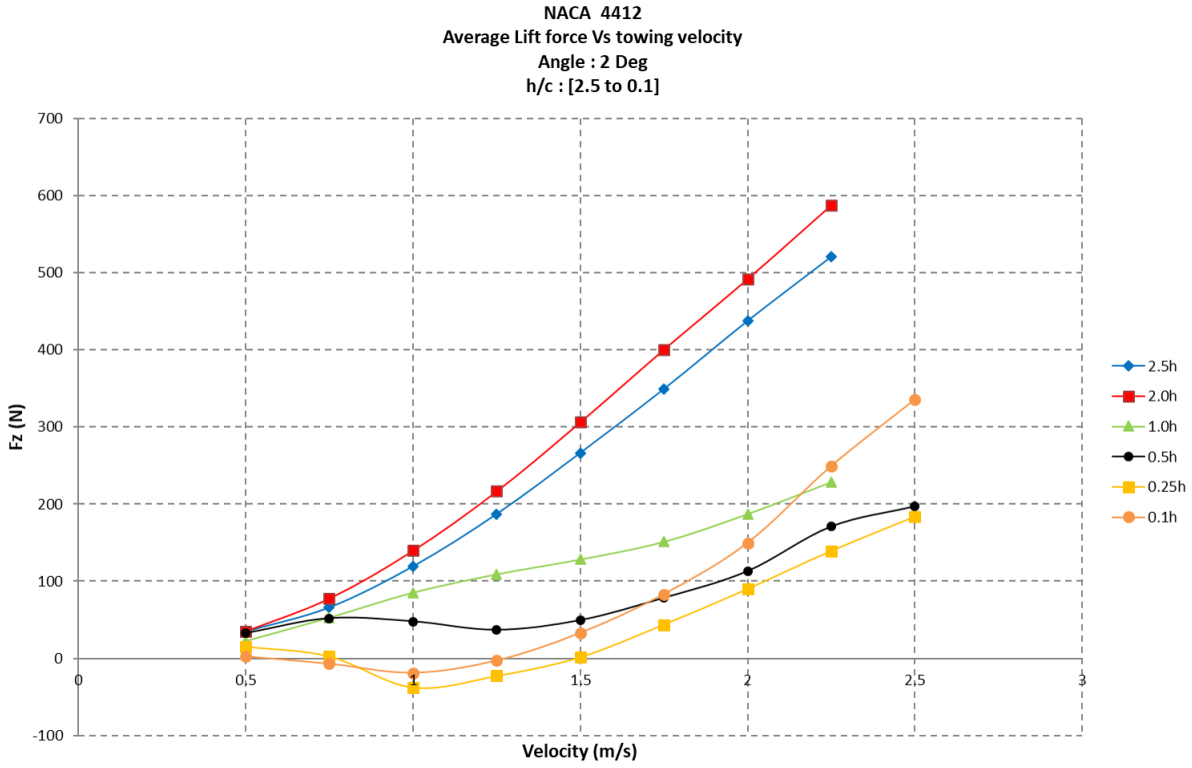

Figure 162: Lift force (F (N)) plotted against velocity for an angle of attack of 2 Degrees at the whole range of submergences.

This also shows that the forces at a submergence 2.0 c are consistently higher than for a greater submergence of 2.5 c as illustrated in Figures 163 and 164.

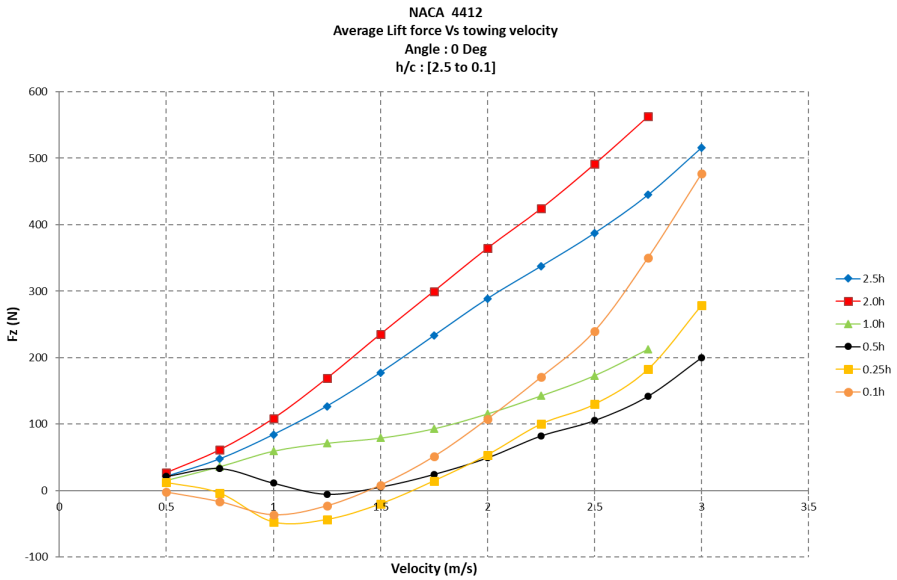

Figure 163: Lift force (F (N)) plotted against velocity for an angle of attack of 0 Degree at the whole range of submergences.

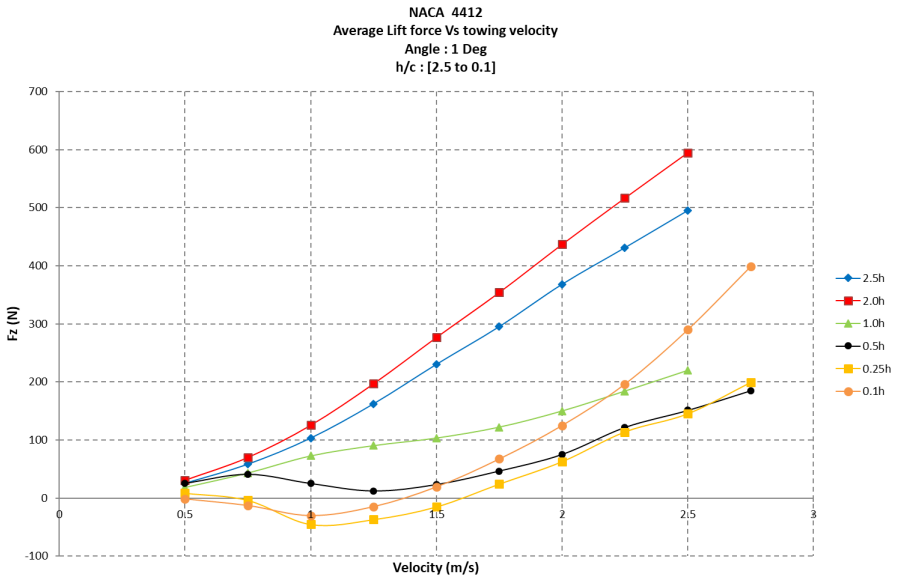

Figure 164: Lift force (F (N)) plotted against velocity for an angle of attack of 1 Degree at the whole range of submergences.

It can also be seen that at higher angles of attack (6,8 and 10 degrees) there is less difference between 2.0 and 2.5 c. Also for the same angles, the trend stays the same for a submergence of 1.0 c until a speed of 1.0m/s is reached. This is illustrated clearly in Figure 165 and further supported by : 165, 166 and 167.

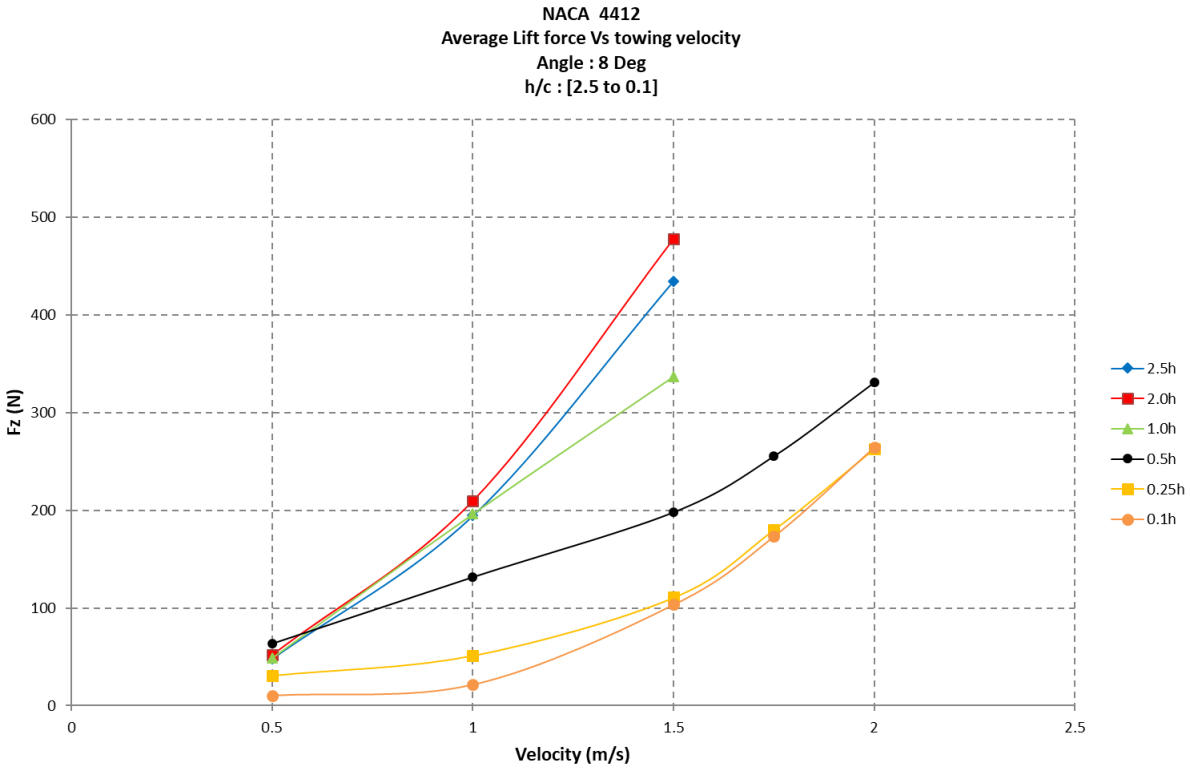

Figure 165: Lift force (F (N)) plotted against velocity for an angle of attack of 8 Degrees for the whole range of submergences.

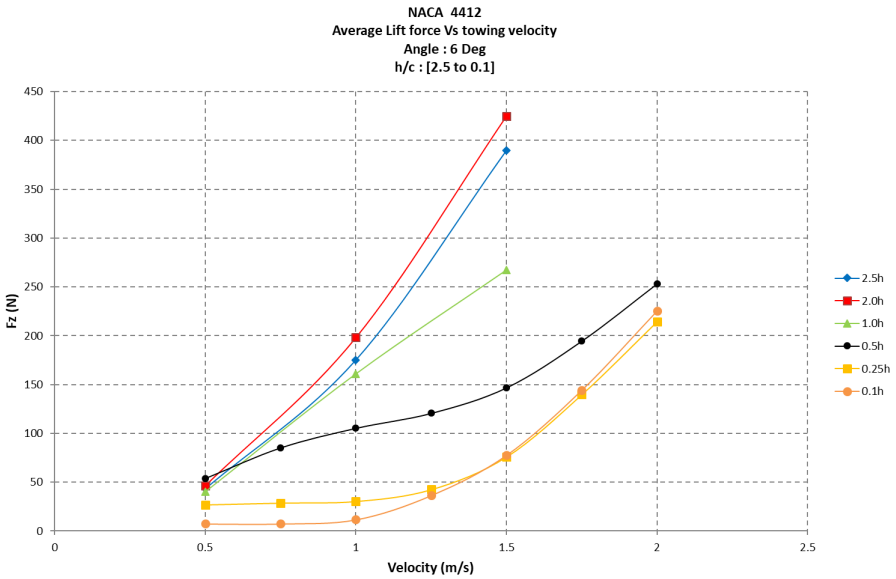

Figure 166: Lift force (F (N)) plotted against velocity for an angle of attack of 6 Degrees for the whole range of submergences.

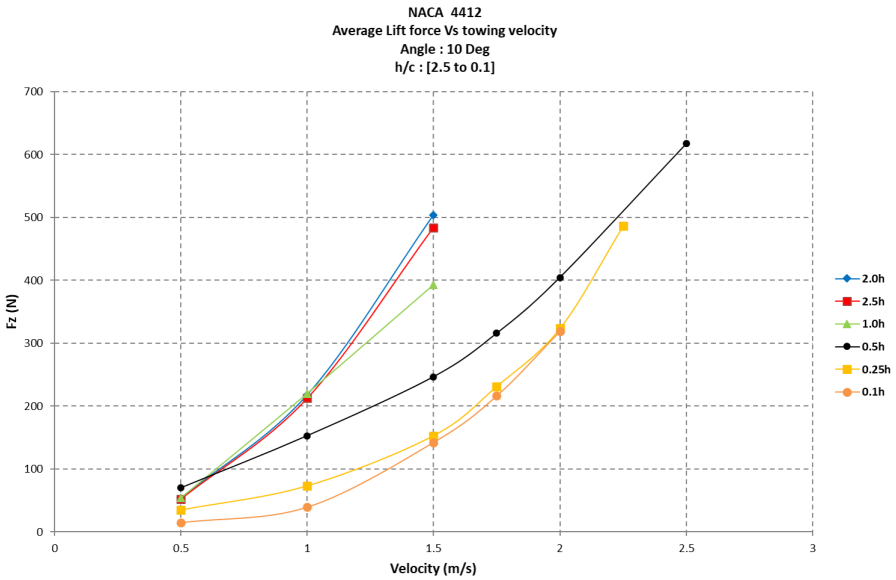

Figure 167: Lift force (F (N)) plotted against velocity for an angle of attack of 10 Degrees for the whole range of submergences.

9.2.3 Drag analysis

As seen before, at a higher submergence, the lift values vary between 2.0 chords and 2.5 chords. However, the drag values do not seem to vary greatly - in fact as seen in Figure 168, submergence does not seem to affect Drag forces until a speed of 1.0 m/s is reached.

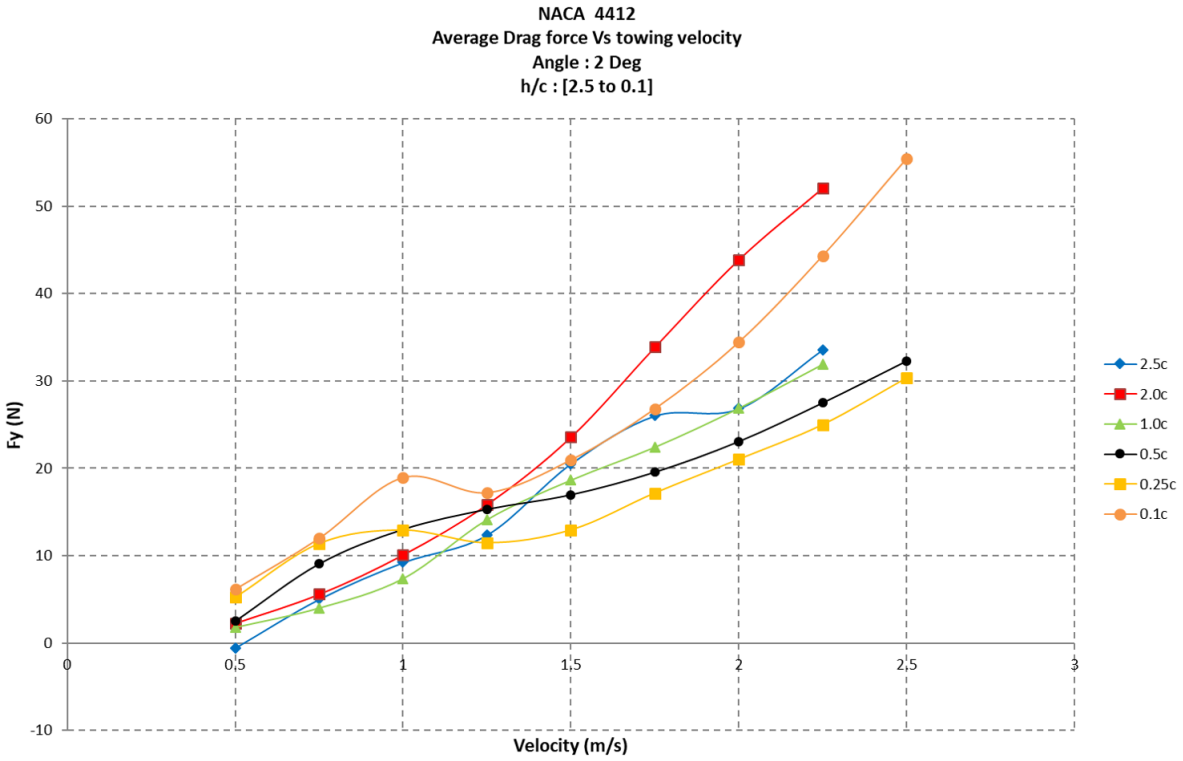

Figure 168: Drag force (F (N)) plotted against velocity for an angle of attack of 2 Degrees at the whole range of submergences.

This is confirmed by Figures 170 and 169.

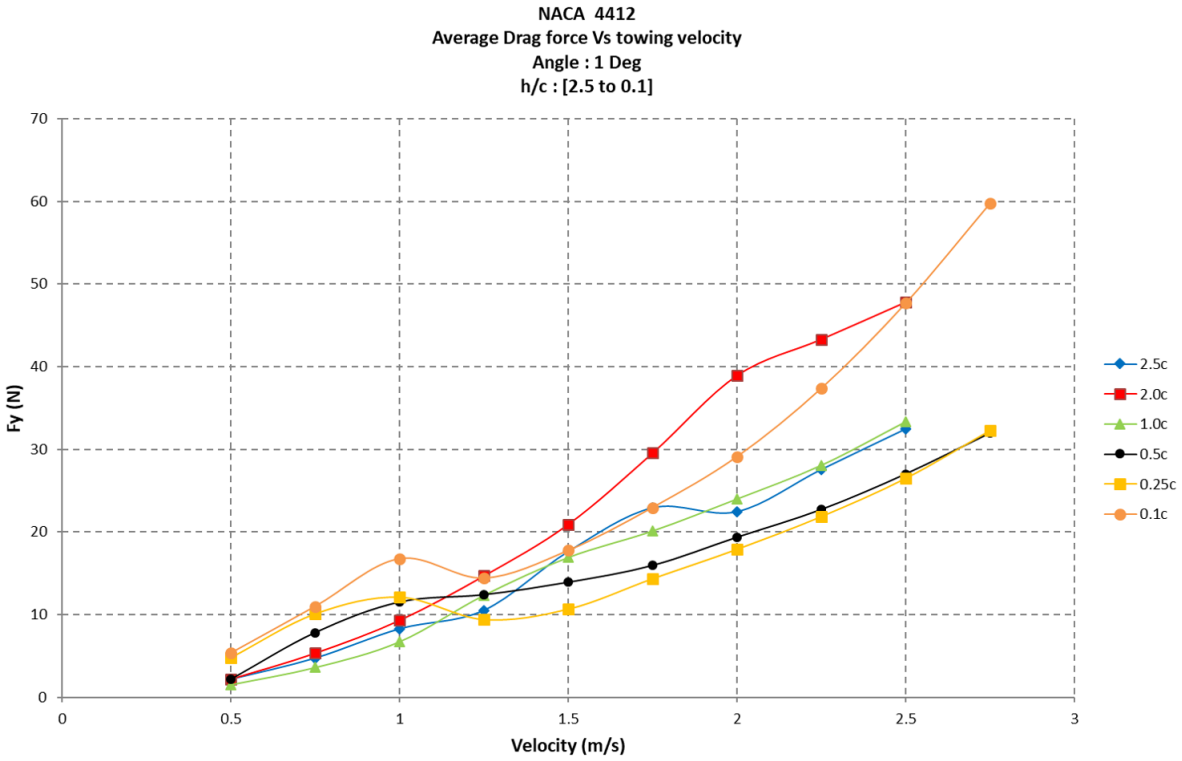

Figure 169: Drag force (F (N)) plotted against velocity for an angle of attack of 1 Degree at the whole range of submergences.

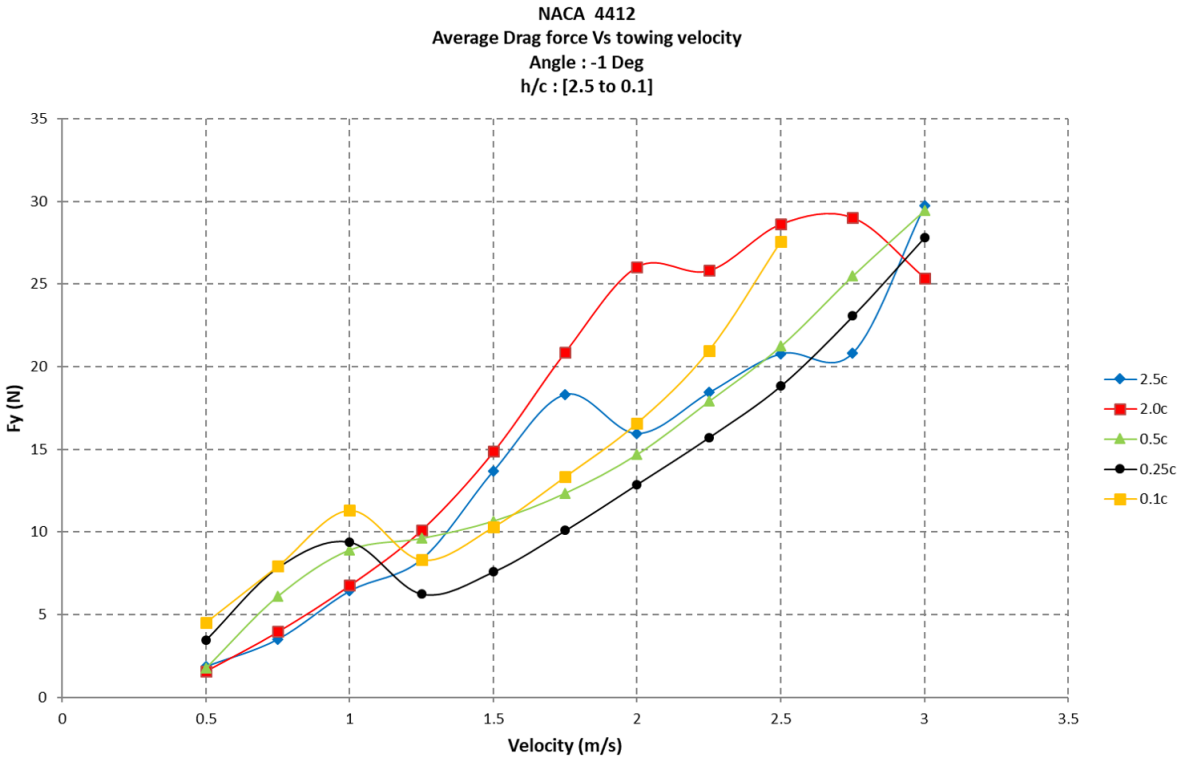

Figure 170: Drag force (F (N)) plotted against velocity for an angle of attack of -1 Degrees at the whole range of submergences.

As shown in Figures 171 and 172, drag forces are lower at deeper submergences until a speed of 1.0 m/s is reached.

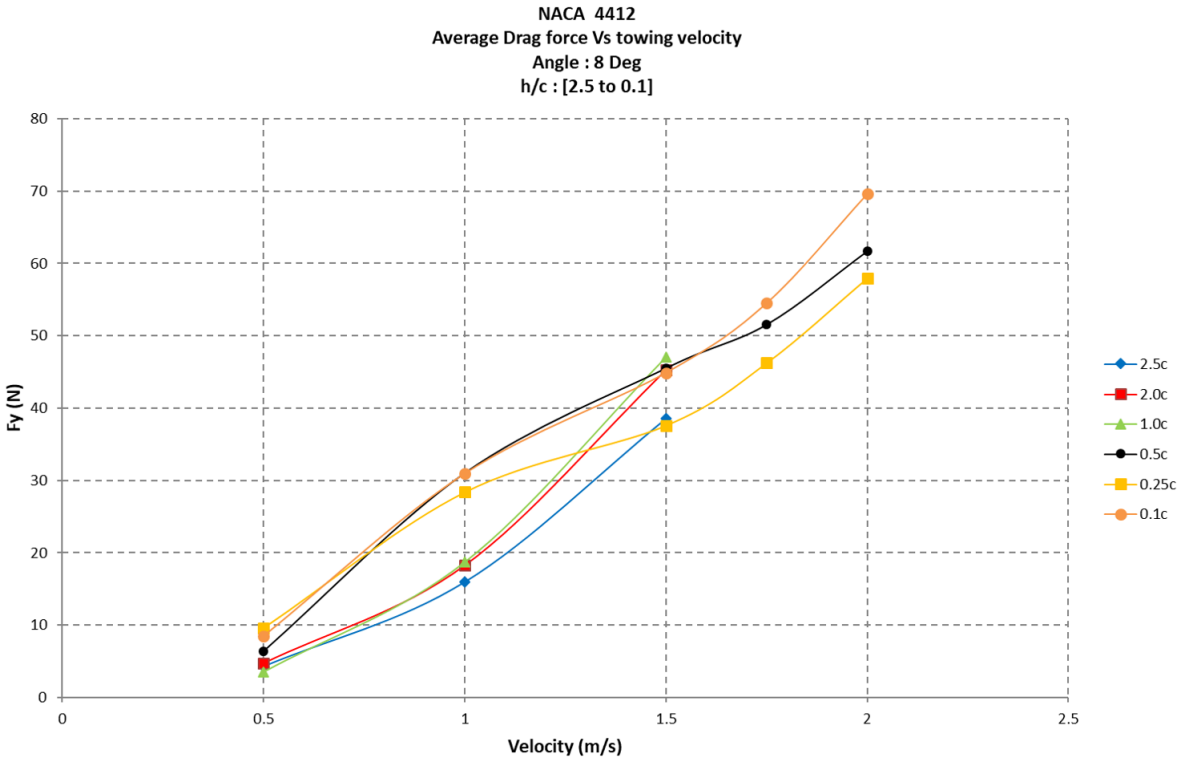

Figure 171: Drag force (F (N)) plotted against velocity for an angle of attack of 8 Degrees for the whole range of submergences.

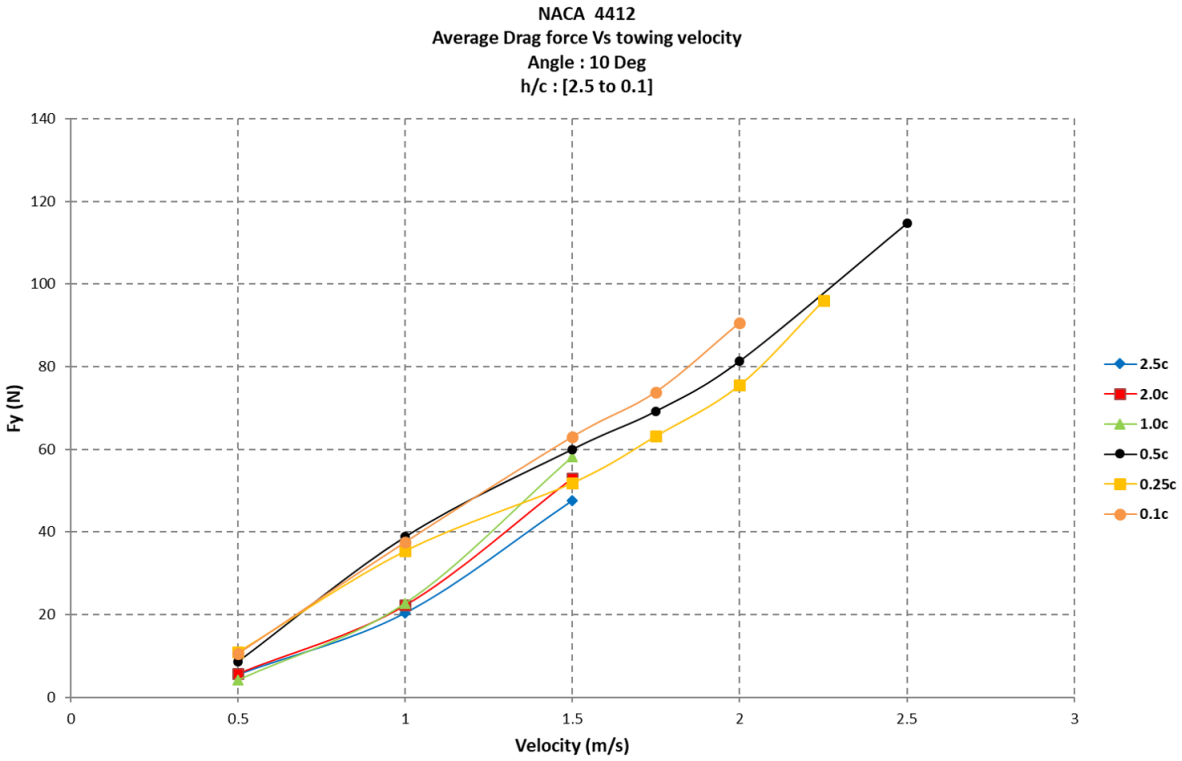

Figure 172: Drag force (F (N)) plotted against velocity for an angle of attack of 10 Degrees for the whole range of submergences.

9.2.4 Conclusion

It has been shown that at the higher submergence of 2.5 chords, lift forces are lower than at a submergence of 2.0 chords. The effect of the tank size will be detailed in 9.3. On the other hand, the drag forces do not seem to be affected by the higher submergence.

9.3 Effect of tank

As seen in Figure 112 the negative lift forces are observed at shallower submergences (0.1, 0.25 and 0.5).At the other end of the curves, a slight decrease can be seen between a submergence of 2.0 and 2.5 chords. This decrease is consistent across all angles. It could be due to tank effect as the hydrofoil draws nearer to the tank bottom. By using the Formula 14 ([24]), corrected values for Cd can be produced. Those results are presented in Figures 173 and 174.

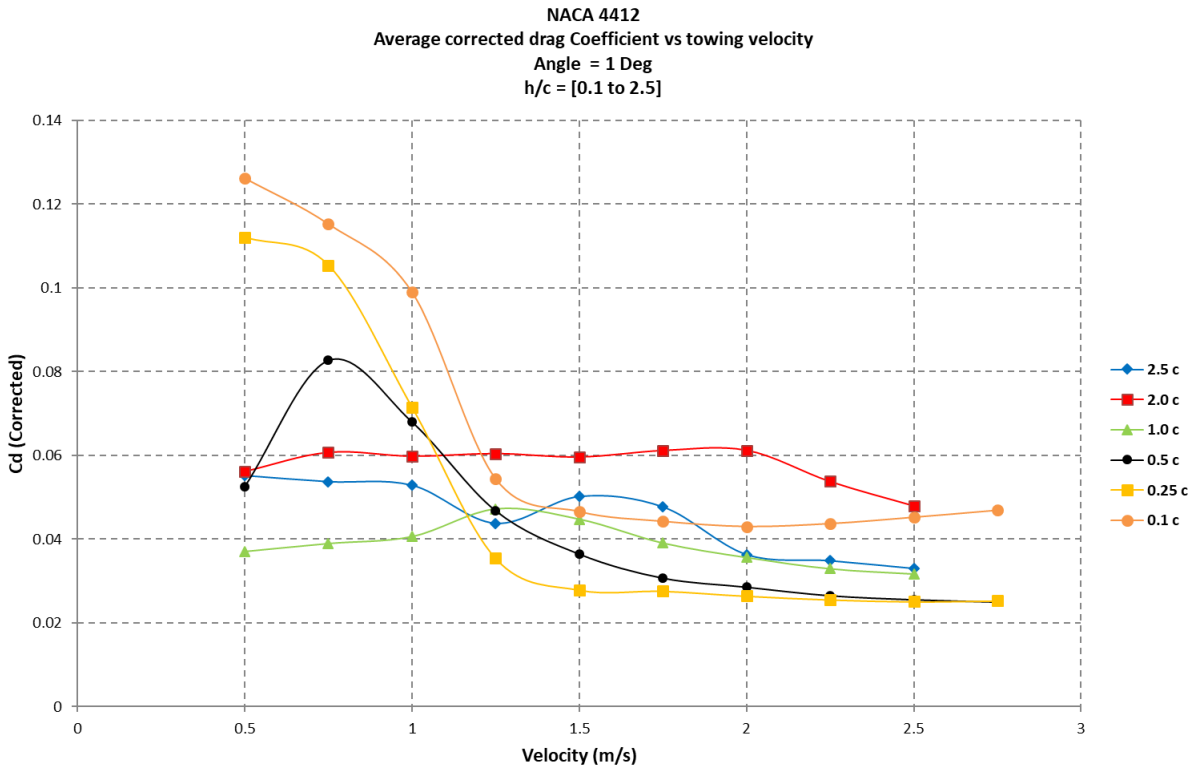

Figure 173: Average corrected drag coefficient plotted against velocity for an angle of attack of 1 Degree for the whole range of submergences.

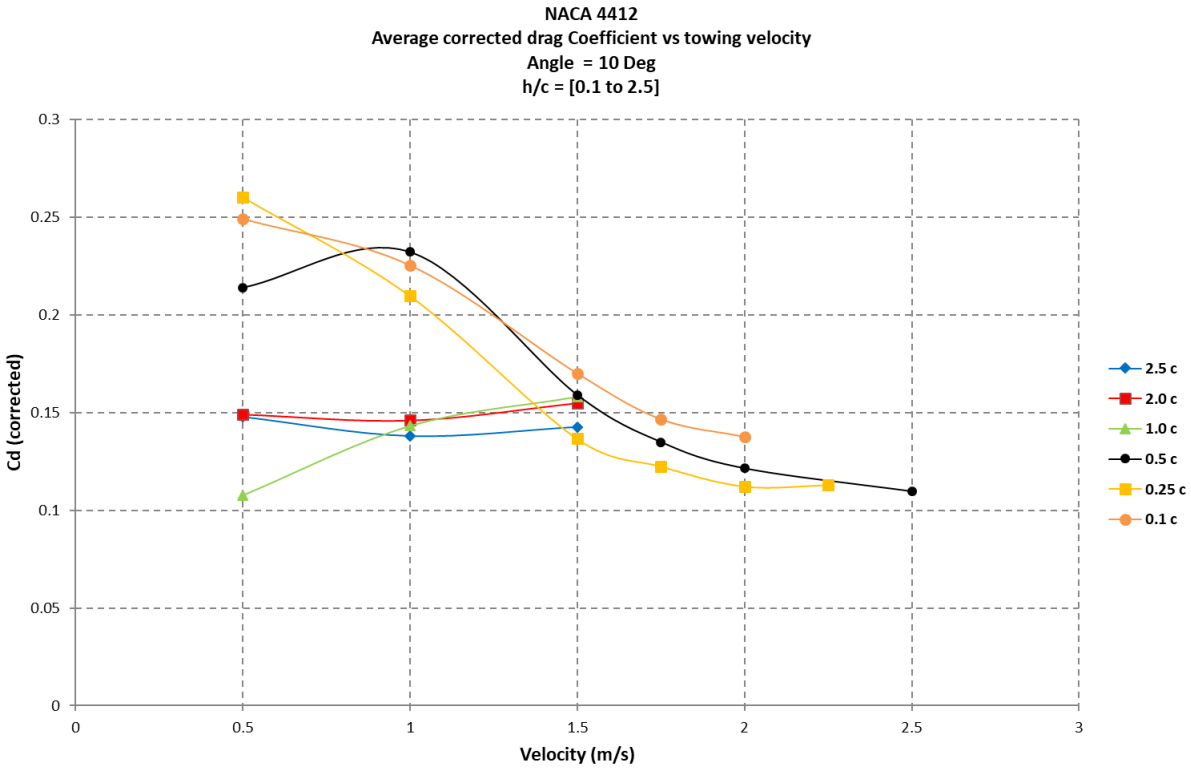

Figure 174: Average corrected drag coefficient plotted against velocity for an angle of attack of 10 Degrees for the whole range of submergences.

Those values can be compared to those of Figures 175 and 176

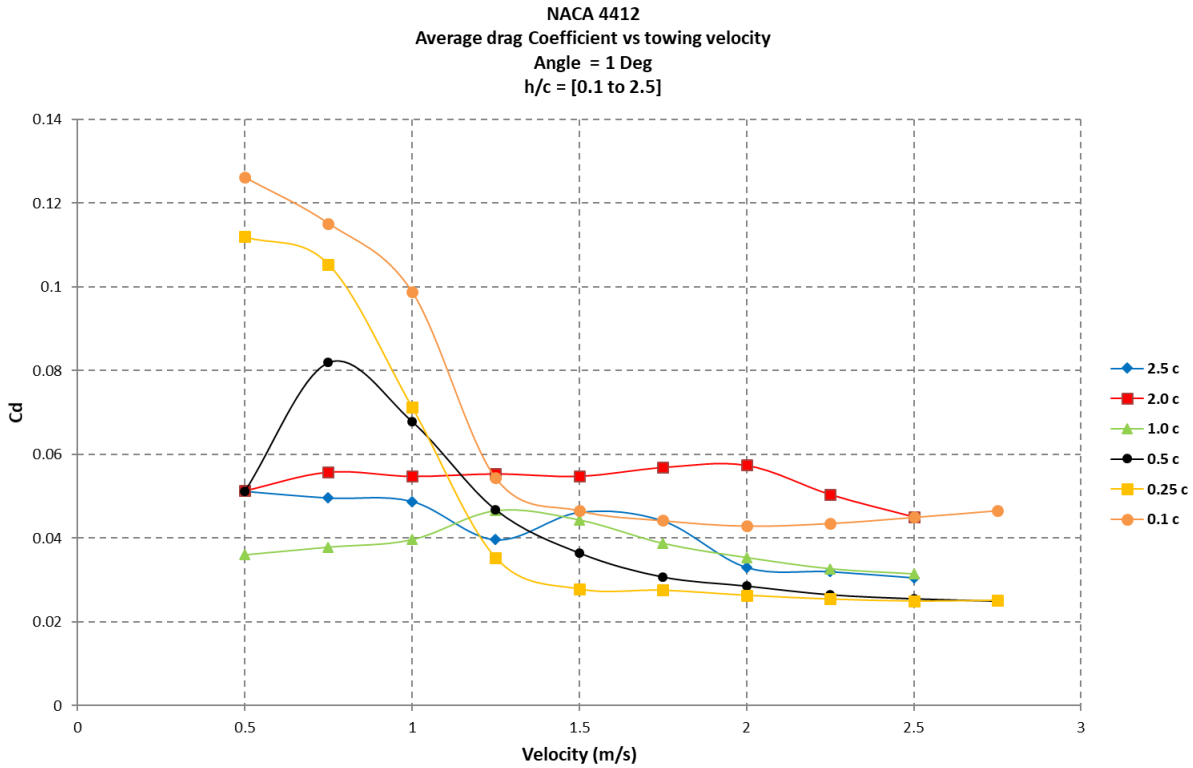

Figure 175: Average drag coefficient plotted against velocity for an angle of attack of 1 Degree for the whole range of submergences.

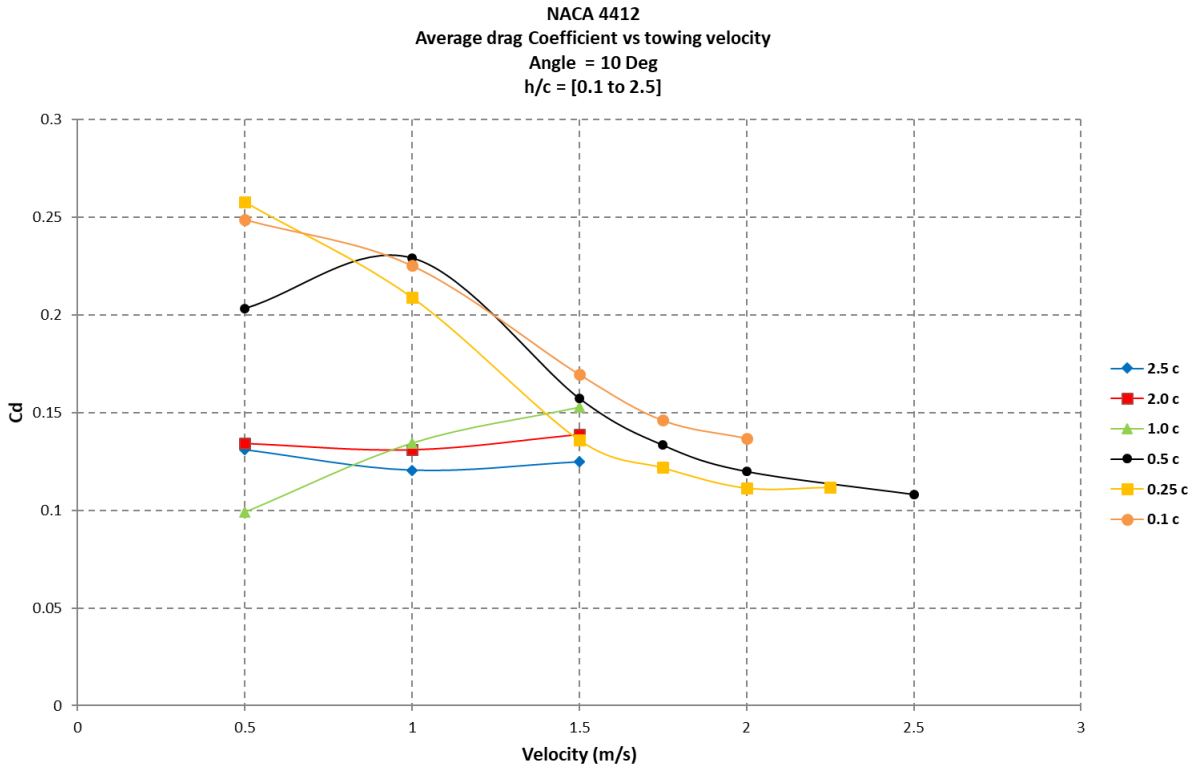

Figure 176: Average drag coefficient plotted against velocity for an angle of attack of 10 Degrees for the whole range of submergences.

The changes are minimal and only affect deeper submergences. A better view of those corrections is presented in Figures 177 and 178. The comparison of the drag and corrected drag coefficients for an an angle of 1 and 10 degrees at submergences of 2.5 and 0.1 chords.

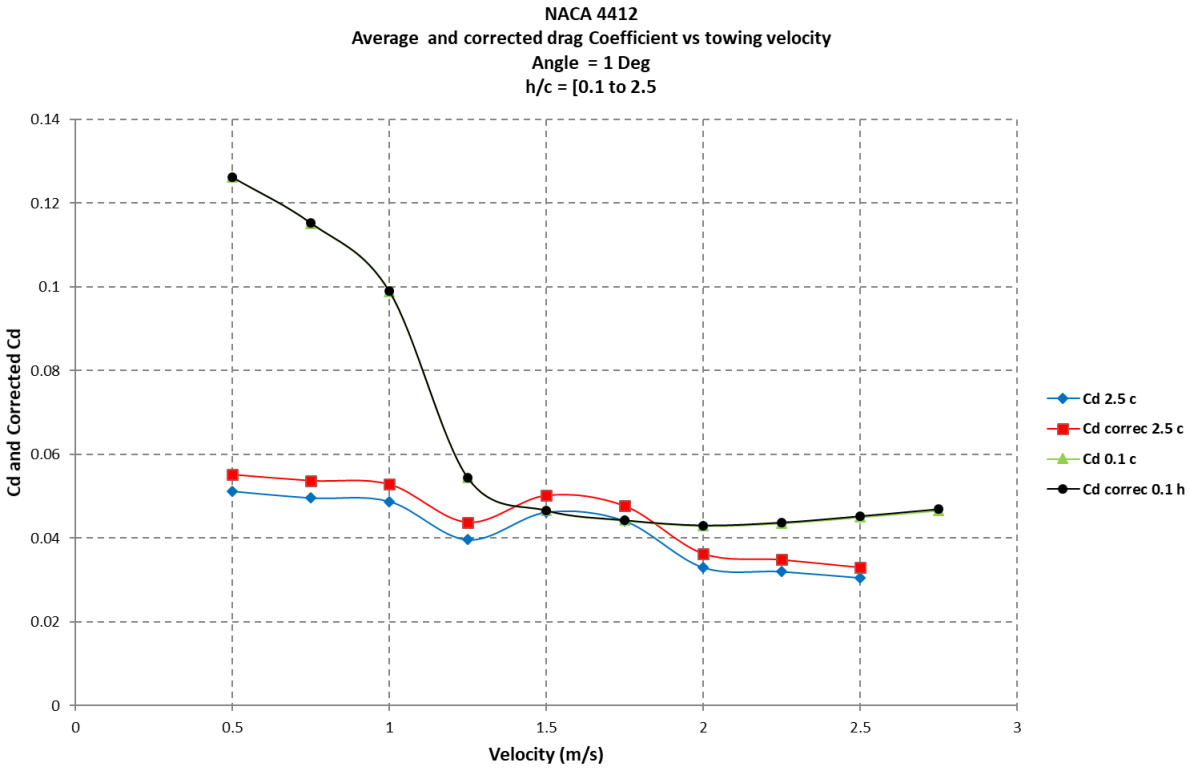

Figure 177: Comparison of drag and corrected drag coefficients plotted against velocity for an angle of attack of 1 Degree at a submergence of 2.5 and 0.1 chords.

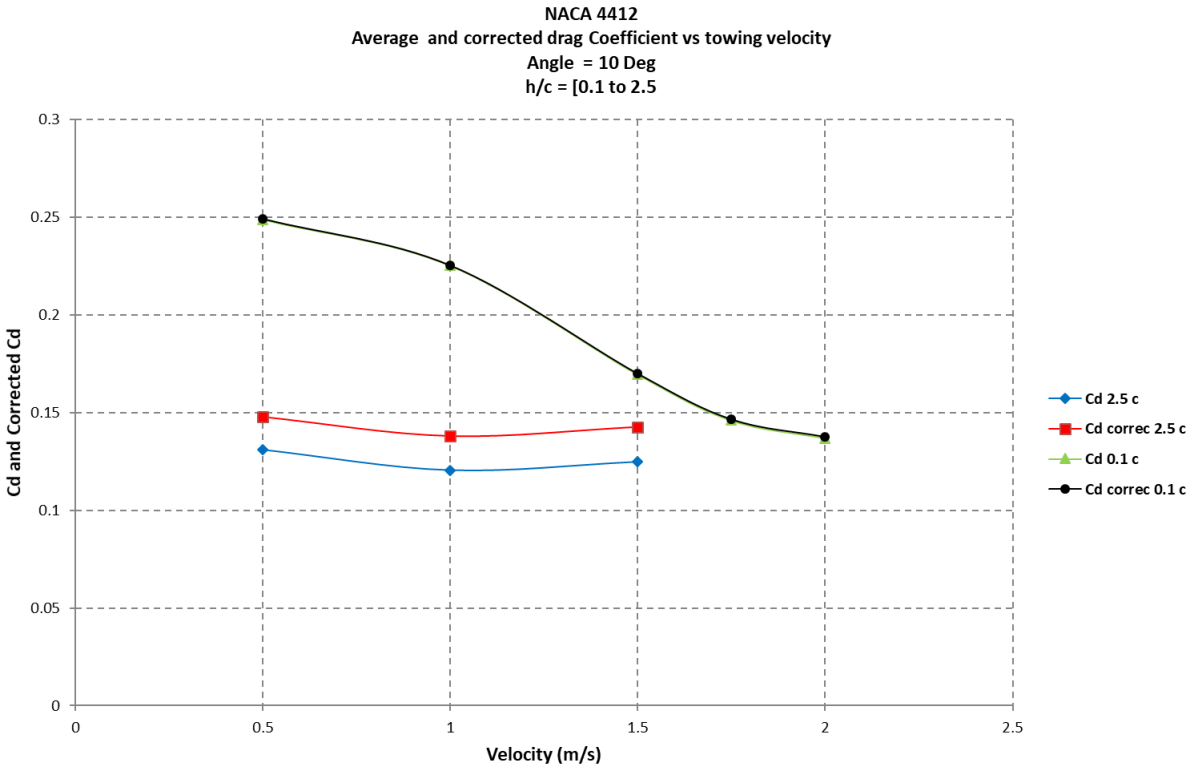

Figure 178: Comparison of drag and corrected drag coefficients plotted against velocity for an angle of attack of 10 Degrees at a submergence of 2.5 and 0.1 chords.

9.3.1 Conclusion

The effect of the bottom of the tank, has an influence on the drag results but not in a significant manner. This was to be expected as drag is a lot less influenced than lift. Some variations of lift that have been observed can be related to effects of the bottom of the tank. This leads to recommendation of testing in a bigger tank to measure this effect for comparison.

9.4 Effect of rig (Side struts)

The main contributing factor to the generation of negative lift could be the test configuration and rig set-up. The rig configuration "is in the way" of the formation of physical effects, most notably the Wing tip effect (which was in part studied by B. Waldin, R. Fontana and C. Shuford in 1951 [49]) (as seen in 4.2.5) This can be seen in Figure 179. This is due mostly to the fact that the foil is held by struts on each side as shown in Figures 40 and 41, which prevents the tip effect from occurring.

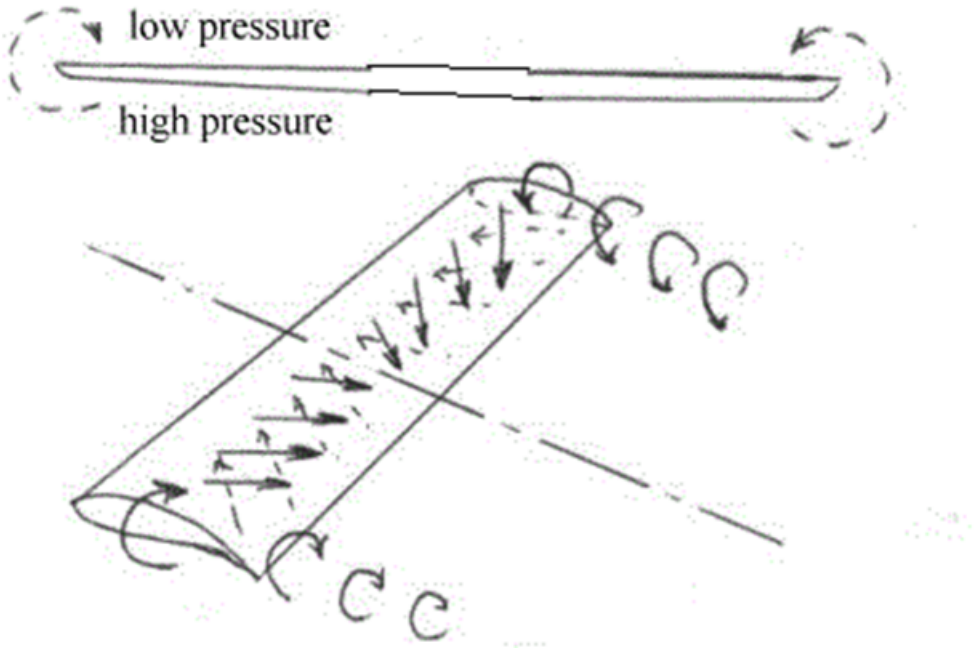

Figure 179: Visualisation of the tip effect [25]

As previously mentioned, the experiments undertaken in Cranfield university closely resemble one of the configurations tested by Waldin, Fontana and Shuford in 1951 [49]. The results of that paper, shown in Figure 13 or Figure 182 below are comparable to the data from recent tests shown in Figures 180 and 181.
Comparable testing was also led by Waldin, Shuford and Mcgehee in 1952 [22].

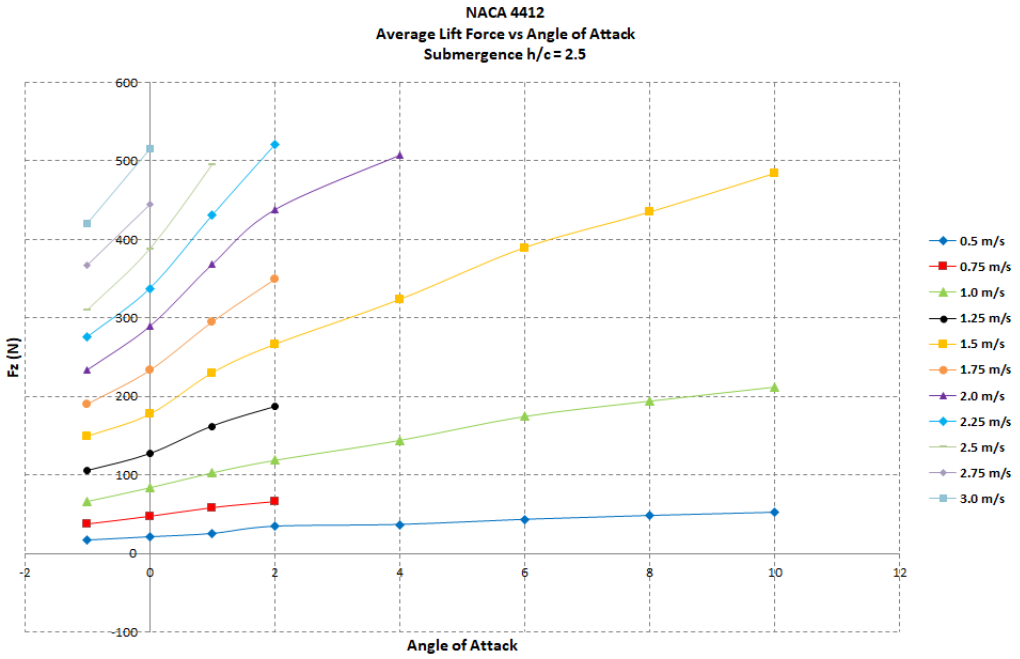

Figure 180: Average Lift force plotted against the angle of attack for velocities ranging from 0.5 m/s to 3.0 m/s at a submergence of 2.5 chords.

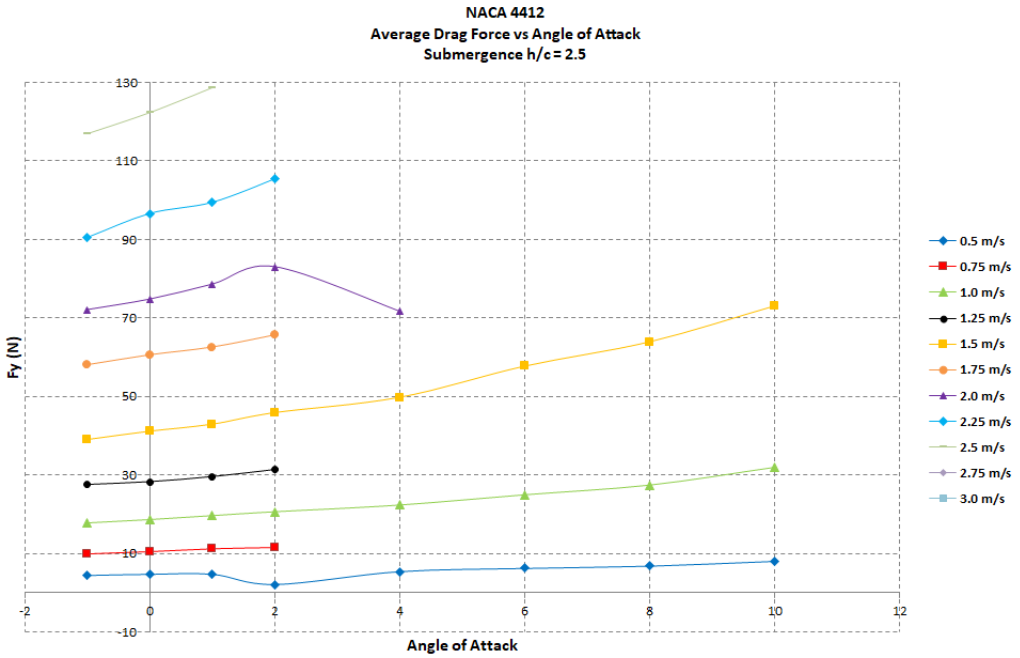

Figure 181: Average Drag force plotted against the angle of attack for velocities ranging from 0.5 m/s to 3.0 m/s at a submergence of 2.5 chords.

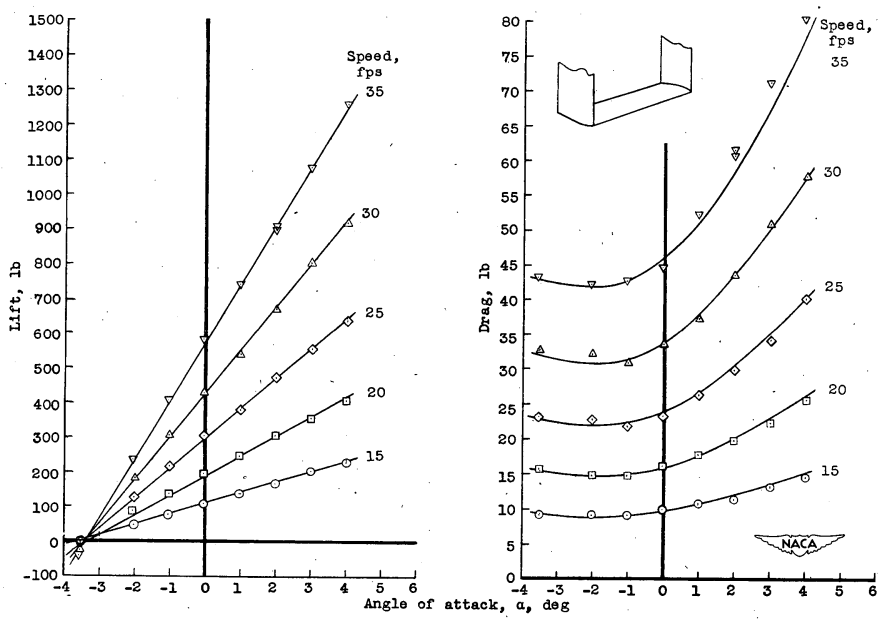

(c) Depth, 2.54 chords.

Figure 13.- Continued.

Figure 182: Results from the testing at Langley by Waldin, Fontana and Shuford [22] for a submergence of 2.54 chords

The experiments shown in Figure 182 show that although speeds are higher (ranging between 4.6 and 10.6 m/s), The form remains similar.
As shown by Daskovsky in 2000 [20], see Figure 183, it is possible to generate negative lift coefficient.

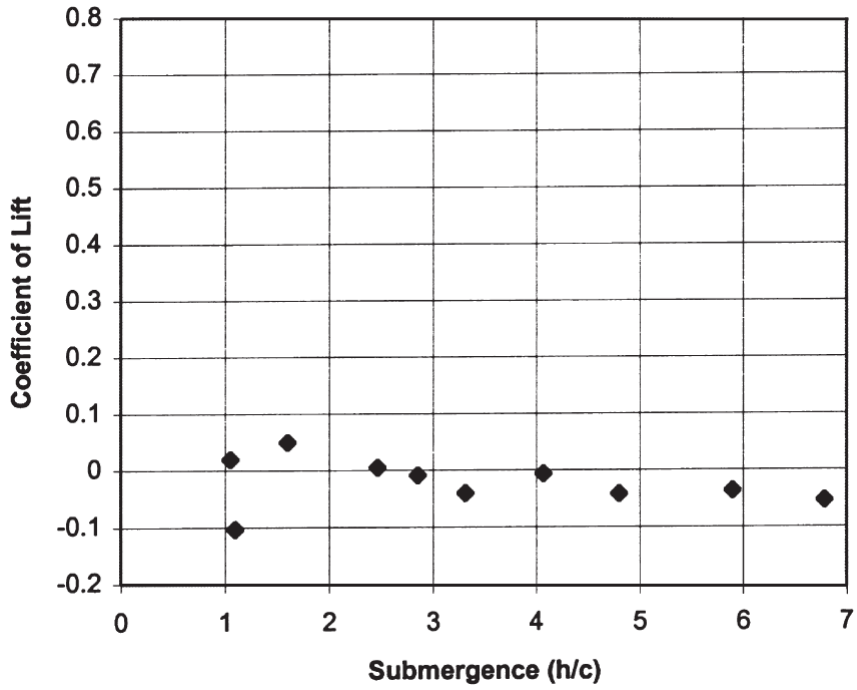

Figure 183: Coefficient of lift [20]

9.4.1 Conclusion

As previously seen, experiments led by Daskovsky [20] and many others (At the Langley towing tank for example : [24], [43] and [50]) the hydrofoils described here are held by a single strut in the middle (compared to the one studied here which is held on both sides). This means that in the experiment presented here, wing tip effects are perturbed. The tip effect is thus widely suppressed and impacts the lift characteristics of the hydrofoil.

9.5 Carriage smoothness

9.5.1 Introduction

When at the standard deviation of the data, a problem arises. An investigation into the phenomenon is presented below.

9.5.2 Investigation

In Figures 184 and 185 a peak can be seen at 1.0 m/s velocity. Although these curves are not perfect, a clear peak is seen.

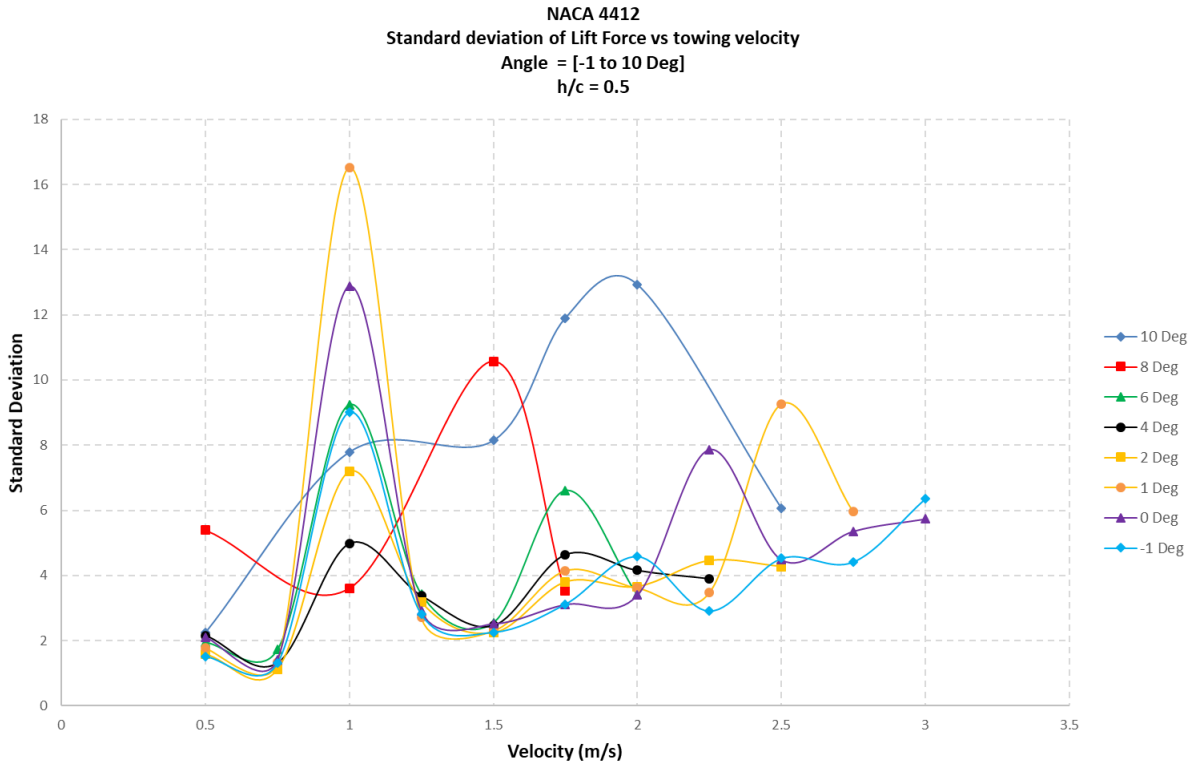

Figure 184: Standard deviation plotted against the velocity, Submergence of 0.5 and an angle of Attack ranging from -1 to 10 degrees.

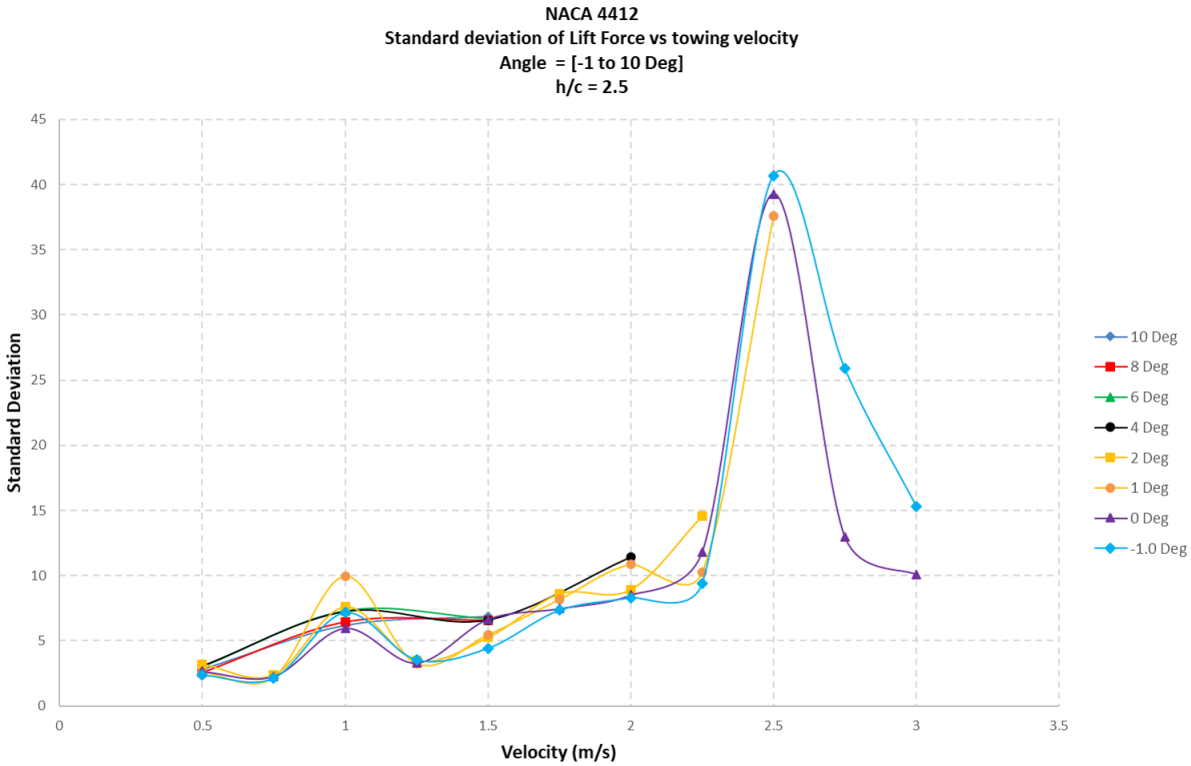

Figure 185: Standard deviation plotted against the velocity, Submergence of 2.5 and an angle of Attack ranging from -1 to 10 degrees.

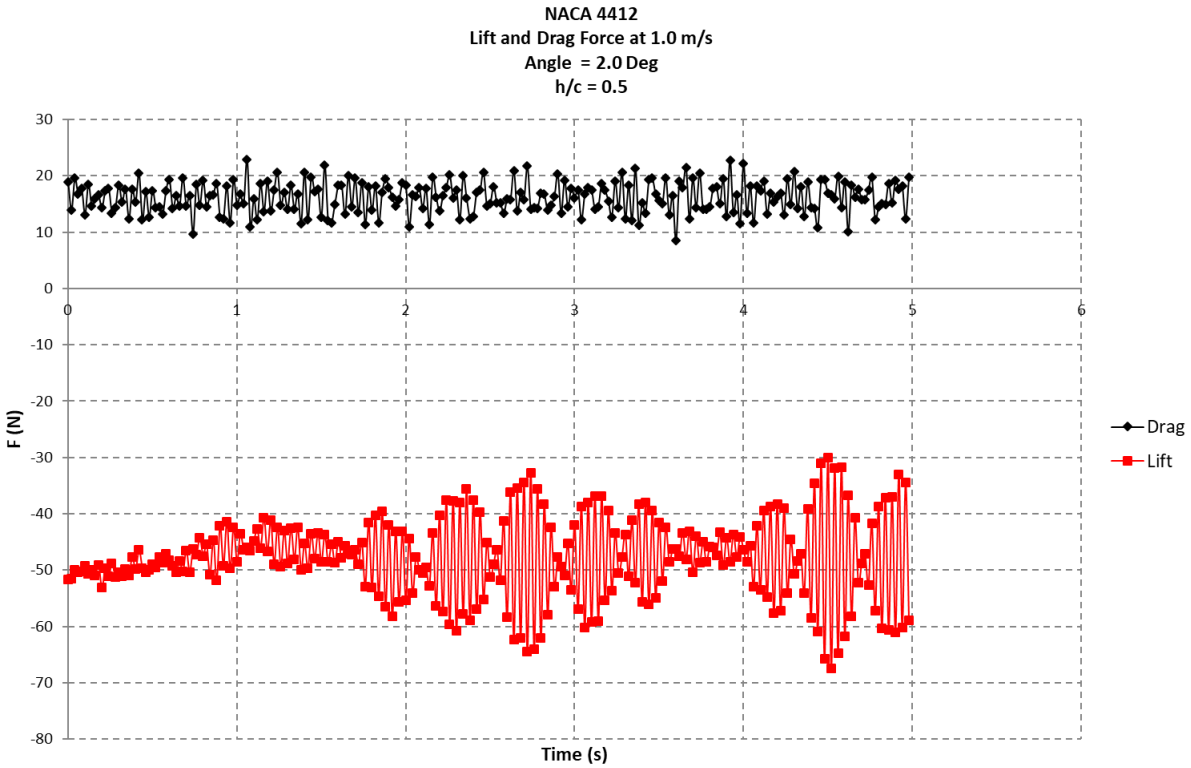

Figure 186: Raw output from the balance for 1.0 m/s, Lift and Drag forces (N) plotted against time, Submergence of 0.5 and an angle of Attack of 2.0 Deg.

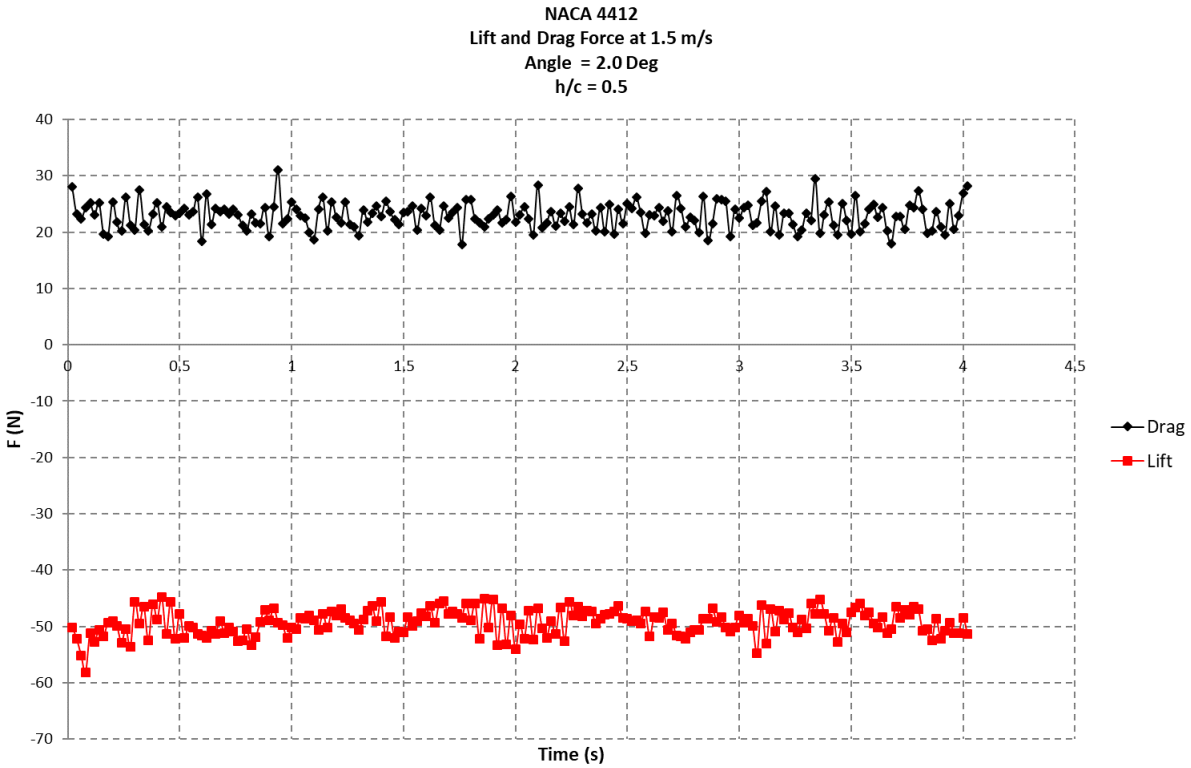

Figure 187: Raw output from the balance for 1.5 m/s, Lift and Drag forces (N) plotted against time, Submergence of 0.5 and an angle of Attack of 2.0 Deg.

Figure 186 shows the raw signal coming from the balance. When comparing to the same angle of attack and submergence (As seen in Figure 187) for a different speed the difference is clear.
A general trend can also be seen, the higher the speed, the higher the standard deviation 184 185.

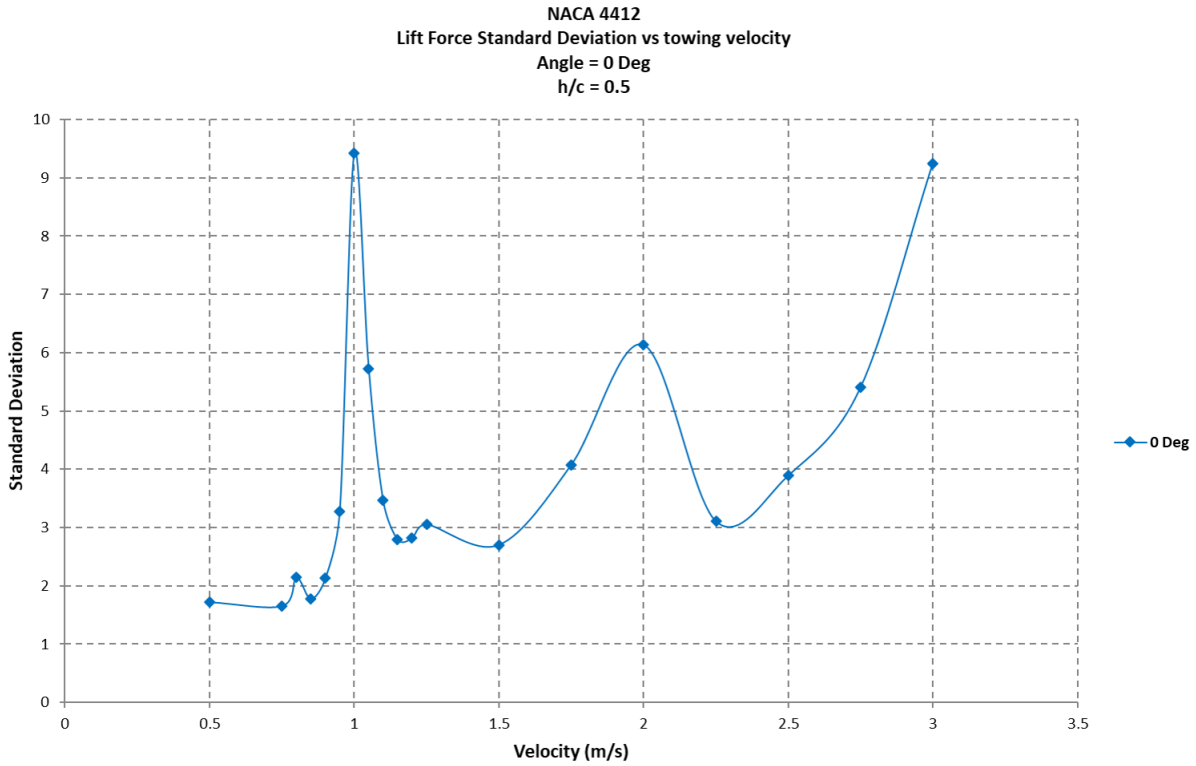

Figure 188: Standard deviation plotted against the velocity, Submergence of 0.5 and an angle of Attack of 0.0 Deg.

Figure 188 Details a series of extra tests undertaken at an angle of attack of 0 degree for a submergence of 0.5 chords. More speeds were used here (from 0.75 m/s to 1.25 m/s in increments of 0.05m/s). The results still show a significant peak at 1.0 m/s.

9.5.3 Conclusion

It can be concluded from evidence provided above that there is a physical phenomenon happening at those velocities. The preferred explanation for this phenomenon, is the smoothness at which the carriage is towed when the input of velocity is 1.0 m/s. It could be that at this speed, the carriage motor can not maintain a steady speed. Another explanation could be that at those velocities the tank enters in a resonance state.

10 Discussion

It is known that some effects can change the results compared to what physical theory says:

- Too close to the surface, where there is no sufficient water above the hydrofoil, the lift generated can be perturbed.
- Conversely, the lift can also be perturbed when the hydrofoil is too close to the bottom of the tank.
- The waves of the hydrofoils and struts can also create resonance effects, or unwanted effects while bouncing off the walls of the tank.
- The steadiness of the towing speed can also affect results.

It is therefore important to look at the experimental results and see when they are consistent with the theory from the physics, or on the contrary when we find unexpected results.
Below are some comments about the experimented behaviour of the drag and lift depending on the three parameters studied:

- The velocity.
- The submergence.
- The angle of attack of the hydrofoil

The physical formula of drag and lift are shown in 1.3.1.2.

10.1 Effect of the velocity:

According to the physics, the drag and lift are correlated to the square of the velocity.

What we observe in the experiment, for instance in 80 or 84 (lift force vs towing velocity) is coherent with the physics.

We can also observe a correct behaviour for the drag force with struts only 148.

With the hydrofoil, we can see the drag forces evolving with the square of the velocity only for important angles. An explanation of why the curves do not follow the physics for lower angles is that the drag is smaller at lower angles and the correction of the drag due to the struts is proportionally more important. Therefore, a small error of measurement of the drag generated by the struts means a proportionally higher error in the drag of the hydrofoil

corrected from the drag of the struts.

This explanation seems to be validated by the fact that measures of drag at lower submergence are closer to the physical expectations (for instance 89), because at lower submergences the drag of the struts reduces.
As seen in section 7, the error also increases with velocity.

10.2 Effect of submergence:

This effect is not represented in the formula of drag and lift shown in 1.3.1.2. Indeed, this formula is calculated for a homogeneous fluid: this is not a problem for aeroplanes, but for ships, the hydrofoils often operate close to the surface, and when the layer of water is too thin, it might change the lift and drag characteristics
.

The effect of submergence is greater for lift than for drag, because both the lift and the submergence are on the same axis. This is clearly seen in the experiments, for instance if figures 51 and 61 are taken, It is seen that drag varies in proportions of roughly 1 to 2 depending on submergence. Lift can change in proportions of 1 to 5 in the same conditions, especially at high speeds.

10.3 Effect of the free surface:

It has been regularly seen in the data, that below a submergence of 1 chord, the results can be erratic (50 58,..).
Trends also be observed in the zone between a submergence of 1 and 2 chords, they change when a submergence higher than 2 chords is reached. In theory, in a tank of infinite depth, when the submergence increases the effects of drag (corrected form the struts) and lift should reach a steady state.
At a great depth, the effect of the free surface should be null. This means that in a tank of sufficient depth, a stable zone should appear when the hydrofoil is sufficiently far from the surface and from the bottom of the tank. In the testing conditions in the Ocean's test system laboratory in Cranfield the effect of the bottom of the tank is observed before the effects of the surface proximity are null.
A solution would be to test smaller hydrofoils at higher speeds in a tank of this size or test the same hydrofoil in a bigger tank.

10.4 Effect of angle of attack of the hydrofoil:

As the angle increases, the projected surface increases, therefore the drag and the lift increase.

For the lift, it can be clearly observed, for instance in figure 80 or 84.

For the drag, this effect can also be seen, for instance in fig 85. This effect is less regular at higher velocities and lower angles. Again, one reason for greater error in this configuration is the proportionally important drag of the struts compared the overall drag of the hydrofoil.

11 Conclusions

During this test session, a substantial number of test were carried out covering angles from -1 to 10 degrees, a velocity ranging from 0.5 to 3.0 m/s and a submergence ranging from h/c = 2.5 to h/c = 0.1. It should provide a good starting point to investigate Lift and Drag characteristics of the NACA 4412 near the water surface.
With these tests it has been able to conclude positively on the efficiency of cost effective small-scale testing in the Cranfield research lab.
Interesting behaviour has been observed (negative lift...)
Negative was anticipated as it had been seen by Daskowsky ([20]) and could be due to the fact that the flow has trouble establishing itself over the Hydrofoil at low submergence and high speeds.

1. At all angles, two dips are seen one at h/c = 0.25 and another from h/c = 2.0. There is no data point for a submergence greater than h/c = 2.5, making an extrapolation on the trend of the curves is impossible. The dip in lift forces and lift coefficient could be because of the tank floor.

2. The effect of depth is seen particularly from a submergence of 1.0 chord. Negative lift forces are seen at low angles and low submergences.

3. The effects of the variation of velocity are only seen at low velocities. The combination with shallow submergence and small angles, creates negative lift.

4. The effect of the bottom of the tank, has an influence on the results but not in a significant manner.

5. It has been shown that at lower angles and at shallow submergence (0.1, 0.25 and 0.5 chords), negative lift is created. Also shown here is that drag is affected by the shallower submergences from a speed of 1.0 m/s. The study of the wave elevation in the wake of the foil also contributes to this analysis.

6. A decrease in lift and lift coefficient has been seen at shallower submergences in 9.1 and it can be concluded that the effect is amplified by the angle of attack.

7. The influence of side struts has been investigated and their influence detailed in 9.4.
   The effect of the struts on the test rig was also detailed by Lee, C. M. Park, I. R. Chun, H. H. et al. in 2001 [51]. These results are in accordance to the results presented. This shows that free surface effect becomes a factor after a submergence of 3 chords. Since the size of the tank did not permit testing at submergences lower than 2.5 chords, tests at a submergence of 3 or more chords were not possible.

8. Carriage smoothness at certain speeds could be a factor. This hypothesis comes from the difference in signals recorded for the 1 m/s velocity.
   Because the lift is affected for different speeds other than 1.0 m/s, this phenomenon doesn't contribute to the native lift forces generated at lower speeds.
   This has been detailed in 9.5.3.

9. The impact of the tank size has been noticed in previous sections (9.4 and 9.3), the ground effect could influence the results if deeper submergences where tested.

The effect of the proximity to the water surface are particularly important from a submergence of 1.0 chord and less. It can therefore be concluded that at a submergence higher than 1.0 chord (between 1.0 and 2.5 chords) we enter in a more stable flow where surface proximity as less of an impact.

12 Future work

Testing accomplished so far has wielded interesting results. Here are the next steps to deepen and improve analysis of the interaction of a the NACA 4412 hydrofoil near the water surface.

1. As previously detailed, the priority now is to try and test in such a way that the struts do not influence the creation of the flow and particularly the tip effect. In order to achieve this, testing with a middle strut (as done in [24] [43], [22], [50]), will be undertaken. An hydrofoil with the same span (1130 mm) and same profile (NACA 4412) but only supported by a middle strut, and the same profile (NACA 4412) with a shorter span (500mm) also held by a single strut. This will help see the influence of the tank wall on the lift and drag characteristics of the profile.
   At the time of writing, a second NACA 4412 hydrofoil with a middle strut (NACA 0024 seen in Figure 189 below) was being prepared to continue the work.

Figure 189: New 4412 hydrofoil supported by a middle strut in the Ocean Systems Test Laboratory. The middle strut here is a 0012 NACA profile. It was chosen to reduce drag.

2. Another aspect that would be interesting to look at would be angles from -10 degrees. It is known that lift should be null for angles of -4 degrees ([35]), so complying to that could help improve the analysis.

3. Compensate for windage as in [39] by hanging struts from the balance and running just clear of the water surface. This would give a component

of the drag generated by air against the struts, above the water surface. This drag component would then be incorporated in the results. It is reasonable to think that the windage component of the struts would be negligible compared to the drag created in the water.

4. The use of different instrumentation to record the speed of the carriage, could enable further insight in the problem that develops at 1.0 m/s.

5. Test in bigger tanks using the same set-up so as to isolate the effect of our tank. Once the effect of the tank size in the the Ocean's Test Laboratory is known, it will be possible to continue tests in said tank and apply coefficients to results, so as to make them more representative.

13 Appendices

The appendices for this thesis are presented in a separate file.

Bibliography

[1] Unknown, "The Speediest Boat," *National Geographic*, p. 875, 1911.

[2] "vs-7.jpg." [Online]. Available: http://www.foils.org/gallery/vs-7.jpg

[3] J. Hilton, "DIMOC," 1984. [Online]. Available: http://www.dimoc.mil/{#}guid=06d5e73c7c35e295f1edb6b37ecde86aa9a7eae3

[4] "Sarancha class/p420." [Online]. Available: http://www.bluebird-electric.net/hydrofoils.htm

[5] "Turya class." [Online]. Available: https://upload.wikimedia.org/wikipedia/commons/4/4d/BTK{_}pr.206M2.jpg

[6] Evgeniy, "Priluki - ShipSpotting.com - Ship Photos and Ship Tracker," 2011. [Online]. Available: http://www.shipspotting.com/gallery/photo.php?lid=1399103

[7] "KEY DATES :: L'HYDROPTÈRE - Alain Thébault." [Online]. Available: http://hydroptere.com/en/the-dream/the-beginning/

[8] "Class A." [Online]. Available: http://gpsailing.org/?p=7725

[9] "Groupama Class C." [Online]. Available: https://www.rcgroups.com/forums/showthread.php?2190004-Fire-Arrow-Foiling-Trimaran-Test-Model/page6

[10] "Nacra F20 FCS - Nacra Sailing - Worlds best catamarans." [Online]. Available: http://www.nacrasailing.com/project/nacra-f20-fcs/

[11] "Flying phamtom." [Online]. Available: http://www.catsailingnews.com/2014/05/nacra-f20-fcs-vs-flying-phantom.html

[12] Thierry Martinez, "mothfoil," 2015. [Online]. Available: http://www.mothworlds.org/sorrento/videos/

[13] Calver Will, "Learning to Fly- A test ride on Stratis, the foiling SL33," 2014. [Online]. Available: http://www.sail-world.com/Australia/Learning-to-Fly--A-test-ride-on-Stratis,-the-foiling-SL33/127036?source=google.co.uk

[14] S. Van der Borch, "PHOTOS: Sky is limit for full foiling GC32," 2014. [Online]. Available: http://www.sailingscuttlebutt.com/2014/04/19/photos-sky-limit-full-foiling-gc32/

[15] J. Tronet, "The 8 Stages of Kite Foiling by Jeremie Tronet — — The Best Kitesurfing Holidays in the Caribbean." [Online]. Available: http://www.kitesurfgrenadines.com/the-8-stages-of-kite-foiling-by-jeremie-tronet/

[16] "America's cup web," 2016. [Online]. Available: https://www.americascup.com/en/ac35-The-Boats.html

[17] B. W. McCormick, *Aerodynamics of V/STOL flight*. Dover Publications, 1999. [Online]. Available: https://commons.wikimedia.org/wiki/File:Airfoil{_}geometry.svg

[18] Anonymous, "File:Aerofoil1.jpg - SKYbrary Aviation Safety," 2011. [Online]. Available: http://www.skybrary.aero/index.php/File:Aerofoil1.jpg

[19] ARLIN STOLTZFUS, "Stoltzfus Research Group at IBBR," 2015. [Online]. Available: http://www.molevol.org/why-the-four-fundamental-forces-view-is-mistaken/

[20] M. Daskovsky, "The hydrofoil in surface proximity, theory and experiment," *Ocean Engineering*, vol. 27, no. 10, pp. 1129–1159, 2000.

[21] Olivier Cleynen, "File:Aircraft wing lift distribution showing trailing vortices (1).svg - Wikimedia Commons," 2011. [Online]. Available: https://commons.wikimedia.org/wiki/File:Aircraft{_}wing{_}lift{_}distribution{_}showing{_}trailing{_}vortices{_}(1).svg

[22] K. Waldin, C. L. Shuford, and J. R. McGehee, "A theoretical and experimental investigation of the lift and drag characteristics of the hydrofoils at subcritical and supercritical speeds," National Advisory Committee for Aeronautics, Langley, Tech. Rep., 1952.

[23] C. CRERAR, "U.S., Japan and Germany Join Australian Stealth Research," 2016. [Online]. Available: http://www.maritime-executive.com/article/us-japan-and-germany-join-australian-stealth-research

[24] K. L. Wadlin, J. R. McGehee, and J. A. Ramsen, "Naca Research Memorandum, Tank Tests At Subcavitation Speeds of an Aspect-Ratio-1O Hydrofoil With a Single Strut," National Advisory Committee for Aeronautics, Langley, Tech. Rep., 1950. [Online]. Available: http://digital.library.unt.edu/ark:/67531/metadc53485/m2/1/high{_}res{_}d/19810068686.pdf{%}5Cnhttp://digital.library.unt.edu/ark:/67531/metadc53558/m2/1/high{_}res{_}d/19810068858.pdf

[25] Unknown, "Trailing Vortices Producing Downwash." [Online]. Available: http://www.pilotfriend.com/training/flight{_}training/aero/lift.htm

[26] Ian Hamilton, "The Hydrofoil As a Weapon," *Pacific Defence Reporter*, 1981.

[27] Robert V. Bruce, *Alexander Graham Bell and the Conquest of Solitude*, 1973.

[28] "Forlanini." [Online]. Available: http://www.foils.org/gallery/forlani.htm

[29] "Alexander Graham Bell and the Hydrofoils [1906-1921]." [Online]. Available: http://www.lesliefield.com/other{_}history/alexander{_}graham{_}bell{_}and{_}the{_}hydrofoils.htm

[30] "German Navy Proves Hydrofoils Unfit." [Online]. Available: http://www.foils.org/trag.htm

[31] "WAR AT SEA - NYTimes.com." [Online]. Available: http://www.nytimes.com/1988/05/29/magazine/war-at-sea.html

[32] "HISTORY OF THE AMERICA'S CUP - 35th America's Cup." [Online]. Available: https://www.americascup.com/en/history.html

[33] "Projects - VPLP Design." [Online]. Available: http://www.vplp.fr/

[34] "Présentation officielle du Figaro 3 - Course au Large." [Online]. Available: http://www.courseaularge.com/presentation-officielle-figaro-3.html

[35] I. H. Abbott and Albert E. Von Doenhoff, *Theory of wing sections*, 1949.

[36] G. Biplane, "REPORT No. 151," no. 151.

[37] C. Bai, J. Li, and Z. Wu, "Generalized Kutta-Joukowski theorem for multi-vortex and multi-airfoil flow with vortex production - A general model," *Chinese Journal of Aeronautics*, vol. 27, no. 5, pp. 1037–1050, 2014. [Online]. Available: http://dx.doi.org/10.1016/j.cja.2014.03.014

[38] P. DuCane, "High speed small craft," in *Principles of hydrofoils*, 1972.

[39] K. E. Ward and N. S. Land, "Preliminary tests in the NACA tank to investigate the fundamental characteristics of hydrofoils," National Advisory Committee for Aeronautics, Langley, Tech. Rep., 1940.

[40] R. M. Pinkerton, "Calculated and measured pressure distributions over the midspan section of the NACA 4412 airfoil," Langley Memorial Aeronautical Laboratory, Langley Field, Tech. Rep., 1936.

[41] Kotchin, "On the notion of profiles of any form below the surface of a heavy fluid," 1951.

[42] Vladimorov, "Approximate hydrodynamic design of a finite span hydrofoil," 1937.

[43] Y. SHEN, "Recent studies of struts and foils for high-speed application," *Archive Set 136*, vol. 16, no. 1, pp. 71–82, 1963. [Online]. Available: http://dx.doi.org/10.2514/6.1976-851

[44] C. Harwood, Y. Young, and S. Ceccio, "Ventilated cavities on a surface-piercing hydrofoil at moderate Froude numbers: Cavity formation, elimination and stability," *Journal of Fluid Mechanics*, vol. 800, no. 2016, pp. 5–56, 2016.

[45] S. Longo, L. Chiapponi, and M. Clavero, "Experimental analysis of the coherent structures and turbulence past a hydrofoil in stalling condition beneath a water-air interface," *European Journal of Mechanics, B/Fluids*, vol. 43, pp. 172–182, 2014. [Online]. Available: http://dx.doi.org/10.1016/j.euromechflu.2013.08.007

[46] M. Sedlar, B. Ji, T. Kratky, T. Rebok, and R. Huzlik, "Numerical and experimental investigation of three-dimensional cavitating flow around the straight NACA2412 hydrofoil," *Ocean Engineering*, vol. 123, pp. 357–382, 2016.

[47] Z. LIU, B.-s. HYUN, M.-r. KIM, and J.-y. JIN, "Experimental and numerical study for hydrodynamic characteristics of an oscillating hydrofoil," *Journal of Hydrodynamics, Ser. B*, vol. 20, no. 3, pp. 280–287, 2008. [Online]. Available: http://www.sciencedirect.com/science/article/pii/S100160580860058X

[48] E. G. Reid, *Applied Wing Theory*, first edit ed. New York: McGraw-Hill Book Company, Inc, 1932.

[49] B. K. L. Wadlin, R. E. Fontana, and C. L. Shuford, "Tee Effect of End Plates , End Struts , and Depth of," 1951.

[50] J. R. Binns, P. A. Brandner, and J. Plouhinec, "THE EFFECT OF HEEL ANGLE AND FREE-SURFACE PROXIMITY ON THE PERFORMANCE AND STRUT WAKE OF A MOTH SAILING DINGHY RUDDER T-FOIL," *3rd High Performance Yacht Design Conference, issue August 2008*, 2008.

[51] C. M. Lee, I. R. Park, H. H. Chun, and S. J. Lee, "Effect of free surface and strut on fins attached to a strut," *Ocean Engineering*, vol. 28, no. 1, pp. 159–177, 2001.